# MODELING RELAYS FOR POWER SYSTEM PROTECTION STUDIES

A Thesis
Submitted to the College of Graduate Studies and Research
in Partial Fulfillment of the Requirements
For the Degree of
Doctor of Philosophy
in the
Department of Electrical Engineering
University of Saskatchewan
Saskatoon, Saskatchewan
Canada
by

**SANDRO GIANNY AQUILES PEREZ**

# PERMISSION TO USE

In presenting this thesis in partial fulfillment of the requirements for a Doctor of Philosophy degree from the University of Saskatchewan, the author agrees that the Libraries of this University may make it freely available for inspection. The author further agrees that permission for copying of this thesis in any manner, in whole or in part, for scholarly purposes may be granted by the professors who supervised the thesis work or, in their absence, by the Head of the Department of Electrical Engineering or the Dean of the College of Engineering. It is understood that any copying or publication or use of this thesis or part thereof for financial gain shall not be allowed without the author's written permission. It is also understood that due recognition shall be given to the author and the University of Saskatchewan in any scholarly use which may be made of any material in this thesis.

Request for permission to copy or to make other use of material in this thesis in whole or part should be addressed to:

Head of the Department of Electrical Engineering,
University of Saskatchewan,
Saskatoon, Saskatchewan, Canada S7N 5A9

# ABSTRACT

Numerical relays are the result of the application of microprocessor technology in relay industry. Numerical relays have the ability to communicate with its peers, are economical and are easy to operate, adjust and repair. Modeling of digital and numerical relays is important to adjust and settle protection equipment in electrical facilities and to train protection personnel. Designing of numerical relays is employed to produce new prototypes and protection algorithms. Computer models of numerical relays for the study of protection systems are greatly enhanced when working along with an electromagnetic transient program (emtp). A literature survey has revealed that previous modeling techniques presented a lack of automation in the generation of relay models, or show high complexity in linking the numerical relay models with the power system modeled in the emtp.

This thesis describes a new approach of modeling and designing of numerical relays. The proposed methodology employs a Visual C++-based program (PLSA) to obtain from the user the specifications of the relay to be designed, and to process this information to generate the FORTRAN code that represents the functional blocks of the relay. This generated code is incorporated in a PSCAD/EMTDC case using a resource called *component*, which facilitates the creation of user-custom models in PSCAD/EMTDC. Convenient electrical and logical signals are connected to the inputs and outputs of the PSCAD/EMTDC *component*. Further additions of digital relay models into the PSCAD/EMTDC case constitute the protection system model. The thesis describes a procedure for designing distance and differential relay models, but the methodology may be extended to design models of other relay elements.

A number of protection system studies were performed with the structure created with the proposed methodology. Adjustment of distance and differential relays were studied. Relay performance under CT saturation and the effects of the removal of anti-aliasing analog filter were investigated. Local and remote backup distance protection of

transmission lines was simulated. The adjustment of differential protection of power transformer to overcome the effects of inrush current was performed. Power transformer differential protection responses to internal and external faults were considered.

Additionally, a set of tests were performed to investigate the consistency of the relay models generated with the proposed methodology. The results showed that the numerical relay models respond satisfactorily according with the expected results of the tests.

# ACKNOWLEDGEMENTS

The author expresses his gratitude and appreciation for Dr. M. S. Sachdev and Dr. T. S. Sidhu for their supervision of this work. Their advice and assistance in the preparation of this thesis are thankfully acknowledged.

The author also wishes to thank the advisory committee members for their suggestions and advice. Assistance provided by the computing staff of the College of Engineering as also the laboratory and secretarial staff of the Department of Electrical Engineering is thankfully acknowledged.

The author is greatly indebted to his wife Leticia Sánchez Pérez and his children Pablo Farid and Selvi Xiomara Aquiles Sánchez, for their continued love, support and patience. The author also recognizes his parents, Gilberto Javier Aquiles López and Rebeca Pérez de Aquiles, for their constant encouragement and loving support in the making of this work the author gratefully acknowledges them. Special acknowledgements to Mrs. Alice Williams for her love and support are dearly recognized. To his brothers Juan Gilberto, Royer Bladimir and Malcom and his family members for their love and moral presence the author thankfully acknowledges them. Kind acknowledges are conveyed to Eli Pajuelo and Fernando Cux and their families for their unselfish friendship.

Financial support provided by the National Polytechnic Institute (IPN) through the Superior School of Mechanic and Electric Engineering (ESIME) in Mexico is immensely thanked and acknowledged. Also, financial support during the first three years of this project provided by the National Association of Universities and Institutions of Superior Education (ANUIES) through the SUPERA scholarship is acknowledged. It is greatly acknowledged the leave provided by Dr. M. S. Sachdev.

*Lovingly dedicated to*

*my beautiful wife Leticia,*

*and to my dear children Pablo Farid and Selvi Xiomara.*

*You are the light of my life.*

***To the memory of mi uncle***

***German Perez Cruz***

***(1960-2003)***

# TABLE OF CONTENTS

**4. PROTECTION SYSTEM MODEL DESIGNING METHODOLOGY**

**5. PROTECTION SYSTEM STUDIES**

# LIST OF FIGURES

**Page**

# LIST OF TABLES

**Page**

# LIST OF SYMBOLS AND ACRONYM

| | |
|---|---|
| IEEE | The Institute of Electrical and Electronics Engineers |
| EPRI | The Electric Power Research Institute |
| emtp | Electromagnetic transient program |
| EMTP | The Electromagnetic Transient Program |
| BPA | The Bonneville Power Administration |
| DCG | The Development Coordination Group |
| WAPA | The Western Area Power Administration |
| ATP | Alternative Transient Program |
| TACS | Transient Analysis of Control Systems |
| RTDS | Real Time Digital Simulator |
| MFC | Microsoft Foundation Classes |
| DC | Direct Current |
| MV | Medium Voltage |
| HV | High Voltage |
| EHV | Extra-High Voltage |
| kV | Kilovolts |
| kA | Kiloamperes |
| s | Seconds |
| ms | Milliseconds |
| Hz | Hertz |
| dB | Decibels |
| R | Resistance axis on impedance plane |
| X | Reactance axis on impedance plane |
| $e$ | Number that is the base of natural logarithms, equal to 2.71828183… |
| $\pi$ | Number expressing the ratio of the circumference of a circle to its diameter, equal to 3.14159265… |
| *INT* | Truncation operation |
| *RON* | Rounding operation |
| *arg(.)* | argument of phasor |
| *Re(.)* | Real part of a complex number |

| | |
|---|---|
| $Im(.)$ | Imaginary part of a complex number |
| $j$ | Imaginary numbers unit used in electricity |
| $a$ | Phasor operator equal to $1\angle 120°$ |
| $W_1(.)$ | Even Walsh function |
| $W_2(.)$ | Odd Walsh function |
| $V_a$ | Voltage of phase a |
| $V_a$ | Voltage of phase b |
| $V_a$ | Voltage of phase c |
| $I_a$ | Current of phase a |
| $I_a$ | Current of phase b |
| $I_a$ | Current of phase c |
| $V_1$ | Positive-sequence voltage at the relay location |
| $V_2$ | Negative-sequence voltage at the relay location |
| $V_0$ | Zero-sequence voltage at the relay location |
| $I_1$ | Positive-sequence current at the relay location |
| $I_2$ | Negative-sequence current at the relay location |
| $I_0$ | Zero-sequence current at the relay location |
| $S_1$, $S_2$ | Phase comparator signals |
| $S_O$ | Operating signal of amplitude comparator |
| $S_R$ | Restraining signal of amplitude comparator |
| $V_r$ | Voltage input signal in the distance relay comparator |
| $I_r$ | Current input signal in the distance relay comparator |
| $\varphi_r$ | Angle in which the voltage leads the current in the distance relay comparator |
| $Z_r\angle\varphi_r$ | Ratio of the line voltage and line current in the distance relay comparator. System impedance seen from relay location. |
| $Z_R\angle\theta$ | Constant parameter representing the impedance of the protected portion of the line in the distance relay comparator |
| $Z_{R1}\angle\theta_1$ | Constant parameter in the distance relay comparator |
| $Z_{R2}\angle\theta_2$ | Constant parameter in the distance relay comparator |
| $R_f$ | Arc-fault resistance |
| $V_{pol}$ | Polarization voltage in polarized mho distance relays |
| $V_{faulty}$ | Input voltage of polarized mho distance relays |

| | |
|---|---|
| $V_{healthy}$ | Healthy voltage of polarized mho distance relays |
| $V_p$ | Cross-polarized element of polarized mho distance relays |
| $k_p$ | Multiplication constant in polarized mho distance relay |
| $Z_{L1}$ | Positive-sequence impedance from the fault to the relay location |
| $Z_{L0}$ | Zero-sequence current impedance from the fault to the relay location |
| $V_{1F}$ | Positive-sequence voltage at the fault location |
| $V_{2F}$ | Negative-sequence voltage at the fault location |
| $V_{0F}$ | Zero-sequence voltage at the fault location |
| $I_{a(comp)}$ | Compensated current in a ground distance relay |
| $K_0$ | Compensating factor of ground distance relay current |
| $Z_{seen}$ | Apparent impedance seen or calculated by a distance relay |
| $I_{As}$ | The secondary current in the pilot wire of current transformer A |
| $I_{Bs}$ | The secondary current in the pilot wire of current transformer B |
| $I_p$ | Current entering a differential protected unit |
| $a_A$ | Transformation ratio of current transformer A |
| $a_B$ | Transformation ratio of current transformer B |
| $I_{Ae}$ | Excitation current of current transformer A converted to the secondary |
| $I_{Be}$ | Excitation current of current transformer B converted to the secondary |
| $I_{op}$ | Fundamental harmonic of the operating current in differential relays |
| $I_{rt}$ | Unfiltered restraining current in differential relays |
| $SLP$ | Slope of a differential relay characteristic |
| $I_{2h}$, $I_{3h}$, $I_{4h,}$ $I_{5h}$ | Second-, third-, fourth- and fifth-harmonic current, respectively |
| $k_2$, $k_3$, $k_{4,}$ $k_5$ | Multiplying factor of the second-, third-, fourth- and fifth-harmonic current in a harmonic restraint or blocking differential relay, respectively |
| $I_{D1}$, $I_{D2}$ | Currents on the pilot wires of the current transformers of a differential protection |
| $k$ | Compensation factor for the restraining current in a differential relay |
| $\omega_p$ | Pass band frequency of a IIR filter in radian/s |
| $\omega_s$ | Stop band frequency of a IIR filter in radian/s |
| $f_p$ | Pass band frequency of a IIR filter in Hz |
| $f_s$ | Stop band frequency of a IIR filter in Hz |
| $\delta_p$ | Tolerance of the magnitude response in the pass band |
| $\delta_s$ | Tolerance of the magnitude response in the stop band |

| | |
|---|---|
| $G_p$ | Pass band gain in dB |
| $G_s$ | Stop band gain in dB |
| $N$ | Order of an IIR filter |
| $\omega_0$ | Cutoff frequency |
| T | Sampling interval |
| $s$ | Laplace transform variable |
| $z$ | Z-transform variable |
| $CT$ | Current Transformer |
| $VT$ | Voltage Transformer |
| $I_s$ | Secondary current of a current transformer |
| $E_s$ | Secondary excitation current of a current transformer |
| $Z_B$ | Impedance burden connected to the secondary of a current transformer |
| $I_p$ | Current in the primary circuit of a current transformer |
| CTR | Current transformer rate |
| ADC, A/D | Analog-to-Digital Converter |
| $Z_{10}$ | Integer value of base 10 |
| $b$ | Word size of a microprocessor |
| FP | Equivalent floating-point output on an analog-to-digital converter |
| DSP | Digital Signal Processor |
| DFT | Discrete Fourier Transform |
| LSE | Least Square Error |
| $\theta$ | Displacement angle of the signal from a reference on a phasor estimation algorithm |
| $V_p$ | Peak value of the signal on a phasor estimation algorithm |
| $[A]^{-L}$ | Left pseudo-inverse matrix of $[A]$ |
| MOV | Metal Oxide Varistor |
| PLSA | Program to generate digital relay models developed in the present thesis |
| *CPLSADoc* | Document object in PLSA |
| *CRelay* | Relay object in PLSA |
| *CPLSAView* | View object in PLSA |
| *UCCS.f* | Subroutine of distance relay comparators generated by PLSA |
| *PhDsP* | Phase Distance Relay P, designed for protection system studies |
| *PhDsQ* | Phase Distance Relay Q, designed for protection system studies |
| *GrDsP* | Ground Distance Relay P, designed for protection system studies |

| | |
|---|---|
| *SPhDiffR1* | Single-Phase Differential Relay 1, designed for protection system studies |
| *PhDistRel1* | Distance relay model auxiliary in the explanation of the proposed protection system modeling and designing methodology |
| *T1, T5, T11* | Transmission lines 1, 5 and 11, respectively, from the test power system |
| *Tr7* | Power transformer 7 from the test power system |
| *Brk6, Brk9* | Power breakers 6 and 9, respectively, from the test power system |
| *Difa* | Angle difference of the composite signals $S_1$ and $S_2$ on a phase comparator of a distance relay |
| *Difm* | Amplitude difference of the composite signals $S_O$ and $S_R$ on an amplitude comparator of a distance relay |
| *STORx* | PSCAD/EMTDC storing arrays for user variables |
| *NSTORx* | PSCAD/EMTDC accessing indexes of the *STORx* arrays |
| *Dsout* | Section of the relay model in PSCAD/EMTDC used to store the relay model code |

# 1. INTRODUCTION

## 1.1 Importance of protection systems

Modern civilization makes use of large amounts of energy to generate goods and services. From the industrial plants, the providers of public services to the ordinary man, all of them need energy to satisfy and create the well being of modern society. The purpose of electric power systems is to provide energy for human use in a secure, reliable and economic manner. Electric power systems are made up of facilities and equipment that generate, transmit and distribute electrical energy. Electric power systems are one of the largest and more complex systems man has ever built.

The importance of the services that power systems offer and the high amount of investments that represent the facilities and equipments, make the normal and constant operation of power systems critical and strategic for every society. Faults and failures normally occur in power systems. Due to the great amounts of energy involved, faults represent a threat to the operation and security of power systems if the faults are not promptly corrected. Power systems need an auxiliary system that must take corrective actions on the occurrence of a fault. This auxiliary system is known as protection system.

Protection systems are sets of equipments, schemes and policies dedicated to detect faults in the protected elements of the power systems, to disconnect the faulted element and to reestablish the service, if it was the case. Because power systems operate in different operating states, different fault scenarios may occur. Protection systems must

provide different schemes and equipments to detect and to react to each and every one of these fault scenarios, from the most simple of them to the most complex and compelling.

## 1.2 Introduction to protective relays

One of the most important equipments employed in the protection of power systems are protective relays. These are one of the most flexible, economic and well-known devices that provide reliable, fast and inexpensive protection.

Relay is defined by the IEEE as "an electric device that is designed to interpret input conditions in a prescribed manner, and; after specified conditions are met, to respond to cause contact operation or similar abrupt changes in associated electric control circuits [32]". Relays acquire signals from the power system (electrical, magnetic, heat, pressure, etc.) and process them with a designed process or algorithm. IEEE defines a protective relay as "a relay whose function is to detect defective lines or apparatus or other power conditions of an abnormal or dangerous nature and to initiate appropriate control circuit action [32]".

Protective relays have provided protection since the beginning of the electric industry, and have encountered great transformations with time as power systems have grown in size and complexity. Early protective relays were constructed using solenoids and electromagnetic actuators. Those relays were bulky and heavy devices that needed lot of space to be mounted. Because of their development and use over several decades, electromechanical relays evolved to become standard accepted devices. Even modern relays use most of the principles of operation of electromechanical relays.

Solid-state relays replaced electromechanical actuators by analog electronic elements. Even when the protection systems based on electromechanical relays had proved to be reliable, solid-state relays gained confidence of protection engineers because of their

advantages of lower costs, reduced space and weight, and ease to set, maintain and operate.

The developments in digital technology led to the incorporation of microprocessors in the construction of relays. Digital and numerical relays are sophisticated, multiple-purpose equipment with the capacity to record signals during faults, monitor themselves and communicate with their peers. Numerical relays employ microprocessors especially constructed to process digital signals, which make them faster and more powerful, while preserving their economic advantages.

## 1.3 Investigation topics on protective relaying

The developments in relaying technology have not solved definitively all the protection issues, and, therefore, substantial investigations and research on protection and protective relaying continues [25]. The following are the most relevant topics currently being investigated in the field of protective relaying.

- Setting and adjustment of relays and interrelation of protective relays with different component of the power system, especially control elements
- Behavior of relays during different operating states of power systems (steady-state, faulted system, etc.)
- Designing of new relay algorithms, relay functions and protection schemes
- Engineering of new relay products
- Education and training of protection personal

Most of the times, it is impossible to investigate the mentioned topics on real systems due to operation, security and economical restrictions. Several approaches and resources have been developed to overcome these difficulties. These include Real Time Digital Simulators (RTDS), Real Time Playback Simulators (RTPS) and software packages for modeling protective relays.

Computer models of protective relays offer an economical and feasible alternative to investigate the performance of relays and protection systems. Computer models of relays permit investigators to observe in a very detailed way the performance of processes in each internal module of the relay.

Designing new relaying algorithms or new relaying equipment is also improved with relay modeling because relay designs are refined before prototypes are built and tested. For specific problems and conflicting scenarios, use of models open the possibility of creating new solutions when known approaches do not work satisfactorily.

## 1.4 Literature review on modeling of protection systems

Relay models have been used for a long time by manufacturers, consultants and academics for designing new prototypes and algorithms, to check and optimize the performance of relays already installed in power systems and to train new protection personnel.

Relay manufacturers were the first to develop relay models for evaluating the performance of their designs. Those models implemented the processes by substituting the values of inputs in equations representing the relays to check if the outcomes were acceptable. The characteristics of overcurrent relays were the first to be modeled. Mathematical models [45], [46] were developed in the form of algebraic equations for representing time-current characteristics of overcurrent relays. The first transient model of a distance relay was presented in [47], where the ninth-order state space mathematical model of a mho element was developed.

Electromagnetic transient programs are computer software developments that simulate transients of multiphase networks, and their use has been popular and generally

approved. When working with computer models of relay, electromagnetic transient programs are powerful tools for protection investigations and studies.

The Electromagnetic Transient Program (EMTP) was the first software that simulates the transient nature of power systems [43]. EMTP, which is based on the algorithm proposed by Hermann W. Dommel [42], was presented to the public domain by the Bonneville Power Administration (BPA) in the late 1960's.

To rationalize the development of the program, the EMTP Development Coordination Group (DCG) was founded in 1982. Original members of the DCG included BPA, the US Bureau of Reclamation, Western Area Power Administration (WAPA), the Canadian Electrical Association, Ontario Hydro and Hydro-Quebec. The DCG and the Electric Power Research Institute (EPRI) started the initiative of commercial sale of the EMTP in 1984. The first version of the DCG EMTP was released in 1987.

The Alternative Transient Program (ATP) is the free version of EMTP, and today it is widely used for power system simulation [26, 43]. Complex networks and control systems can be simulated with ATP. ATP has extensive modeling capabilities and additional features such as the Transient Analysis of Control Systems (TACS) and MODELS, which enable modeling of control systems and components with non-linear characteristics, respectively. However, while having strong features for programming in simulation tasks, MODELS has limited memory allocation size for data arrays [49].

PSCAD/EMTDC is an electromagnetic transient analysis program developed by the Manitoba HVDC Research Center. The program encompasses a wide variety of steady state and transient power system studies [44]. The primary solution engine is EMTDC, which represents and solves differential equations for the entire power system in time domain employing the electromagnetic transient algorithm proposed by Dommel [42]. The graphical user interface is named PSCAD, and it provides powerful means of visualizing the transient performance of the systems. Together, PSCAD and EMTDC

provide a fast, accurate and flexible solution for the simulation of electrical equipments or systems.

MATLAB integrates mathematical computing, visualization, and a powerful language to provide a flexible environment for technical computing [54]. MATLAB possesses a flexible software structure comprising libraries, models and programs that enable integration of different model components in a single package. SIMULINK is a package in MATLAB for obtaining time domain solutions. This package shows an open system where new libraries and models can be added with relative ease [55]. The Power System Block Set enables transient modeling of basic components of power systems [56]. The combination of MATLAB, SIMULINK and the Power System Block Set permits users to model and simulate real-time power and related protection systems with high accuracy.

Some techniques that have been developed towards computational interfacing between electromagnetic transient programs and external programs are outlined in the paragraphs that follow.

J. Mahseredjian, G. Benmouyal, X. Lombard, M. Zouiti, B. Bressac, L. Gérin-Lajolie presented in 1998 a programmed link between MATLAB and EMTP [28]. The link permits the users to call FORTRAN routines contained in the MATLAB library and Toolboxes of the MATLAB from the general network simulator of EMTP. This enables external run-time access to the computational engine of MATLAB [51].

A. M. Gole and A. Daneshpooy developed in 1997 an open-system interface between MATLAB and PSCAD/EMTDC [57]. The authors employed a PSCAD/EMTDC application called DSDYN to call a FORTRAN subroutine. The FORTRAN subroutine starts the MATLAB engine and sets up the data communication pipe between the PSCAD/EMTDC and the MATLAB engine. Data from the transient simulation in PSCAD/EMTDC is passed through this data communication pipe to the MATLAB and

processed. However, the literature survey has not found a development in relay modeling that had used this technique.

The works presented in the past on modeling of digital and numerical relays have used two different approaches: The first approach has modeled the power system and the relay in the same electromagnetic transient program ([27], [48], [49], [53], [59]), while the second approach has modeled the power system in the electromagnetic transient program and the relay in an external program [29]. In the second approach, the interface between the electromagnetic transient program and relay models is crucial. The following is a description of the works developed in the past on modeling of digital and numerical relays. The works were found by a literature survey conducted for this thesis and are presented in the ascendant chronological order.

One of the earliest works on modeling relay algorithms was presented in 1990 by M. S. Sachdev, M. Nagpal, and T. Adu [22]. The authors introduced an interactive software programmed in APL for evaluating algorithms of digital relays. The software included signal processing and protection modules used in typical digital relays. The data for testing the performance of digital relay designs could be generated either by facilities included in the software, recorded from a power system location or generated by other softwares.

In 1993, Wilson and Nordstrom modeled one measuring unit of a distance digital relay using MODELS of EMTP [48]. The input filter, analog-to-digital converter, fundamental frequency phasor calculator and relay measuring principle were modeled separately in MODELS. The simulations were compared with laboratory test results obtained by applying digitally generated waveforms to the actual relay.

In 1994, A. K. S. Chaudhary, Kwa-Sur Tam and A. G. Phadke developed specific models of relays for line protection and transformer differential protection and models of current and capacitor voltage transformers for the EPRI/DCG EMTP version 2.0 [27]. The authors made several changes to the main subroutine of EMTP to link it with user-

defined FORTRAN subroutines that simulate relay algorithms. The elements modeled permitted the user to simulate dynamic interactions between the power system and the protection system.

In 1995, P. G. McLaren, G. W. Swift, Z. Zhang, E. Dirks, R. P. Jayasinghe, and I. Fernando modeled a new positive-sequence directional element of a numerical distance relay simulated in PSCAD/EMTDC [59]. The subroutines representing the relay were linked to the electromagnetic transient engine of EMTDC, and the model was incorporated to the relay library of the graphical routine PSCAD. The relay models were tested using a Real Time Digital Simulator (RTDS).

In 1997, T.S. Sidhu, M. Hfuda, and M. S. Sachdev presented a unified approach in MATLAB to produce computer models of distance, differential and overcurrent relays [23]. The approach is composed of two MATLAB programs. The first program is an interactive environment for collecting the design specifications. The second program produces the program code and logic of the relay model. The input data entered to the relay model is generated by direct mathematic function sampled at specific rates.

M. Kezunovic and Q. Chen presented in 1997 a work where the power system transients are simulated using ATP and the protective relay is modeled in MATLAB [29]. The interaction between both systems was implemented in a closed-loop employing an "interaction buffer" for communication. The approach also permitted the simulation of the relay model in other high level languages while maintaining the link. Minor modifications to the ATP program were included to establish the interaction between the power system modeled in ATP and the external relay model.

In 1997, R. W. Wall and B. K. Johnson developed an educational tool for investigating relay concepts by modeling digital relays using TACS functions within EMTP in a closed-loop [58]. The TACS functions were used to model dynamics associated with analog-to-digital conversion and sampling systems.

M. Kezunovic and B. Kasztenny presented in 1999 new SIMULINK libraries for modeling digital protective relays for teaching protective relay concepts [53]. The MATLAB software package with SIMULINK was utilized for developing customized relay model libraries. Power systems were modeled in the Power Block Set Toolbox and were set to interact with the digital relay libraries in the open-system environment of SIMULINK.

In 2000, Chul-Hwan Kim, Myung-Hee Lee, R. K. Aggarwal and A. T. Johns presented the implementation of a distance relay algorithm using EMTP MODELS for educational purposes [49]. All the procedures for the simulation of a digital relay system were integrated in an EMTP file. The modeling of the power system and the protective system were integrated in one program module. The authors implemented an anti-aliasing low-pass filter and the DC-offset removal filter in order to extract the fundamental frequency current and voltage phasors, which were used for calculating the apparent impedance.

## 1.5 Objectives of the research

Digital and numerical relays offer flexible, economic and feasible protection to electric power systems. These relays are widely used in today's power systems. Designing and modeling of numerical relays are crucial tasks in developing new devices and algorithms. Modeling of digital and numerical relays is employed by utility engineers and educators to assess the performance of relays installed in power systems and to train new protection personnel. Digital and numerical relay models are employed by manufacturers and researchers to develop new relay prototypes and protection algorithms.

The literature survey reported in the previous section outlines the principal research works that have been done in the area of relay modeling. An important part of these activities was focused on the modeling of numerical relays. The survey has shown that

the modeling of relays is a powerful tool when working along with an electromagnetic transient programs either in an open- or closed-loop structure. At the same time, the literature survey has revealed the following issues related to the modeling techniques.

- Most of the techniques show a lack of automation and generalization in their processes. This means that the modeling techniques are not computer-aided for successive relay model designing. A whole new modeling process has to be planned and carried out thoroughly every time a new relay model has to be produced.
- The techniques that offer generality in the modeling process [53] employ software that is not the standard in the industry to perform power transient studies.
- The techniques modeling the power system and the digital relay in the same emtp present the difficulty of setting a link between the electromagnetic transient engine and the relay model. To set up the link, it is necessary to have an in depth knowledge of the structure of the emtp to make proper modifications. The amount of work that this task takes can be as big as the modeling process itself.

The objective of the proposed research was to develop a methodology for designing protection systems. This methodology should facilitate the process of designing numerical relay models. The methodology should embed the models within a power system modeled in an electromagnetic transient program in a closed-loop structure to recreate the protection system working along with the modeled power system. With this arrangement, the methodology should help in investigating the interaction between the protection system and the power system under specific scenarios.

A computer program should be developed to design custom relay models. This program should be provided with relevant data related to the relay of interest. With this information, the program must generate computational products that mimic the relay performance. These computational products might not have direct one to one correspondence to the actual microprocessor machine language coding within the

numerical relay, but they are expected to show the same response under transient and steady state conditions than its real counterpart has.

The designed relay models should be such that they can be included as natural elements of the emtp employed. The designed numerical relay models and the power system model in the emtp must constitute a single computational unit. The embedding of the designed relay models must be a simple and straight forward process. The successive addition of generated numerical relay models into the electromagnetic transient program case should build the model of the protection system. The interaction of the numerical relay models with the electromagnetic transient program must implement the topology of the power system model during the simulation of the case (closed loop structure). The structure constituted by the designed relay models and the model of the power system in the emtp should be flexible enough to permit the user to perform a wide range of protection system studies of diverse complexity. This structure also should allow analyzing the performance of the designed relay models in different levels ranging from the internal response of different modules that constitute the numerical relays to the interaction between different numerical relays that constitute a protection system.

## 1.6 Outline of the thesis

The thesis is organized in seven chapters and four appendices. The subject and organization of the thesis are described in the first chapter. The importance of protection of power system is discussed in this chapter. A brief introduction on protective relaying and designing of digital and numerical relay models is also included. Important conclusions and objectives of the research are drawn from the literature review on modeling techniques of digital relays proposed in the past.

In Chapter 2, an overview of power system protection and protection philosophy are presented. Special attention is given to the description and operating principles of distance and differential relays. The setting and adjustment of protection zones,

comparators and operating characteristics of distance relays are discussed. The calculation of apparent impedance and zero sequence compensation for ground distance relays are also included. The principle of operation of differential relays is examined. Percentage restrain differential relays are introduced. Finally, the protection of power transformers with differential relays is addressed.

The major internal modules of the generalized numerical relay are presented in Chapter 3. These modules are the analog signal scaling module, analog anti-aliasing filtering module, analog-to-digital conversion module, phasor estimation algorithm module and relay logic module. The most common techniques and methods employed in each module of the generalized numerical relay are enumerated and reviewed.

The proposed methodology for designing models of protection systems is presented in Chapters 4. The computer program developed in this project to design and model numerical relays (PLSA) is introduced. The computational structure of PLSA, the role of PLSA in the methodology for designing the protection system models is discussed. The use of PLSA to design relay models is described. The procedure to embed the generated relay model in a PSCAD/EMTDC case is outlined. The computational resource of PSCAD/EMTDC (*component*) that is used as a base to construct the numerical relay model in the PSCAD/EMTDC case is briefly examined. The procedure to create a new PSCAD/EMTDC *component* is presented. The process to customize the *component* as a numerical relay model is also described. The final setting of the numerical relay model in a PSCAD/EMTDC case is also included.

In Chapter 5, protection system studies performed with the proposed methodology are presented. The studies are divided in two types, studies of distance relays protecting a transmission line and studies of differential relays protecting a power transformer. The studies performed with distance and differential relay models are enumerated. The adjustment and parameter setting of the distance and differential relays are reported. The performance of the distance and differential relay models in the event of faults of different nature are included. The responses of the distance and differential relay

models to CT saturation are reviewed, as well as the response of the relay models when anti-aliasing filter are not used. The response and the issues of differential relay models in the presence of inrush current are also reported.

The consistency tests performed on the relay models are presented in Chapter 6. The distance relay characteristic curve consistency tests are introduced. Results obtained with the distance relay characteristic curve consistency tests are reported and the conclusions are drawn. Decimation applied to the consistency of numerical relay models is described. The outcomes obtained with decimation applied to the consistency of numerical relay models are shown and conclusions are developed.

A brief summary of the research conducted for this project and important conclusions drawn thereof are outlined in Chapter 7. This chapter is followed by a list of references. In appendix A, some technical aspects important for the programming of PLSA in Visual C++ are introduced. The grammatical rules that must prevail in the FORTRAN code of the relay models, which are to be embedded in the PSCAD/EMTDC cases, are reported in appendix B. The parameters to construct the variable names to gain access to the internal signals of the relay models generated with PLSA are presented in appendix C. The connectivity and electrical parameters of the test power system employed in Chapter 6 to perform the protection system studies are presented in appendix D.

Specifically, the project has made the following contribution:

- A new methodology for designing models of protection systems and including digital and numerical relay models in a PSCAD/EMTDC case have been developed. This methodology establishes a closed loop structure between the protection systems and power systems. In depth analysis of the internal variables of the numerical relay models and observations of the interactions of the numerical relay models between themselves or with other elements of the power system are feasible with this structure. The structure flexibility permits the

simulation of practically any power and protection system study. Additionally, the proposed methodology can be employed in designing new numerical relay prototypes, new protection algorithms and methods.

- A user-friendly Visual C++-based program (PLSA), which helps in designing numerical relay models, for use with PSCAD/EMTDC has been developed. PLSA acquires from the user data and parameters of a numerical relay to generate computational equivalents of the relay.
- A technique for embedding numerical relay models designed with PLSA in cases of the electromagnetic transient program PSCAD/EMTDC has been introduced. The technique employs a user-custom structure to insert numerical relay models inside a PSCAD/EMTDC case.

## 1.7 Summary

The importance of protection systems has been discussed briefly in this chapter. Protective relaying concepts and modeling of relays has been introduced as well. A review of the literature on modeling of relays and the interaction with models of power system has been reported. The principal computer programs to conduct electromagnetic transient studies of power systems have been enumerated and examined. The principal works in the research field of modeling of protection systems and their interactions with power systems modeled in electromagnetic transient programs have been reviewed. The objectives of the thesis have been outlined. The organization of the thesis is described and the contributions that the research has made have been outlined.

# 2. POWER SYSTEM PROTECTION

## 2.1 Introduction

Basic concepts of protection systems, relaying and computer modeling of relays have been briefly introduced in Chapter 1. A literature review of modeling of relays and interaction of relay models with models of power systems in electromagnetic transient programs has been presented in that chapter. The objectives and organization of the thesis and specific contributions of this research project have been outlined in Chapter 1.

This chapter presents an overview of distance and differential protection systems, because methodologies for designing and modeling these systems are developed later in this thesis. The important aspects of distance protection are discussed. These aspects include the principles of operation of amplitude and phase comparators, and the operating characteristics and criteria to set distance protection zones. The calculation of the apparent impedance and zero-sequence compensation in ground distance relays is reviewed. The principles of operation of differential protection, including the use of percentage differential relays, are discussed. Finally, protection of power transformers with differential relays and issues relevant to this application are addressed.

## 2.2 Power system protection philosophy

The main purpose of power systems is to generate, transmit, and distribute electric energy to customers without interruptions and in the most economical and safe manner.

To achieve these objectives, power systems are divided in generation, transformation, transmission and distribution subsystems.

Generation consists of converting energy from different forms, such as thermal, hydraulic or nuclear, to electrical energy. Transformation consists of changing the voltage levels to those that are convenient for transmitting or distributing electrical energy. The role of transmission is to transport energy from generally geographically far away locations, where electric energy is generated, to load centers where it is consumed. The distribution consists of supplying energy to customers at a convenient voltage level.

All subsystems described above are composed of costly components and machines. Protection of these elements is crucial. However, the principal elements to protect in a power system are generators, power transformers, transmission lines and distribution circuits.

The philosophy of protection ensures that, in the event of a fault, the faulted element must be disconnected from the system for isolating the fault to prevent further damage to the components of the system through which the fault currents were flowing. To achieve this objective, it is a common practice to interconnect major elements, such as generators, power transformers, transmission lines, etc, by using circuit breakers. However, it is a usual practice to control one element with a set of circuit breakers.

In Figure 2.1 are shown the protection zones of a simple power system. Each zone protects a single element of the power system. The protection zones overlap around circuit breakers. The purpose is to make certain that no section of the system is left unprotected. The consequence of this practice is that a fault in an overlapping zone opens circuit breakers to isolate more than one element from the system. [21].

Back-up protection is provided to ensure that the faulted element of the system is disconnected even if the primary protection fails to isolate the faulted element. Back-up

protection can be provided locally or from a remote location. Local back-up protection is provided by equipment that is in addition to the equipment provided for primary protection whereas remote back-up protection is provided by equipment that is physically located at substations away from the location where equipment for primary protection is located.

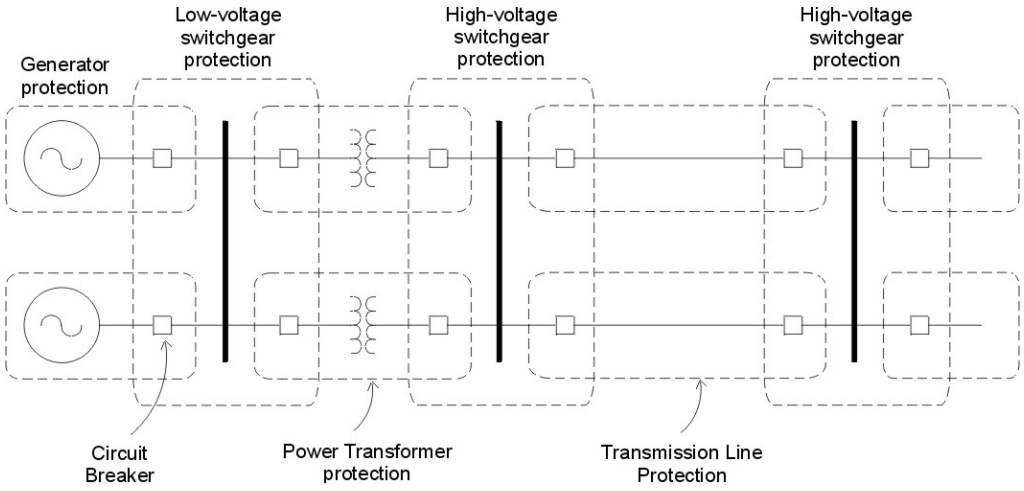


**Figure 2.1:** Primary relay protection zones [21]

This research project is dedicated mainly to study and model two of the most widely used relays, namely, distance relays and differential relays. Distance relays are studied and modeled for protection of transmission lines and differential relays are studied and modeled for protection of power transformers.

## 2.3 Distance protection

Transmission lines electrically connect different elements in a power system. Electrical power that is generated at relatively low voltage levels is raised to a higher voltage level to be transported on transmission lines for supplying energy to loads.

Transmission lines generally use voltages of 115 kV and higher. The level of voltage of transmission lines requires that line conductors be supported on adequate insulation and

remain sufficiently clear of the ground to assure proper operation of the system and safety of personnel. These requirements result in high cost in the construction of transmission lines and their maintenance. To safeguard the investment in a transmission line, several types of protection techniques are used. Directional, over-current, distance and pilot are some of these techniques.

A single technique or combinations of two or more techniques are employed to detect line to ground and line-to-line faults on transmission lines.

Distance protection has been widely used for protecting transmission and subtransmission circuits because of its suitability, simplicity, economy and reliability. In addition, selectivity and remote back-up protection are natural advantages of this type of protection.

Distance relays use voltages and currents acquired at the relay location to calculate the apparent impedance of the protected line. The calculated apparent impedance is compared with predetermined impedance that is called reach of the relay. During normal operation, the apparent impedance must be larger that the impedance-reach of the relay. If the apparent impedance is less than the impedance-reach, then it is concluded that a fault has occurred in the protected line between the relay location and the impedance reach of the relay. Under these conditions, the distance relay energizes the circuits to trip appropriate circuit breakers to isolate the faulted line from the rest of the system.

### 2.3.1 Distance relay zones

Selectivity in distance relays is provided by using different impedance reaches in conjunction with different time delays associated with those settings [3]. The combination of an impedance reach and its associated time delay is known as a protection zone. It is common to provide distance relays with three protection zones but,

depending on the application, extra zones can be included in the relay. The incidence of a fault within a protection zone of a distance relay must initiate and complete the operation of the relay.

The impedance reach of zone-1 is usually set between 80% and 85% of the transmission line impedance, leaving the remaining 20% to 15% of the line impedance as a safety margin. This is done because errors are introduced by inaccuracies of current and voltage transformers and processes used in the relay for calculating impedances. These errors could make the relay over-reach causing the relay to operate for faults in other than its own protection zone. No intentional delay is provided to zone-1 protection.

To allow selectivity, time setting of zone-2 must be graded with the operating time of zone-1 relays. Zone-2 setting must cover the 15% of the transmission line not protected by zone-1 and a substantial part of the lines emanating from the remote bus. A usual practice is to set the impedance-reach to include a maximum of 50% impedance of the shortest line emanating from the remote bus.

The main function of zone-3 is to offer remote back-up protection for faults occurring in lines emanating from the remote bus. For a radial system, it is a common practice to set the reach of zone-3 to cover 100% of the shortest line emanating from the remote bus. Some times, zone-3 is set to reach to 120% the impedance of the shortest line out of the remote bus. When multiple lines emanate from the remote bus and a fault occurs on one of those lines, the currents contributed via the healthy buses connected to the remote bus affect the calculation of the apparent impedance by the local distance relay. The current contribution by the healthy lines is known as in-feed and must be taken into account in determining the setting of zone-3 relays.

In Figure 2.2 are shown typical distance zones that provide local and back-up protection to a transmission system. In this figure, protection zones are specified according to the numerical identification of the associated breakers [2].

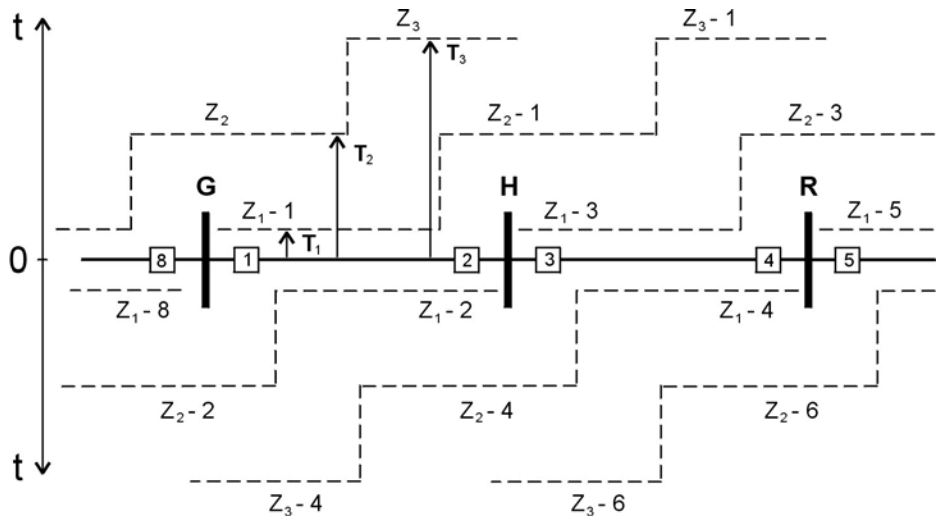


**Figure 2.2:** Distance relay protection zones **[2]**

In some situations, it is convenient to provide distance relays with a fourth protection zone. Zone-4 is employed to provide back-up protection to the local bus bar, normally by establishing a reverse reach setting of 25% of the impedance of zone-1 [3]. Zone-4 is also used as a fault detector in some logics to control the operation of the zone timers [40]. In Table 2.1 are summarized some of the typical criteria used for selecting the time delay settings of numerical distance relays [40].

## 2.3.2 Impedance diagram

The calculated apparent impedance of the system, the locus of the impedance of the protected line and the impedance-reach of distance relays can be represented in a complex plane that has the resistance and the reactance as coordinate axes. This complex plane is known as impedance plane.

In the impedance plane the protected line is represented by a straight line, drawn from the origin to the point corresponding to the impedance of the line in steady state; the impedance-reach or operating characteristic of a distance relay is represented by a fixed

shape. The impedance of the line must lie inside the area of the operating characteristic of the distance relay protecting the line.

The apparent impedance seen by the distance relay during normal operation is the load impedance of the system, which is normally inductive and relatively larger in magnitude than the line impedance.

<table>
<tr><td rowspan="3">Zone-1</td><td colspan="2">This zone operates without intentional delay. The operating times are</td></tr>
<tr><td>Medium Voltage (MV) and High Voltage (HV)</td><td>20-30 ms</td></tr>
<tr><td>Extra-High Voltage (EHV)</td><td>15-25 ms</td></tr>
<tr><td rowspan="5">Zone-2</td><td colspan="2">Must allow Zone-1 of neighboring feeder to clear the fault. The zone-2 operating time is the sum of the following times:</td></tr>
<tr><td>Zone-1 operating time of protected line</td><td>(Referred above)</td></tr>
<tr><td>+ circuit-breaker operating time of the protected line</td><td>From 2 cycles in EHV up to 4 cycles in MV</td></tr>
<tr><td>+ fault detector re-setting time</td><td>Approx. 20 ms</td></tr>
<tr><td>+ errors of the internal timers<br>+ safety margin</td><td>1% of set time, minimum 10 ms<br>50 ms</td></tr>
<tr><td>Zone-3</td><td colspan="2">Same procedure as for Zone-2, wherein the operating time of Zone-1 of the protected line is replaced by the operating time of Zone-2 of the protected line.</td></tr>
</table>

**Table 2.1:** Typical criteria used for time zone setting of numerical distance relays

When a fault occurs on the line, the value of the apparent impedance tends to be equal to the impedance between the relay location and the fault location. Therefore, the apparent impedance moves from the load impedance to the point of the short-circuit impedance when a fault occurs. This point is inside the operating characteristic of the distance relay and, therefore, the relay initiates the opening of circuit breakers that control the line.

In Figure 2.3 is shown a plot, in the impedance plane, of the operating characteristics of the three zones of distance relays located at bus G (shown as solid lines) and at bus H (shown as dotted lines) of the power system shown in Figure 2.2 [3].

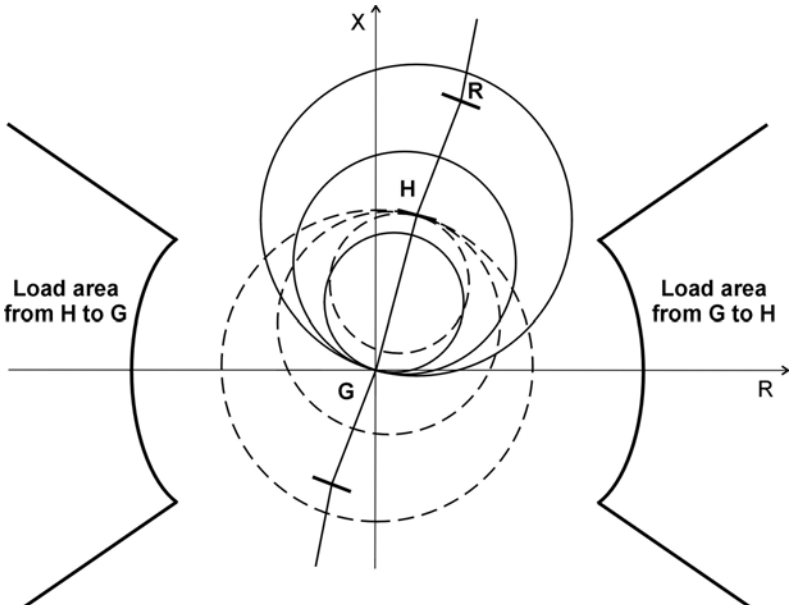


**Figure 2.3:** Distance relay protection zones in the impedance plane for relays provided at buses G and H (of Figure 2.2) for protecting the line from Bus G to Bus H [2]

### 2.3.3 Input signals of distance relays

In Table 2.2 are shown the input signals employed by ground and phase distance relays. In this table, $K_0$ is a compensating factor. The determination and use of $K_0$ is explained in section 2.3.6.

### 2.3.4 Comparators for distance protection

Comparators are measuring units that combine voltages and currents acquired by the relay to form two composite signals. The difference in phase or magnitude of these

composite signals is used to discriminate between a normal operating condition and a fault on the protected line. A phase comparator checks the difference between the phase angles of the two composite signals and operates if the difference is within a specified range. A magnitude comparator compares the amplitude of the two composite signals and operates if the amplitude of one signal is greater than the amplitude of the other signal.

| Distance Element | Voltage signal | Current signals |
|---|---|---|
| Phase A | $V_a$ | $I_a+K_0 3I_0$ |
| Phase B | $V_b$ | $I_b+K_0 3I_0$ |
| Phase C | $V_c$ | $I_c+K_0 3I_0$ |
| Phase A – Phase B | $V_a - V_b$ | $I_a - I_b$ |
| Phase B – Phase C | $V_b - V_c$ | $I_b - I_c$ |
| Phase C – Phase A | $V_c - V_a$ | $I_c - I_a$ |

**Table 2.2:** Input signals of ground and phase distance relays

The composite signals in a phase comparator are denoted by $S_1$ and $S_2$. An angular displacement is considered positive if $S_1$ leads $S_2$. A phase comparator operates if the following condition is satisfied [39].

$$-90° \le \arg(S_1) - \arg(S_2) \le 90° \tag{2.1}$$

The composite signals in an amplitude comparator are denoted by $S_O$ and $S_R$, operating and restraining signals, respectively. The comparator operates if the following condition is satisfied.

$$|S_O| \ge |S_R| \tag{2.2}$$

## 2.3.5 Distance protection characteristics

The parameters of the composite signals in a comparator determine the shape, size and position of the operating characteristic in the impedance plane. The operating characteristics of distance relays are usually geometric figures, such as circles, straight lines or their combinations. However, in numerical relays it is possible to design operating characteristics of almost any shape. The most common operating characteristics employed by distance relays are impedance, offset impedance, mho, mho polarized, reactance, and quadrilateral characteristics.

The methods used for obtaining different operating characteristics by the phase and magnitude comparators are presented in the following sections [39]. Special attention is given to the mho-polarized characteristic because this has been the most commonly used characteristic for a long time.

### 2.3.5.1 Impedance characteristic

#### 2.3.5.1.1 Impedance characteristic phase comparator

The phase comparator signals $S_1$ and $S_2$ for obtaining impedance characteristics are defined by the following expressions.

$$S_1 = -V_r \angle 0° + Z_R \angle \theta \cdot I_r \angle -\varphi_r \tag{2.3}$$

$$S_2 = V_r \angle 0° + Z_R \angle \theta \cdot I_r \angle -\varphi_r , \tag{2.4}$$

where,

$S_1$, $S_2$ are the phase comparator signals

$V_r$ is the voltage applied to the relay

$I_r$ is the current applied to the relay

$\varphi_r$ is the angle by which the voltage leads the current

$Z_R\angle\theta$ is the impedance reach of the relay used for protecting the line.

By dividing these equations by the line current, $I_r\angle$-$\varphi_r$, the following expressions can be obtained.

$$S_1' = -Z_r\angle\varphi_r + Z_R\angle\theta \tag{2.5}$$

$$S_2' = Z_r\angle\varphi_r + Z_R\angle\theta\,, \tag{2.6}$$

where,

$Z_r\angle\varphi_r$ is the ratio of the line voltage and current; impedance seen by the relay.

The vectors impedances $S'_1$ and $S'_2$ are representations of the voltage phasors $S_1$ and $S_2$. $S'_1$ and $S'_2$ are determined by the constant parameter $Z_R\angle\theta$ and the system impedance $Z_r\angle\varphi_r$. The locations of $S'_1$ and $S'_2$ in the impedance plane are shown in Figure 2.4. Since the parameter $Z_R\angle\theta$ is constant, the system impedance $Z_r\angle\varphi_r$ determines the value of the angle difference between $S'_1$ and $S'_2$.

In Figure 2.4(a) is shown the case of the system impedance $Z_r\angle\varphi_r$ laying inside the operating characteristic of the relay. In this case, the angle difference between $S'_1$ and $S'_2$ is less than 90 degrees, fulfilling the condition (2.1). In Figure 2.4(b) is shown the case when of the system impedance $Z_r\angle\varphi_r$ laying outside the operating characteristic. In this case, the angle difference between $S'_1$ and $S'_2$ is more than 90 degrees, and the operating condition expressed in Equation 2.1 is not satisfied.

The cases of the first quadrant presented in Figure 2.4(a) and 2.4(b) can be extended for the rest of the quadrants in the impedance plane. In this manner, the impedances $S'_1$ and

$S'_2$ describe a circular operating characteristic with center at the origin and radius equal to $|Z_R|$.

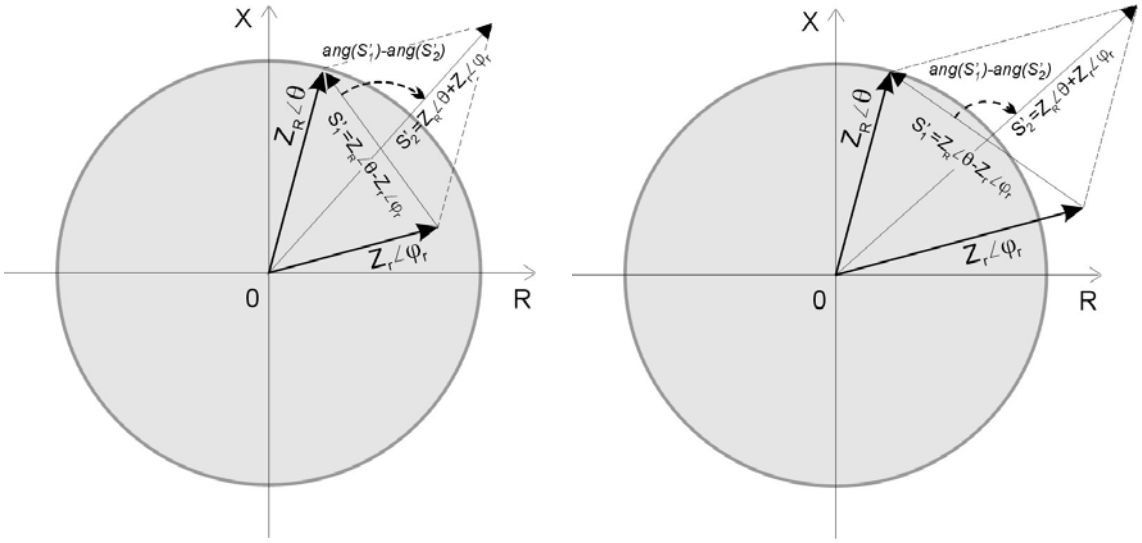


a) Operating condition b) Non-operating condition

**Figure 2.4:** Definition of the impedance characteristic phase comparator

#### 2.3.5.1.2 Impedance characteristic amplitude comparator

The amplitude comparator signals, $S_O$ and $S_R$, for obtaining the impedance characteristic are as follows.

$$S_O = Z_R \angle \theta \cdot I_r \angle -\varphi_r \tag{2.7}$$

$$S_R = V_r \angle 0° \tag{2.8}$$

By dividing these equations by the line current $I_r\angle$-$\varphi_r$, provides the following equations.

$$S'_O = Z_R \angle \theta \tag{2.9}$$

$$S'_R = Z_r \angle \varphi_r \tag{2.10}$$

The impedances $S'_O$ and $S'_R$ are equivalent representations of the voltages $S_O$ and $S_R$. Figure 2.5 shows the location of $S'_O$ and $S'_R$ in the impedance plane. In Figure 2.5(a) is shown the case of the system impedance $Z_r \angle \varphi_r$ laying inside the operating characteristic. In this case, the absolute value of $Z_r \angle \varphi_r$ can be less than or equal to the absolute value of $Z_R \angle \theta$, fulfilling the condition of Equation 2.2. In Figure 2.5(b) is shown the case of the system impedance $Z_r \angle \varphi_r$ laying outside the operating characteristic. For this, the condition in Equation 2.2 is not met.

Since $Z_R \angle \theta$ is a constant parameter, its absolute value defines a circular characteristic with center at the origin and radius equal to $|Z_R|$.

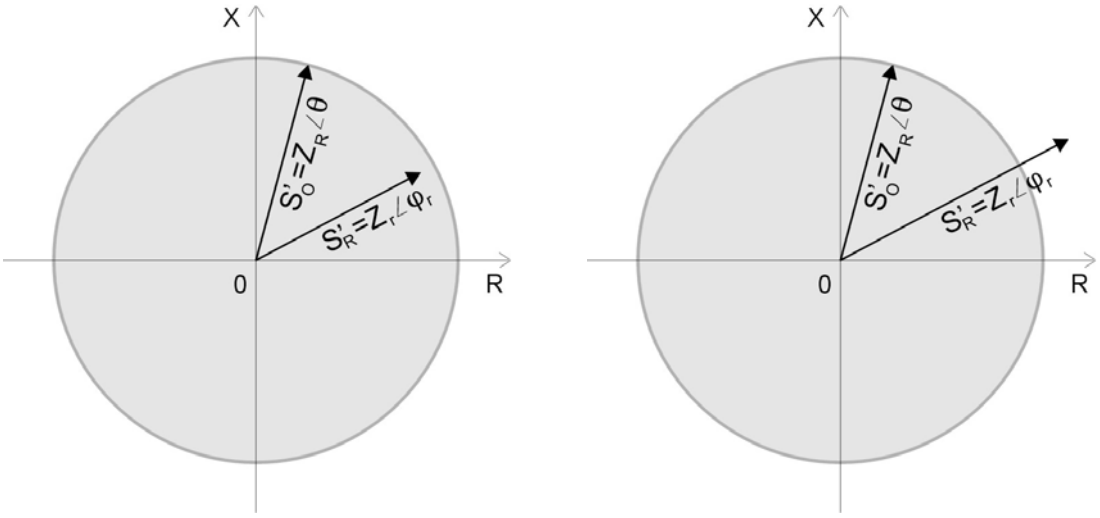


a) Operating condition b) Non-operating condition

**Figure 2.5:** Definition of the impedance characteristic amplitude comparator

### 2.3.5.2 Mho characteristic

#### 2.3.5.2.1 Mho characteristic phase comparator

The phase comparator signals $S_1$ and $S_2$ for producing the mho characteristic are defined as follows.

$$S_1 = -V_r \angle 0° + Z_R \angle \theta \cdot I_r \angle -\varphi_r \tag{2.11}$$

$$S_2 = V_r \angle 0° \tag{2.12}$$

Dividing these equations by the line current $I_r \angle -\varphi_r$, give the following equations.

$$S_1' = -Z_r \angle \varphi_r + Z_R \angle \theta \tag{2.13}$$

$$S_2' = Z_r \angle \varphi_r \tag{2.14}$$

As seen in Figure 2.6, the impedances $S'_1$ and $S'_2$ are placed in the extremes of the constant impedance $Z_R \angle \theta$. When the system impedance $Z_r \angle \varphi_r$ is inside the operating characteristic, as shown on Figure 2.6(a), the angle between $S'_1$ and $S'_2$ fulfills Equation 2.1, and the relay operates. In Figure 2.6(b) is shown the case of $Z_r \angle \varphi_r$ laying outside the operating characteristic. Now, the angle between $S'_1$ and $S'_2$ is outside the range specified in Equation 2.1, and the relay does not operate.

The constant parameter $Z_R \angle \theta$ marks the diameter of the circular characteristic that passes through the origin.

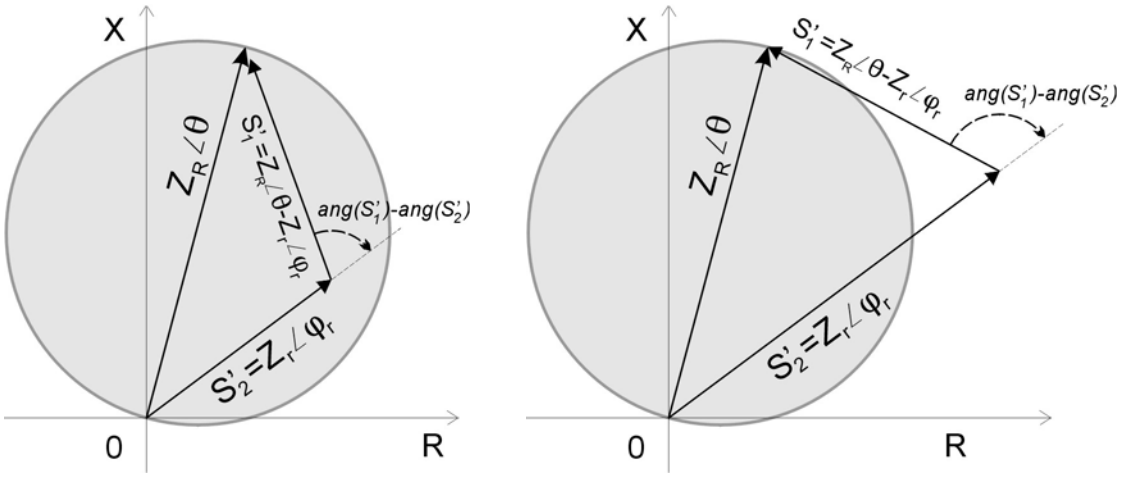


a) Operating condition b) Non-operating condition

**Figure 2.6:** Definition of the mho characteristic phase comparator

#### 2.3.5.2.2 Mho characteristic amplitude comparator

The following $S_O$ and $S_R$ inputs are used in amplitude comparators that implement the mho characteristic. In Figure 2.7, the radius of the mho circular characteristic is $Z_R\angle\theta$.

$$S_O = Z_R\angle\theta \cdot I_r\angle -\varphi_r \tag{2.15}$$

$$S_R = -V_r\angle 0° + Z_R\angle\theta \cdot I_r\angle -\varphi_r \tag{2.16}$$

Dividing these equations by $I_r\angle\text{-}\varphi_r$ leads to the following equations.

$$S_O' = Z_R\angle\theta \tag{2.17}$$

$$S_R' = -Z_r\angle\varphi_r + Z_R\angle\theta \tag{2.18}$$

When the system impedance $Z_r\angle\varphi_r$ is inside the characteristic, the absolute value of the impedance $S'_R$ is less than the absolute value of the radius $S'_O$ as is shown in Figure 2.7(a); the condition specified in Equation 2.2 is satisfied and the relay operates. When the system impedance $Z_r\angle\varphi_r$ is outside the characteristic, the absolute value of $S'_R$ is larger than the absolute value of $S'_O$ and the relay does not operate as is shown in Figure 2.7(b).

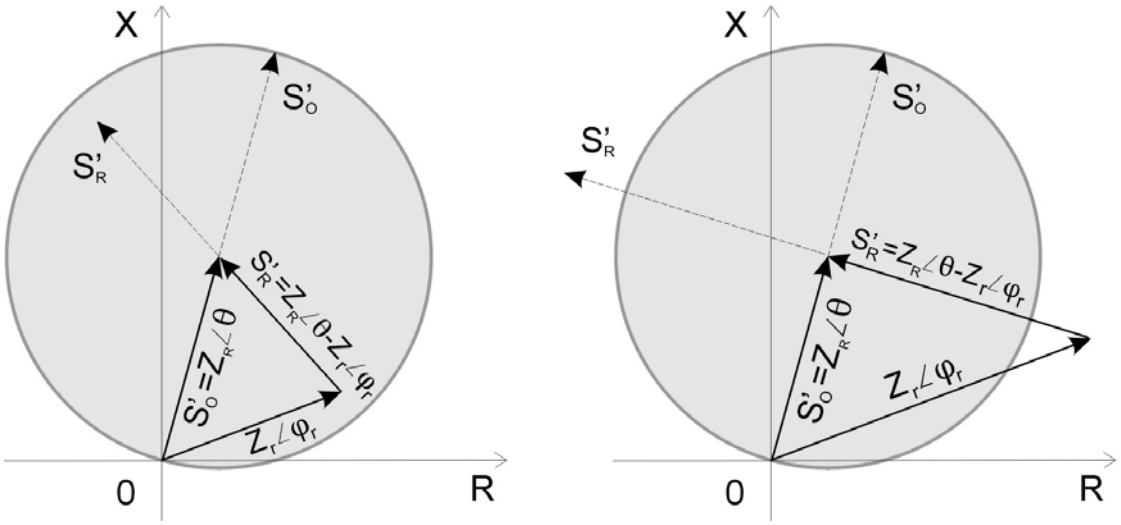


a) Operating condition b) Non-operating condition

**Figure 2.7:** Definition of the mho characteristic amplitude comparator

### 2.3.5.3 Offset-impedance characteristic

#### 2.3.5.3.1 Offset-impedance characteristic phase comparator

The following $S_1$ and $S_2$ inputs are applied to obtain an offset-impedance characteristic.

$$S_1 = -V_r\angle 0° + Z_{R1}\angle\theta_1 \cdot I_r\angle -\varphi_r \tag{2.19}$$

$$S_2 = V_r\angle 0° - Z_{R2}\angle\theta_2 \cdot I_r\angle -\varphi_r \tag{2.20}$$

Simplifying,

$$S_1' = -Z_r \angle \varphi_r + Z_{R1} \angle \theta_1 \tag{2.21}$$

$$S_2' = Z_r \angle \varphi_r - Z_{R2} \angle \theta_2 \tag{2.22}$$

In Figure 2.8 are shown the impedances $S'_1$ and $S'_2$ and the constant impedances $Z_{R1}$ and $Z_{R2}$. In Figure 2.8(a) is illustrated the case of the system impedance $Z_r \angle \varphi_r$ laying inside the operating characteristic. For this case, the angle between $S'_1$ and $S'_2$ fulfills the condition specified in Equation 2.1, and the relay operates. In Figure 2.8(b) is shown the case of $Z_r \angle \varphi_r$ laying outside the operating characteristic. Now, the angle between $S'_1$ and $S'_2$ does not meet the condition specified in Equation 2.1, and the relay does not operate.

The diameter of the offset-impedance characteristic includes the origin in it.

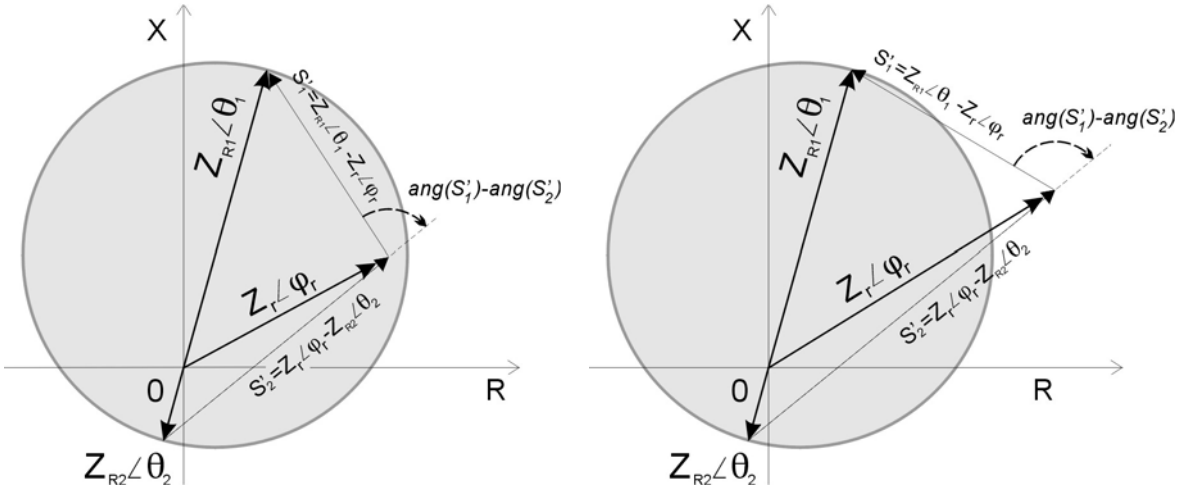


a) Operating condition b) Non-operating condition

**Figure 2.8:** Definition of the offset-impedance characteristic by a phase comparator

#### 2.3.5.3.2 Offset-impedance characteristic amplitude comparator

The following $S_O$ and $S_R$ inputs are used in offset-impedance amplitude comparators

$$S_O = (Z_{R2}\angle\theta_1 \cdot I_r\angle -\varphi_r) - (Z_{R1}\angle\theta_1 \cdot I_r\angle -\varphi_r) \tag{2.23}$$

$$S_R = -V_r\angle 0° + Z_{R2}\angle\theta_2 \cdot I_r\angle -\varphi_r \tag{2.24}$$

Dividing these equations by $I_r\angle$-$\varphi$ provides the following equations.

$$S'_O = Z_{R2}\angle\theta_1 - Z_{R1}\angle\theta_1 \tag{2.25}$$

$$S'_R = -Z_r\angle\varphi_r + Z_{R2}\angle\theta_2 \tag{2.26}$$

As shown in Figure 2.9, the radius of offset-impedance circular characteristic is determined by the values of $Z_{R1}\angle\theta_1$ and $Z_{R2}\angle\theta_2$. When the system impedance $Z_r\angle\varphi_r$ is inside the characteristic, the absolute value of $S'_R$ is less than or equal to the absolute value of the radius $S'_O$ as is shown in Figure 2.9(a). In the case when the system impedance $Z_r\angle\varphi_r$ is outside the characteristic, the absolute value of $S'_R$ is more than the absolute value of $S'_O$ as is shown in Figure 2.9(b).

### 2.3.5.4 Reactance characteristic

#### 2.3.5.4.1 Reactance characteristic phase comparator

The amplitude comparator signals, $S_1$ and $S_2$, for obtaining the reactance characteristic are as follows.

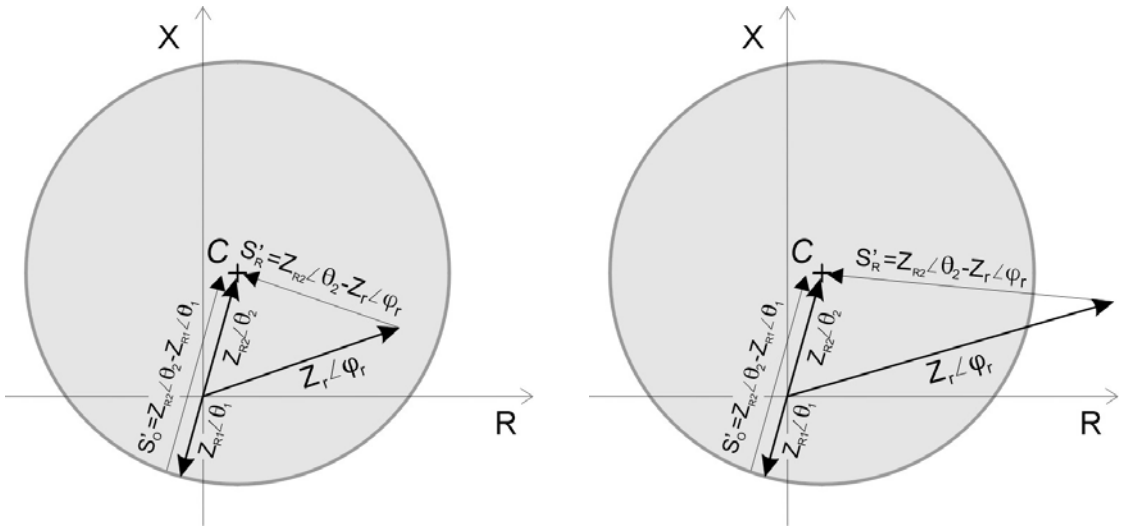


a) Operating condition b) Non-operating condition

**Figure 2.9:** Definition of the offset-impedance characteristic amplitude comparator

$$S_1 = -V_r\angle 0° + X_R\angle 90° \cdot I_r\angle -\varphi_r \tag{2.27}$$

$$S_2 = X_R\angle 90° \cdot I_r\angle -\varphi_r \tag{2.28}$$

Dividing these equations by the line current $I_r\angle$-$\varphi_r$ results in

$$S_1' = -Z_r\angle\varphi_r + X_R\angle 90° \tag{2.29}$$

$$S_2' = X_R\angle 90° \tag{2.30}$$

The constant reactance $X_R\angle 90°$ determines the height of the reactance characteristic, as shown in Figure 2.10. When the system impedance $Z_r\angle\varphi_r$ lies inside the operating characteristic, the angle between $S'_1$ and $S'_2$ satisfies the condition specified in Equation 2.1, as is depicted in Figure 2.10(a). When the system impedance $Z_r\angle\varphi_r$ lies outside the operating characteristic, the angle between $S'_1$ and $S'_2$ does not meet the condition specified in Equation 2.1 as shown in Figure 2.10(b).

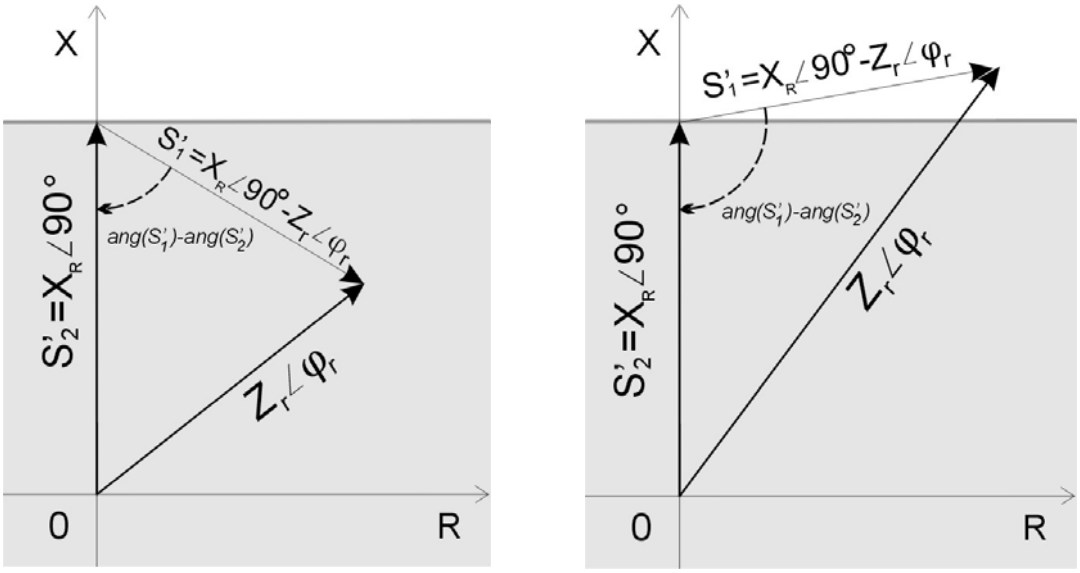


a) Operating condition b) Non-operating condition

**Figure 2.10:** Definition of the reactance characteristic phase comparator

### 2.3.5.4.2 Reactance characteristic amplitude comparator

The following is a set of expression of the amplitude comparator signals $S_O$ and $S_R$ for the reactance characteristic. In Figure 2.11 is shown the reactance characteristic defined by the reactance $X_R \angle 90°$.

$$S_O = -V_r \angle 0° + 2 \cdot X_R \angle 90° \cdot I_r \angle -\varphi_r \tag{2.31}$$

$$S_R = V_r \angle 0° \tag{2.32}$$

Simplifying,

$$S'_O = -Z_r \angle \varphi_r + 2 \cdot X_R \angle 90° \tag{2.33}$$

$$S'_R = Z_r \angle \varphi_r \tag{2.34}$$

When the system impedance $Z_r\angle\varphi_r$ is inside the operating characteristic, the magnitude of $S'_R$ is less than or equal to the magnitude of $S'_R$, as is shown in Figure 2.11(a). When the system impedance $Z_r\angle\varphi_r$ is outside the operating characteristic, the magnitude of $S'_R$ is greater than $S'_O$ as is shown in Figure 2.11(b).

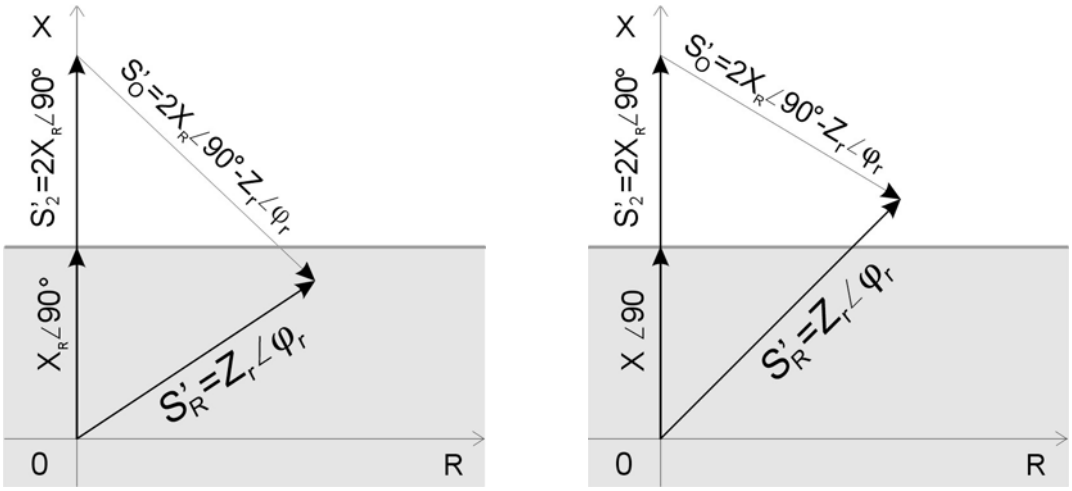


a) Operating condition b) Non-operating condition

**Figure 2.11:** Definition of the reactance characteristic amplitude comparator.

### 2.3.5.5 Quadrilateral characteristic

In numerical relays, the computed apparent impedance is compared with the borders of a pre-defined operating characteristic that could be of any predetermined shape of the operating characteristic [40]. A quadrilateral characteristic can be defined in numerical relays by specifying the corners of the quadrilateral, as shown in Figure 2.12. Quadrilateral characteristics are commonly employed for protecting transmission lines because they can be set to accommodate pre-determined arc resistance while maintaining sufficient margin from the load region. These features make quadrilateral characteristic very useful for protecting short transmission lines, where arc resistances could be a major part of the apparent impedance.

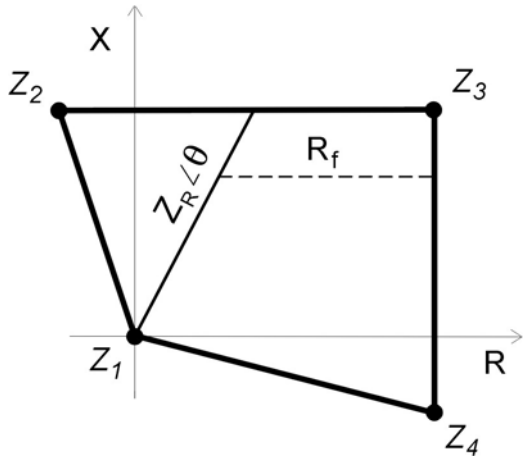


**Figure 2.12:** Quadrilateral characteristic of a distance relay

### 2.3.5.6 Polarized mho characteristic

Mho characteristics have been used worldwide for many years because they combine distance protection and directionality. Their advantages and limitations are well understood. For these reasons, mho elements continue to be emulated in the algorithms of relays built with numerical technology [3]. During faults directly in front of or behind the voltage transformers, short circuit impedance becomes practically zero and a secure relay decision is no longer possible. To achieve directional sensitivity in such cases, cross-polarized and memory polarized mho elements are designed and built for use on high voltage systems [40].

#### 2.3.5.6.1 Cross-polarization

Cross-polarization consists of supplementing the voltage of the faulted phase with a voltage of the healthy phase that is in quadrature with the voltage of the faulted phase [40]. In Figure 2.13 are shown the selection of the cross-polarization voltages for a ground distance relay and a phase distance relay. In Figure 2.13(a), the voltage $V_{bc}$ is the cross-polarized voltage used in relays trying to detect phase A to ground faults. In Figure 2.13(b), the voltage phasor $V_{ca}$-$V_{ab}$ is the cross-polarized voltage used in relays

detecting phase-B to phase-C faults. In Table 2.3 are listed the voltages signals used as cross-polarizing voltages for the different distance relay elements.

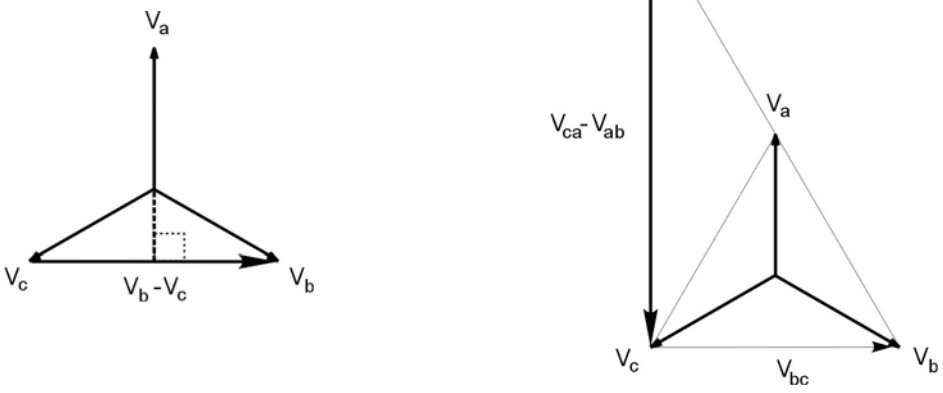


(a) Cross-polarized phasor of $V_a$ (b) Cross-polarized phasor of $V_{bc}$

**Figure 2.13:** Cross-polarized elements for ground and phase distance relays

| Protected line | Cross-Polarized Element $V_p$ |
|---|---|
| Phase A | $V_{bc}$ |
| Phase B | $V_{ca}$ |
| Phase C | $V_{ab}$ |
| Phase A – Phase B | $V_{bc}$ - $V_{ca}$ |
| Phase B – Phase C | $V_{ca}$ - $V_{ab}$ |
| Phase C – Phase A | $V_{ab}$ - $V_{bc}$ |

**Table 2.3:** Cross-polarization elements of mho distance relays

The total voltage applied to the measuring unit of a cross-polarized relay can be expressed by the following equation.

$$V_{Pol} = V_{faulty} + k_p \cdot V_{healthy}\,, \tag{2.35}$$

where,

$V_{pol}$ is the polarization voltage

$V_{faulty}$ is the input voltage of the mho distance relay

$V_{healthy}$ is the cross-polarized voltage applied to the mho distance relay

$k_p$ is the multiplication constant in polarized mho distance relay

To bring the cross-polarizing voltage in phase with the voltage of the faulted phase, the cross-polarizing voltage is rotated by 90° in the positive direction and is divided by a factor of √3. The healthy voltage and the modified polarizing voltage become equal as expressed mathematically by the following equation.

$$V_{healthy} = \frac{1}{\sqrt{3}} \cdot e^{j\frac{\pi}{2}} \cdot V_p \tag{2.36}$$

$V_p$ is the cross-polarized element of polarized mho distance relays

**2.3.5.6.2 Voltage memory**

In the event of a close-in three-phase fault, no healthy phase voltage is available. To solve this problem, a phase voltage memory system, which provides a signal of pre-fault voltage reference during a fault, is employed. Numerical technology has made it possible to generate a voltage reference for as long as desired, but frequency compensation to avoid deviation from the system frequency must be implemented. The following equation defines the polarized voltage when memory polarization is used [40].

$$V_{Pol} = V_{faulty} + k_p \cdot V_{memory} \tag{2.37}$$

A value of 0.1 to 0.2 for $k_p$ is sufficient and is generally used.

### 2.3.6 Zero-sequence current compensation

In Figure 2.14(b) is shown the sequence-networks connection for the phase A-to-ground fault on a transmission line shown in Figure 2.14(a) [41].

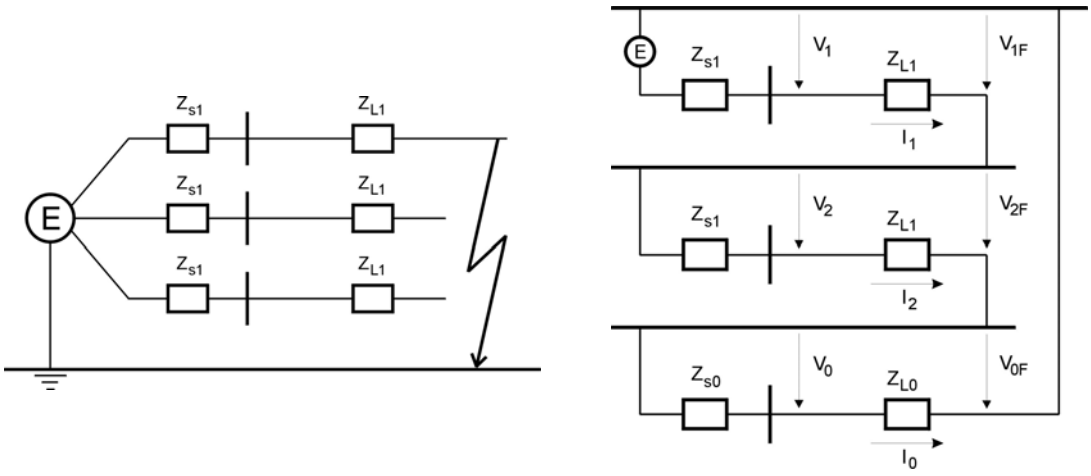


(a) Single phase-to-ground fault (b) Sequence network

**Figure 2.14:** Sequence-networks connection for a phase A-to-ground fault in a transmission line

From Figure 2.14(b), the voltage at the relay location $V_a$ can be calculated as follows:

$$V_a = V_1 + V_2 + V_0 , \tag{2.38}$$

where,

$V_1$ is the positive-sequence voltage at the relay location

$V_2$ is the negative-sequence voltage at the relay location

$V_0$ is the zero-sequence voltage at the relay location

The sequence voltages are equal to

$$
\begin{aligned}
V_1 &= I_1 Z_{L1} + V_{1F} \\
V_2 &= I_2 Z_{L1} + V_{2F} \\
V_0 &= I_0 Z_{L0} + V_{0F}.
\end{aligned}
\tag{2.39}
$$

where,

$I_1$ is the positive-sequence current at the relay location

$I_2$ is the negative-sequence current at the relay location

$I_0$ is the zero-sequence current at the relay location

$Z_{L1}$ is the positive-sequence impedance from the fault to the relay location

$Z_{L0}$ is the zero-sequence impedance from the fault to the relay location

$V_{1F}$ is the positive-sequence voltage at the fault location

$V_{2F}$ is the negative-sequence voltage at the fault location

$V_{0F}$ is the zero-sequence voltage at the fault location

Therefore,

$$
V_a = I_1 Z_{L1} + I_2 Z_{L1} + I_0 Z_{L0} + (V_{1F} + V_{2F} + V_{0F}) . \tag{2.40}
$$

But,

$$
V_{1F} + V_{2F} + V_{0F} = 0 . \tag{2.41}
$$

And therefore,

$$
\begin{aligned}
V_a &= (I_1 + I_2) Z_{L1} + I_0 Z_{L0} \\
&= (I_1 + I_2 + I_0) Z_{L1} + I_0 (Z_{L0} - Z_{L1}) \\
&= (I_1 + I_2 + I_0) Z_{L1} + 3 I_0 \left( \frac{Z_{L0} - Z_{L1}}{3} \right)
\end{aligned}
\tag{2.42}
$$

Because $I_a = I_1 + I_2 + I_0$, Equation 2.42 becomes

$$V_a = I_a Z_{L1} + 3I_0 \left( \frac{Z_{L0} - Z_{L1}}{3Z_{L1}} \right) Z_{L1} \\ = I_a Z_{L1} + K_0 3I_0 Z_{L1} \tag{2.43}$$

The compensated current $I_{a(comp)}$ can be defined as

$$I_{a(comp)} = I_a + K_0 3I_0 . \tag{2.44}$$

The ratio of the voltage $V_a$ to the compensated current $I_{a(comp)}$ now yields

$$\frac{V_a}{I_{a(comp)}} = Z_{L1} . \tag{2.46}$$

Depending on the manner $I_0$ is provided to the relay, the $K_0$ factor may be expressed as [60]

$$K_0 = \frac{Z_{L0} - Z_{L1}}{3Z_{L1}} . \tag{2.47}$$

## 2.3.7 Computation of the apparent impedance

In the case of phase distance relays, phase-to-phase voltages and differences between line currents are used. For example, a relay designed to detect phase-B to phase-C faults computes the impedance as expressed in the following equation

$$Z_{seen} = \frac{V_b - V_c}{I_b - I_c} = \frac{V_{bc}}{I_{bc}} . \tag{2.48}$$

In terms of the real and imaginary parts of the phasors, Equation 2.48 can be written in the following form.

$$Z_{seen} = \frac{V_{bc}}{I_{bc}} = \frac{\mathrm{Re}(V_{bc}) + j\,\mathrm{Im}(V_{bc})}{\mathrm{Re}(I_{bc}) + j\,\mathrm{Im}(I_{bc})} = \frac{V_r + jV_i}{I_r + jI_i} \tag{2.49}$$

It can be shown that the impedance seen in this phase distance relay can be expressed as follows.

$$Z_{seen} = \left( \frac{V_r \cdot I_r + V_i \cdot I_i}{{I_r}^2 + {I_i}^2} \right) + j\left( \frac{V_i \cdot I_r - V_r \cdot I_i}{{I_r}^2 + {I_i}^2} \right). \tag{2.50}$$

The ground distance relay protecting phase-A computes the apparent impedance using the following equation.

$$Z_{seen} = \frac{V_a}{I_a + K_0 3I_0} \tag{2.51}$$

## 2.4 Differential protection

Differential protection is one of the most reliable and popular techniques in power system protection. Differential protection compares the currents that enter with the currents that leave a zone. If the net sum of the currents that enter and the currents that leave a protection zone is essentially zero, it is concluded that there is no fault in the protection zone. However, if the net sum is not zero, the differential protection concludes that a fault exists in the zone and takes steps to isolate the zone from the rest of the system.

In 1904, British engineers Charles H. Merz and Bernard Price developed the first approach for differential protection. The advantages of the scheme proposed by Merz and Price were soon recognized and the technique has been extensively applied since then [4]. However, it soon became apparent that differential protection operated

incorrectly due to mismatch of current transformers provided at the two ends of the zone, differences in the relay circuitry and due to inrush currents or excessive currents caused by system over-voltages at the transformer terminals. Over the years, various methods have been developed to ensure correct operation of differential relays.

### 2.4.1 Differential principle

In Figure 2.15 is shown one phase of a three-phase differential protection system. Multiple circuits may exist, but the example is sufficient to explain the basic principle of differential protection [2]. It can be observed from Figure 2.15 that the protection zone is delimited by a couple of current transformers. Due to its very nature, differential protection does not provide backup protection to other system components. For this reason, differential protection is categorized as unit protective scheme. The conductors bringing the current from the current transformers to the differential relay are in some situations called pilot wires.

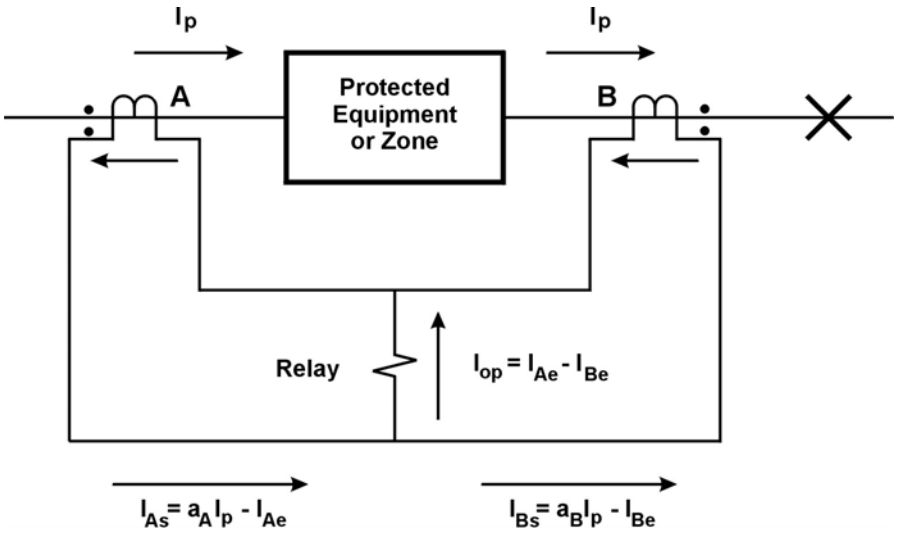


**Figure 2.15:** Differential relay currents during normal operation or external fault

Under normal conditions, the current $I_p$ entering the protected unit would be equal to the current leaving it at every instant. Consider current transformer A. The secondary current in the pilot wire of current transformer A is equal to

$$I_{As} = a_A I_p - I_{Ae}, \tag{2.52}$$

where,

$a_A$ is the transformation ratio of current transformer A

$I_{Ae}$ is the excitation current of current transformer A in the secondary

For the current transformer B, the equation is similar and is as follows.

$$I_{Bs} = a_B I_p - I_{Be}, \tag{2.53}$$

where,

$a_B$ is the transformation ratio of current transformer B

$I_{Be}$ is the excitation current of current transformer B in the secondary

Assuming equal transformation ratios, $a_A = a_B = a$, the relay operation current $I_{op}$ is given by

$$I_{op} = I_{Ae} - I_{Be} \tag{2.54}$$

During normal system operation and during external faults, the relay operating current $I_{op}$ is small, but never zero. This happens due to several factors that are explained later in section 2.4.3.2.

In the event of a fault in the protection zone, the input current is no longer equal to the output current. The operating current of the differential relay is now the sum of the input currents feeding the fault as shown in Figure 2.16.

$$I_{op} = a(I_{F1} + I_{F2}) - I_{Ae} - I_{Be} \tag{2.55}$$

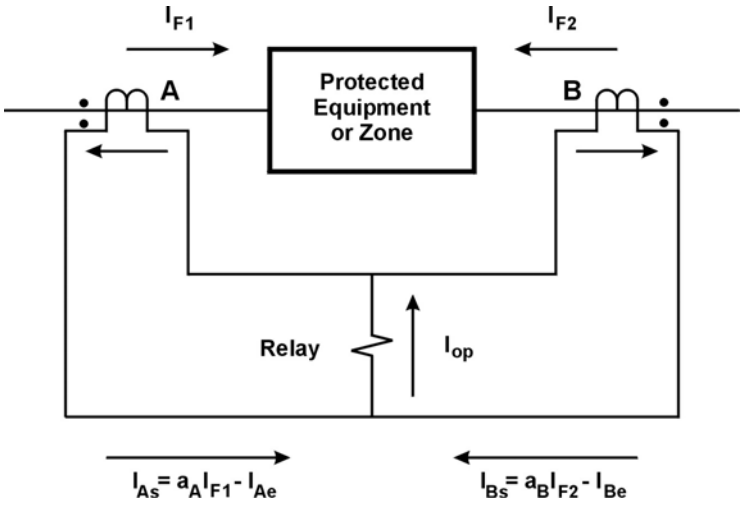


**Figure 2.16:** Differential relay currents during internal fault

## 2.4.2 Percentage restraint differential protection

Except for very light internal faults, good discrimination is available to detect faults inside the differential zone. Percentage differential protection overcomes the problems related with the identification of light internal faults while keeping the advantages of the basic differential scheme [1]. In general, the operating current in the differential relay is equal to

$$I_{op} = \left| I_{D1} + I_{D2} \right|, \tag{2.56}$$

where,

$I_{D1}$, $I_{D2}$ are the currents on the pilot wires of the current transformers

For their operation, percentage restrain relays employ a restraining current. The following are the most common ways to obtain the restraint current, where $k$ is a compensation factor, generally taken as 0.5 or 1.

$$I_{rt} = k\left|I_{D1} - I_{D2}\right| \tag{2.57}$$

$$I_{rt} = k\left(\left|I_{D1}\right| + \left|I_{D2}\right|\right) \tag{2.58}$$

$$I_{rt} = Max\left(\left|I_{D1}\right|, \left|I_{D2}\right|\right), \tag{2.59}$$

Percentage restraint differential protection employs the restraint current $I_{rt}$, together with the operating current $I_{op}$, to define the relay operation on a coordinate plane, as shown in Figure 2.17. A line divides the coordinate plane in two parts. The upper part is the operating region while the lower part is the restraining region. This dividing line is called the characteristic of the differential relay. Typical characteristic of differential relays present a small slope for low currents to allow sensitivity to light internal faults. At higher currents, the slope of the characteristic is much higher, which requires that the operating current, $I_{op}$, be higher in order to cause operation of the differential relay.

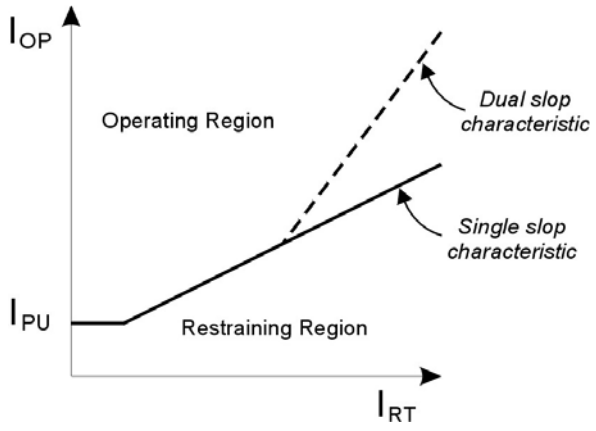


**Figure 2.17:** Characteristic of a percentage differential relay

The operation of a percentage-differential relay can be expressed by the following equation.

$$I_{op} > SLP_i \cdot I_{rt}, \tag{2.60}$$

where $SLP_i$ is the slope of the *i-th* characteristic of the differential relay.

## 2.4.3 Differential protection of power transformers

Over-current, differential and gas accumulator are three types of protection that are normally applied to protect power transformers.

Overcurrent protection provided the first type of transformer protection, and it is still in use for small capacity transformers. Differential protection replaced overcurrent technology as the principal electrical protection for power transformers. An electric arc in oil decomposes the oil producing gases. The emission of gas is used in gas accumulator and rate-of-pressure-rise relays to detect internal arcing faults.

### 2.4.3.1 Types of faults on power transformers

Faults on power transformers can be classified as through faults and internal faults. A through fault is located outside the protection zone of the transformer. The unit protection of the transformer should not operate for through faults. The transformer must be disconnected when such faults occur only when the faults are not cleared by other relays in pre-specified time. Internal faults can be phase-to-phase and phase-to-ground faults. Internal faults are dangerous for the integrity of the power transformer. These internal faults can be classified into two groups.

Group I: Electrical faults that cause immediate serious damage but are generally detectable by unbalance of current or voltage. Amongst them are the following.

- Phase-to-earth fault
- Phase-to-phase fault
- Short circuit between turns of high-voltage or low-voltage windings
- Faults to earth fault on a tertiary winding or short circuit between turns of a tertiary winding

Group II: These include incipient faults, which are initially minor faults but cause substantial damage if they are not detected and taken care of. These faults cannot be detected by monitoring currents or voltages at terminals of the transformer. Incipient faults include the following:

- A poor electrical connection between conductors
- Core fault which causes arching in oil
- Coolant failure, which causes rise of temperature
- Bad load sharing between transformers in parallel, which can cause overheating due to circulating currents

For a group I fault, the transformer should be isolated as quickly as possible after the occurrence of the fault. The group II faults, though not serious in the incipient stage, may cause major faults in the course of time. Incipient faults should be cleared soon after they are detected.

### 2.4.3.2 Problems of differential protection applied to power transformers

For proper discrimination between internal and external faults, the secondary currents of the current transformers on a differential protection scheme must be identical. A

number of factors affect adversely the balance of the currents being compared. Some of these factors are as follows.

- Two current transformers do not perform equally, even when they are from the same brand and have the same ratio and type.
- The remnant magnetic fluxes in the cores of two current transformers may not be identical and consequently their excitation currents are not identical.
- The saturation of one of the current transformers affects the waveform and reduces the output of the transformer current. The difference of the outputs of the two current transformers manifests as relay operating current.
- Difference in length of the wiring produces a difference in the resistance of the pilot wires, affecting the symmetry of signals. This difficulty is overcome by connecting adjustable resistors to pilot wires.
- The incoming and outgoing sides of a transformer have different voltage levels and the current on both sides of the transformers are different. For this reason, the ratios of current transformers used on the two sides of a differential protection are different. This increases the mismatches of the current transformers. These mismatches are corrected in numerical relay by scaling used in their software.
- The power transformer connection produces a phase displacement from the primary voltages and currents to the secondary voltages and currents. Delta-wye connection, the most common of transformer connections, produces a 30 degree displacement. This problem is also corrected in the software programs of numerical differential relays.
- Tap changing alters the ratio of voltages and currents on the high voltage and low-voltage sides. Enough bias should be provided in order that the variation in secondary currents due to tap changing does not produce relay operation.

However, inrush current is the most sensitive of the issues related with differential protection of power transformers.

### 2.4.3.2.1 Magnetizing inrush

When the excitation of a transformer is removed, the magnetizing current goes to zero, and the flux, following the hysteresis loop, falls to some residual value. If the transformer were reenergized at the instant the voltage waveform correspond to the residual magnetic density within the core, there would be a smooth continuation of the previous operation with no transients. However, in practice, the instant when switching takes place cannot be controlled, and a magnetizing transient occurs, almost inevitably. The transient generates a current known as inrush current. The magnitude of this inrush current can be several times the load current and flows only on one side of the differential relay, which tends to operate if some form of restraint is not provided. In Figure 2.18 is shown a typical curve of inrush current due to the energization of a power transformer.

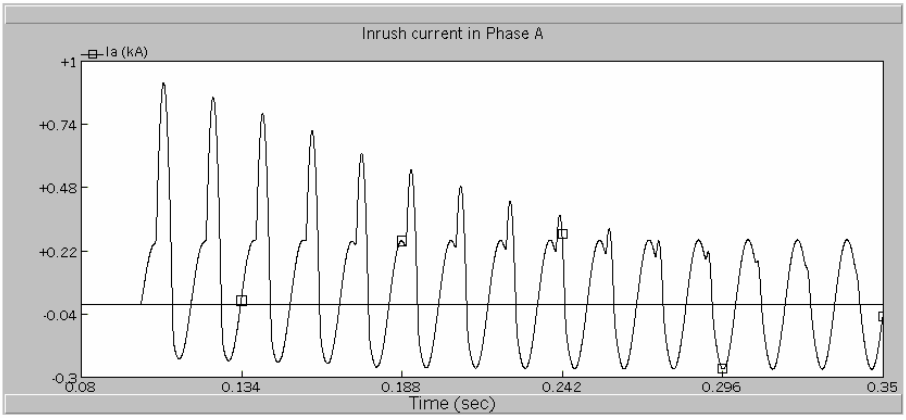


**Figure 2.18:** Typical magnetizing inrush current in a power transformer

Typically, inrush currents are composed of unipolar or bipolar pulses, separated by intervals of very low values of current. The inrush current decays rapidly during the first few cycles, and then decays slowly. Time constants for the inrush currents vary from 10 cycles for small units to 60 seconds for large units. The factors that determine the magnitude and duration of magnetizing current inrush include the following:

- Size of transformer
- Size of power system
- Type of magnetic material in the core
- Residual flux in the transformer before switching on

Maximum inrush current occurs if the transformer is energized when voltage wave is passing through zero. At this instant, the current and flux reach their maximum value in highly inductive circuit. If there is residual flux in the transformer, the required flux may be in the same or opposite direction. Accordingly, the magnetizing current will be less or more. If the magnetizing current is more, it will saturate the core and increase the magnetizing current component further.

### 2.4.3.3 Differential protection restraint for magnetizing inrush current

Early transformer differential relay designs used time delay, or a temporary desensitization of the relay to override the inrush current. This technique increased the time to operate. Other designs used an additional voltage signal on a substation to restrain or to block the differential relay operation. However, for a stand-alone differential relay the additional voltage signal is not always available.

The methods presently used to discriminate inrush currents from internal faults fall in two groups: those using harmonics to restrain or block relay operation, and those based on wave shape identification.

#### 2.4.3.3.1 Harmonic-based methods

The magnetizing inrush currents have high component of even and odd harmonics. In Table 2.4 are shown typical amplitudes of the harmonics, compared with the fundamental (100%) [1].

| Harmonic components in magnetizing inrush current | Amplitude (% of fundamental) |
|---|---|
| D. C. | 55 |
| 2nd harmonic | 63 |
| 3rd harmonic | 26.8 |
| 4th harmonic | 5.1 |
| 5th harmonic | 4.1 |
| 6th harmonic | 3.7 |
| 7th harmonic | 2.4 |

**Table 2.4:** Percentage of harmonics in typical magnetizing inrush current

Given that harmonic content of the short circuit currents is negligible, the harmonic-based methods are used for either restraining or blocking the relay from operation during initial current inrush. Harmonic-based methods allow the differential relay to remain sensitive to fault currents while keeping the relay from operating due to magnetizing currents.

**Harmonic restrain techniques**: The original harmonic-restrained differential relay used all harmonics to provide the restrain function [7], [8], [9]. The resulting high level of harmonics restraint provided security for inrush conditions at the expense of operating speed for internal faults with CT saturation. As a result, the harmonic-restrained differential relay compares the fundamental component of the operating current with a restraint signal consisting of the unfiltered restraint current plus the harmonics of the operating current. The differential relay operation condition can be expressed as

$$I_{op} > SLP_i \cdot I_{rt} + k_2 I_{2h} + k_3 I_{3h} + \ldots, \tag{2.61}$$

where,

$I_{op}$ is the fundamental component of the operating current

$I_{2h}$, $I_{3h}$, ... are higher harmonics of the operating current

$I_{rt}$ is the unfiltered restrain current

$k_1$, $k_2$, ... are constant coefficients

A more recent set of techniques use only the second harmonic to identify inrush currents and the fifth harmonic to avoid misoperations for transformer due to over-excitation [10, 11]. The basic operating equation for one phase can be expressed as follows.

$$I_{op} > SLP_i \cdot I_{rt} + k_2 I_{2h} + k_5 I_{5h} \tag{2.62}$$

Common harmonic restrain for three-phase transformer differential protection is a technique where the harmonic restrain quantity is proportional to the sum of the second and fifth-harmonic components of the three relay elements. The relay operation is of the following form:

$$I_{op} > SLP_i \cdot I_{rt} + \sum_{n=1}^{3} (k_2 I_{2hn} + k_5 I_{5hn}) \tag{2.63}$$

**Harmonic blocking techniques**: Typically, numerical transformer differential relays use second- and fifth-harmonic blocking logic [10]. A tripping signal requires that Equation 2.60 and the following conditions are satisfied

$$I_{op} < k_2 I_{2h} \tag{2.64}$$

$$I_{op} < k_5 I_{5h} \tag{2.65}$$

In Figure 2.19 are shown the logic diagrams of harmonic restraint and harmonic blocking differential elements.

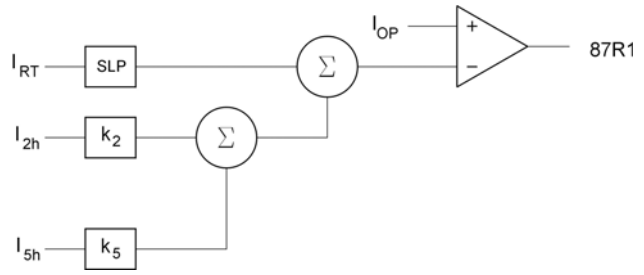


**(a)** Harmonic restraint

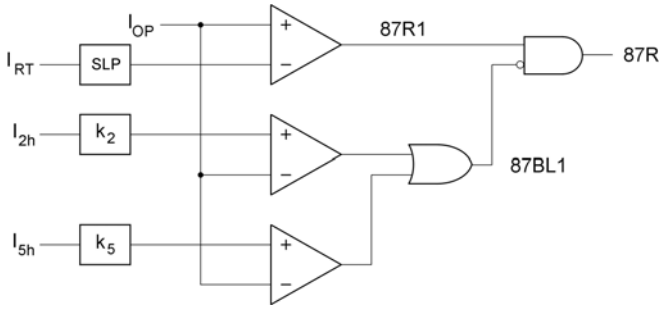


**(b)** Harmonic blocking

**Figure 2.19:** Logic diagrams of differential elements employing harmonic-based methods

In Figure 2.20 are shown the three-phase version of the logic diagrams of independent harmonic blocking differential element and independent harmonic restrain. The relay is composed of three differential elements of the types shown in Figure 2.19. In both cases, a tripping signal results when any one of the relay elements asserts.

#### 2.4.3.3.2 Wave shape recognition methods

Other methods for discriminating internal faults from inrush conditions are based on direct recognition of the shape of the differential current [1]. Wave shape recognition methods are divided between those methods that are based on the identification of the separation of different current peaks [12], [13], [14], [15], [16] and those methods that use DC offset or asymmetry in the differential current [17], [18], [19], [20].

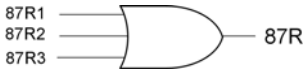


**(a)** Independent harmonic restraint

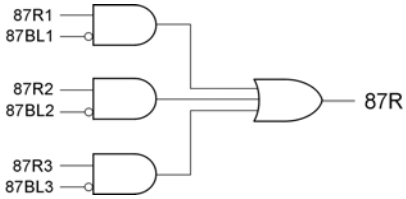


**(b)** Independent harmonic blocking

**Figure 2.20:** Logic diagrams of three-phase differential elements employing harmonic-based methods

A well-known principle [14], [15] recognizes the length of the time intervals during which the differential current is near zero. In Figure 2.21 is depicted the basic concept behind this low current differential method.

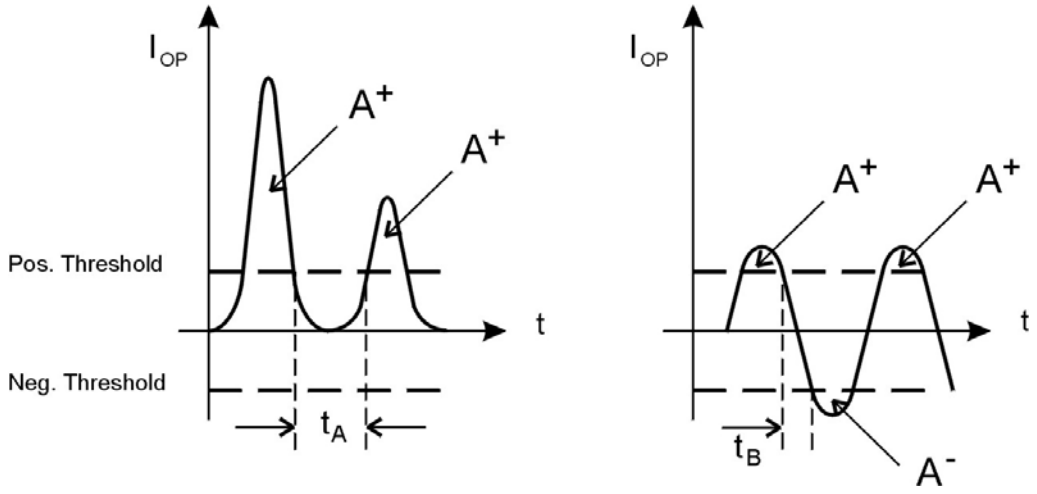


(a) Inrush current (b) Internal fault current

**Figure 2.21:** Differential relay blocking based on recognition of low-currents intervals

The differential current is compared with equal positive and negative thresholds to determine the duration of the intervals during which the absolute value of the current is less than the absolute value of the threshold. The time intervals are then compared with a value equal to one-quarter cycle. If the low current intervals of currents $t_A$ are greater than one-quarter cycle as shown in Figure 2.21(a) the relay is blocked. On the other hand, if the low current intervals $t_B$ are less than one-quarter cycle, shown in Figure 2.21(b), the relay operates.

Some techniques belonging to the second group of wave shape recognition methods compare the amplitudes of the positive and negative semi-cycles of the differential current with given thresholds [13], [18]. Another alternative [19] used difference of the absolute values of the positive and negative semi-cycles of the differential current for restrain. More recently, another technique [20] proposed making separate percentage-differential comparison on both semi-cycles of the differential current.

## 2.5 Summary

The description and operating principles of distance and differential protection have been described in this chapter. Key aspects of distance relay protection, such as protection zones, comparators and operating characteristic, have been discussed. Methods of calculating the apparent impedance and zero-sequence compensation have been reviewed. The differential protection principle and the percentage restraint differential protection have been introduced. The differential protection of power transformers, together with the problems and issues of their application, has also been presented.

# 3. DIGITAL AND NUMERICAL RELAYS

## 3.1 Introduction

Previous chapters presented basic concepts of protection and principles of operation of distance and differential relays. Modern digital and numerical relays are widely employed in protection systems nowadays. Designing and modeling of numerical relay require establishing a generalized numerical relay structure, which is composed by the more relevant and common internal modules employed by typical numerical relays. The present chapter discusses the functionality of each of the internal modules of the generalized numerical relay, namely signal conditioning and scaling module, analog anti-aliasing filtering module, analog-to-digital conversion module, phasor estimation algorithm and relay logic. The most common techniques and methods employed in each of these internal modules are enumerated and reviewed.

## 3.2 Relay performance and relay technology

The following characteristics are related with a good performance of a relay in a power system [2], [3].

**Reliability:** The reliability of a relay is directly in correspondence with the concepts of dependability and security. A relay is said to be dependable when it operates in the occurrence of a fault relevant to its protection zone. Security is reached either when the relay will not operate for a fault outside its operating zone, or when the system is in a healthy state.

**Selectivity:** Selectivity is the ability that a relay has to only open those breakers that isolate the faulted element. Selectivity discrimination can be achieved by time grading or by unit protection. Selectivity by time grading means that different zones of operation are graded by time and that in the occurrence of a fault, although a number of protections equipment respond, only those relevant to the faulty zone complete the tripping function. Selectivity by unit protection means that the relay will only operate under certain fault conditions occurring within a clearly defined zone.

**Speed:** In the occurrence of a fault, the greater the time in which the fault is affecting the power system, the greater is the risk that the power system falls into an unstable operation point. Relays are therefore required to clear the fault as quickly as possible.

**Sensitivity:** The relay is said to be sensitive if the relay operates to the minimum value of faulted input signals.

### 3.2.1 Relay technology

The relay application for protection of power system date back nearly 100 years ago. Since then, the technology employed to construct relays have improved dramatically relay size, weight, cost and functionality. Based on the technology employed for their construction, relays can be chronologically classified as electromechanical, static or solid-state, digital and numerical [3].

**Electromechanical relays:** The first relays employed in the electric industry were electromechanical devices. These relays worked based on creating a mechanical force to operate the relay contacts in response to a fault situation. The mechanical force was established by the flow of a current that reflected the fault current through windings mounted in magnetic cores. Due to the nature of its principle of operation, electromechanical relays are relatively heavier and bulkier than relays constructed with

other technologies. Besides, the burden of these relays can be extremely high, affecting protection purposes. However, electromechanical relays were so largely employed, tested and known that even modern relays employ their principle of operation, and still represent a good choice for certain conditions of application.

**Solid-state relays:** With the advances on electronics, the electromechanical technology presented in the relays of the first generation started to be replaced by static relays in the early 60's. Static relays defined the operating characteristic based in analog circuitry rather than in the action of windings and coils. The advantages that static relays showed over electromechanical relays were a reduced size, weight and electrical burden. However, static relays showed some disadvantages since analog circuitry is extremely affected by electromagnetic interference and the ranges of current and voltages values are strongly restricted in analog circuits, affecting the sensitivity of the relay.

**Digital relays:** Incorporating microprocessor into the architecture of relay to implement relay and logic functions started happening in the 80's. Digital relays incorporated analog-to-digital converter (ADC) to sample the analog signals incoming from instrument transformers, and used microprocessor to define the logic of the relay. Digital relays presented an improvement in accuracy and control over incoming signals, and the use of more complexes relay algorithms, extra relay functions and complementary task.

**Numerical relays:** The difference between numerical relays and digital relays lies in the kind of microprocessor used. Numerical relays use digital signal processors (DSP) cards, which contain dedicated microprocessors especially designed to perform digital signal processing.

## 3.3 Digital and numerical relay models

Modeling and simulation of electric power systems has been a common practice for more than thirty years. Computer models of major power system components have been used in software packages such as short circuit programs, load flow, stability programs, and electromagnetic transient programs. Relay system modeling has been performed in a lesser degree.

A successful relay model must produce the same output for the same inputs than its real counterpart, even when there would not be a direct correspondence to the actual microprocessor machine language coding within the relay.

Utility engineers and consultants use relay models to select the relay types suited for a particular application, and to analyze the performance of relays that appear to either operate incorrectly or fail to operate on the occurrence of a fault. Instead of using actual prototypes, manufacturers use relay model designing to expedite and economize the process of developing new relays. Electric power utilities use computer-based relay models to confirm how the relay would perform during systems disturbances and normal operating conditions and to make the necessary corrective adjustment on the relay settings. The software models could be used for training young and inexperienced engineers and technicians. Researchers use relay model designing to investigate and improve protection design and algorithms. However, choosing appropriate settings for the steady state operation of overcurrent relays and distance relays is presently the most familiar use of relay models [25].

The purpose for which a relay model is to be used determines the amount of detail required in the representation of the actual relay. Based on this, digital and numerical relay models can be divided into two categories. The models of the first category consider only the fundamental frequency components of voltages and currents. Phasor-based models were the first to be widely used to design and apply relays. The models of the second category take into consideration the high frequency and decaying DC

components of voltages and currents in addition to the fundamental frequency components [25]. These models are called transient models of relays.

### 3.3.1 Phasor relay models

The primary limitation of phasor models is their inability to handle and account for some components of the inputs, such as the DC offset, nonlinearities of current transformers and voltage transformers, and protective relay memory circuits losing stored voltage or current data.

In spite of their limitations, phasor models provide the ability to observe, usually by graphical plots, the margin between the boundary of operation and the parameters that are calculated by the relay. This ability, which is common to all relay models, is very helpful in developing reliable protection applications and settings. Phasor-based models can be used, among others, for the following purposes.

- Modeling of time-graded overcurrent characteristics
- Setting and adjustment of instantaneous relays
- Modeling of the characteristic of a directional overcurrent relay on the complex plane
- Modeling of the characteristic of a power relay plotted in the P-Q plane
- Modeling of the characteristic of a percentage restrained differential relay plotted in the differential-restrain current plane

### 3.3.2 Transient relay models

Transient relay models mimic the behavior of digital and numerical relays including their performance in the transient state and the impact of the transient components in the

input signal. Some of the situations that require transient models for proper evaluation of relay performance are as follows.

- Transformer or capacitor inrush
- Current transformer or capacitance voltage transformer transient
- Current transformer steady state saturation
- Presence of harmonics
- Presence of transient direct current offset
- Evolving faults
- Power system swing and dynamics of rotating machines
- Time varying machine impedances (sub-transient, transient and steady state)
- Protection of series capacitors

The availability of detailed information of the internal functioning of relays is critical in the process of producing a close-to-real transient relay model. Accordingly to the available information, transient models can be categorized in generic and detailed models.

**Generic models:** Generic models give considerable insight into the operation of the relay type but may not be suitable for marginal cases and precise timing. They may not have detailed logic provided in specific implementation of the generic principle in a specific relay. This logic is often applied to make specific functions interact with other functions to make a protection system. Because of this limitation generic model determine the best use for checking specific functions, rather than complete systems that are made up of numerous interacting functions.

**Detailed models:** Detailed models preserve all the advantages of being able to examine the internal operation of any function. Detailed models are more useful than generic models for checking the performance of complete systems since all logic is represented. Unfortunately, detailed models are not as readily available as the generic models because they may include trade secrets of the manufacturers.

Manufacturers are in position to design accurate transient models, particularly for new digital relays, for the reason that, in the designing process, the software model may precede the hardware design. Where algorithms and hardware are known in detail very precise performance can be achieved in the modeling.

## 3.4 Generalized numerical relay structure

McLaren was the first to propose the concept of Open System Relaying, where different relay functions can be obtained from the same hardware just by modifying microprocessor programming [3]. Modern relay technology has shown recently a tendency towards this direction.

The generalized numerical relay concept, which is directly derived from open system relaying, consists of a minimum set of hardware modules and functions of modern digital and numerical relays. With the generalized numerical relay and with the amount of information commonly available, it is possible to recreate the majority of modern digital and numerical relay equipment. The following hardware modules and functions constitute the generalized numerical relay.

- **Isolation and analog signal scaling:** Current and voltage waveforms from instrument transformers are acquired and scaled down to convenient voltage levels for use in the digital and numerical relays.
- **Analog anti-aliasing filtering:** Low-pass filters are used to avoid the phenomena of aliasing in which the high frequency components of the inputs appear to be parts of the fundamental frequency components.
- **Analog-to-digital conversion:** Because digital processors can process numerical or logical data only, the waveforms of inputs must be sampled at discrete times. To achieve this, each analog signal is passed through a sample-

and-hold module, and conveyed, one at a time, to an Analog-to-Digital Converter (ADC) by a multiplexer.

- **Phasor estimation algorithm:** A software algorithm implemented in a microprocessor estimates the amplitude and phase of the waveforms provided to the relay.
- **Relay algorithm and trip logic:** The equations and parameters specific to the protection algorithm and the associated trip logic are implemented in the software of the microprocessor used in the relay. The microprocessor calculates the phasors representing the inputs, acquires the status of the switches, performs protective relay calculations, and finally provides outputs for controlling the circuit breakers. The processor may also support communications, self-testing, target display, time clocks, and other tasks [25].

In Figure 3.1 is shown the schematic of a generalized numerical relay structure. The functionalities of each module of the generalized relay model are developed in next sections.

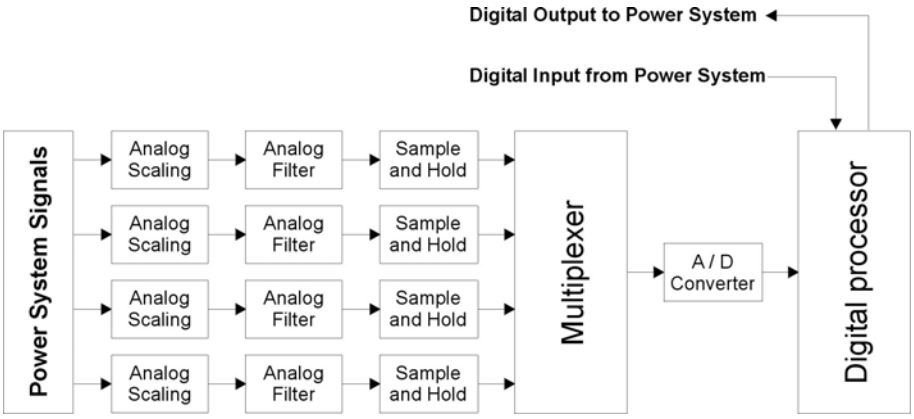


**Figure 3.1:** Generalized numerical relay structure

## 3.4.1 Isolation and analog signal scaling module

The isolation and analog signal scaling module acquires the voltage and current signals from the transducers of the power system. This module provides electrical isolation

from the power system and scales down the acquired inputs to levels suitable for use by the data acquisition system. Since analog-to-digital converters accept only voltage signals, this module also converts currents to equivalent voltages.

In Figure 3.2 is shown a schematic diagram of the circuit for isolation and analog scaling of a voltage signal. The output of a voltage transformer is applied to an auxiliary transformer that reduces the voltage level and provides electrical isolation to the rest of the relay equipment. After the auxiliary voltage transformer, the voltage is further reduced by a potentiometer to a level suitable for use by the data acquisition system. A metal oxide varistor (MOV) is used at the input of the auxiliary transformer to protect the data acquisition system from transients in the input signals.

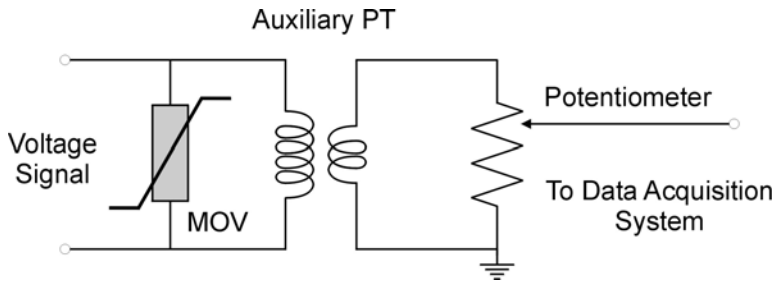


**Figure 3.2:** Isolation and analog scaling of a voltage signal

In Figure 3.3 is shown the isolation and analog scaling circuit used for processing currents. A current from a current transformer is reduced to a lower level by an auxiliary current transformer. The secondary of the auxiliary current transformer is passed to a resistor to convert the current to an equivalent voltage.

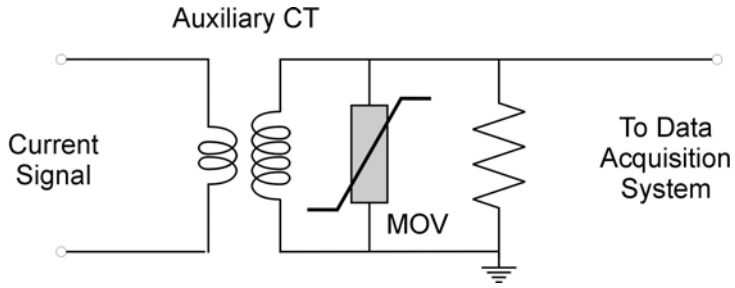


**Figure 3.3:** Isolation and analog scaling of a current signal

### 3.4.2 Anti-aliasing filter module

The analog inputs must be applied to low-pass filters and their outputs should be sampled and quantized. The use of low-pass filter is necessary to limit the effects of noise and unwanted components of frequencies over the folding frequency (half of the sampling frequency).

The nature of the relaying task dictates the total amount of filtering required. Distance protection based on impedance measurements uses information contained in the sinusoidal steady state components of 60 Hz. Therefore, filtering must preserve the steady state components and reject other components. Common analog low-pass filters used in these relays are of third to fifth order with cutoff frequency of about 90 Hz. The cutoff frequency of 90 Hz implies that a sampling rate of at least three samples per cycle (180 Hz) must be used in order that that the information needed to perform the distance relay functions is retained and errors due to aliasing are avoided. In practice, the sampling rate must be at least four samples per cycle (240 Hz).

In a transformer differential relay, inrush currents may be detected by checking the levels of second and fifth harmonics in the differential current. A cutoff frequency of 360 Hz is a practical choice. To guarantee proper observation of the fundamental, second and fifth harmonics, and to avoid aliasing, a sampling rate of at least 720 Hz (12 samples per second) is required [33].

#### 3.4.2.1 Practical filters specifications

An ideal filter has a pass band with unity gain and a stop band of zero gain. The transition from the pass band to the stop band is abrupt. However, in practical filters the transition from pass band to stop band is gradual, and takes place over a finite band of frequencies [35]. Moreover, for realizable filters, the gain cannot be zero over a finite band (Paley-Wiener conditions). As a result, there cannot be a true stop band for

practical filters. Therefore, stop band is better defined as a band over which the gain is less than a specified level. Similarly, pass band is also a band over which the gain is between 1 and a specified level.

### 3.4.2.2 Low-pass filter specifications

Low-pass filters are designed to pass frequencies, from zero to a frequency $\omega_p$ with an approximately unity gain [34]. The frequency range [0, $\omega_p$] is called the pass band of the filter. High frequencies, from a frequency $\omega_s$ and up, are attenuated. The frequency range [$\omega_s$, $\infty$] is called the stop band of the filter. The frequency range [$\omega_p$, $\omega_s$], between the pass and the stop band, is called the transition band.

A graphical description of the specifications of a low-pass filter is provided in Figure 3.4. The hatched areas in the pass band and in the stop band indicate forbidden magnitude values in these bands. In the transition band there are no forbidden values, but it is usually required that the magnitude decrease monotonically in this band.

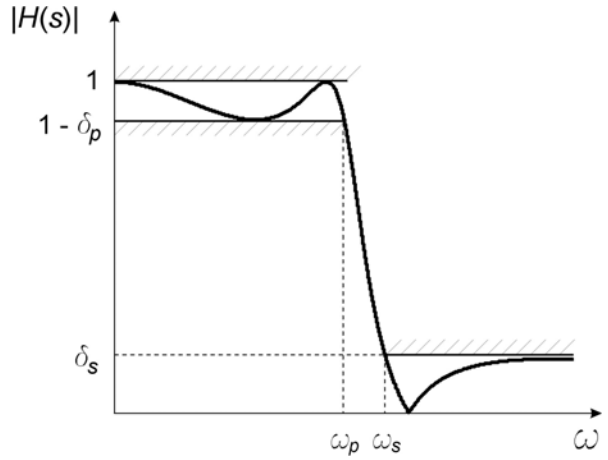


**Figure 3.4:** Specifications of a low-pass filter

The parameter $\delta_p$ is the tolerance of the magnitude response in the pass band. The desired (nominal) magnitude response in the pass band is 1. The parameter $\delta_s$ is the tolerance of the magnitude response in the stop band. The nominal magnitude response

in the stop band is zero. The –3 dB frequency is called the cutoff frequency, and it is defined as the frequency at which the magnitude response of the filter is $1/\sqrt{2}$ of its nominal value in the pass band. In Procedures for designing a family of IIR filters, which includes Butterworth, Chebyshev, and Elliptic filters, is presented.

### 3.4.2.3 Butterworth filters

The amplitude response $|H(\omega)|$ of an $N^{th}$ order Butterworth low pass filter is given by [35]

$$H(\omega) = \frac{1}{\sqrt{1 + (\omega/\omega_0)^{2N}}}, \tag{3.1}$$

where,

$N$ is the order of the filter

$\omega_0$ is the cutoff frequency

The procedure for designing Butterworth filters starts calculating the order of the filter ($N$) using the following expression.

$$N \geq \frac{\log\left(10^{-G_s/10} - 1\right) - \log\left(10^{-G_p/10} - 1\right)}{2\log\left(\omega_s/\omega_p\right)}, \tag{3.2}$$

where,

$G_p$ is the pass band gain in dB

$G_s$ is the stop band gain in dB

$[0, \omega_p]$ is the pass band frequency in radians

$[\omega_s, +\infty]$ is the stop band frequency in radians

Knowing the order of the filter $N$, the pass band frequency $\omega_p$ and the stop band frequency $\omega_s$, the cutoff frequency $\omega_c$ can be calculated employing either of the following equations.

$$\omega_c = \frac{\omega_p}{\left(10^{-G_p/10} - 1\right)^{1/2N}} \tag{3.3}$$

$$\omega_c = \frac{\omega_s}{\left(10^{-G_s/10} - 1\right)^{1/2N}} \tag{3.4}$$

The cut-off frequencies provided by Equations 3.3 and 3.4 are different; the choice of selecting a value is up to the designer and is influenced by the need to fulfill the requirements either in the pass band or in the stop band.

The poles of the normalized transfer function are determined by the following equation.

$$s_k = e^{\frac{j\pi}{2n}(2k+n-1)} \qquad k = 1, 2, \ldots, n \tag{3.5}$$

The normalized transfer function is determined by the values of the poles by using the following equation.

$$\hat{H}(s) = \frac{1}{(s - s_1)(s - s_2)\ldots(s - s_n)} \tag{3.6}$$

The final filter transfer function is obtained by replacing

$$H(s) = \hat{H}\left(s/\omega_c\right). \tag{3.7}$$

In Figure 3.5 is shown the frequency response of a 3rd order, 180 Hz cutoff frequency Butterworth filter whose transfer function is

$$H(s) = \frac{1446625279.519}{s^3 + 2261.9449\,s^2 + 2558197.2576\,s + 1446625279.519}.$$

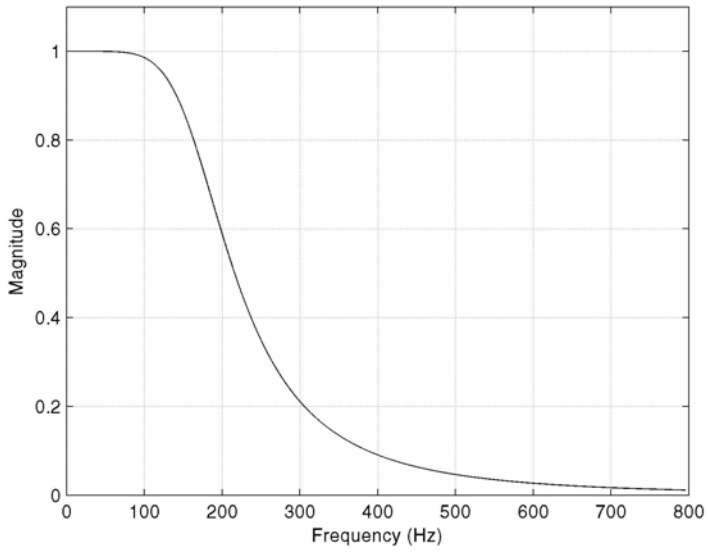


**Figure 3.5:** Frequency response of a Butterworth filter

### 3.4.2.4 Chebyshev filters

Chebyshev has noted that cos ($N\alpha$) is a polynomial of degree $N$ in cos $\alpha$. Even more, cosh ($N\alpha$) is the same polynomial of degree $N$ in cosh $\alpha$. Correspondingly, Chebyshev polynomial of degree $N$ is defined as [34]:

$$T_N(x) = \begin{cases} \cos(N \cos^{-1} x), & |x| \le 1, \\ \cosh(N \cosh^{-1} x), & |x| > 1, \end{cases} \tag{3.8}$$

Chebyshev polynomials can be constructed by the following recursive formula:

$$T_N(x) = 2xT_{N-1}(x) - T_{N-2}(x),\ T_0(x) = 1,\ T_1(x) = x \tag{3.9}$$

The main properties of Chebyshev polynomials are:

- For $|x| \leq 1$, $|T_N(x)| \leq 1$, and it oscillates between +1 and –1 proportional to $N$.
- For $|x| > 1$, $|T_N(x)| > 1$, and it is monotonically increasing in $|x|$.
- Chebyshev polynomials of odd orders are odd functions of $x$, and Chebyshev polynomials of even orders are even functions of $x$.

These properties are used for the construction of filters that are equiripple in either the pass band or stop band. The equiripple property provides sharp transition between the pass band and the stop band. As a result, the order of a Chebyshev filter needed to achieve given specifications is usually smaller than that of a Butterworth filter.

There are two kinds of Chebyshev filters: The first is equiripple in the pass band and monotonically decreasing in the stop band; it is known commonly as Chebyshev I. The second filter is monotonically decreasing in the pass band and equiripple in the stop band; it is known as Chebyshev II or Inverse Chebyshev.

#### 3.4.2.4.1 Chebyshev I filters

Chebyshev I filter is defined by the square magnitude frequency response [34]:

$$|H(\omega)|^2 = \frac{1}{1+\varepsilon^2 T_N^2(\omega/\omega_0)}, \tag{3.10}$$

where,

$N$ is the order of the filter

$\varepsilon = \sqrt{1-\delta_p)^{-2}-1}$

$\delta_p$ is the ripple band

$\omega_0$ is the cutoff frequency

The properties of Chebyshev I filters are:

- For $0 \le \omega \le \omega_0$, the properties of Chebyshev functions are as follows.

$$\frac{1}{1+\varepsilon^2} \le \left|H(\omega)\right|^2 \le 1 \tag{3.11}$$

- It can be shown that

$$H(0) = \begin{cases} \sqrt{\dfrac{1}{1+\varepsilon^2}}, & N \text{ even} \\ 1, & N \text{ odd} \end{cases} \tag{3.12}$$

- For $\omega > \omega_0$, the response is monotonically decreasing, because of the monotonic behavior of $T_N(x)$ for $|x|>1$. Furthermore, since $T_N(x)$ is an $N$th-order polynomial, the asymptotic attenuation of the filter is 20 dB per decade.
- The poles of the $N$th-order low pass filter of Chebyshev I type are given by

$$\begin{aligned} s_k = &-\omega_0 \sinh\left(\frac{1}{N}\sinh^{-1}\frac{1}{\varepsilon}\right)\sin\left[\frac{(2k+1)\pi}{2N}\right] \\ &+ j\omega_0 \cosh\left(\frac{1}{N}\sinh^{-1}\frac{1}{\varepsilon}\right)\cos\left[\frac{(2k+1)\pi}{2N}\right] \end{aligned} \tag{3.13}$$

  For $0 \le k \le N-1$

- The poles are located on an ellipse whose principal horizontal radius is $\sinh[N^{-1}(\sinh^{-1}\varepsilon^{-1})]$, and its principal vertical radius is $\cosh[(N^{-1}\sinh^{-1}\varepsilon^{-1})]$.
- A low pass Chebyshev I filter has no zeros.
- The transfer function of a Chebyshev I filter is given by

$$H(s) = H(0)\prod_{k=0}^{N-1}\frac{-s_k}{s-s_k} \tag{3.14}$$

In Figure 3.6 is shown the frequency response of a 3rd order, 180 Hz cutoff frequency Chebyshev I filter whose transfer function is

$$H(s) = \frac{1005963718.4905}{\mathrm{s}^3 + 1647.9864\,\mathrm{s}^2 + 1899804.6259\,\mathrm{s} + 1005963718.4905}.$$

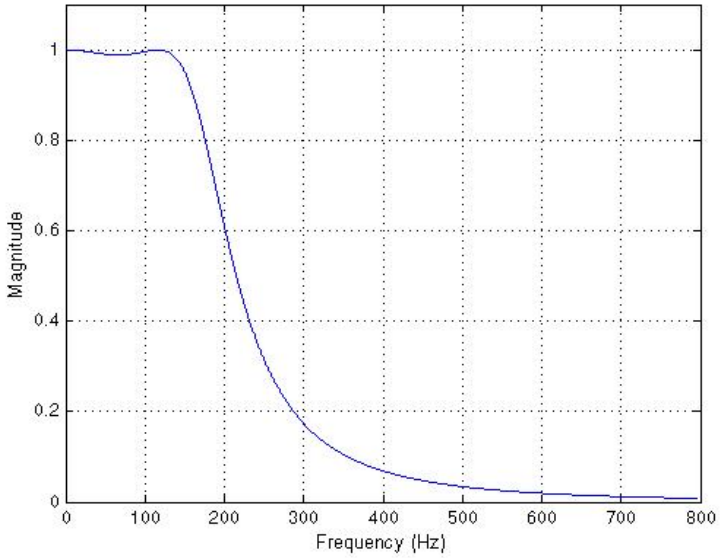


**Figure 3.6:** Frequency response of a Chebyshev I filter

### 3.4.2.4.2 Chebyshev II filters

Chebyshev II filter is defined by the frequency response defined by the following equation [34].

$$\begin{aligned}\left|H(\omega)\right|^2 &= 1 - \frac{1}{1+\varepsilon^2 T_N^2\left(\omega/\omega_0\right)} \\ &= \frac{\varepsilon^2 T_N^2\left(\omega/\omega_0\right)}{1+\varepsilon^2 T_N^2\left(\omega/\omega_0\right)}\end{aligned} \tag{3.15}$$

The salient properties of Chebyshev II filters are:

- For $\omega \geq \omega_0$, the bounds of the frequency response are defined by the following equation.

$$0 \leq \left|H(\omega)\right|^2 \leq \frac{\varepsilon^2}{1+\varepsilon^2} \tag{3.16}$$

- $|H(0)|^2 = 1$ for all $N$, $\omega_0$, and $\varepsilon > 0$
- For $0 \leq \omega \leq \omega_0$, the response is monotonically decreasing, because of the monotone behavior of $T_N(x)$ for $|x| > 1$.
- The poles of the $N$th-order low pass filter of Chebyshev II type are inversely proportional to those of a type I Chebyshev filter of the same order. The poles of the filter, $v_k$, for $0 \leq k \leq N$-1 are determined as follows.

$$v_k = \frac{\omega_0^2}{s_k}, \quad 0 \leq k \leq N - 1, \tag{3.17}$$

The poles $s_k$ are given by Equation 3.14; these poles are not located in an ellipse.

- The zeros of A Chebyshev II filter are given by the following equation.

$$u_k = \frac{j\omega_0}{\cos\left[\frac{(2k+1)\pi}{2N}\right]}, \quad 0 \leq k \leq N - 1 \tag{3.18}$$

- When $N$ is even, there are $N$ finite zeros. When $N$ is odd, there are only $N$-1 zeros, since $k = (N\text{-}1) / 2$ gives a zero at infinity.
- The transfer function of a Chebyshev II filter is given by

$$H(s) = \prod_{k=0}^{N-1} \frac{v_k (s - u_k)}{u_k (s - v_k)} \tag{3.19}$$

Where $(s\text{-}u_k) / u_k$ is replaced by –1 if $u_k = \infty$.

In Figure 3.7 is shown the frequency response of a 3rd order, 180 Hz cutoff frequency Chebyshev II filter defined by the transfer function

$$H(s) = \frac{379.33\,s^2 + 2023093451.6247}{s^3 + 2430.0089\,s^2 + 2880525.9979\,s + 2023093451.6247}.$$

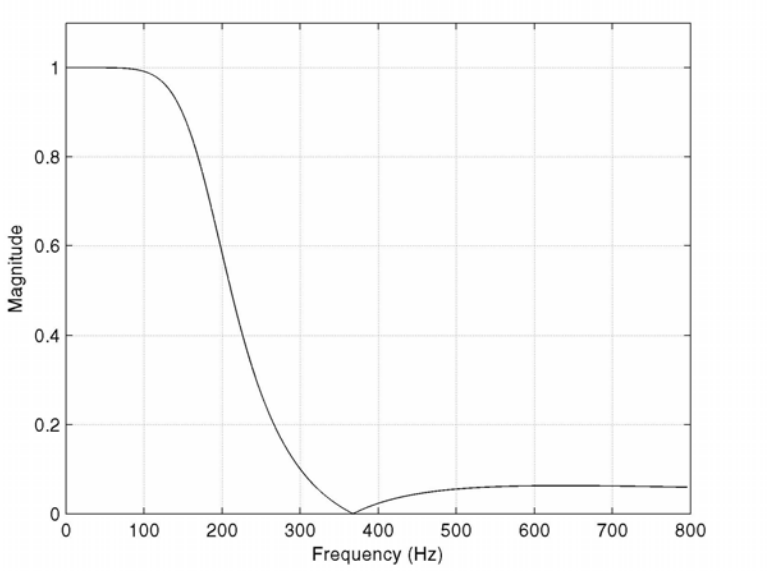


**Figure 3.7:** Frequency response of a Chebyshev II filter

### 3.4.2.5 Elliptic filters

An elliptic integral of the first kind is defined as follows [36].

$$u(\phi, k) = \int_0^{\phi} \frac{dy}{\sqrt{1 - k^2 \sin^2(y)}} \tag{3.20}$$

A special evaluation of Equation 3.20, known as the complete elliptic integral, is as follows.

$$K = u(\pi/2, k) \tag{3.21}$$

The trigonometric functions of the inverse of Equation 3.21 are defined as Jacobian elliptic trigonometric functions of $u$ with modulus $k$; the functions are as follows.

$$\begin{aligned} sn(u,k) &= \sin[\phi(u,k)]; \quad nc(u,k) = \sec[\phi(u,k)]; \\ cn(u,k) &= \cos[\phi(u,k)]; \quad ns(u,k) = \csc[\phi(u,k)]; \\ sc(u,k) &= \tan[\phi(u,k)]; \quad cs(u,k) = \cot[\phi(u,k)]. \end{aligned} \tag{3.22}$$

These Jacobian elliptic trigonometric functions are periodic functions with period of $4K$, if $u$ is real. Hence, $K$ is also called the quarter period. The quarter period or complete elliptic integral, as a function of the modulus $k$, is $K = \pi/2$ when the modulus $k = 0$. The value of $K$ does not change too much until $k$ approaches 1, when $K$ increases rapidly and tends to infinite.

Another parameter, the complementary modulus $k'$, is defined as follows

$$k^2 + k'^2 = 1 \tag{3.23}$$

Some of the most important properties for the elliptic functions, as functions of a complex variable, are as follows.

$$sn(jv,k) = j\, sc(v,k'); \quad cn(jv,k) = nc(v,k') \tag{3.24}$$

These relationships indicate that the elliptic functions are periodic in both the real and imaginary part of the argument, with periods related to $K$ and $K'$ respectively.

Noticing the similarity between the Chebyshev polynomials defined in Equation 3.8, the Chebyshev rational function is defined as a function of moduli $k$ and $k_1$ as follows.

$$R_N(x) = sn\left[n\ angsn(\omega, k), k_1\right] \tag{3.25}$$

The Chebyshev rational functions present equiripple properties, and are used in the construction of filters. Elliptic filters are equiripple in both the pass band and the stop band. They achieve the minimal possible order for given specifications. A low pass elliptic filter is defined by the frequency response as follows [34].

$$\left|H(\omega)\right|^2 = \frac{1}{1+\varepsilon^2 R_N^2\left(\omega/\omega_0\right)}, \tag{3.26}$$

In this equation, $R_N(x)$ is a Chebyshev rational function of degree $N$. The main properties of this function are as follows.

- It is an even function of $x$ for even values of $N$, and an odd function of $x$ for odd values of $N$ (similar to Chebyshev polynomials).
- In the range of $-1 \le x \le 1$, the function oscillates between –1 and 1 and all its zeros are in this range. Therefore, $|H(\omega)|^2$ oscillates between 1 and $1 / (1 + \varepsilon^2)$ for $-0 \le |\omega| \le \omega_0$.
- In the range $1 < |x| < \infty$, $|R_N(x)|$ oscillates between $1/d$ and $\infty$, where

$$d = \left(\frac{10^{Gp/10}-1}{10^{Gs/10}-1}\right)^{1/2} \tag{3.27}$$

As a result, $|H(\omega)|$ oscillates between 0 and $1 / (1 + \varepsilon^2 / d^2)$ in the range $\omega_0 \le |\omega| \le .\infty$. The order of the filter $N$ is the smallest integer satisfying

$$N = \frac{KK'_1}{K'K_1} \tag{3.28}$$

The locations of the zeros of the filter transfer function are defined by

$$\omega_{zi} = \frac{\pm 1}{k\, sn(iK/N, k)} \quad \text{for } i = \begin{cases} 0, 2, 4, ..., N-1 & N \text{ odd} \\ 1, 3, 5, ..., N-1 & N \text{ even} \end{cases} \tag{3.29}$$

The locations of the poles of the transfer function are defined by

$$s_{pi} = j\, sn\left( \frac{Ki}{N} + \frac{angsn[j(1/\varepsilon), k_1]}{n} j, k \right) \text{for } i = \begin{cases} 0, 2, 4, ..., N-1 & N \text{ odd} \\ 1, 3, 5, ..., N-1 & N \text{ even} \end{cases} \tag{3.30}$$

In Figure 3.8 is shown the frequency response of a 3rd order, 180 Hz cutoff frequency Elliptic filter whose transfer function

$$H(s) = \frac{307.7872\,s^2 + 1.2189^{-10}\,s + 1326185001.3231}{s^3 + 1695.2265\,s^2 + 2018954.6201\,s + 1326185001.3231}.$$

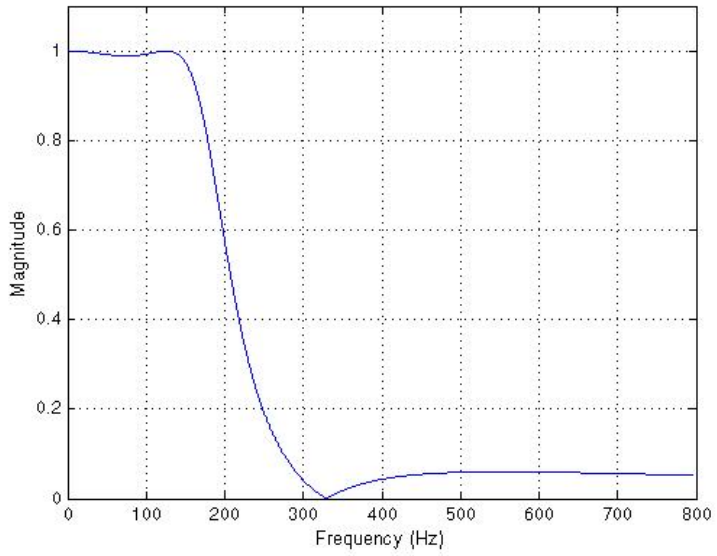


**Figure 3.8:** Frequency response of an Elliptic filter

### 3.4.2.6 Bilinear transformation

In order to be modeled, an analog filter must be transformed into an IIR digital filter. Several transformation methods can be used for this purpose but bilinear transformation is commonly used because of its simplicity and convenience in implementation. The bilinear transformation consists of the following substitution [34].

$$s \leftarrow \frac{2}{T} \cdot \frac{z-1}{z+1}, \tag{3.31}$$

where,

$T$ is the sampling interval

$s$ is the Laplace transform variable

$z$ is the z-transform variable

If the transfer function of an analog filter is *H(s)*, the transfer function of its corresponding digital filter is

$$H(z) = H(s)\Big|_{s=\frac{2(z-1)}{T(z+1)}} \tag{3.32}$$

The bilinear transformation preserves the number of poles and the order of the filter. The number of zeroes increases to match the number of poles.

Ideally, the frequency response of the digital filter should be close to that of the analog filter, fulfilling

$$\Omega = \omega T \tag{3.33}$$

where,

$\Omega$ is the digital-domain frequency

$\omega$ is the analog-domain frequency

However, the relationship of digital and analog frequencies in the bilinear transformation is given by

$$\Omega = 2 \cdot \tan^{-1}\left(\frac{\omega T}{2}\right). \tag{3.34}$$

The digital frequency $\Omega$ is *warped* with respect to the analog frequency $\omega$. At low frequencies, $\Omega \approx \omega T$, which is a linear relationship. The analog high frequencies are mapped to $\Omega = \pm\pi$.

To overcome the frequency warping introduced by bilinear transformation, it is a common practice to *prewarp* the specifications of the analog filter, in order that, after warping, they will be located at the desired frequencies. For this reason, it is necessary to design the analog filter using the following band edges equations:

$$\omega_p = \frac{2}{T}\tan\left(\frac{\Omega_p}{2}\right), \quad \omega_s = \frac{2}{T}\tan\left(\frac{\Omega_s}{2}\right). \tag{3.35}$$

After the analog filter has been transformed using the bilinear transformation, the resulting digital filter will have its band edges placed in the desired places.

### 3.4.2.7 Digital filter realization

Realization of a digital filter is made in two stages [34]:

1. *Construction of a block diagram of the filter*. Such a block diagram is known as realization of the filter. A realization is essentially a flow graph of signals in the

filter. It includes operations such as delays, additions, and multiplication of signals by constant coefficients.

2. *Implementation of the realization*, in either software or hardware.

#### 3.4.2.7.1 Building blocks of digital filters

Any digital system that is linear, time invariant, rational, and causal can be realized using three basic types of elements [34].

**Unit delay:** Its purpose is to hold the input for a unit of time (physically equal to the sampling interval T) before it is delivered to the output. Mathematically, it performs the following operation.

$$y[n] = x[n - a] \tag{3.36}$$

Unit delay is depicted schematically in Figure 3.9(a). The letter *D*, indicating delay, sometimes is replaced by $z^{-1}$, which is the delay operator in the *z* domain. Unit delay can be implemented in software in a storage variable, which changes its value when instructed by the program.

**Adder:** The purpose of the adder is to add two or more signals appearing at the input at a specific time. Mathematically, it performs the operations like the one shown in the following equation.

$$y[n] = x_1[n] + x_2[n] + ... \tag{3.37}$$

An adder is depicted schematically in Figure 3.9(b).

**Multiplier:** The purpose of this element is to multiply a signal (a varying quantity) by a constant number, such as the one shown in the following equation.

$$y[n] = ax[n] \tag{3.38}$$

A multiplier is depicted schematically in Figure 3.9(c). There is no specific symbol for the multiplier, but to show its operation, a constant factor is placed above or besides the signal line.

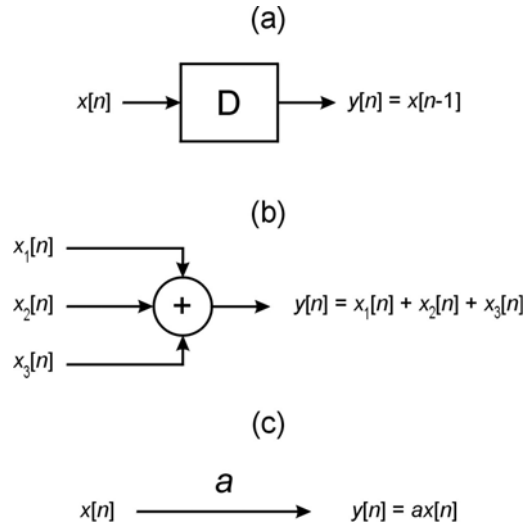


**Figure 3.9:** Basic elements to build digital filters
**(a)** Unit delay, **(b)** Adder, **(c)** Multiplier

### 3.4.2.7.2 Direct realization of IIR systems

Let *H(z)* be a rational, causal, stable transfer function in which the order of the polynomials in the numerator and denominator are equal. This transfer function can be mathematically expresses as follow [34].

$$H(z) = \frac{b(z)}{a(z)} = \frac{b_0 + b_1 z^{-1} + ... + b_N z^{-N}}{1 + a_1 z^{-1} + ... + a_N z^{-N}} \tag{3.39}$$

It can be shown that an auxiliary signal $u[n]$, the input $x[n]$ and the output $y[n]$ defined by the following equations represent the use of the transfer function defined by Equation 3.39.

$$u[n] = -a_1 u[n-1] - \ldots - a_N u[n-N] + x[n] \tag{3.40}$$

$$y[n] = -b_0 u[n] + b_1 u[n-1] + \ldots + b_N u[n-N] \tag{3.41}$$

In Figure 3.10 is shown a realization of these equations. By passing $u[n]$ through a chain of $N$ delay elements, signals $\{u[n\text{-}1],\ u[n\text{-}2],\ \ldots,\ u[n\text{-}N]\}$ are obtained. Then $u[n]$ is formed as a linear combination of the delayed signals and the input signal $x[n]$. $N$ multipliers are needed for using the coefficients $\{-a_1,\ \ldots,\ -a_N\}$, and $N$ binary adders to form the sum. The realization uses feedback; it builds the present value of the signal $u[n]$ from its past values and the present value of the input signal $x[n]$.

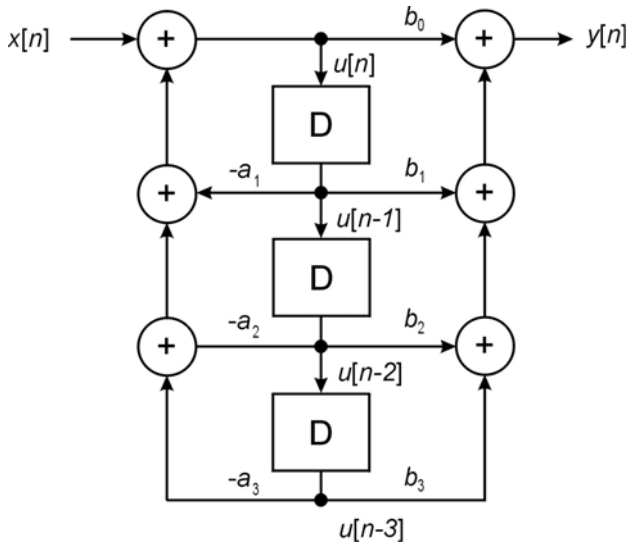


**Figure 3.10:** Direct realization of a digital IIR system

To generate the output $y[n]$ from the auxiliary signal $u[n]$ and its delayed values, $N$+1 multipliers for using the coefficients $\{b_0,\ \ldots,\ b_N\}$ are added in addition to $N$ delay elements. The realization shown in Figure 3.10 is called a direct realization. In this

realization, the number of delay elements, *N,* is equal to the orders of the polynomials in the numerator and denominator of the transfer function. As well, there are 2*N*+1 multipliers and 2*N* adders. The realization is recursive, since it generates present values of its internal signals from past values of these signals.

### 3.4.3 Analog-to-digital converter

An analog-to-digital converter (A/D converter or ADC) takes the instantaneous value of an analog voltage and converts it into an *n*-bit binary number that can be easily manipulated by a microprocessor. The *n*-bit number is a binary fraction representing the ratio between the input voltage and the full-scale voltage of the converter. A number of techniques can be used to achieve this conversion. The full-input voltage ranges for an ADC are typically 0 to +5 or 0 to +10 volts for unipolar operations, and –5 to +5 or –10 to +10 volts for bipolar operation [37].

#### 3.4.3.1 Sample-and-hold techniques

The basic function of a sample-and-hold in an analog input system is to capture an input signal and hold it constant during the subsequent ADC conversion cycle. For the sake of illustration, a very simple circuit consisting of only a switch and a hold capacitor $C_H$ is shown in Figure 3.11. When the switch is closed, the capacitor charges up to the level of the input signal. The capacitor holds the charge to this level when the switch is opened.

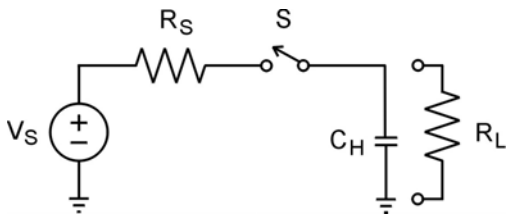


**Figure 3.11:** Simple sample-and-hold circuit

In Figure 3.12 is shown the operation of a sample-and-hold system in the time domain. Up until time $T_1$, the output is in the hold mode. At time $T_1$, the circuit is told to reacquire the input. The acquisition time $T_{AC}$ is the time required for the circuit output to become equal to its input. The output then follows the input until the circuit is again put in the hold mode at $T_2$. A small amount of time $T_{AP}$, the aperture time, is required for the circuit to actually switch to hold mode. During this time the output signal may change slightly from the value at $T_2$, such variation is called aperture uncertainty. Typical values for acquisition time, aperture time, and aperture uncertainty are 5, 0.005 and 0.01 microseconds, respectively [37].

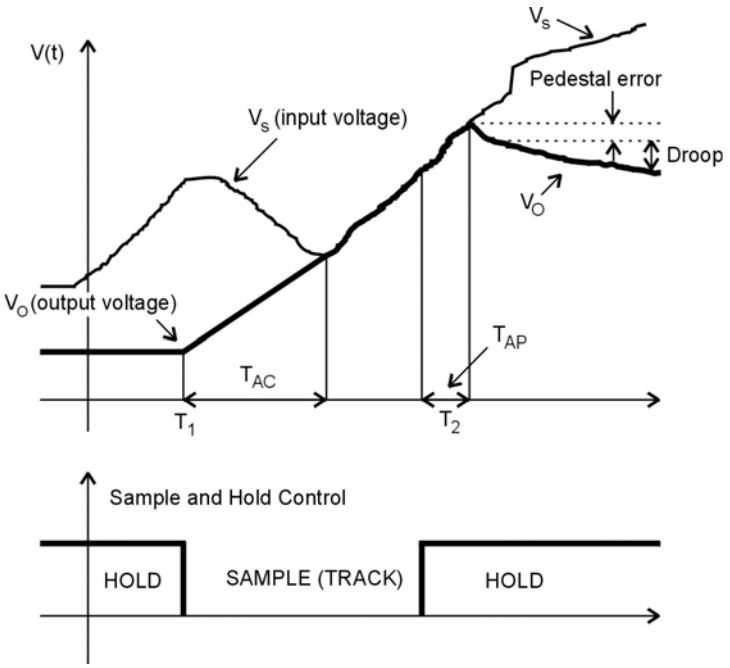


**Figure 3.12:** Operation of the sample-and-hold circuit in the time domain

The sample-and-hold is used in the numerical relay for analog–to-digital conversion. A comparison of the most common ADC techniques is displayed in Table 3.1 [37]. The medium-speed, medium-cost successive approximation ADC is a common choice in digital protection and control systems.

| Converter | Conversion rate | Cost / complexity | Comments |
|---|---|---|---|
| Tracking | | Low | Needs slowly varying input signal; output always available |
| Counter ramp | Slow | Low | Need stable input |
| Single ramp | Slow | Low | Lack stability with time and temperature |
| Dual ramp | Slow | Medium | Integrates input signal; can be used at high resolutions – 20 bits or more |
| Successive approximation | Fast | Medium | Need stable input |
| Parallel flash | Fastest | High | Output always available |

**Table 3.1:** Comparison of ADC techniques

### 3.4.3.2 Multiplexing

The analog multiplexer consists of an array of analog switches controlled with digital logic. The analog multiplexer uses the digital control logic to select a specific analog input and direct it to its output. In the generalized relay model of Figure 3.1, the analog multiplexer is applied to select one sample-and-hold output channel at a time for subsequent analog scaling and analog-to-digital conversion. During a sampling interval, the multiplexer brings all the sampled-and-held signals one at a time for analog-to-digital conversion. The multiplexer is not relevant for modeling of numerical relays, because the multiplexer does not affect the analog inputs. For the purposes of this thesis, it is assumed that the multiplexing process is accomplished seamlessly.

### 3.4.3.3 Software modeling of ADC

Software modeling of an ADC is reduced to calculating the number that is proportional to the level of the analog input. Software modeling of the ADC requires that the following information is available.

- Word size of the converter in number of bits used in the quantization process
- Range of the analog input quantized by the converter without saturation
- Whether the ADC truncates or rounds the input to the next higher integer value
- The method used for representing the negative numbers

Suppose that the ADC has a word size of $(b+1)$ bits and a range of $-Y$ to $+Y$. For a positive input of $X$ volts, the digitized value $Z_{10}$ is defined as follows.

$$Z_{10} = INT \text{ or } RON\left[\frac{X\left(2^b - 1\right)}{Y}\right], \tag{3.42}$$

where,

$Z_{10}$ is the integer value of base 10
$INT$ is the truncation operation
$RON$ is the rounding operation

For a negative input of $X$ volts, the digitized value $Z_{10}$ is calculated by one of the following representations.

- One's complement representation

$$Z_{10} = \left[2^{b+1} - 1\right] - INT \text{ or } RON\left[\frac{|X|\left(2^b - 1\right)}{Y}\right] \tag{3.43}$$

- Two's complement representation

$$Z_{10} = INT \text{ or } RON\left[\frac{(2Y - |X|)2^b}{Y}\right] \tag{3.44}$$

- Sign and magnitude representation

$$Z_{10} = 2^b - INT \text{ or } RON\left[\frac{|X|(2^b - 1)}{Y}\right] \tag{3.45}$$

$Z_{10}$ is always an integer, irrespective of whether an input is an integer or not. When the output $Z_{10}$ is converted to its binary equivalent, the result provides the state of an ADC output bits. However, such an output must account for the resolution of the ADC converter in order to provide proper output value. An ADC converter refers to the output of the ADC converter changes by one *least significant bit* (LSB) whose worth is given by the following equation.

$$\text{Resolution} = \frac{\text{Y}}{2^{\text{b}} - 1} \tag{3.46}$$

The floating point representation of an ADC output can be computed considering whether an input is positive or negative, and the method used for representing negative numbers. For positive numbers, the equivalent floating-point output (FP) can be computed by using the following equation.

$$\text{FP} = Z_{10} \cdot \text{Resolution} \tag{3.47}$$

The following equations can be used for determining the floating point representations of negative numbers represented by the One's complement, Two's complement and Sign and Magnitude methods, respectively.

$$\mathrm{FP} = \left[Z_{10} - 2^{b+1} + 1\right] \cdot \text{Resolution} \tag{3.48}$$

$$\mathrm{FP} = \left[Z_{10} - 2^{b+1}\right] \cdot \text{Resolution} \tag{3.49}$$

$$\mathrm{FP} = \left[Z_{10} - 2^{b}\right] \cdot \text{Resolution} \tag{3.50}$$

### 3.4.3.4 Numerical example of analog-to-digital conversion

The following examples illustrate the application of the conversion formulas given in the previous section. The integer representation, resolution and floating-point output for an input voltage of 1.25 volts applied to a 16-bit ADC that can receive inputs in the –10 to 10 volts range are calculated in this example.

Word size = b+1 = 16 bits

Y = 10

$X = 1.25$

$$Z_{10} = RON\left[\frac{(1.25)(2^{15} - 1)}{10}\right]$$
$$= 4096$$

$$\text{Resolution} = \frac{10}{2^{15} - 1}$$
$$= 0.0003052782611350246$$

$$FP = Z_{10} \cdot \text{Resolution}$$
$$= 1.25041975760906$$

The integer representation, resolution and floating-point output for an input voltages of –1.25 volts applied to a 16-bit ADC that can receive inputs in the –10 to 10 volts range are calculated using the One's complement, the Two's complement and the Sign and Magnitude methods in the following examples.

$X = -1.25$

- One's complement method

$$Z_{10} = (2^{16} - 1) - RON\left[\frac{|-1.25|(2^{15} - 1)}{10}\right]$$
$$= 61439$$
$$\text{FP} = \left[61439 - 2^{16} + 1\right] \cdot 0.0003052782611$$
$$= -1.25041975760906$$

- Two's complement method

$$Z_{10} = RON\left[\frac{(2[10] - |-1.25|)2^{15}}{10}\right]$$
$$= 61440$$
$$\text{FP} = \left[61440 - 2^{16}\right] \cdot 0.0003052792611$$
$$= -1.25041975760906$$

- Sign and Magnitude method

$$Z_{10} = 2^{15} - RON\left[\frac{|-1.25|(2^{15} - 1)}{10}\right]$$
$$= 28672$$
$$\text{FP} = \left[28672 - 2^{15}\right] \cdot 0.0003052782611$$
$$= -1.25041975760906$$

### 3.4.4 Phasor estimation algorithms

Algorithms are programs used in microprocessors that manipulate the samples of voltages and currents to produce parameters of interest. Most of the existing algorithms proposed for use in numerical relays can be grouped in two categories. The first type is based on a model of the waveform itself. The second type involves a model of the element being protected, such a transmission line or a power transformer [25].

The types of algorithms applied in the present thesis are related with waveform-model algorithms. The parameters of interest for the relaying application are contained in the waveform description. Application of the waveform-model algorithms includes the following processes.

- The peak value of sinusoidal current for overcurrent protection
- The fundamental frequency voltage and current phasors for distance relaying
- The magnitude of harmonics in waveforms of currents for harmonic restrain in transformer protection
- The fundamental frequency of a periodic signal for frequency relays

The information necessary for waveform algorithms is taken from sampling the signals at equal intervals over a pre-specified time period usually referred to as a data window. After the required parameters are calculated, a new sample is incorporated to the data window, and the oldest sample is discarded. The calculations of the required parameters are performed and the process continues seamlessly. Some of the waveform-model algorithms are described in this section. These algorithms can be divided in the following categories.

- Non-recursive
    - Short window algorithms
        - Miki and Mikano
        - Mann and Morrison

        - Rockefeller and Udren
        - Gilbert and Shovlin
    - Long window algorithm
        - Discrete Fourier Transform
        - Walsh Functions
        - Least Square Error
- Recursive
    - Kalman Filtering
    - Recursive Least Square Error

### 3.4.4.1 Non-recursive short window techniques

Short window techniques make the assumption that the signals are sinusoids of the nominal frequency, and that the system frequency is invariant. Depending on the technique, only two or three samples are necessary to estimate phasors with short window algorithms. A phasor is a representation of a sinusoidal voltage or current of the nominal frequency, $f_0$, and its positive going zero crossing is $\theta$ radians ahead of the time equal to zero. The mathematical representation of a phasor is as follows.

$$\begin{aligned} \vec{V} &= |V| e^{j\theta} \\ &= |V| \left( \cos\theta + j \sin\theta \right) \end{aligned}, \tag{3.51}$$

The real and imaginary parts of the phasor are expressed as follows.

$$\mathrm{Re}(\vec{V}) = |V| \cdot \cos\theta \tag{3.52}$$

$$\mathrm{Im}(\vec{V}) = |V| \cdot \sin\theta \tag{3.53}$$

The magnitude and phase of the phasor can be calculated using the real and the imaginary parts of the phasor as follows.

$$|V| = \sqrt{\mathrm{Re}(\vec{V})^2 + \mathrm{Im}(\vec{V})^2} \tag{3.54}$$

$$\tan\theta = \frac{\mathrm{Im}(\vec{V})}{\mathrm{Re}(\vec{V})} \tag{3.55}$$

Following sections are dedicated to describe the commonly used non-recursive short window techniques.

#### 3.4.4.1.1 Miki and Mikano technique

Figure 3.13 shows a typical waveform of a voltage that can be defined by

$$v(t) = V_p \sin(\omega_0 t + \theta), \tag{3.56}$$

where,

| | |
|---|---|
| $v$ | is the voltage waveform as a function of time |
| $V_p$ | is the peak value of the voltage |
| $\omega_0$ | is the fundamental angular frequency = $2\pi f$ |
| $\theta$ | is the displacement angle of the signal from a reference |

The voltage is sampled every $\Delta t$ seconds. Two samples of the waveform are shown in Figure 3.13. At $t=0$, Equation 3.56

$$\begin{aligned} v(0) &= v_0 \\ &= V_p \sin\theta \end{aligned} \tag{3.57}$$

represents the imaginary part of the phasor $V$.

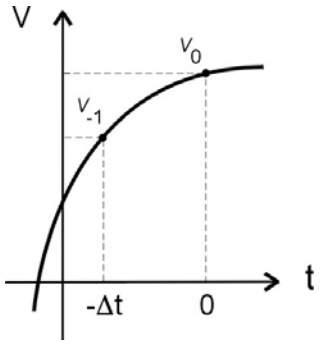


**Figure 3.13:** A voltage waveform sampled two times

Evaluating Equation 3.56 at $t=\Delta t$, and at $t=-\Delta t$, becomes

$$\begin{aligned} v(\Delta t) &= v_{+1} \\ &= V_p \sin\left(\omega_0 \Delta t + \theta\right) \end{aligned} \tag{3.58}$$

$$\begin{aligned} v(-\Delta t) &= v_{-1} \\ &= V_p \sin\left(-\omega_0 \Delta t + \theta\right) \end{aligned} \tag{3.59}$$

Expanding the sine $(-\Delta t+\theta)$ by using the well known trigonometric identity provides

$$v_{-1} = V_p \left[\sin(-\omega_0 \Delta t)\cos\theta + \cos(-\omega_0 \Delta t)\sin\theta\right]. \tag{3.60}$$

Substituting $V_p \sin\theta$ from Equation 3.57 and rearranging provides

$$V_p \cos\theta = \frac{v_{-1} - v_0 \cos(-\omega_0 \Delta t)}{\sin(-\omega_0 \Delta t)}, \tag{3.61}$$

This is the real part of the voltage phasor.

### 3.4.4.1.2 Mann and Morrison technique

In Figure 3.14 is shown a typical sinusoid waveform defined by Equation 3.56. The waveform is sampled every $\Delta t$ seconds, and three samples of the voltage are shown in Figure 3.14. Consider that Equation 3.57 represents the imaginary part of vector *V*.

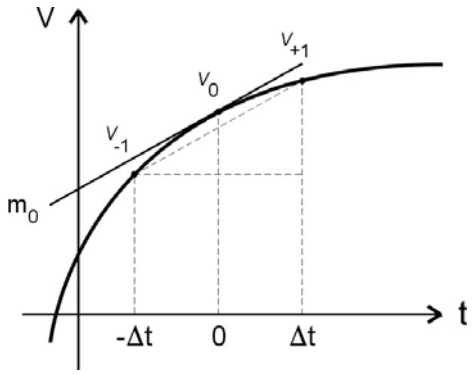


**Figure 3.14:** Mann and Morrison phasor estimation technique

Differentiating both sides of Equation 3.56 produces the following expression.

$$v' = \omega_0 V_p \cos(\omega_0 \Delta t + \theta). \tag{3.62}$$

Evaluating this equation at *t=0* provides

$$\begin{aligned} v'_0 &= \omega_0 V_p \cos\theta \\ &= m_0 \end{aligned} \tag{3.63}$$

In Figure 3.14, the slope of the line joining $v_{-1}$ and $v_{+1}$ is almost the same that $m_0$.Therefore

$$\omega_0 V_p \cos\theta \approx \frac{v_{+1} - v_{-1}}{2\Delta t}. \tag{3.64}$$

Rearranging this equation provides the real part of phasor *V*.

$$V_p \cos\theta = \frac{v_{+1} - v_{-1}}{2\omega_0 \Delta t}. \tag{3.65}$$

#### 3.4.4.1.3 Rockefeller and Udren technique

The second derivative of Equation 3.56 is

$$v'' = -\omega_0^2 V_p \sin(\omega_0 t + \theta). \tag{3.66}$$

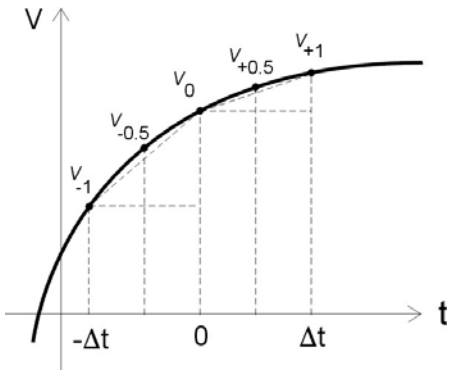


**Figure 3.15:** Rockefeller and Udren phasor estimation technique

Intermediate points $v_{-0.5}$ and $v_{+0.5}$ between the three samples $v_{-1}$, $v_0$ and $v_{+1}$ are shown in Figure 5.15. The slope of the line joining $v_{-1}$ and $v_0$ is almost the same that the slope of the tangent at $v_{-0.5}$. Similarly, the slope of the waveform at $v_{+0.5}$ is the same as the slope of the line joining $v_0$ and $v_{+1}$. The following equations express this observation.

$$v'_{+0.5} = \frac{v_0 - v_{-1}}{\Delta t}, \tag{3.67}$$

$$v'_{-0.5} = \frac{v_{+1} - v_0}{\Delta t}. \tag{3.68}$$

The second derivative of the waveform in $t$=0 is equal to

$$v''_0 = \frac{v'_{+0.5} - v'_{-0.5}}{\Delta t}. \tag{3.69}$$

Substituting for $v'_{+0.5}$ and $v'_{-0.5}$ from Equations 3.67 and 3.68 in Equation 3.69 gives

$$v''_0 = \frac{-v_{-1} + 2v_0 - v_{+1}}{(\Delta t)^2}. \tag{3.70}$$

Substituting this equation in Equation (3.66) provides

$$-\omega_0^2 V_p \sin\theta \approx \frac{-v_{-1} + 2v_0 - v_{+1}}{(\Delta t)^2}. \tag{3.71}$$

Summarizing, the real part of vector $V$ at $t = 0$ is the same as Equation 3.64, as in Mann and Morrison algorithm. The imaginary part provided by Equation 3.71, is

$$V_p \sin\theta = \frac{v_{-1} - 2v_0 + v_{+1}}{(\omega_0 \Delta t)^2} \tag{3.72}$$

#### 3.4.4.1.4 Gilbert and Shovlin technique

The product of $v_{-1}$ and $v_{+1}$ defined by Equations 3.58 and 3.59 provides the following expression.

$$v_{-1} \cdot v_{+1} = V_p \sin(-\omega_0 \Delta t + \theta) \cdot V_p \sin(\omega_0 \Delta t + \theta). \tag{3.73}$$

Using a well-known trigonometric equivalence, the right hand side of this equation can be expands and the following equation follows.

$$v_{-1} \cdot v_{+1} = V_p^2[\sin(-\omega_0 \Delta t)\cos\theta + \cos(-\omega_0 \Delta t)\sin\theta)] \\ [\sin(-\omega_0 \Delta t)\cos\theta + \cos(-\omega_0 \Delta t)\sin\theta)] \quad (3.74)$$

Further simplification of this equation produces the following equation.

$$v_{-1} \cdot v_{+1} = V_p^2[-\sin^2(\omega_0 \Delta t)\cos^2\theta + \cos^2(\omega_0 \Delta t)\sin^2\theta)]. \quad (3.75)$$

The operation suggested in the following expression is developed employing Equation 3.57.

$$v_0^2 - v_{-1} \cdot v_{+1} = V_p^2 \sin^2\theta - v_{-1} \cdot v_{+1}. \quad (3.76)$$

Replacing Equation 3.75 in Equation 3.76, and simplifying produces

$$v_0^2 - v_{-1} \cdot v_{+1} = V_p^2 \sin^2(\omega_0 \Delta t). \quad (3.77)$$

Thus, the magnitude of the phasor is given by

$$V_p^2 = \frac{v_0^2 - v_{-1}v_{+1}}{\sin^2(\omega_0 \Delta t)}. \quad (3.78)$$

### 3.4.4.2 Advantages and disadvantages of short window techniques

Short window algorithms are simple techniques that use a few samples and can be implemented with few computations. The estimation of phasor with short window techniques is, therefore, relatively quick. However, short window techniques are

adversely affected by the presence of decaying DC and harmonic components in the waveform. Additionally, these techniques amplify the noise, which adversely affects the phasor estimates.

### 3.4.4.3 Non-recursive long window techniques

Long window techniques use data from one-half cycle of the fundamental frequency. Modern numerical relays typically use 64 samples per cycle. Discrete Fourier Transform (DFT), Least Error Square and Walsh Function algorithms are among the most popular phasor estimation techniques employed in numerical relays.

#### 3.4.4.3.1 Discrete Fourier Transform algorithm

A periodic waveform can be expressed as a linear combination of two orthogonal functions. The Discrete Fourier Transform algorithm (DFT) employs the sine and cosine functions, which are well known orthogonal functions, to estimate the phasors of sinusoidal waveforms. Two functions $f(x)$ and $g(x)$ are orthogonal over the interval $[a, b]$ if the following expression is satisfied.

$$\begin{aligned} \langle f(x) \perp g(x) \rangle &\equiv \int_a^b f(x)g(x)dx \\ &= 0 \end{aligned} \tag{3.79}$$

The orthogonality of $f(x) = \sin(x)$ and $g(x) = \cos(x)$ in the interval $[-\pi, +\pi]$ is determined by the following expression.

$$\begin{aligned} \langle \sin(x) \perp \cos(x) \rangle &\equiv \int_{-\pi}^{+\pi} \sin(x)\cos(x)dx \\ &= 0 \end{aligned} \tag{3.80}$$

$W = \langle \sin(x) \perp \cos(x) \rangle$ is an orthonormal basis in the interval [-π, +π]. The projection of a function $f(\omega t)$ over the orthonormal basis $W$ is

$$proj_W[f(\omega t)] = \langle f(\omega t), \sin(\omega t) \rangle \sin(\omega t) + \langle f(\omega t), \cos(\omega t) \rangle \cos(\omega t) . \qquad (3.81)$$

Consider that the phasor of the following sinusoidal waveform is to be estimated.

$$v(\omega t) = V_p \sin(\omega t + \theta). \qquad (3.82)$$

The orthogonality of the sinusoidal waveform and the sine function is evaluated using Equation 3.79 as follows.

$$\begin{aligned} \langle v(\omega t), \sin(\omega t) \rangle &= \int_{-\pi}^{+\pi} (V_p \sin(\omega t + \theta) \sin \omega t) d\omega t \\ &= \pi V_p \cos\theta \end{aligned} . \qquad (3.83)$$

Solving to the well-know expression $V_p \cos\theta$ produces

$$V_p \cos\theta = \frac{1}{\pi} \int_{-\pi}^{+\pi} (V_p \sin(\omega t + \theta) \sin \omega t) d\omega t . \qquad (3.84)$$

Similarly, the evaluation of the orthogonality of the sinusoidal waveform and the cosine function is given by the following equation.

$$\begin{aligned} \langle v(\omega t), \cos(\omega t) \rangle &= \int_{-\pi}^{+\pi} (V_p \sin(\omega t + \theta) \cos \omega t) d\omega t \\ &= \pi V_p \sin\theta \end{aligned} . \qquad (3.85)$$

And,

$$V_p \sin\theta = \frac{1}{\pi}\int_{-\pi}^{+\pi}(V_p \sin(\omega t + \theta)\cos\omega t)d\omega t \,. \tag{3.86}$$

If the voltage waveform of Equation 3.82 is sampled $N$ times at a $\Delta t$ sampling step in the interval of one period, then Equations 3.84 and 3.86 estimate the real and imaginary components of the phasor of the waveform defined by Equation 3.82.

$$\begin{aligned} \mathrm{Re}(V) &= V_p \cos\theta \\ &= \frac{2}{N}\sum_{i=1}^{N} v_i \sin(\omega i \Delta t) \end{aligned} \tag{3.87}$$

$$\begin{aligned} \mathrm{Im}(V) &= V_p \sin\theta \\ &= \frac{2}{N}\sum_{i=1}^{N} v_i \cos(\omega i \Delta t) \end{aligned} \tag{3.88}$$

Equations 3.87 and 3.88 imply that the sine and cosine functions must be sampled at the same rate at which the voltage waveform $v$ was sampled. The first sample in the sampling window of the voltage waveform is multiplied by the first sample in the sine or cosine function, the second sample in the sampling window is multiplied by the second sample in the sine or cosine function, and so on.

#### 3.4.4.3.2 Walsh function technique

The Walsh functions consist of trains of periodic square pulses of states -1 and 1. The initial state of Walsh function is always +1. The even and odd functions, depicted in the Figure 3.16, constitute an orthogonal basis for voltage waveforms in the same manner that the sine and cosine functions constitute a basis for the voltage waveforms in the DFT algorithm.

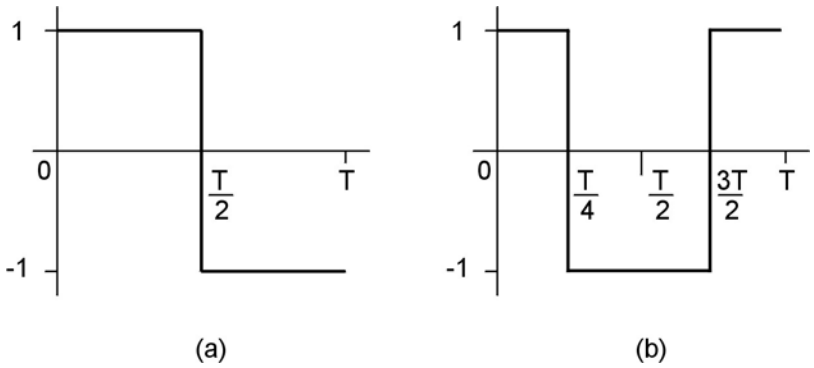


**Figure 3.16:** Walsh functions (a) Even and (b) Odd functions

The real and imaginary components of the phasor estimated by the Walsh function are expressed as following.

$$\begin{aligned} \mathrm{Re}(V) &= V_p \cos\theta \\ &= \frac{2}{N}\sum_{i=1}^{N} v_i W_2(\omega_i \Delta t)\,, \end{aligned} \tag{3.89}$$

$$\begin{aligned} \mathrm{Im}(V) &= V_p \sin\theta \\ &= \frac{2}{N}\sum_{i=1}^{N} v_i W_1(\omega_i \Delta t)\,, \end{aligned} \tag{3.90}$$

where,

$W_1(.)$ is the sampled values of the even Walsh function shown in Figure 3.16(a)

$W_2(.)$ is the sampled values of the odd Walsh function shown in Figure 3.16(b)

As implied, the Walsh functions period is the same as the period of the waveform whose phasor is to be estimated, and they ought to be sampled at the same rate.

### 3.4.4.3.3 Least Square Error technique

Consider a set of measurements that satisfy

$$a + bt = m, \tag{3.91}$$

where,

$m$ is a measurement

$a, b$ are unknown parameters to be estimated

If $\hat{a}$ and $\hat{b}$ are the estimated values, then

$$\hat{a} + \hat{b}t - m = \varepsilon, \tag{3.92}$$

where,

$\varepsilon$ is the error between estimation and measurement.

If $n$ measurements are taken at regular intervals, they can be arranged in the matrix form as follows.

$$\begin{bmatrix} 1 & t_1 \\ 1 & t_2 \\ \dots & \dots \\ 1 & t_n \end{bmatrix} \begin{bmatrix} \hat{a} \\ \hat{b} \end{bmatrix} - \begin{bmatrix} m_1 \\ m_2 \\ \dots \\ m_n \end{bmatrix} = \begin{bmatrix} \varepsilon_1 \\ \varepsilon_2 \\ \dots \\ \varepsilon_n \end{bmatrix}. \tag{3.93}$$

The previous expression also can be written in the following fashion.

$$[A][\hat{x}] - [m] = [\varepsilon]. \tag{3.94}$$

Errors deviated from the actual measurements may be positive or negatives. A better way to assess the error is by finding the error squared.

$$[\varepsilon]^T [\varepsilon] = \left[ [\hat{x}]^T [A]^T [A][\hat{x}] \right] - 2[\hat{x}]^T [A]^T [m] + [m]^T [m] \tag{3.95}$$

The sum of the squares of the errors is minimum if the first derivative of the sum of the squares of the errors is zero. To determine the condition for the minimum sum of the squares of the errors the following equation should be satisfied. Simplifying,

$$\begin{aligned}\frac{d}{dt}\left[[\varepsilon]^T[\varepsilon]\right] &= 2[A]^T[A][\hat{x}] - 2[A]^T[m] \\ &= [0]\end{aligned} \tag{3.96}$$

$$\begin{aligned}[\hat{x}] &= \left[\left[[A]^T[A]\right]^{-1}[A]^T\right][m] \\ &= [A]^{-L}[m]\end{aligned} \tag{3.97}$$

The matrix $[A]^{-L}$ is known as the Left pseudo-inverse matrix of $[A]$. If $[A]$ is a [$n$ x $p$] matrix, with $n$ samples and $p$ unknowns, the Left pseudo-inverse matrix of $[A]$ is a [$p$ x $n$] matrix. If the sampling times are known in advance, the Left pseudo-inverse matrix of $[A]$ can be calculated in advance in an off-line mode. Once the sampling data is available, the phasor representing the waveform can be calculated using Equation (3.97). This procedure is known as the Least Square Error (LSE) algorithm.

In LSE, it is assumed that the sampled waveforms of voltages and currents are sinusoidal waveforms of known frequencies (fundamental frequency and harmonics). Thus, a couple of orthogonal sinusoidal functions, related to each frequency of interest, are included in the LSE estimation process. Consider the following voltage waveform expression.

$$v = V_{np}\sin(n\omega t + \theta_n), \tag{3.98}$$

where,

$n$ is an integer showing the multiple of fundamental frequency

$V_{np}$ is the peak magnitude of the waveform

$\omega$ is the fundamental frequency

$\theta_n$ is the phase displacement of the harmonic from a fixed reference

Equation 3.98 is expanded in the following manner.

$$v = V_{np} \sin\theta_n \cos n\omega t + V_{np} \cos\theta_n \sin n\omega t\,, \tag{3.99}$$

where,

$V_{np}\sin\theta_n$ is real component of the phasor of frequency $n\omega$

$V_{np}\cos\theta_n$ is imaginary component of the phasor of frequency $n\omega$

The DC component can be included as well as a linearly decaying component. Consider that the DC component is of the following form.

$$v = V_0 e^{-\frac{t}{\tau}}. \tag{3.100}$$

The first two terms of the Taylor's series of Equation 3.100 are

$$V_0 e^{-\frac{t}{\tau}} = V_0 - V_0 \frac{t}{\tau}. \tag{3.101}$$

Suppose that the waveform to be estimated is of the form

$$v = \left\{\sum_{n=1}^{N} V_n \cos\theta_n \sin n\omega_0 t\right\} + \left\{\sum_{n=1}^{N} V_n \sin\theta_n \cos n\omega_0 t\right\} + V_0 - \frac{V_0}{\tau} t\,. \tag{3.102}$$

At the time $t$ = 0, the first sample is evaluated by Equation 3.102 in the following manner.

$$
\begin{aligned}
v_0 &= V_1 \sin[\omega_0(0)\Delta t]\cos\theta_1 + V_1 \cos[\omega_0(0)\Delta t]\sin\theta_1 \\
&+ V_2 \sin[2\omega_0(0)\Delta t]\cos\theta_2 + V_2 \cos[2\omega_0(0)\Delta t]\sin\theta_2 \\
&+ \ldots \\
&+ V_N \sin[N\omega_0(0)\Delta t]\cos\theta_N + V_N \cos[N\omega_0(0)\Delta t]\sin\theta_N \\
&+ V_0 - \frac{V_0}{\tau}(0)
\end{aligned}
\tag{3.103}
$$

Similarly, at $t = \Delta t$, the second sample can be expressed as

$$
\begin{aligned}
v_{+1} &= V_1 \sin[\omega_0(1)\Delta t]\cos\theta_1 + V_1 \cos[\omega_0(1)\Delta t]\sin\theta_1 \\
&+ V_2 \sin[2\omega_0(1)\Delta t]\cos\theta_2 + V_2 \cos[2\omega_0(1)\Delta t]\sin\theta_2 \\
&+ \ldots \\
&+ V_N \sin[N\omega_0(1)\Delta t]\cos\theta_N + V_N \cos[N\omega_0(1)\Delta t]\sin\theta_N \\
&+ V_0 - \frac{V_0}{\tau}(1\Delta t)
\end{aligned}
\tag{3.104}
$$

If $N$ samples are processed, the matrix $[A]$ is as follows.

$$
[A] = \begin{bmatrix}
\sin[\omega_0(0)\Delta t] & \sin[\omega_0(0)\Delta t] & \ldots & \sin[N\omega_0(0)\Delta t] & \cos[N\omega_0(0)\Delta t] & 1 & 0 \\
\sin[\omega_0(1)\Delta t] & \cos[\omega_0(1)\Delta t] & \ldots & \sin[N\omega_0(1)\Delta t] & \cos[N\omega_0(1)\Delta t] & 1 & 1 \\
\ldots & \ldots & \ldots & \ldots & \ldots & \ldots & \ldots \\
\sin[\omega_0(N-1)\Delta t] & \cos[\omega_0(N-1)\Delta t] & \ldots & \sin[N\omega_0(N-1)\Delta t] & \sin[N\omega_0(N-1)\Delta t] & 1 & N-1
\end{bmatrix}
\tag{3.105}
$$

The Left pseudo-inverse matrix of $[A]$ is calculated using Equation 3.97. The real and imaginary components of the estimated sinusoidals are estimated as following.

$$
\begin{bmatrix}
V_1 \sin\theta_1 \\
V_1 \cos\theta_1 \\
V_2 \sin\theta_2 \\
V_2 \cos\theta_2 \\
\ldots \\
V_N \sin\theta_N \\
V_N \cos\theta_N \\
V_0 \\
-\frac{V_0}{\tau}
\end{bmatrix}
= [A]^{-L}
\begin{bmatrix}
v_0 \\
v_{+1} \\
v_{+2} \\
v_{+3} \\
\ldots \\
v_{N-3} \\
v_{N-2} \\
v_{N-1} \\
v_N
\end{bmatrix}
\tag{3.106}
$$

### 3.4.5 Relay algorithm and trip logic implementation

The estimated phasors of voltages and currents are used in the implementation of protection algorithms in numerical relays. A relay algorithm is a set of equations whose evaluation and comparison with certain predetermined levels determines the operation of the relay. The equations and parameters that represent the relay algorithm of distance and differential relays have been developed in chapter 2, and are implemented through computational code at the interior of the relay microprocessor.

## 3.5 Summary

This chapter has given an overview on relay technology. Numerical relays concepts and the numerical relay modeling have also been described. The structure of a generalized numerical relay has been established so that the modeling of numerical relays is simplified. Major relevant modules and functions of a generalized numerical relay have been outlined. These modules include signal conditioning and scaling module, analog anti-aliasing filtering module, analog-to-digital conversion module, phasor estimation algorithm and relay logic. Basic concepts and information concerning each module has been presented. The most common techniques and methods employed in each module have also been described and developed.

# 4. PROTECTION SYSTEM MODEL DESIGNING METHODOLOGY

## 4.1 Introduction

The principles of operation and application procedures of distance and differential relays have been presented in previous chapters. The concept of generalized numerical relay, whose structure is constituted by the typical operational modules and functions of modern digital and numerical relays, has been introduced. The importance of the use of generalized numerical relay for model designing of numerical and digital relays has been also addressed.

A new methodology for modeling numerical relays is proposed in this chapter. The proposed protection system model designing methodology is divided in two major steps. The first step consists of designing numerical and digital relay models with the help of a computer program developed in the present thesis project. For designing, the numerical and digital relay model structure is based in the structure of the generalized numerical relay. The second step of the proposed methodology consists on embedding the designed numerical relay models into a power system modeled in an electromagnetic transient program (emtp).

The details of the proposed protection system model designing methodology are discussed extensively in this chapter. The computer program to design numerical and digital relay models (PLSA) is presented. The role of PLSA in the protection system model designing methodology is underlined. The computational structure of PLSA is

examined. The use of PLSA for designing numerical relay models is described. An account of the final products of the model designing process with PLSA is listed. The procedure to embed the PLSA-designed relay models in a PSCAD/EMTDC case is outlined. A description of the computational structure of PSCAD/EMTDC (*component*), used as the foundation of numerical relay model embed in the PSCAD/EMTDC case, is briefly done. The procedure to initialize a *component* and to use the final products of PLSA to customize the *component* as a numerical relay model is shown. The considerations to connect and set the numerical relay model in a PSCAD/EMTDC are commented. Additionally, the benefits that the proposed methodology offers for the designing of numerical relay are discussed.

## 4.2 Proposed protection system model designing methodology

A literature review of modeling of relays and interaction of relay models with models of power systems in electromagnetic transient programs has been presented in chapter 1. This literature review has shown that previous approaches for modeling numerical relays are not computer-aided for successive relay model designing and do not have a pattern or basic structure to construct the model. In the other side, those approaches that do offer generality in the modeling process employ software that is not the standard in the protection industry to perform power transient studies. The review also showed that the approaches that model the power system and the numerical relay in the same emtp present the difficulty of setting a link between the emtp engine and the relay model. The amount of work that this task presents can be as big as the modeling process itself.

The present project has proposed a new approach on relay model designing. The proposed methodology consists on employing a program to design numerical relay models and embedding the designed numerical relay models inside a power system model, in a manner that the numerical relay models and the modeled power system form a single computational unit within the chosen emtp. This proposed approach offers automation and generalization in the designing of numerical and digital relay models

and it does not require modifying the internal subroutines of the emtp or compiling an external signal-processing program with the emtp.

### 4.2.1 Tools required in the methodology

The following are the two major tools necessary to develop the proposed protection system model designing methodology.

- An electromagnetic transient program (emtp) to model and simulate the normal, faulted and transitory operation states of power systems.
- A computer program to design digital and numerical relay models accordingly to the specifications and adjustments required to protect the elements of the power system modeled in the emtp.

For the purposes of the present project, the emtp selected to model the power system is PSCAD/EMTDC. PSCAD/EMTDC is a program developed in the Manitoba HVDC Research Centre (Manitoba Hydro) [44]. The primary solution engine is known as EMTDC, and the graphical user interface is named PSCAD. A more extensive introduction of PSCAD/EMTDC has been given in section 1.4.

Additionally, a Visual C++-based computer program, named PLSA, has been created to design numerical relay models. The user of PLSA enters, through a friendly user interface, data related to the specific relay that is to be designed or modeled. Once PLSA has obtained the data from the user, it processes the information and creates a piece of code that represents the different internal modules and functions of the numerical relay model. PLSA stores the piece of code generated on a FORTRAN file, for storage purposes. For each numerical relay model, a FORTRAN file is created, keeping a sequence of variables between files, which will give consistency to the simulation once they are incorporated to the modeled power system on PSCAD/EMTDC.

### 4.2.2 Description of the methodology

The proposed methodology requires that a power system must be first modeled in PSCAD/EMTDC. For that, PSCAD/EMTDC provides a complete library of the typical elements presented in typical power systems.

The modeling of protection system is initiated by modeling each of the numerical relays belonging to the protection system. For this, the data and parameters of each of the numerical relays are entered in a PLSA project. The final product of the PLSA project is a set of files containing the code of the numerical relay models.

To incorporate the relays in the power system modeled in PSCAD/EMTDC, a feature of PSCAD/EMTDC called *components* is employed. A PSCAD/EMTDC *component* is a computational resource to create user-custom models. PSCAD/EMTDC *components* share the same computational structure as the models belonging to the PSCAD/EMTDC libraries. This structure is constituted by an icon that activates the element in the graphical interface PSCAD, an editor to add code to process the inputs and to address the outputs of the element, and associated dialog boxes to provide parameters and/or to gain access to the internal variables of the element.

For each of the relay model to be incorporated in the project, a PSCAD/EMTDC *component* must be initialized. The initialized *components* must be provided with the necessary number of input and outputs accordingly with the type of relay modeled. The internal variables to be monitored and the graphs to illustrate them are created. The code generated by PLSA related to the specific relay is incorporated in the editor of the *component*. Finally, electrical and logical signals are connected to the inputs and outputs of the initialized *components*. After this described procedure, each of the initialized *components* becomes a numerical relay model and the protection system is ready for simulation with its associated power system in PSCAD/EMTDC.

The main difference between digital and numerical relays is the type of microprocessor they use as Central Processor Unit (CPU). While digital relays use multi-purpose microprocessors, numerical relays employ digital signal processors, which are special-purpose microprocessors that provide ultra-fast instruction sequences, such as shift and add, and multiply and add, which are commonly used in math-intensive signal processing applications. Digital signal processors make numerical relays faster and more efficient than their digital counterparts. However, digital and numerical relays sample their inputs at the same sampling rate, and they run all their processes in the lapse of the same time step. Under this premise, the relay models designed with the proposed methodology include numerical and digital relays. Hence, from hereafter in this thesis the concept of numerical relays includes the concept of digital relays.

Summarizing, the proposed methodology to design model of protection systems can be outlined in the following manner.

1. Model power system in a PSCAD/EMTDC case
2. Use PLSA to design the numerical or digital relay models protecting the elements of the power system modeled in PSCAD/EMTDC
3. Embed numerical or digital relay models in the PSCAD/EMTDC case
    (a) Initialize an PSCAD/EMTDC *component* in the graphical interface PSCAD with the convenient number of inputs and outputs, in accordance with the information given by auxiliary files generated by PLSA
    (b) Create a dialog boxes to gain access to specific internal variables of the relay model
    (c) Insert the related code generated by PLSA in the editor of the *component* in PSCAD/EMTDC
    (d) Provide the relay model with the convenient inputs from the power system model in PSCAD and address the outputs
    (e) Repeat steps (a) to (e) for every relay modeled in PLSA
4. Use the modeled protection system in power system studies

### 4.2.3 Structure of PLSA

PLSA has been programmed using the Microsoft Foundation Classes MFC in Visual C++ version 6.0. Under the concept of Document/View architecture, PLSA has been created as a Single Document Interface program, which means that one single document class is initialized to store and control all the data collected by PLSA. For further reading and a more extensive explanation on the subject of object-oriented programming, MFC and Visual C++, please refer to appendix A of the thesis.

#### 4.2.3.1 Document class CPLSADoc

CPLSADoc is the Document class and the core of PLSA. CPLSADoc is in charge of the most critical and important processes. Briefly, CPLSADoc performs the following tasks.

- Initializes the Relay Data Dialog Boxes, that are the interface between the user and PLSA
- Initializes a new object of CRelay, that is the relay data store class
- Retrieves from Relay Data Dialog Boxes the relay data provided by the user and store the relay data in the related CRelay object
- With the relay data performs a series of calculations, such as:
    - The transfer function coefficients of the anti-aliasing filter
    - The coefficients of the digital filter for digital simulation of the anti-aliasing filter by bilinear transforming
    - The analog-to-digital conversion equations
    - The phasor estimator algorithm equations
- Writes in an auxiliary file the general information of the relay model and the necessary information to customize the initialized *component* of PSCAD/EMTDC, such as the number, order of connectivity and names of the channels, signals assigned to the channels, etc.

- Writes in a FORTRAN file the code of the relay model
- For distance relays models, writes in an auxiliary file the subroutine of the relay comparator
- For long window techniques, writes in an auxiliary file the subroutine of the phasor estimator algorithm

EMTDC provides a dynamic memory array to store the variables employed by user-custom models. This memory array is updated every time step of the EMTDC simulation. If two or more user-custom models are employed in the same PSCAD/EMTDC case, then specific portions of the dynamic memory array must be assigned to each of the user-custom models present in the PSCAD/EMTDC case. CPLSADoc manages the assignation of portions of the dynamic memory array to each of the numerical relay modeled to avoid any further conflict. CPLSADoc also takes all the consideration in the generated code to match the frequency of the simulation in EMTDC and the sampling frequency of the signals.

#### 4.2.3.2 Relay class object CRelay

PLSA may be used to design several relay models for the same PSCAD/EMTDC case. The class CRelay of PLSA was created to store and manage the information of the relay models participating in the same PSCAD/EMTDC case. A new object of the class CRelay is initialized every time a new relay is designed in PLSA.

The internal structure of CRelay is constituted by the particular values and parameter that the user has entered to specify the numerical relay currently modeled, and the functions to serialize, store and access such values and parameters in PLSA.

The CRelay class objects containing the data of the numerical relay models to embed in the same PSCAD/EMTDC case are stored on an MFC array class or collection. MFC provides lists, arrays, and maps collections. PLSA employs an MFC array collection

template class. This array template class provides PLSA with a dynamically sized, ordered, and integer-indexed array of CRelay objects. When a project in PLSA is finished, PLSA saves in a file the collection template allocating the CRelay class objects. The template files are retrieved at runtime from PLSA to make available the information of the related relay models.

#### 4.2.3.3 View class CPLSAView

The PLSA user interacts with the data stored and organized in the CRelay array template through the CPLSAView class. The CPLSAView class is a class derived from the MFC list view class CListCtrl. The CListCtrl class encapsulates the functionality of a list view control. The list view control displays a collection of items, each of them consisting of an icon (from an image list) and a label. In addition to an icon and label, each item has information displayed in columns to the right of the icon and label. Class CListCtrl provides several functions for inserting, deleting, finding, and modifying these items. A designed relay model appears as an item in the view of PLSA.

#### 4.2.3.4 PLSA flux diagram

In Figure 4.1 is shown the flux diagram of the program PLSA.

### 4.2.4 Using PLSA to design numerical relay models

When PLSA is initiated, the main window of the program appears in the computer screen. The main window of PLSA is shown in Figure 4.2. The main window has a Windows-style toolbar and menu, and a view-list where the relevant information of the generated relay models is shown. It is through the main window that the user interacts

with the PLSA to design numerical relay models or to gain access to the information of the stored relay models.

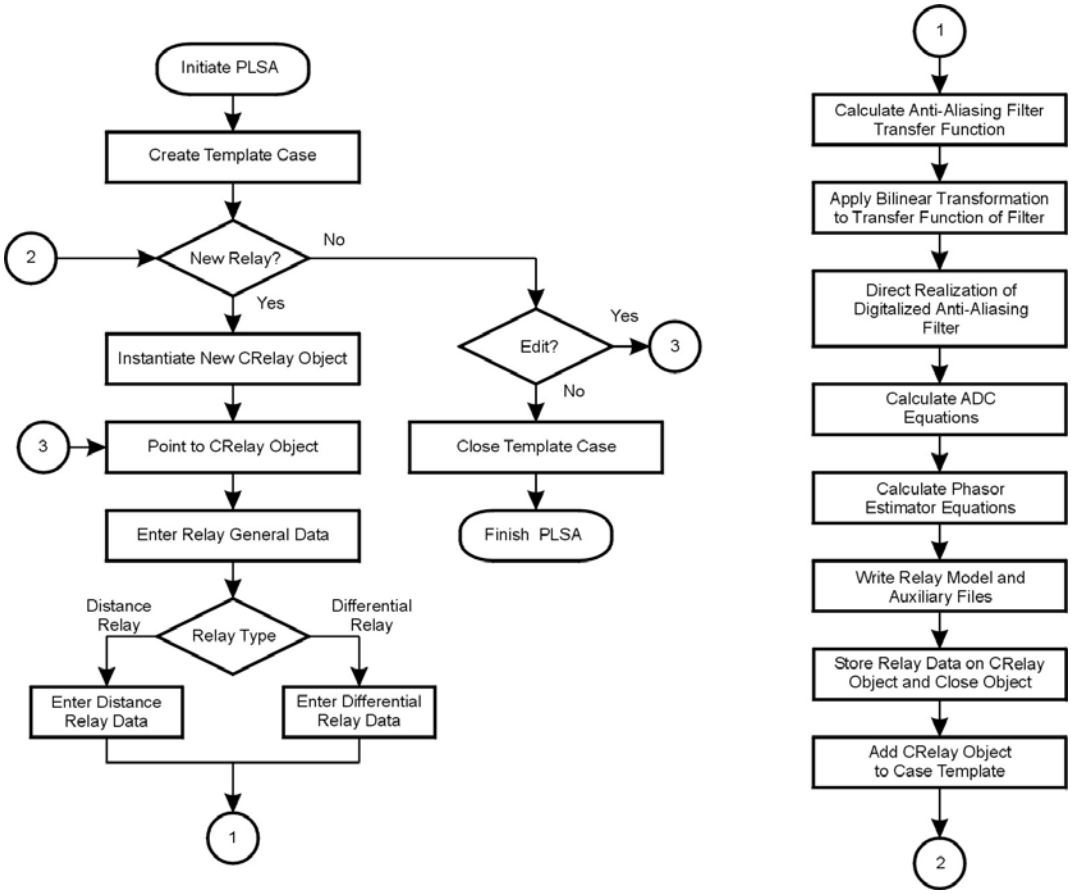


**Figure 4.1:** Flux diagram of the program to design numerical relay models PLSA

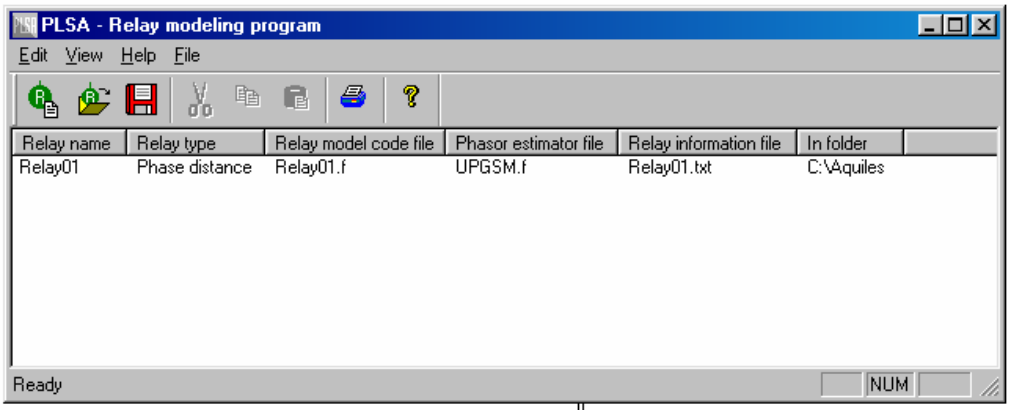


**Figure 4.2:** Main window of PLSA

#### 4.2.4.1 New Relay Dialog Box

The process to start the designing of a new numerical relay model may be started by either clicking in the *New Relay* icon  on the main menu, or by clicking *Edit* in the main toolbar and then selecting *New Relay*, as shown in Figure 4.2. Proceeding in either way makes the *New Relay Dialog Box* to pop up. The appearance of the *New Relay Dialog Box* is shown in Figure 4.3. The *New Relay Dialog Box* is a tabbed dialog box composed of five different sheets, where the relevant information of the relay is entered by the user. The five sheets of the *New Relay Dialog Box* are the following.

1. General information
2. Analog signal scaling
3. Channels information
4. Analog-to-Digital conversion
5. Phasor estimation information

The *New Relay Dialog Box* sheets are navigated using the *Back* and *Next* buttons. There is not a specific order to fill the data fields of the sheets. The following sections describe the data sheets of the *New Relay Dialog Box* and the specific information that is requested on each of these data sheets.

##### 4.2.4.1.1 General information sheet

When the *New Relay Dialog Box* is activated, the initial sheet that is shown is the *General information* sheet. The data that is requested to enter in the *General information* sheet is the following.

- *Relay name*: The name of the relay used for visualization in the *Relay List* of the PLSA main window. This name is also used to name the FORTRAN file containing the related numerical relay model code.

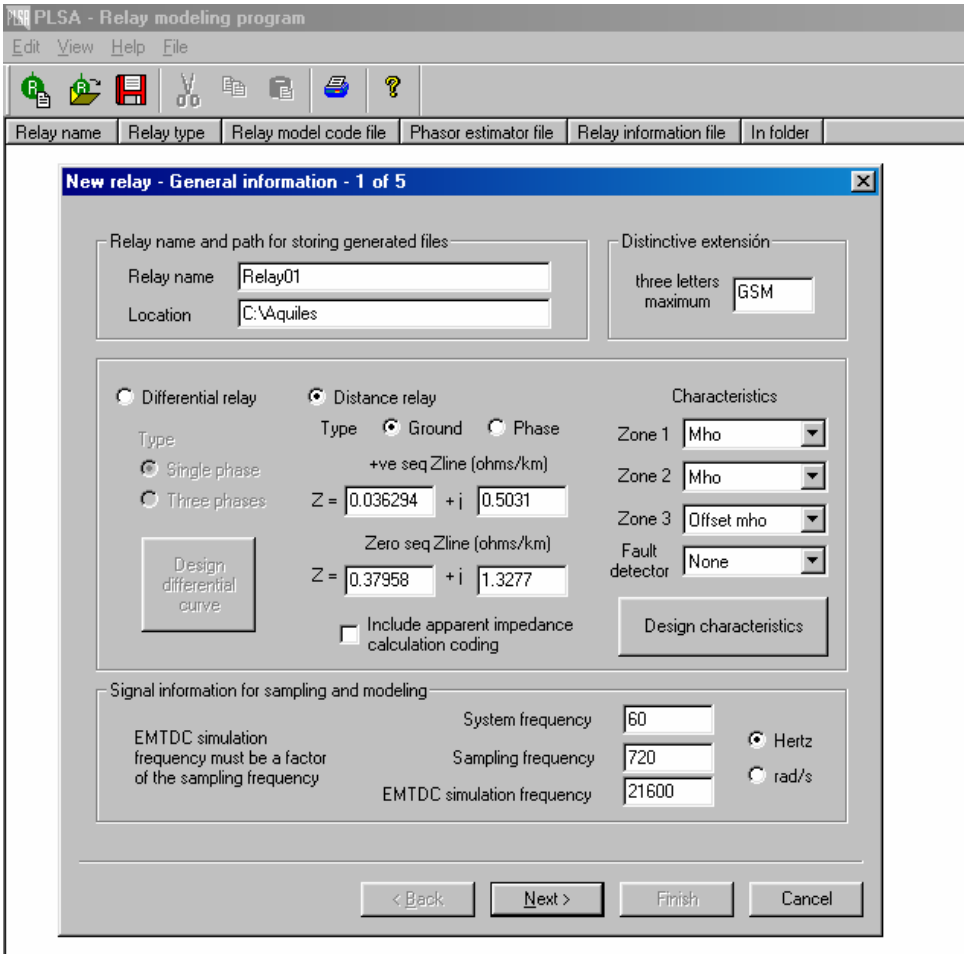


**Figure 4.3:** *New relay* dialog box and *General information* sheet

- *Location*: The computer folder where the FORTRAN file containing the numerical relay model code and auxiliary files generated by PLSA are stored at the end of the modeling procedure.
- *Distinctive extension*: Unique set of three letters used to differentiate the variables related to the numerical relay model currently designed.
- *Relay type*: It can be chosen between differential and distance relay. If it is chosen to design a differential relay, then the following information is requested:
    - *Differential relay type:* To choose between *Single-phase* or *Three-phase* differential relay.
    - *Differential curve:* The *Differential Curve* window is activated when the "*Design differential relay*" button is hit, as shown in Figure 4.4. This

window request information of the coordinates of the *Pickup current* [*Ipx*, *Ipy*], the *First slope angle* (*Alpha1*), the coordinates of the *Change of slope* point [*Isx*, *Isy*] and the *Second slope angle* (*Alpha2*).

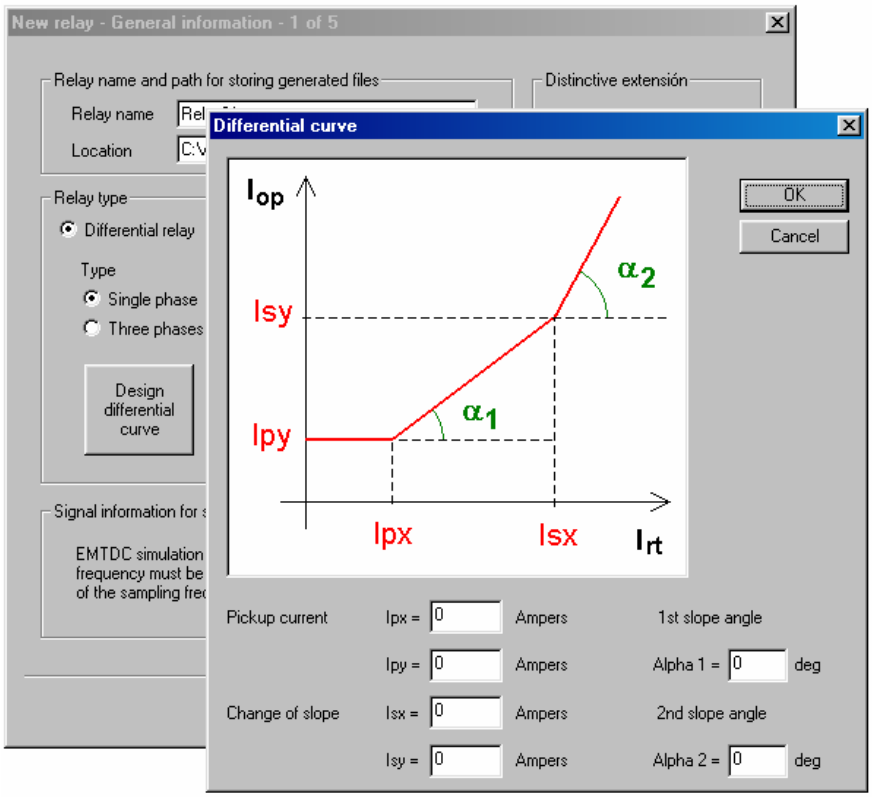


**Figure 4.4:** *Differential curve* window

If distance relay design is chosen, then the following information is requested.

- *Distance relay type*: To choose between *Ground* and *Phase* relay. If *Ground* relay is chosen, then it is asked to enter the data of the positive and zero sequence transmission line impedance, necessary for current compensation calculations.
- *Include apparent impedance calculation coding*: When this checkbox is selected, PLSA includes in the generated code the calculations of the apparent impedance seen by the relay. The names of the variables of the apparent impedance are described in appendix C of this thesis.

- *Characteristics*: This section adds the protection zones desired to the numerical relay model and specify in the drop lists the characteristics of the zones. The drop lists allows selecting between impedance, offset mho, mho, mho polarized and reactance characteristics for zone-1, zone-2, zone-3 and fault detector.
- *Characteristic parameters*: When the "*Design characteristics*" button is hit, the *Distance Relay Characteristic* window is activated, as shown in Figure 4.5. This *Distance Relay Characteristic* window requests information of the parameters of the distance relay characteristic of the protection zones, one zone at a time. The information requested is the characteristic reach impedances $Z_R$, the type of coordinates used to express the parameter impedances (*Rectangular* or *Polar* coordinates), the *Time delay after activation* of the zone, the *Comparator* type (*Phase* or *Magnitude*), the *Polarization* method (*Cross polarization* or *Voltage memory*) –for mho-polarized characteristic-, and the multiplication constant in the mho-polarized distance relay $K_p$, as explained in section 2.3.5.6.1.

- *System frequency*: Typically 60 Hz or 50 Hz.
- *Sampling frequency*: The frequency in which the system signals are sampled for quantization.
- *EMTDC simulation frequency*: The frequency in which PSCAD/EMTDC simulates the operation of the power system. This frequency must be an integer multiple of the *Sampling Frequency*. The PSCAD/EMTDC case simulation step must be set accordingly to this number.

#### 4.2.4.1.2 Analog signal scaling sheet

The appearance of the *Analog signal scaling* sheet is shown in Figure 4.6. The data requested in the *Analog signal scaling* sheet is the following.

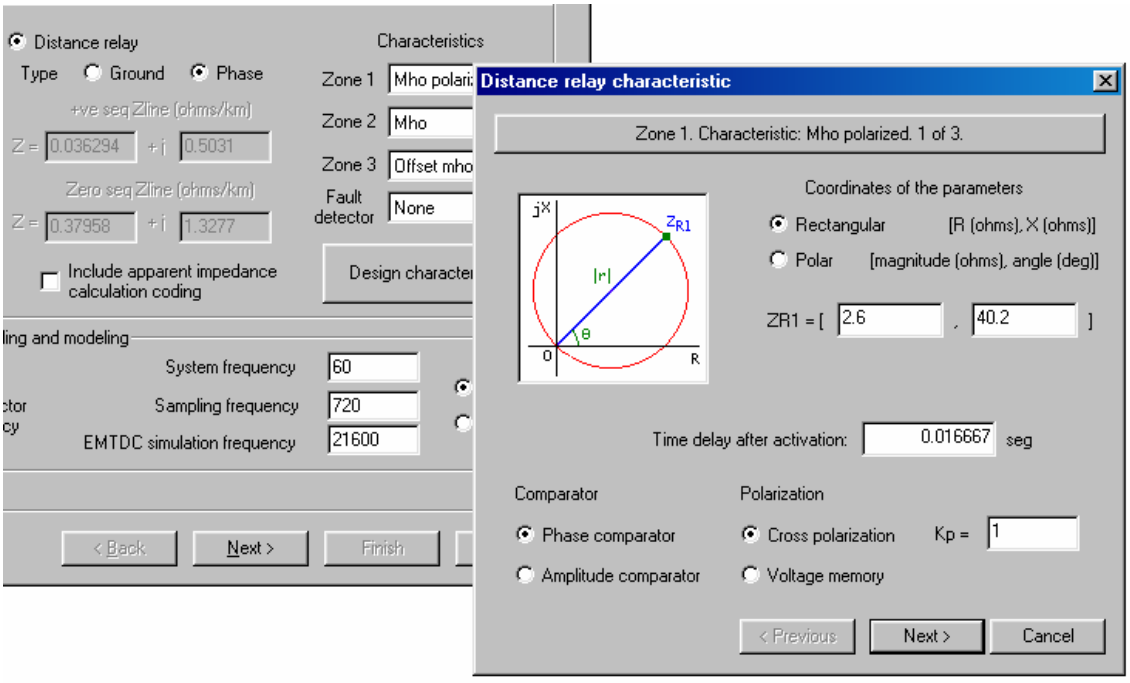


**Figure 4.5:** *Distance relay characteristic* window

- *Current and voltage scaling factors*: PSCAD/EMTDC and PLSA could be using different units for current and voltage signals. To match the units, it is requested to enter the scale factors that convert the PSCAD/EMTDC currents into amperes and the PSCAD/EMTDC voltages into volts.
- *Auxiliary current and voltage transformer rate*: It is transformer rate of the auxiliary current and voltage transformers employed to scale down the current and voltage system signals to the operational voltage levels of the numerical relay.
- *Internal voltage to scale*: Voltage range to which the current and voltage input signals are scaled down for further digitalization. The scale-down voltage range can be chosen to be between zero and a positive value of voltage $x$ ([0, x]), or between $-x$ and $+x$ ([$-x$, $x$]). In both cases, it is required to enter the voltage value $x$.

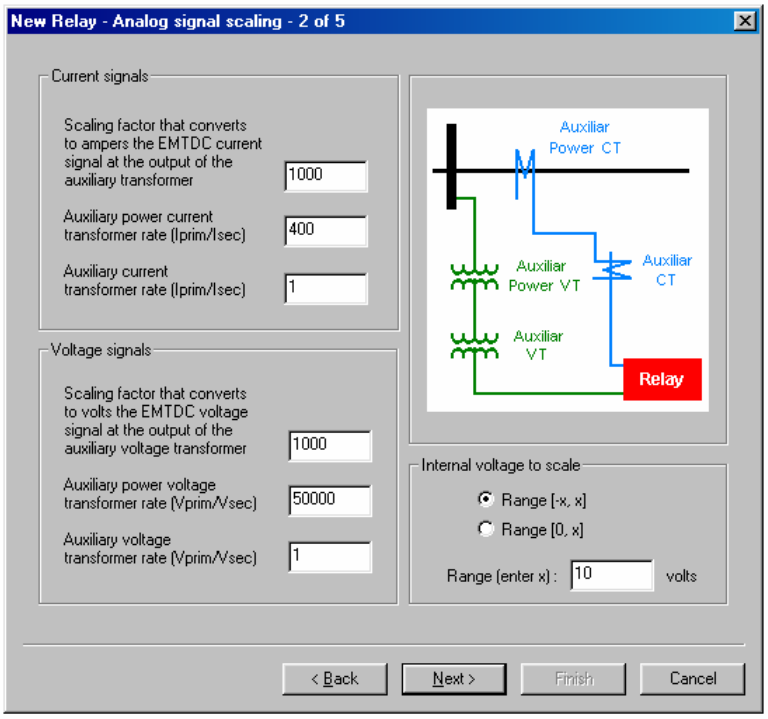


**Figure 4.6:** *Analog signal scaling* sheet

#### 4.2.4.1.3 Channel information sheet

The *Channel information* sheet is depicted in Figure 4.7. The *Channel information* sheet shows in this sheet the information related to the channels that is used in the embedding of the relay model in the PSCAD/EMTDC case. The *Channel information* sheet writes in the column *Signal* the information of the specific input that must be connected to each channel in PSCAD/EMTDC case. Also, the *Channel information* sheet writes in the column *Channel name in the model* the information of the variable assigned to the channel in the PSCAD/EMTDC relay model. Additional channels may be included for user-custom purposes. The rest of the information required by the *Channel information* sheet is the following.

- *Absolute peak value*: Expected maximum absolute value of the voltage or current input before the CT's and VT's. The *absolute peak value* is employed to confine the input signal into the scaled voltage range used by the relay model.

The values entered must be specified in kilo-amperes (kA) for currents and in kilovolts (kV) for voltages.

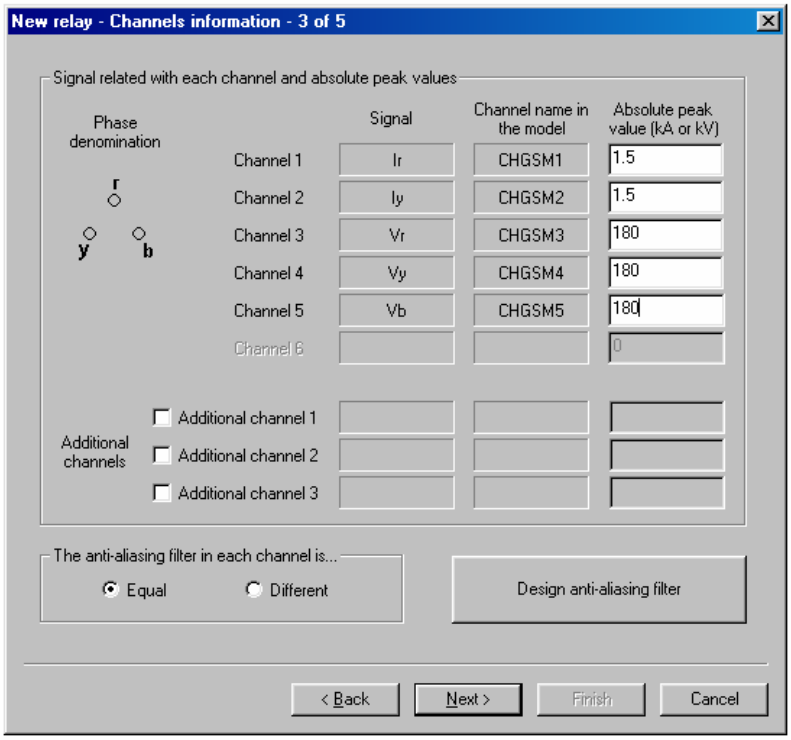


**Figure 4.7:** *Channel information* sheet

- *Same anti-aliasing filter in all channels*: If *Equal* is chosen, only one anti-aliasing filter is designed. If *Different* is chosen, one anti-aliasing filter is designed per each channel.
- *Anti-aliasing filter design information*: When the "*Design anti-aliasing filter*" button is clicked, the *Filter modeling* window is activated, as shown in Figure 4.8. This *Filter modeling* window requests information related to the anti-aliasing filter. The window offers the possibility to design the filter by *Approximation* or by *Transfer Function*. The *Approximation* designing requires choosing between a *Butterworth*, *Chebyshev I*, *Chebyshev II*, *Elliptic* or *Bessel* filter. It is also required to provide the data related to the *Pass band gain* and *Pass band frequency* and the *Stop band gain* and *Stop band frequency*. If the *Transfer Function* designing is chosen, it is necessary to specify the *Filter order*, and provide the coefficients of the *Numerator* and *Denominator* of the transfer

function of the analog filter. As discussed in section 3.4.2.6, it is important that the *Transfer Function* data of the analog filter provided to PLSA had been prewarped to the PSCAD/EMTDC frequency of simulation, to avoid the problems of warping created by the use of the bilinear transformation.

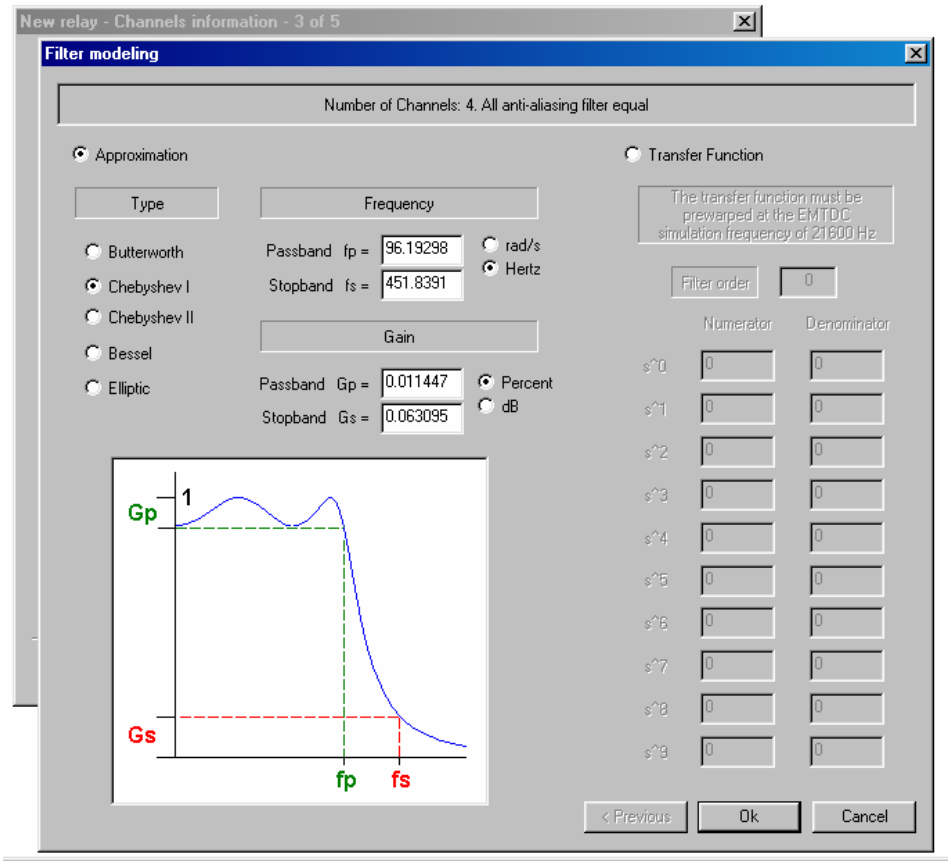


**Figure 4.8:** *Filter modeling* window

#### 4.2.4.1.4 Analog-to-digital conversion sheet

In Figure 4.9 is shown the appearance of the *Analog-to-digital conversion* sheet. The information requested is the following.

- *Digital word size*: Number of bits in the microprocessor word of the relay.
- *Nearest integer*: Operation used for getting the nearest integer into the analog to digital conversion. The options are *Truncation* or *Rounding* operations.

- *Negative numbers*: Conversion method to use for converting negative analog numbers into digital numbers. The options are *One's complement*, *Two's complement* and *Magnitude and Sign* methods.

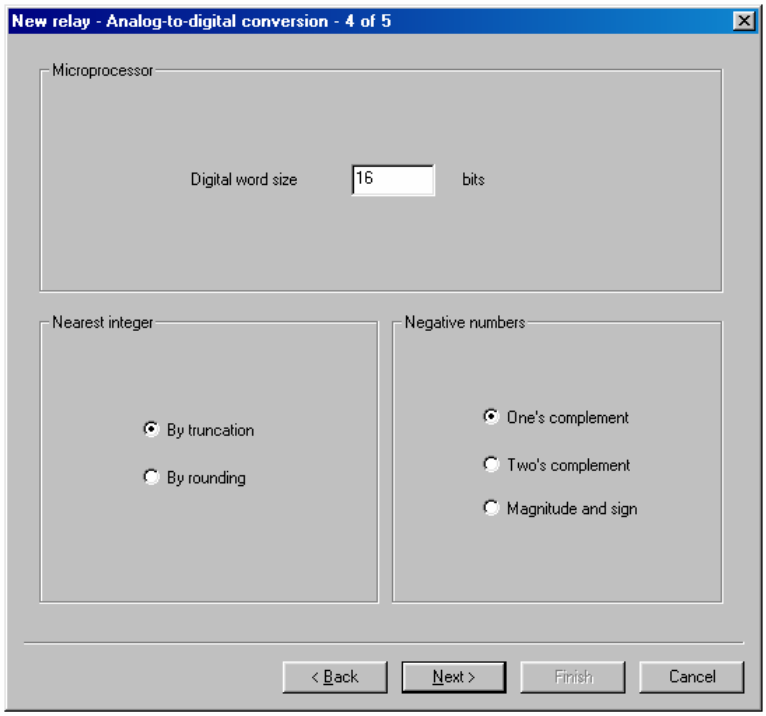


**Figure 4.9:** *Analog-to-digital conversion* sheet

#### 4.2.4.1.5 Phasor estimation information sheet

The *Phasor estimation information sheet* is depicted in Figure 4.10. The information requested in this sheet is the following.

- *Phasor estimator algorithm*: To choose between *Short window* and *Long window* methods. The options of *Short window* methods are *Miki and Makino* method, *Mann and Morrison* method, and *Rockefeller and Udren* method. The options of *Long window* methods are *Least error square* method, *Discrete Fourier Transform* method, and *Walsh functions* method.
- *Samples per data window*: PLSA shows the number of samples per data window employed by the *Phasor estimator algorithm*. For *short window* methods, the *samples per data window* may be 2 or 3. For *long window* methods, the number

of *samples per data window* is based in the *System frequency* and the *Sampling frequency* values.

- *Long window subroutine filename*: The user must enter the name of the file to store the *Long window algorithm* subroutine. Two or more relay models can use the same long-window phasor estimator subroutine, as long as they sample their input signals at the same sampling frequency. For this, it must be entered the same *long window subroutine filename* in the designing of the relay models sharing the same phasor estimator subroutine.
- *Harmonic participating in the long window matrix:* For *Least error square* method, PLSA enquires for the harmonics and decaying DC participating and estimated in the left-pseudo inverse matrix.

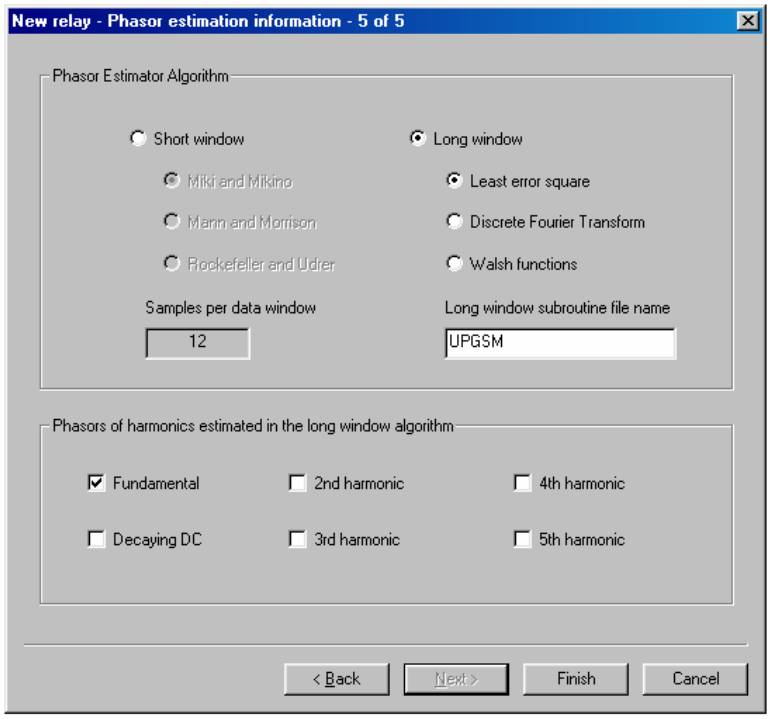


**Figure 4.10:** *Phasor estimation information* sheet

#### 4.2.4.1.6 Finishing the designing of a relay model

To let PLSA know that the relay data entered in the sheets is the wished to be used for the modeling of related numerical relay, the *Phasor estimation information* sheet must

be active. Once placed in the *Phasor estimation information* sheet, PLSA activates the "Finish" button, as shown in Figure 4.10. Clicking the "Finish" button closes the *New Relay Dialog Box* and the item correspondent with the recently designed relay model is added in the PLSA view-list, as depicted in Figure 4.2. PLSA process the data entered by the user in the *New Relay Dialog Box* and the final products associated with the recently designed relay model are stored in the folder specified by the user. The process explained in the section 4.2.4.1 is applied to each of the numerical relay participating in the same PSCAD/EMTDC case.

### 4.2.4.2 Final products of PLSA

After finishing the designing of numerical relays, PLSA generates several files. These files are of three classes.

- The files of the first class contain the FORTRAN coding of the modules and functions of the generalized numerical relay customized with the parameters provided to PLSA. There is one first class file for each of the numerical relays designed with PLSA. The name of these files are formed by PLSA with the relay name provided by the user and the extension **.f*.
- The files of the second class are auxiliary files created to store subroutines used by the FORTRAN code of the related first class file. The number of these auxiliary files depends of the type of numerical relay designed, as follows.
    - If a long window technique is used as phasor estimator, a second class file is created to store the subroutine containing the phasor estimator algorithm. This second class file is written in FORTRAN. The filename is formed by PLSA with the name provided by the user (as explained in section 4.2.4.1.5) and the extension **.f*.
    - If the modeling corresponds to a distance relay, an auxiliary file is created to store the subroutine containing the equations of the distance relay comparator. This second class file is also written in FORTRAN, and it is

named automatically by PLSA as *UCCS.f*. This file is used universally by any distance relay designed with PLSA. Only one version of *UCCS.f* is created, even if there is more than one distance relay model in the same PLSA project.

- Files of third class are informative text files. There is one of these third class files per file of the first class. The informative text files summarizes the data collected by PLSA to design the associated relay model, the names of the first and second class files associated with the relay model and the information necessary to embed the relay model in PSCAD/EMTDC, such as number of channels, signal connected to the channels, channel variable names to use in the PSCAD/EMTDC case, and the order that these channel must keep in the related EMTDC/PSCAD *component*. These informative text files are named with the relay name provided by the user with the extension **.txt*.

In Table 4.1 is presented a summary of the files generated for each of the numerical relays models designed in the same PLSA project.

| File class | File name | Content | Number of files |
|---|---|---|---|
| First | *RelayName.f* | FORTRAN code of the numerical relay model | 1 |
| Second | *UserDefined.f* | FORTRAN code of the long-window phasor estimator subroutines associated with the relay(s) model(s). | Depending on the preference of the user. |
| | *UCCS.f* | FORTRAN code of the distance relay comparator subroutine. All distance relay models use this file. | 1 |
| Third | *RelayName.txt* | Summary of the data used to model the numerical relay, file names of the first and second class files associated with the relay model and information for embedding the relay model | 1 |

**Table 4.1:** Files generated by PLSA to embed relay models in a PSCAD/EMTDC case

The files generated by PLSA are stored in the folder that the user has specified in the *General information sheet* of PLSA, as pointed in section 4.2.4.1.1. These files are used to embed the numerical relay model in a PSCAD/EMTDC case.

### 4.2.5. Embedding numerical relay models in a PSCAD/EMTDC case

In the PSCAD/EMTDC case, for each of the relay models to embed, the user must initialize a PSCAD/EMTDC *component*. *Components* are the basic building blocks of PSCAD/EMTDC elements. *Components* can be electrical, control, documentary or simply decorative elements. *Components* have external connection points to interact with other elements in PSCAD/EMTDC. These connections can be inputs and outputs of electrical, logic, or numerical nature. *Components* can fashion dialog boxes to inquire for parameters and data from the user. *Components* process their inputs in a flexible manner, and can perform inner algebraic and trigonometric operations. However, the most useful feature that *components* provide to this project is that they can be used to incorporate user-defined models in PSCAD/EMTDC.

An initialized PSCAD/EMTDC *component* is customized to make a numerical relay model in the PSCAD/EMTDC case. The user has the choice of initializing either part or all the numerical relay models in the PSCAD/EMTDC case, as long as the numerical relay models were designed in the same PLSA project.

The procedure to customize the PSCAD/EMTDC components in numerical relay models is explained in following sections with the embedding of a phase numerical distance relay model, designed with PLSA, in a PSCAD/EMTDC case. In this example, a phase digital distance relay was designed using the proposed designing methodology and named *PhDistRel1*. In PLSA, *PhDistRel1* was given *GSM* as its three distinctive letters (section 4.2.4.1.1). *PhDistRel1* employed the least error square algorithm as phasor estimator and the filename provided for this subroutine was *UPGSM*. The files of *PhDistRel1* generated by PLSA were *PhDistRel1.f, UPGSM.f, UCCS.f* and

*PhDistRel1.txt*, which are the files to store the FORTRAN code of the relay model, the long window-phasor estimator subroutine, the comparators subroutine and the associated informative text file, respectively.

### 4.2.5.1 Initializing a new PSCAD/EMTDC *component*

The simplest manner to initialize a new *component* in a PSCAD/EMTDC case is by employing the PSCAD/EMTDC *Component Wizard*. The *Component Wizard* is a dialog box in PSCAD/EMTDC that creates the template of a new *component* based on the parameters entered by the user. To initialize a new *component* with the *Component Wizard*, the following procedure must be undertaken.

1. The PSCAD/EMTDC case is opened by double-clicking on the case name in the *Project Tree*.
2. It is right-clicked on the background of the main window of PSCAD. In the menu that appears, the option *Special* is selected.
3. In the next menu that appears, the option *Create New Component* is selected as shown in Figure 4.11, to activate the *Component Wizard* definition window shown in Figure 4.12.

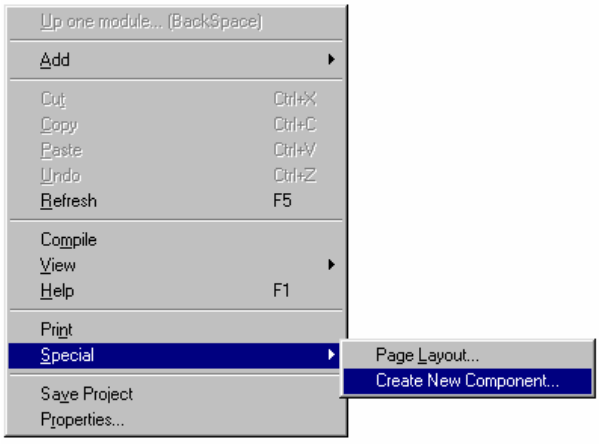


**Figure 4.11:** Activating the *Component Wizard* window

4. A short alphanumeric name (starting with a letter and without spaces) is provided to set the *Definition Name* of the *component*. In the example, the *Definition Name* was set as *PhDistRel1*, as shown in Figure 4.12.
5. The front text that the icon of the *component* shows in the graphical interface PSCAD is typed. In the example, the front text was set as *Phase Distance Relay 1*, as depicted in Figure 4.12. The result in the rectangular icon of the *component* in PSCAD is appreciated in Figure 4.14.
6. The number of input and output connections of the *component* is provided to the *Component Wizard*, in accordance with the information provided by the auxiliary text file generated by PLSA. These inputs and outputs are reflected in the rectangular icon of the *component*. It is recommended to set the input in one side of the rectangular component and the outputs in the opposite side. In the example, accordingly with the informative file *PhDistRel1.txt*, four inputs were created in the left side of the icon and one output was created in the right side of the icon, and they were set as shown in Figure 4.12. The *Next* button is hit.
7. The *Component Wizard* presents a connection window as the shown in Figure 4.13 per each input and output specified in the *Component Wizard* definition window. The following procedure is carried out for each of the inputs or outputs specified. The *Connection Name* is typed in the order provided by the informative text file. *Input* is selected in the *Connection Type* for every voltage or current signal entering the relay model, or *Output* for every output as pointed in the informative text file. *Real* is chosen in the *Data type* for all inputs and outputs. The rest of the parameters are left as they are. In Figure 4.13 is shown the *Component Wizard* connection window for the first connection, and the data entered accordingly to the informative file.
8. To review or modify the entered parameters, the *Prev* or *Next* buttons are clicked. The button *Cancel* is clicked to exit the *Component Wizard* without initializing the *component* at any time. The button *Finish* is hit to accept the entered parameters and to close the *Component Wizard* window. The *Prev*, *Next*, *Cancel* and *Finish* buttons are shown in Figure 4.13.

9. The *component* icon shows in the graphical interface PSCAD once the *Component Wizard* window is closed, and the *component* appears as an element in the PSCAD/EMTDC case.

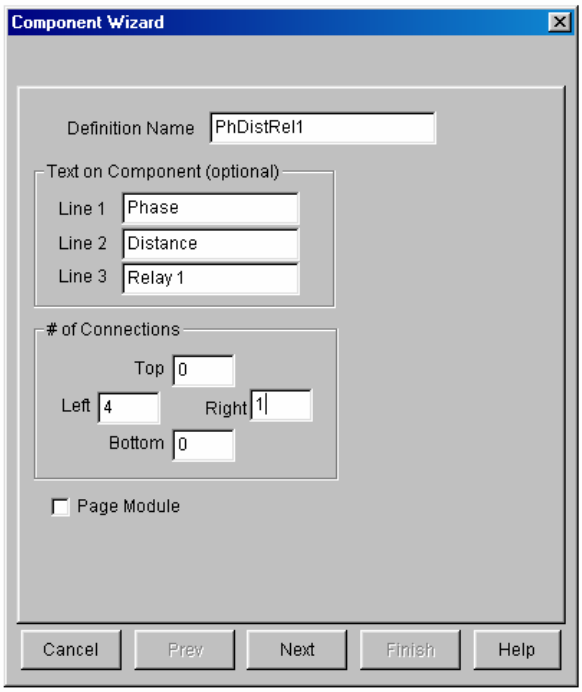


**Figure 4.12:** *Component Wizard* definition window

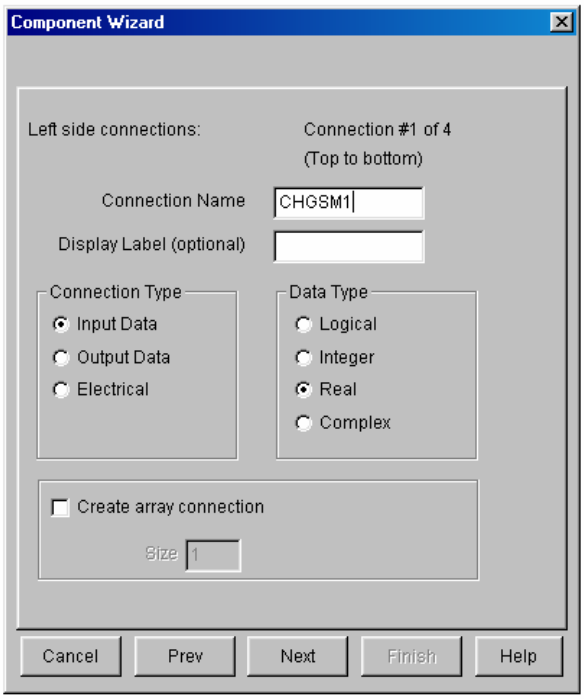


**Figure 4.13:** *Component Wizard* connection window

### 4.2.5.2 Structure of PSCAD/EMTDC *components*

The *component* recently created is employed as the computational base of the numerical relay model in a PSCAD/EMTDC case. *Components* are constituted by an icon in the graphical interface PSCAD, an internal code in FORTRAN and dialog boxes to establish user parameters.

The graphical icon permits the component to interact with other elements in the PSCAD/EMTDC case. The internal code processes the inputs and retrieves the outputs. Through the dialog boxes the user set values to parameters of the internal code of the *component* on the PSCAD/EMTDC case.

The *Component Workshop* is a resource of PSCAD/EMTDC that customizes the icon, internal code and dialog boxes of the *component*. In this thesis, the *Component Workshop* is used to customize the *component* into a numerical relay model in PSCAD/EMTDC cases.

The *Component Workshop* is opened by placing the pointer in the icon of the *component* in PSCAD and right-clicking on it; from the menu that pops the option *Special* is selected and, from the next drop down menu that appears, *Edit Definition…* is chosen, as shown in Figure 4.14.

The *Component Workshop* window and its two main views are shown in Figure 4.15. The left view of the *Component Workshop* is the *tree view*. The *tree view* of the *Component Workshop* shows the three main sections of the *component*, which are the *Graphics*, *Parameters*, and *SectionsNode* sections. The section *Graphics* correspond to the icon, the section *Parameters* correspond to the dialog boxes and *SectionsNode* correspond to the internal code of the component. The right view of the *Component Workshop* is the *edit view*. The edit *view* shows the content of the selected section on the *tree view*. The sections *Graphics* and *Parameters* have graphical editors, and *SectionsNode* has a text editor. The *tree view* with the main sections of the *component*

and the *edit view* are shown in Figure 4.15. It is recommended to leave structure of the section *Graphics* unchanged.

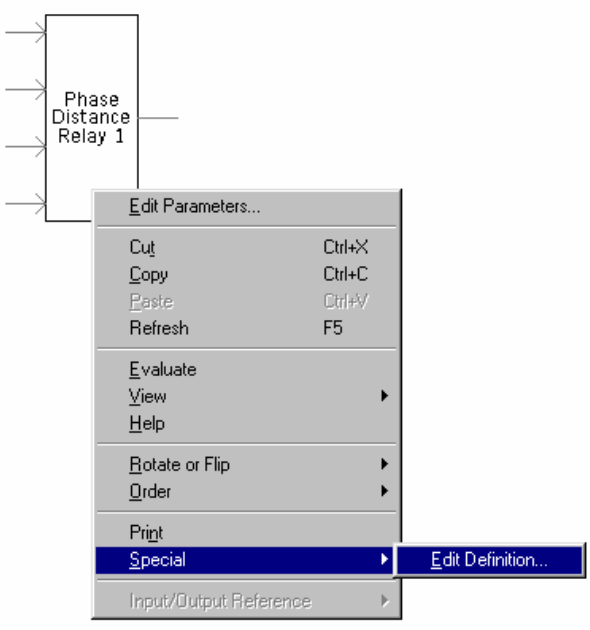


**Figure 4.14:** Opening the *Component Workshop*

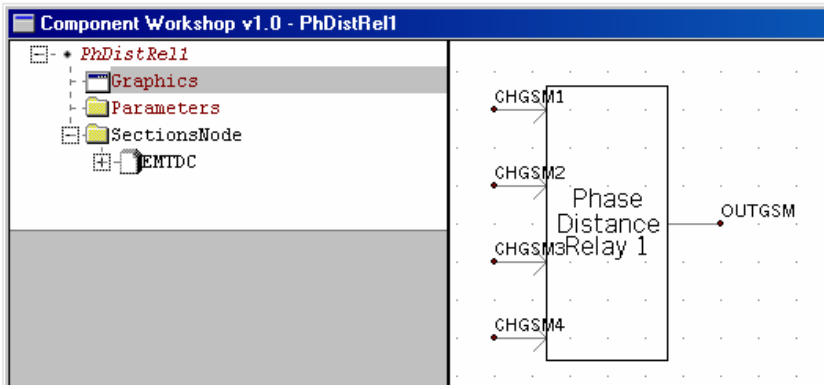


**Figure 4.15:** *Component Workshop* window

### 4.2.5.3 Creating a dialog box to access relay model internal variables

The section *Parameters* permits designing the dialog boxes to assign values to the parameters of the component. In this thesis, the dialog boxes of *Parameter* are employed to gain access to the internal variables of the numerical relay model from the graphical interface PSCAD. The internal variables are possible to plot once the access

to them has been established. Just one *Parameters* dialog box is needed for establishing the access to the internal variables of the *component*, as follows.

1. A new category is created in the section Parameters. For this, a right-click is issued with the pointer positioned on the section *Parameters* in the *tree view* of the *Component Workshop*. From the menu that pops, the option *New* is selected and, from the next menu that appears, *Category* is selected, as depicted in Figure 4.16. A new *Category* named *Untitled* shows as a subsection under the section *Parameters*, as observed in Figure 4.17.

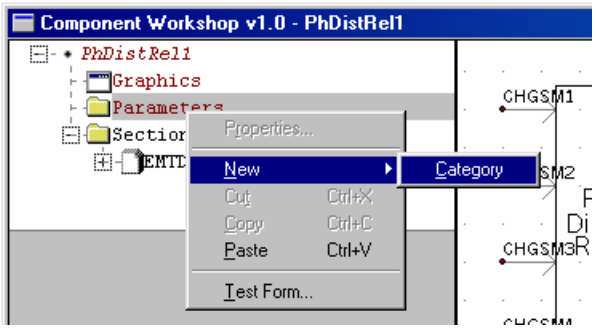


**Figure 4.16:** Creating a new *Parameters* category

2. The category just created is named. A right-click is issued with the pointer positioned on the category *Untitled*, under the section *Parameters* in the *tree view* of the *Component Workshop*. From the menu that pops, *Properties* is selected. The *Category Properties* window appears, as depicted in Figure 4.17. A name for this category is typed in the field *Name*. In the example, the *Category name* is set arbitrarily as *Dist Relay 1 variables*. The default value of *true* in the *Enabled When* field is left unchanged.
3. Entries to the category are added. The new *Dist Relay 1 variables* category is empty and entries are required to be added. The number of entries to add depends on the number of internal variables that the user wishes to access. For the purpose of describing the procedure, just one entry is going to be added. A click is issued on the *Dist Relay 1 variables* category, under the section

*Parameters* in the *tree view* to show the initial dialog box of the *Dist Relay 1 variables* category in the *edit view*. Positioned on the gray area of this initial dialog box a right-click is issued. From the menu that pops, the option *New* is selected. From the next menu that appears, the option *Text Field* is chosen, as shown in Figure 4.18. After this, the *TextBox Properties* window pops up, as shown in Figure 4.19. The *TextBox Properties* window is a resource that customizes the entries of the categories.

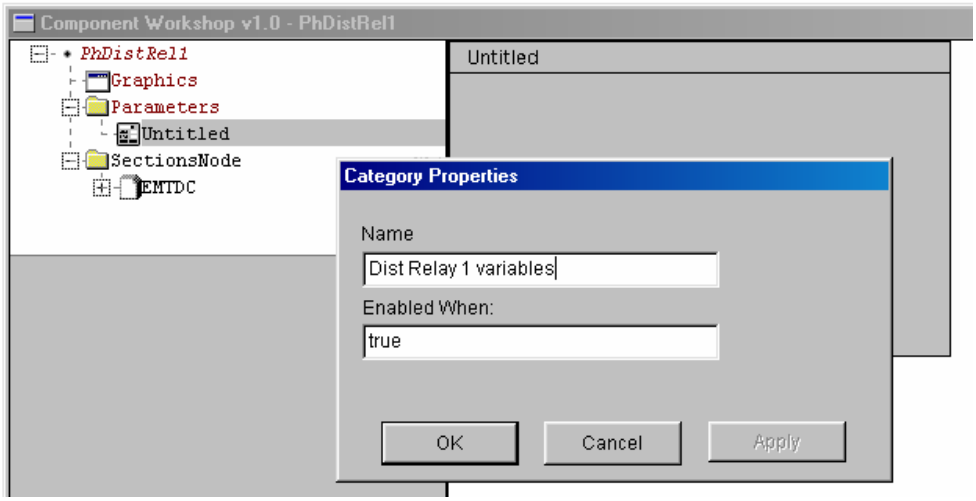


**Figure 4.17:** Naming the new *Category* of *Parameters*

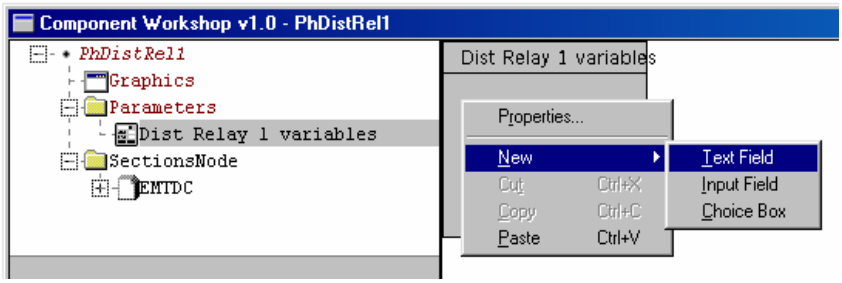


**Figure 4.18:** Adding an entry to the dialog box in the section *Parameters*

4. The entries are customized. In *Symbol* field of the *TextBox Properties* window is written a variable name to handle the internal relay variable to be accessed. These variable name typed in *Symbol* must be different from any other variable

name used in the same PSCAD/EMTDC case. It is recommended that the variable name in *Symbol* has the *three distinctive letters* (section 4.2.4.1.1) related to the particular relay plus a progressive number. In this example, the variable name in *Symbol* has been set *Outgsm1*, as shown in Figure 4.19. The legend appearing besides the entry in the dialog box is typed in *Caption*. In the example, the *Caption* field has been set arbitrarily as *Output 1*, as shown in Figure 4.19. The rest of the fields in the *TextBox Properties* window are left unchanged. The results of these procedures in the *Parameters* dialog box are shown in Figure 4.20.

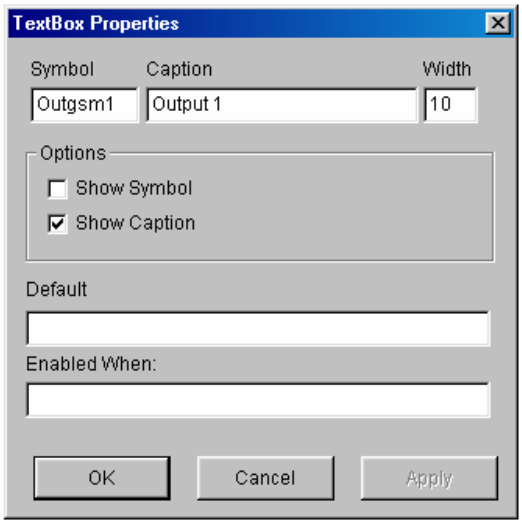


**Figure 4.19:** The *TextBox Properties* window appearance

5. The steps 3 and 4 are repeated for each internal variable of the relay model wished to access.

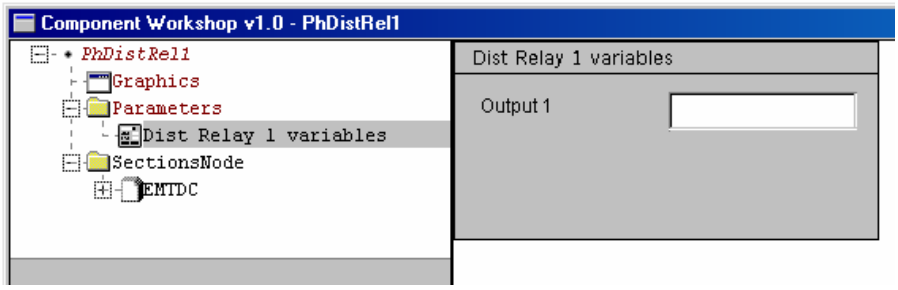


**Figure 4.20:** *Parameter* **Output 1** included into the **Dist Relay 1 variables** *Category*

### 4.2.5.4 Inserting the relay model code in the *component*

The PSCAD/EMTDC *component* is defined as a numerical relay model mainly by the code stored in the section *SectionsNode*. Clicking on the *SectionsNode* in the *tree view* expands the default applications *Fortran*, *Branch* and *Computations* under the subsection *EMTDC*, as shown in Figure 4.21. PSCAD/EMTDC uses this default applications and others for multiple and different purposes. In this thesis the default applications are eliminated and a new application *Dsout* is initialized.

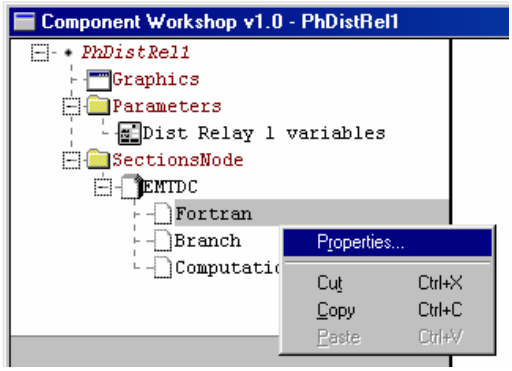


**Figure 4.21:** *SectionsNode* section

The power system modeled in PSCAD/EMTDC is solved in discrete steps of time. Before solving the power system, EMTDC searches for changes occurred to the network. After this, EMTDC solves the power system equations and obtains the currents in the branches and the voltages in the nodes of the power system. The FORTRAN code stored in *Dsout* processes these currents and voltages. Since the relay operation may change the connectivity of the system network, the relay model code is placed in *Dsout*. The changes in the connectivity that the relay may provoke are updated in the network before EMTDC solves the power system equations the next time step.

To eliminate a default application, a right-click is issued in the default application name, and the option *Cut* is selected from the menu that pops, as shown in Figure 4.21. This is repeated to eliminate the rest of the default applications. A new application named *Untitled* is created by right-clicking in the *EMTDC* subsection, and by choosing the

options *New* and *Entry* in consecutive menus that appear. A right-click is made over *Untitled* and the name of the new application is changed to *Dsout*.

The relay model code generated by PLSA is now inserted on *Dsout*. For this, *Dsout* is selected by clicking on it. In the *edit view* appears the blank page of the text editor of *Dsout*. The relay model code in the file generated by PLSA is copied and pasted in the text editor of *Dsout*. It is important to notice that it is the FORTRAN code stored in the file generated by PLSA what is inserted in the text editor of *Dsout*, no the file. In Figure 4.22 it is shown the result of this operation. The FORTRAN syntax employed in the text editor of *Dsout* is described in Appendix B.

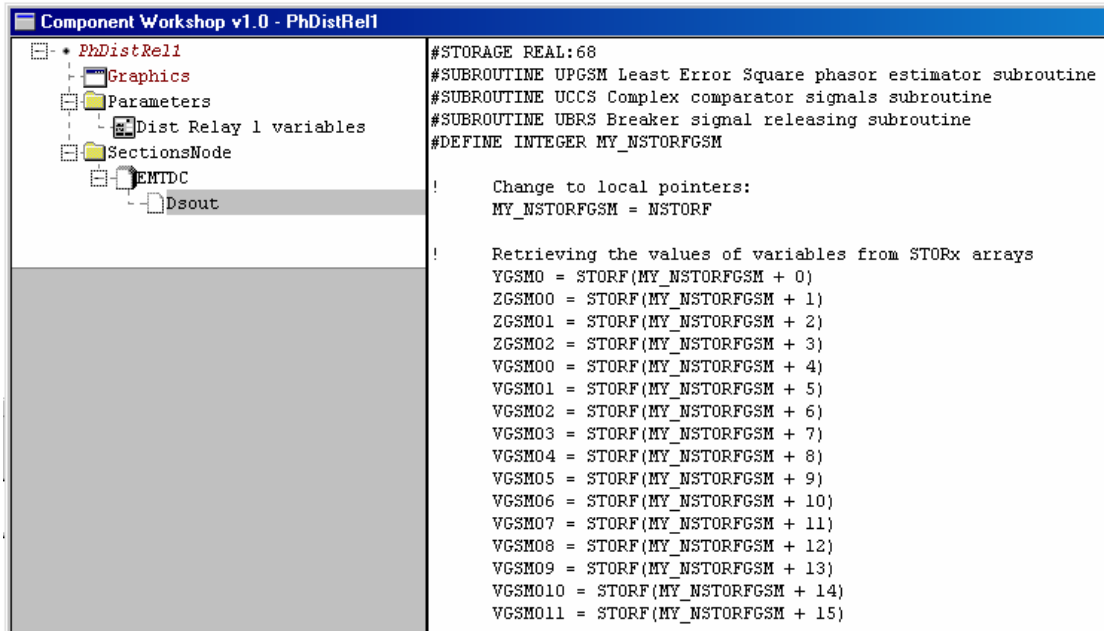


**Figure 4.22:** *Dsout* section and code

### 4.2.5.5 Linking relay model internal variables with the *component* dialog box

PLSA has left at the end of the generated relay model code three code lines to link the internal variables of the relay model with the *Parameters* dialog box, as shown in Figure 4.23. The user can specify the internal variables wished to access in the empty parenthesis *{ }* of these lines. The lines showed in Figure 4.23 use the output variables

*Outgsm1*, *Outgsm2*, and *Outgsm3*, which are valid output variables of the *Parameters* dialog box, as specified in section 4.2.5.3, numeral 4.

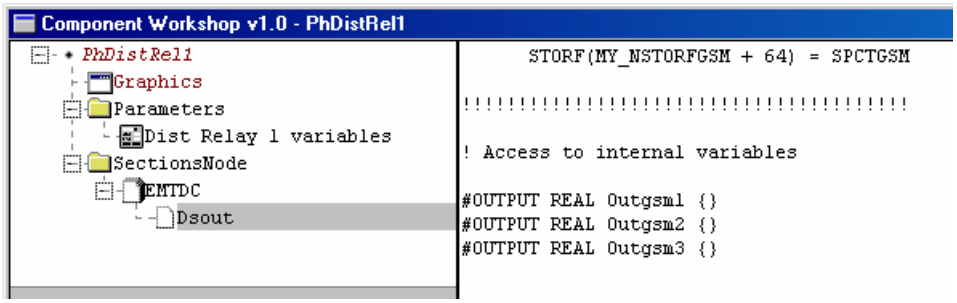


**Figure 4.23:** Code lines left to specify relay model internal variables to access

The user does not necessarily has to use the three default lines left for linking internal variables of the relay model with the *Parameters* dialog box. Depending of the number of internal variables to access, lines can be deleted or new lines can be added. If new lines are added, the added output variables must preserve consistency with variables in the *Parameters* dialog box. In Figure 4.24 is shown the modified relay model code in *Dsout* that relates the output variables *Outgsm1* with the numerical relay model internal variable *DGSM0A*, which is the angular difference provided by the phase comparator of the relay model. In Appendix C the more relevant relay model internal variables are described, as well as the manner to specify the name of these variables.

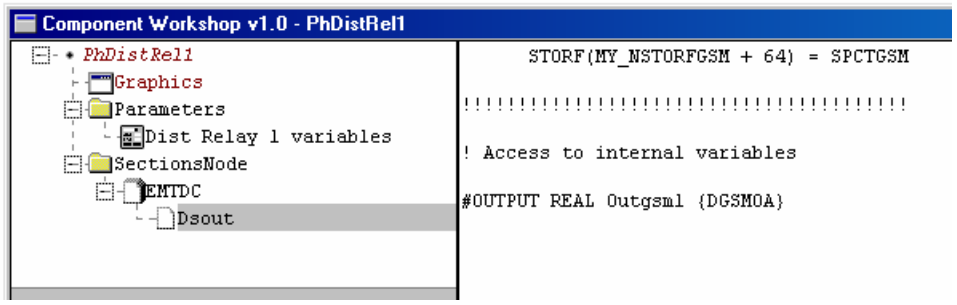


**Figure 4.24:** Code modified to specify the internal variable to access

### 4.2.5.6 Final setting of the numerical relay model in the simulation case

The appearance of the designed numerical phase distance relay model in the simulation case in PSCAD is shown in Figure 4.25. The designed numerical phase distance relay icon shows the front text *Phase Distance Relay 1*. The *Phase Distance Relay 1* protects a transmission line labeled *T5*. The transmission line *T5* has been split in two sections, *T5p* and *T5q*, in order to simulate a double line-to-ground fault at 50% of its length.

The *Phase Distance Relay 1* receives the voltage and current inputs from the secondaries of a voltage transformer (lower-left corner) and two current transformers (low center), respectively, both PSCAD/EMTDC transformers models. The voltage signals are labeled *V3bs* and *V3cs*, and the current signals are labeled *Ibps* and *Icps*. At the output of *Phase Distance Relay 1* there is a label named *Brkp*, which is the logic variable that triggers the associated breaker *Brkp* of *T5* in *Bus 3*.

The auxiliary FORTRAN files *UPGSM.f* and *UCCS.f,* generated by PLSA and containing subroutines usable by *Phase Distance Relay 1*, must be incorporated to the PSCAD/EMTDC case. For this, first it is necessary to move the files *UPGSM.f* and *UCCS.f* from the locations where PLSA originally created them to the PSCAD/EMTDC simulation case folder. After this, two file references to the files *UPGSM.f* and *UCCS.f* are created in PSCAD, as shown in Figure 4.25.

The last step to embed the numerical relay model is to create a channel to plot the numerical relay model wished variables. For this, a double-click is issued on the icon of *Phase Distance Relay 1*. The *Parameter*s dialog box *Dist Relay 1 variables* created in section 4.2.5.3 pops up, as shown in Figure 4.26. In the field *Output1* of the *Parameter*s dialog box *Dist Relay 1 variables* it is written a variable that is linked to the relay model output variable *Outgsm1,* which is related to the internal relay model variable *DGSM0A*. In the example, the variable in the field *Output1* was assigned arbitrarily as *Outp1*, as shown in Figure 4.26. In the lower-right corner of Figure 4.25 it is observed a label of

the variable *Outp1* connected to a PSCAD/EMTDC *Channel* element, to plot *Outp1* and, consequently, to plot the internal relay model variable *DGSM0A*.

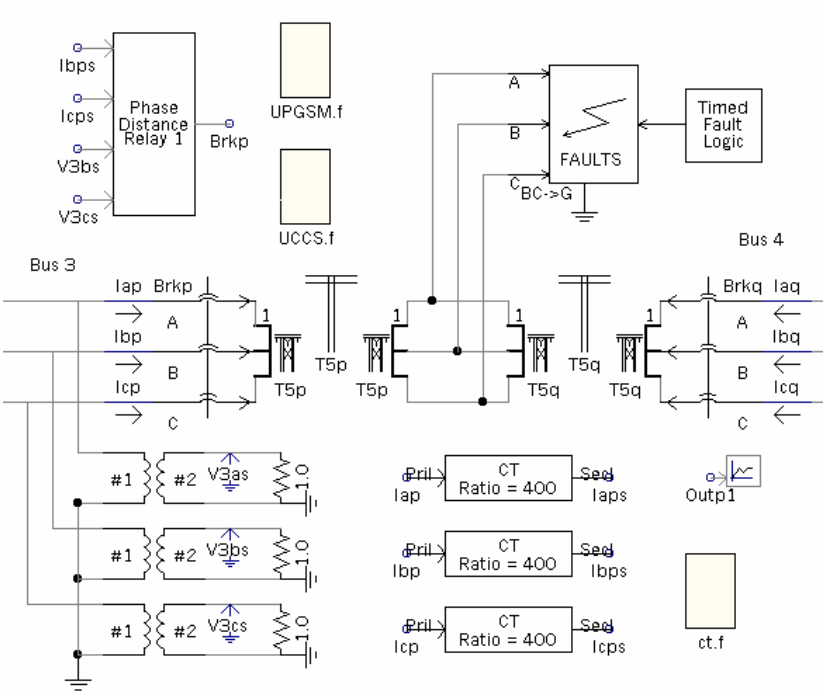


**Figure 4.25:** Final setting of the relay model on the simulation case

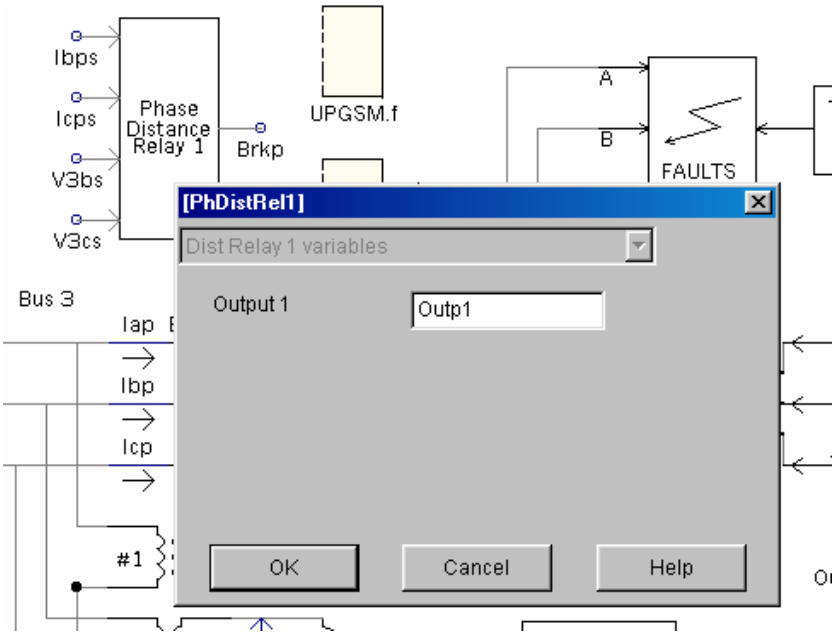


**Figure 4.26:** Assigning a variable in the relay model *Parameters* dialog box

## 4.3 Designing with the proposed protection system model designing methodology

The proposed protection system model designing methodology offers advantages to the process of designing numerical relays. The procedure steps of the proposed methodology are flexible and allow modifications that are useful in the designing of numerical relays models. These advantages for designing numerical relay models are divided as follows.

- Designing with PLSA.
- Designing by modifying the code generated by PLSA.
- Designing with numerical relay models embedded in PSCAD/EMTDC cases.

### 4.3.1 Designing with PLSA

The following are the major advantages that PLSA offers for designing numerical relay models.

- PLSA allows designing numerical relay models of system frequencies different of 60 Hz. PLSA makes all the calculations and considerations to match the system frequency, the PSCAD/EMTDC simulation frequency and the numerical relay sampling frequency.
- The voltage scaling range of the relay input signals can be set accordingly to the need of the user. Different relay internal voltages may be designed modifying the voltage scaling range.
- PLSA gives the option of adding extra channels to the numerical relay models. These additional channels can be used to provide the numerical relay models with signals of the user preference. PLSA assigns a portion of the dynamic memory to the variables related with the additional channels.

- PLSA permits to enter the coefficients of the transfer function of the anti-aliasing filter designed by the user. Provision must be taken to prewarp the user-custom filter before providing the filter transfer function coefficients to PLSA.
- It is possible to choose different digital word size of the processor.

### 4.3.2 Designing by modifying the code generated by PLSA

The files that are the final product of modeling of numerical relays with PLSA contain FORTRAN code that is easily editable. Code of functions that are not contemplated in the generalized numerical relay can be inserted in the FORTRAN code of the files generated by PLSA. Additionally, the parameters of the modules or functions of the generalized numerical relay set by PLSA can be modified accordingly to the needs of the design procedure. The following are the major advantages that the editable code of the files generated by PLSA offer for designing numerical relay models.

- PLSA assigns a portion of the dynamic memory intended for user variables. These variables are updated every PSCAD/EMTDC simulation time step and the user can use them to preserve values of interest.
- It is possible to expand the size of the dynamic memory as long as the added portion is not allocated on portions of the memory already in use.
- PLSA can include in the code the estimation of phasors of harmonics (different from the fundamental) of the input signals. Additional code may be included to make use of the information of the phasors of the harmonics, depending on the needs of the design.
- The phasor estimator algorithm generated by PLSA may be replaced by a phasor estimation technique of the preference of the user.
- User-custom trigger logics are possible to design modifying the code generated by PLSA.
- The trip logic and the apparent impedance seen by the relay model can be used to design user-custom distance relay characteristic.

To edit the code of the embedded numerical relay model, a right-click is issued over the icon of the relay in PSCAD. From the menu that appears, the options *Special* and *Edit Definition* are selected, as shown in Figure 4.27. The *Component Wizard* windows is activated and the code stored in *Dsout* is edited.

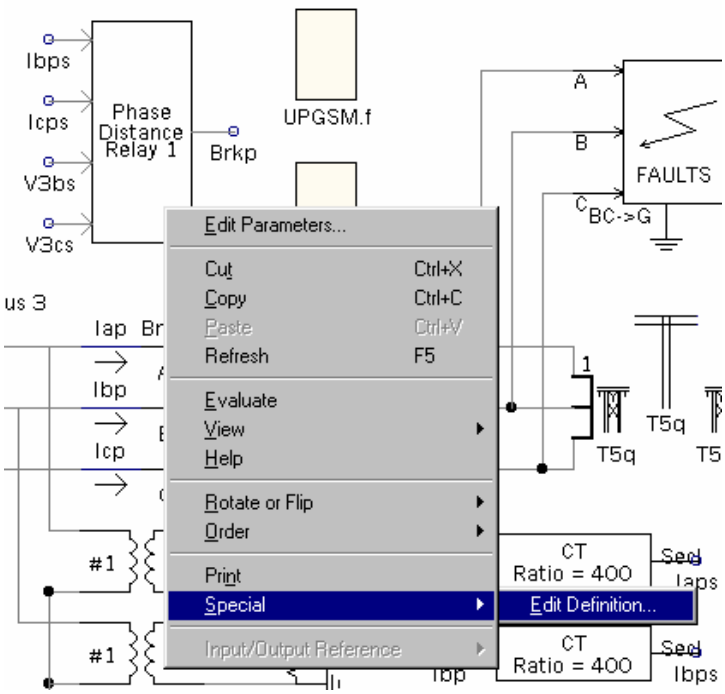


**Figure 4.27:** Activating the *Component Wizard* windows for editing the code of the embedded relay model

### 4.3.3 Designing with the numerical relay model embedded in PSCAD/EMTDC

The numerical relay model designed with the proposed methodology can be used as basic structure for more complete and complex designs. *Components*, the PSCAD/EMTDC structure used in this methodology to embed numerical relay models in PSCAD/EMTDC cases, are flexible structures that can accept modifications and additions required by user-custom designs. The numerical relay models of this

methodology can exploit the full capabilities of PSCAD/EMTDC, since these numerical relay models are natural elements of PSCAD/EMTDC. Thus, the numerical relay models can work along with other PSCAD/EMTDC elements or with other PSCAD/EMTDC procedures.

## 4.4 Summary

In chapter 4 has been described the proposed protection system model designing methodology. The computer program developed in this project to generate numerical relay models (PLSA) has been introduced. The structure and functionality of the computer program PLSA has been discussed. The user interfaces to design the different internal modules of the generalized numerical relay model have been reviewed. The use of PLSA has also been described. The procedure to embed the numerical relay models designed with PLSA in a PSCAD/EMTDC case has been outlined. The description of the PSCAD/EMTDC *component* has been carried out. The procedure to initialize a *component* and to use it together with the final products of PLSA to customize the *component* into numerical relay models has been examined. The considerations to connect and set the numerical relay model in a PSCAD/EMTDC have been conveyed. Finally, the benefits that the proposed protection system model designing methodology offers for the designing of numerical relay have been weighted and enumerated.

# 5. PROTECTION SYSTEM STUDIES

## 5.1 Introduction

The proposed protection system model designing methodology was introduced in chapter 4. The different tools employed by the proposed methodology, the designing of numerical relay models and their embedding in PSCAD/EMTDC cases were also discussed in chapter 4.

The studies of protection system models designed with the proposed methodology are presented in this chapter. These studies are divided in analysis of relay model internal signals, studies of distance relays protecting a transmission line, and studies of differential relays protecting a power transformer. The distance and differential protection studies performed are enumerated. The adjustment and setting of the distance and differential relays are examined. The performance of the distance and differential relay models in fault events of diverse nature is investigated. The responses of the distance and differential relay models to CT saturation are reviewed. The behavior of distance and differential relay models when the anti-aliasing filter is removed is analyzed. The performance of distance relay models actuating as remote back ups is studied. The adjustment issues of differential protections to inrush current are described.

## 5.2 Modeling of the test power system employed in the studies

The first step of the proposed methodology was to model a power system in PSCAD/EMTDC. In Figure 5.1 is shown the 17-bus test system employed to develop

the power system studies performed in the present chapter. This 17-bus test system was developed by the Protection Group of the University of Saskatchewan and was modeled in PSCAD/EMTDC. The information of the electric parameters and data of the 17-bus test system is available in Appendix C of this thesis. The 17-bus test system has two sources representing power systems with excess generation, and two batteries of motors representing power systems that have load in excess of generation.

## 5.3 Designing the numerical relay models employed in the studies

The second step of the proposed methodology was to design the models of the numerical relays protecting the power system using PLSA. Distance and differential relays models were designed to perform the protection system studies. Phase and ground distance relays models were designed to protect transmission line *T5*, located between buses *B3* and *B4* shown in Figure 5.1. A single-phase differential relay model was designed to protect power transformer *Tr7* shown in Figure 5.1.

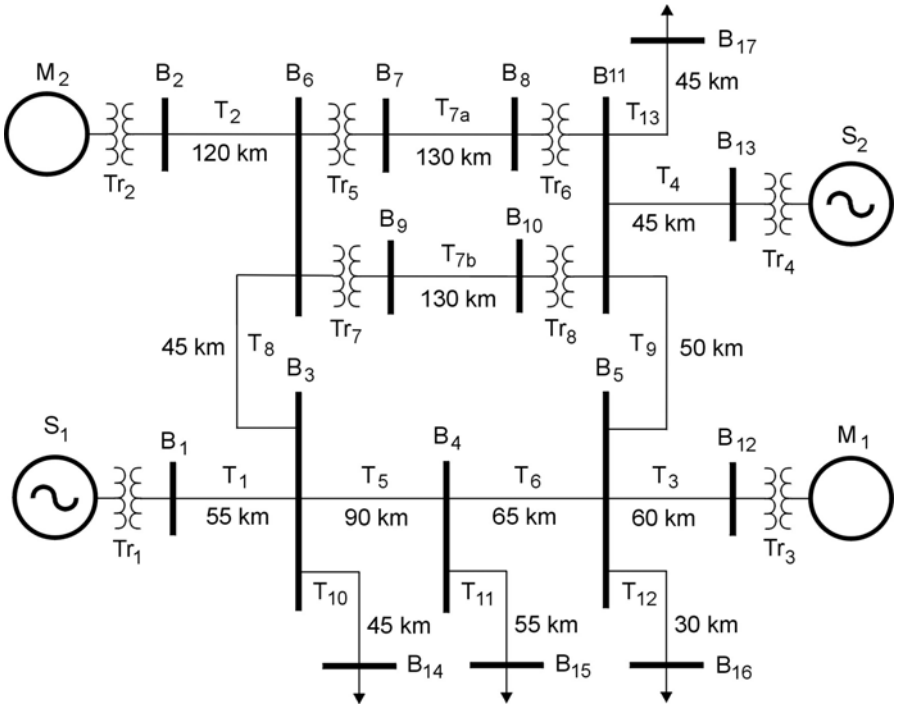


**Figure 5.1:** Seventeen-bus test system

Two phase distance relays models, **Phase Distance Relay P** (*PhDsP*) and **Phase Distance Relay Q** (*PhDsQ*), were designed and embedded in the PSCAD/EMTDC case employing the proposed methodology to protect both sides of the line *T5*. *PhDsP* was set to provide phase distance protection to phases B and C of *T5* from *Bus 3*, while *PhDsQ* was set to provide phase distance protection to phases B and C of *T5* from *Bus 4*. The phase distance protection of transmission line *T5* modeled in PSCAD is shown in Figure 5.2. The transmission line *T5* was divided in two parts to perform faults in its extension, as depicted in Figure 5.2. The portion of *T5* connected to *Bus 3* has been named *T5p*, and the portion of *T5* connected to *Bus 4* is named *T5q*.

The input signals of *PhDsP* were provided by a set of CT's with transforming rates of 2000 A/5 A, and by a set of VT's of transforming rates of 500 kV/10 V. The input signals of *PhDsQ* were provided by a set of CT's with transforming rates of 1500 A/5 A, and by a set of VT's with transforming rates of 500 kV/10 V. Both relay models *PhDsP* and *PhDsQ* employ the auxiliary FORTRAN files *UPEP.f* and *UCCS.f*.

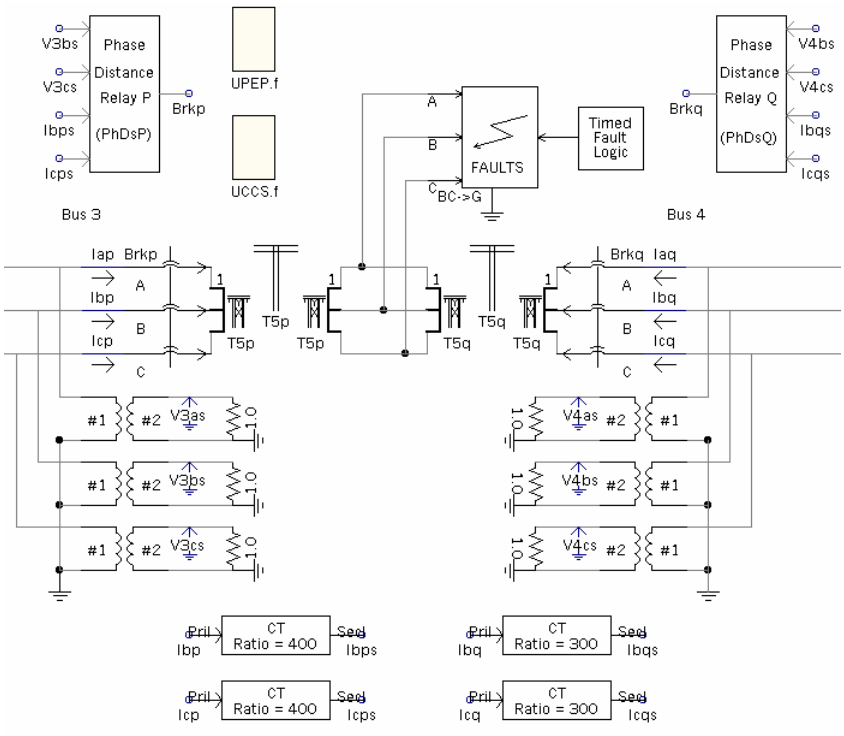


**Figure 5.2:** Phase distance protection of transmission line *T5* in PSCAD

A **Ground Distance Relay P** (*GrDsP)* was designed and embedded in the PSCAD/EMTDC case following the proposed methodology to protect the phase A of the transmission line *T5* from *Bus 3*, as shown in Figure 5.3. The input signals of *GrDsP* were provided by CT's with transforming rates of 2000 A/5 A, and by a set of VT's of transforming rates of 500 kV/10 V. The zero sequence current for current compensation was taken from the addition of the secondary currents of phases A, B, and C. *GrDsP* also employs the auxiliary FORTRAN files *UPEP.f* and *UCCS.f*.

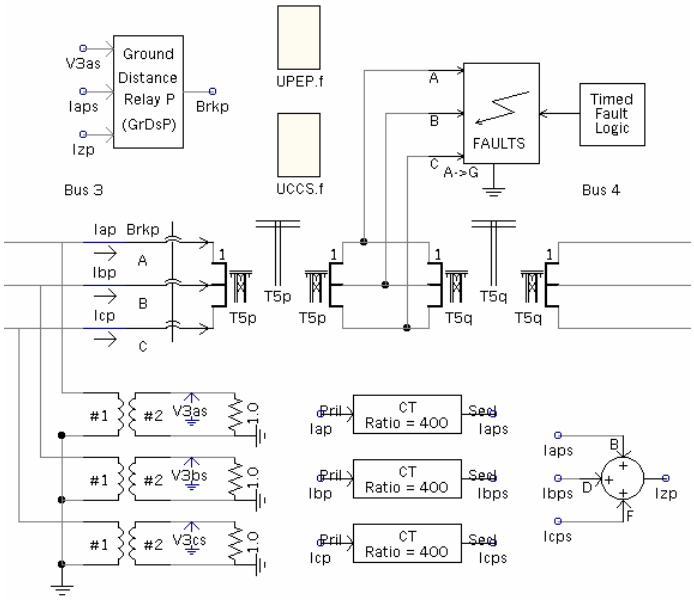


**Figure 5.3:** Ground distance protection of transmission line *T5* in PSCAD

A **Single-Phase Differential Relay** (*SPhDiffR1*) was designed and embedded in the PSCAD/EMTDC case accordingly with the proposed methodology to protect the power transformer $Tr_7$, located between *Bus 6* and *Bus 9*, as shown in Figure 5.4. The input signals of *SPhDiffR1* were provided by a set of CT's, *I6a* and *I9a*, with transforming rates of 1750 A/5 A and 1200 A/5 A, respectively. *SPhDiffR1* employs the auxiliary FORTRAN file *UPEQ.f*. The three-phase fault located in front the current transformers on *Bus 6* represents the maximum fault source of the power transformer $Tr_7$.

The internal modules of the designed relay models *PhDsP*, *PhDsQ*, *GrDsP* and *SPhDiffR1* are all similar, except for the relay algorithm module. The analog signal

scaling modules were set to scale down the acquired current and voltage signals to a range of +10 V to –10 V. The anti-aliasing filtering modules were designed to use a third-order Butterworth, 180 Hz-cutoff frequency, low-pass anti-aliasing filter. The numerical relay models were designed to sample the signal at 720 Hz. The analog-to-digital conversion modules were set to convert the acquired signals into digital values of 16 bits.

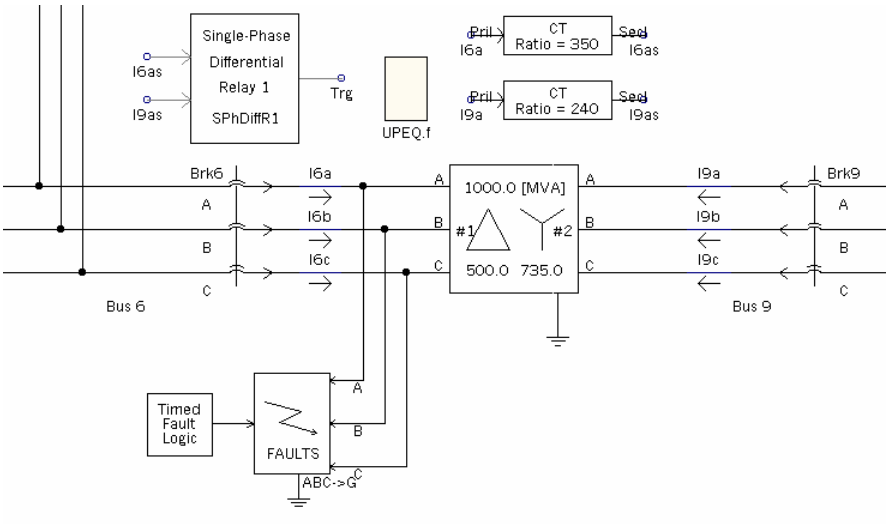


**Figure 5.4:** Single-phase differential protection of power transformer $Tr_7$ in PSCAD

## 5.4 List of protection system studies performed

The protection studies presented in this chapter are divided in analysis of relay model internal signals, studies of distance relays protecting a transmission line, and studies of differential relays protecting a power transformer.

The first of the studies is common for all numerical relay models and they focus in the observation of the relay signals passing analog scaling and conditioning, anti-aliasing analog filtering, analog-to-digital conversion, and phasor estimation algorithm modules.

The studies of distance numerical relays protecting a transmission line performed in this chapter are the following.

- Setting and adjustment of a numerical phase and ground distance relay protecting a transmission line
- Local distance protection of a faulted transmission line (double line-to-ground faults located at 10, 50, and 90% of the transmission line)
- Remote backup distance protection of a faulted transmission line (double line-to-ground faults located at 25, 50, 75 and 100% of the remote transmission line)
- Distance protection performance for a fault behind its location
- Distance protection performance during CT saturation
- Distance protection performance when anti-aliasing filter removed

The studies of differential numerical relays protecting a power transformer performed in this chapter are the following.

- Setting and adjustment of numerical differential relays protecting a transformer
- Adjustment of differential protection for inrush current presented on a transformer
- Performance of the differential protection under transformer internal faults
- Performance of the differential protection under transformer external faults
- Performance of the differential protection of a transformer during CT saturation
- Performance of the differential protection of a transformer when anti-aliasing filter removed

## 5.5 Observation of signals in the modules of numerical relay models

The behavior of the input voltage signal of phase B in *Bus 3*, *V3bs* on Figure 5.2, for a phase B-phase C-to ground fault at 80% of *T5*, at a time of $t$ = 0.2481 seconds, of the phase distance relay model *PhDsP* through the different internal modules of the relay model was observed in this study. The modifications that the voltage signal of phase B ($V_b$) after the analog signal scaling, the analog anti-aliasing filter and the analog-to-digital conversion modules are shown in Figure 5.5, respectively.

In Figure 5.5, the waveform of $V_b$ after the analog signal scaling module is the same shape of the original voltage input but scaled to the range of [+10, -10] volts. The anti-aliasing filtering module smoothed the waveform by removing the high frequency components. A delay of 0.00189 seconds in the voltage waveform due to the anti-aliasing filter was observed. In analog-to-digital conversion module the waveform was sampled at 12 samples per cycle and quantized. In Figure 5.5, the scale chosen to observe the quantized waveform was the voltage in Bus 3. The magnitude and phase of the signal $V_b$ estimated by the phasor estimator algorithm module is shown in Figure 5.6.

The observation of the internal signal renders useful information for protection purposes, such as the adjusting parameters or selecting different alternative for the design of the relay modules. The behavior and response of the relay modules signals under specific events can be analyzed in detail, which can help taking proper corrective measures.

## 5.6 Distance relay studies

Under this section are presented the studies of the distance protection designed with the proposed protection system model designing methodology and listed in section 5.4.

### 5.6.1 Setting and adjustment of distance relays protecting a transmission line

The purpose of these studies was to adjust the three zone characteristics curves of phase and ground distance relays. The studies were divided in the adjustment of phase distance relays, and the adjustment of ground distance relays.

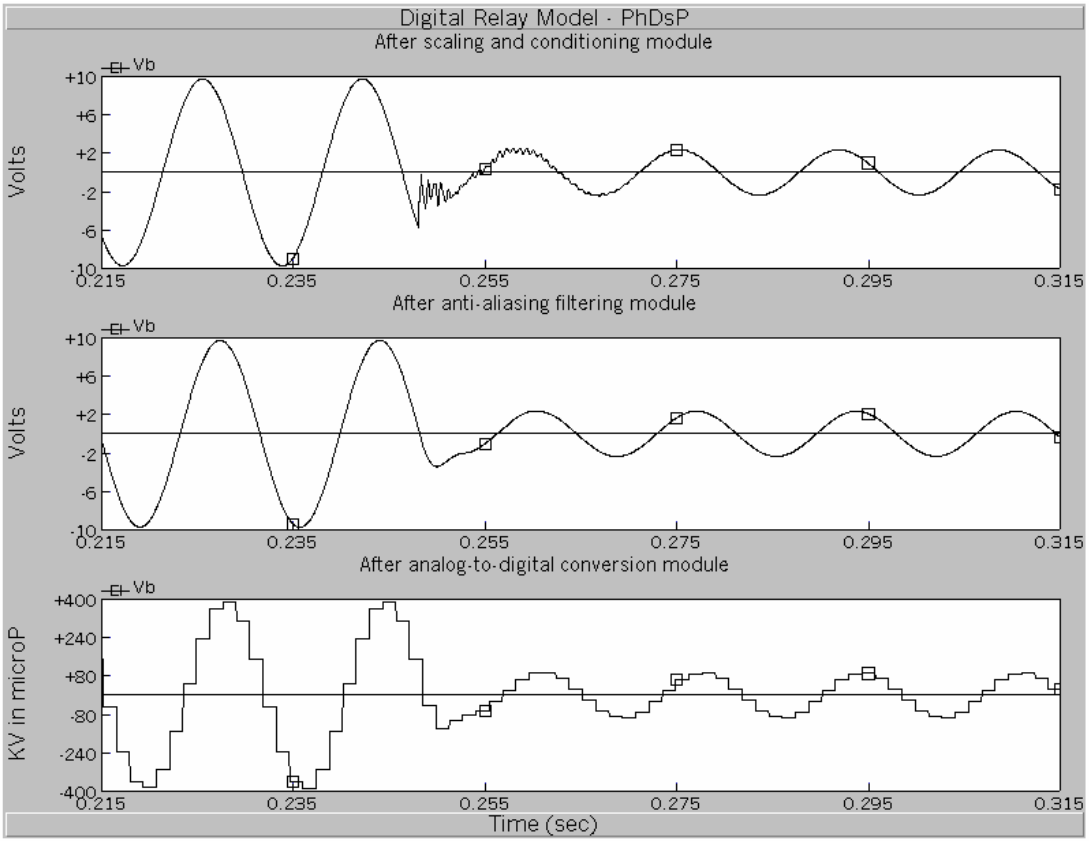


**Figure 5.5:** $V_b$ after scaling and conditioning, anti-aliasing filtering and analog-to-digital conversion modules

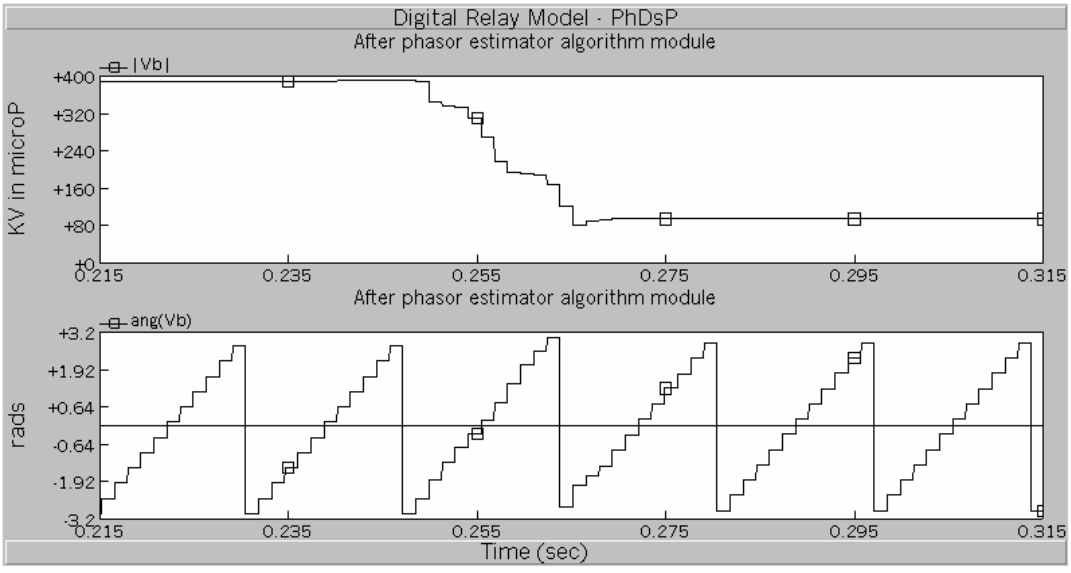


**Figure 5.6:** $V_b$ magnitude and phase after phasor estimator algorithm module

#### 5.6.1.1 Setting and adjustment of numerical phase distance relays

To illustrate this study, the adjustment and setting of phase distance relay *PhDsP* was performed. Mho characteristic were chosen for the three zones of *PhDsP*, all of them employing phase comparators. The purpose of this study was to set the reach adjustments of zone-1, -2 and -3 of *PhDsP*.

##### 5.6.1.1.1 Zone-1 characteristic reach adjustment of phase distance relays

The adjustment of zone-1 was set to protect up to 80% of the impedance of the protected line, as stated in section 2.3.1. A double line-to-ground fault between phase B and C was simulated at 80% of *T5*, at a time of $t$ = 0.2481 seconds, with the arrangement showed in Figure 5.2. As stated in section 2.3.4, the operating condition of the phase comparator is given by the following expression.

$$-90° \leq \arg(S_1) - \arg(S_2) \leq 90° \qquad (5.1)$$

The reach of the characteristic was adjusted with a trial-and-error procedure to meet the condition of Equation 5.1. This is, the reach of the characteristic reach of zone-1 was set to a given impedance value and the double line-to-ground fault was simulated. If the operating condition of Equation 5.1 was not met, then the characteristic reach impedance was given a bigger value. If the operating condition was met, then the characteristic reach impedance was given a smaller value. This procedure finished when the value of the characteristic reach impedance allowed meeting the operating condition but a relative smaller value of this impedance did not. The result was that the reach of the mho characteristic of zone-1 of the phase distance relay model *PhDsP* was set at 24.07 ohms. In Figure 5.7(a) is shown the relevant information of the angular difference of signal $S_1$ and $S_2$ (*Difa*) of the zone-1 phase comparator when the reach of the mho characteristic was adjusted at 24.07 ohms. In Figure 5.7(b) is shown a zooming of Figure 5.7(a), for better appreciation of the proximity of the curve to the value of $-\pi/2$.

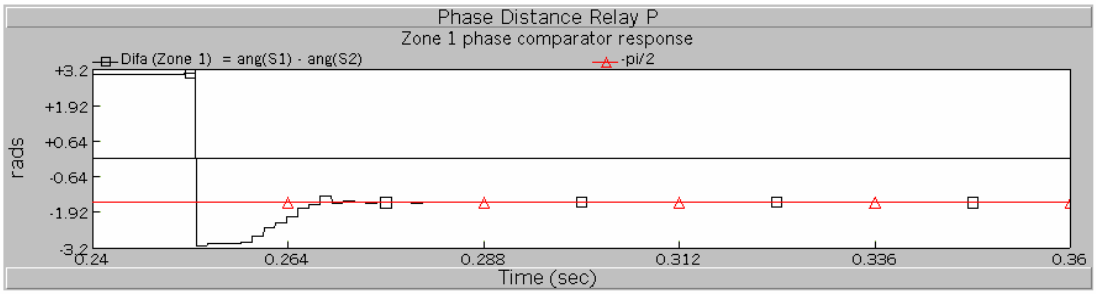


**(a)** View of the relevant information of the simulation

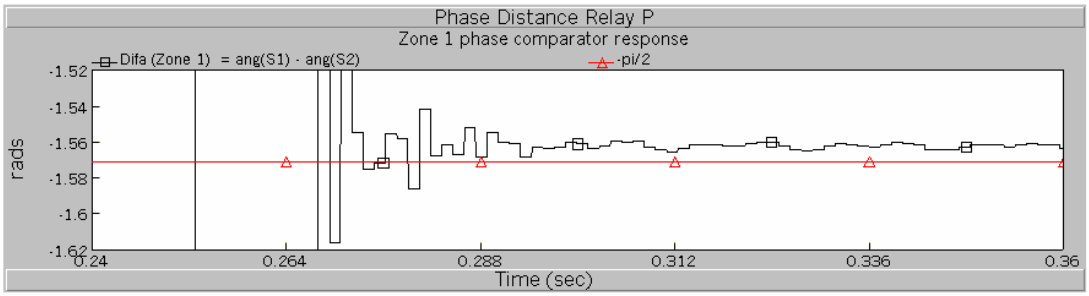


**(b)** Zooming of the previous figure

**Figure 5.7:** Phase comparator response, *PhDsP* zone-1, phase B-phase C-to-ground fault, 80% of *T5* from relay location

In Figure 5.7 is observed that *Difa* oscillates and stabilizes around a given value. The characteristic reach impedance of 24.07 ohms forced that the stable value of *Difa* remained inside the operation condition of Equation 5.1, which makes the zone-1 of *PhDsP* operating for phase B-phase C-to-ground faults at 80% of the protecting line.

#### 5.6.1.1.2 Zone-2 characteristic reach adjustment of phase distance relays

The adjustment of zone-2 of *PhDsP* was set to protect up to 50% of the shortest impedance of the lines *T6* and *T11*, emanating from the remote bus, as stated in section 2.3.1. Phase B- phase C-to-ground faults were simulated at 50% of the lines *T6* and *T11*, at a time of $t$=0.2481 seconds, with the arrangement showed in Figure 5.8. The fault at 50% of transmission line *T6* presented the minor apparent impedance. In Figure 5.8 is shown line *T6* divided in two sections to simulate faults in its extension. The

section of *T6* connected to *Bus 4* was named *T6m*, and the section of *T6* connected to *Bus 5* was named *T6n*. A trial-and-error procedure similar to the used for the adjustment of zone-1 was employed to adjust zone-2 of *PhDsP*. With this procedure, the reach of the mho characteristic of zone-2 of the phase distance relay model *PhDsP* was set at 40.997 ohms. In Figure 5.9(a) is shown the angular difference *Difa* of the zone-2 phase comparator when the reach of the mho characteristic was adjusted at 40.997 ohms. In Figure 5.9(b) is shown a zooming of Figure 5.9(a).

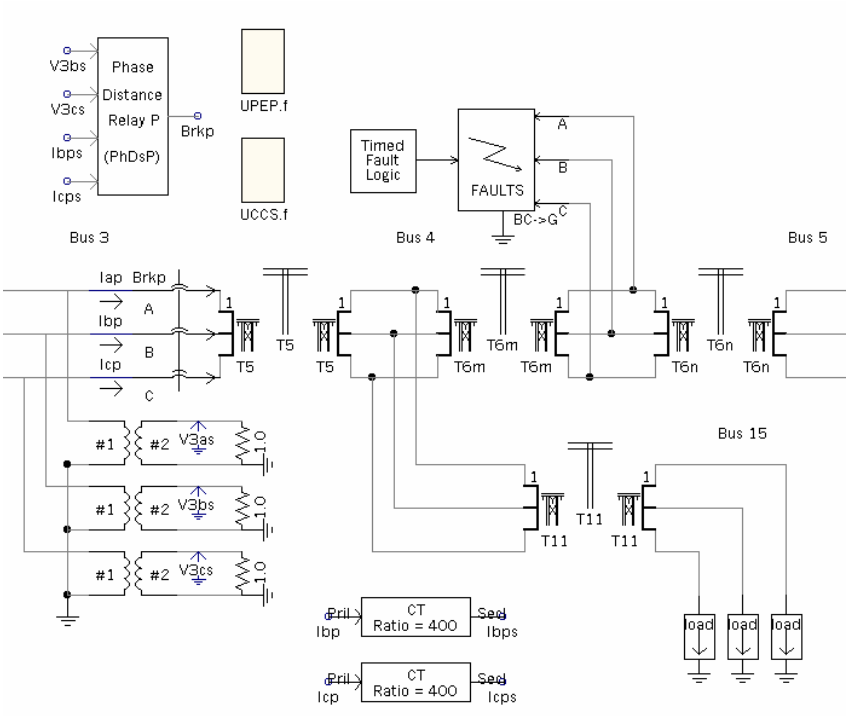


**Figure 5.8:** Double line-to-ground fault at 50% of *T6* for *PhDsP* zone-2 adjustment

#### 5.6.1.1.3 Zone-3 characteristic reach adjustment of phase distance relays

The adjustment of zone-3 of *PhDsP* was set to protect up to 100% of the remote line *T6*, as stated in section 2.3.1. A phase B- phase C-to-ground fault was simulated at 100% of the remote line *T6*, at a time of $t$=0.2481 seconds, with the arrangement showed in Figure 5.10.

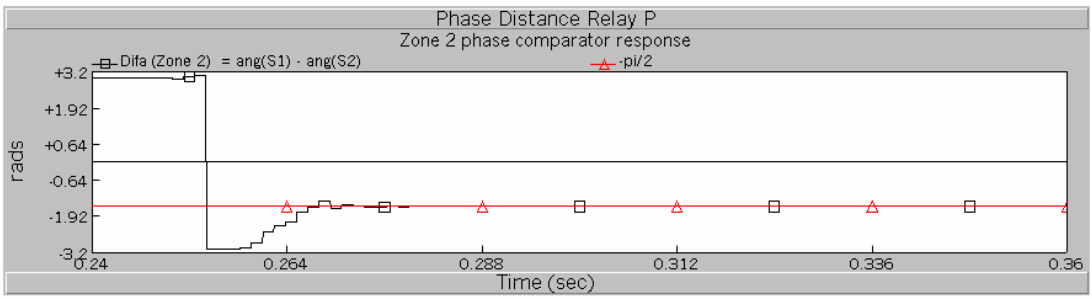


**(a)** View of the relevant information of the simulation

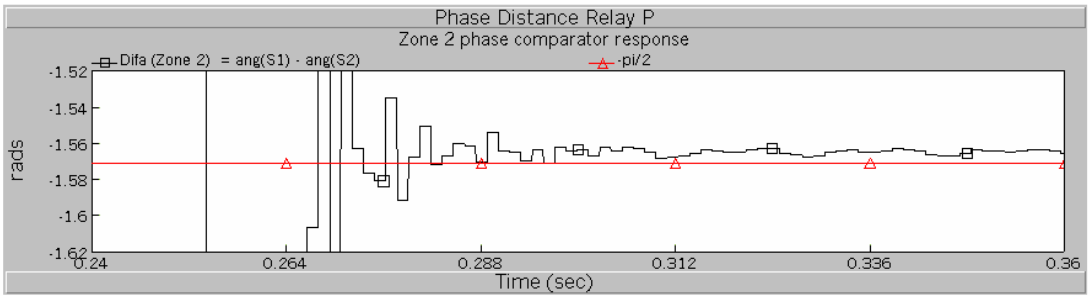


**(b)** Zooming of the previous figure

**Figure 5.9:** Phase comparator response, *PhDsP* zone-2, phase B-phase C-to-ground fault, 50% of remote line *T6*

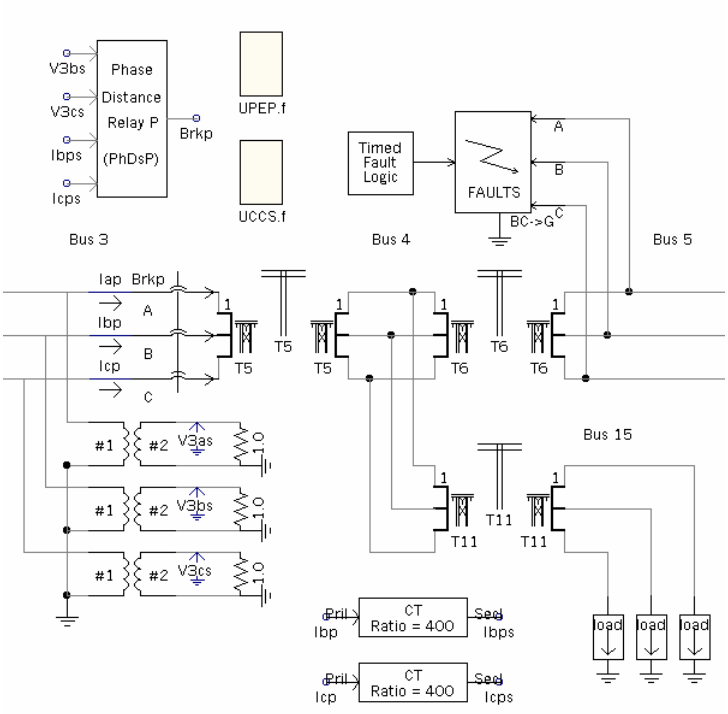


**Figure 5.10:** Double line-to-ground fault at 100% of *T6* for *PhDsP* zone-3 adjustment

A trial-and-error procedure was also employed to adjust zone-3 of *PhDsP*. With this procedure, the reach of the mho characteristic of zone-3 of the phase distance relay model *PhDsP* was set at 51.93 ohms. In Figure 5.11(a) is shown the angular difference *Difa* of the zone-3 phase comparator when the reach of the mho characteristic was adjusted at 51.93 ohms. In Figure 5.11(b) is shown a zooming of Figure 5.11(a).

#### 5.6.1.1.4 Summary of adjustments of phase distance relays

In Table 5.1 are summarized the adjustment of the zones of the phase distance relay *PhDsP*. Time delays were given to the zones of *PhDsP*, as suggested in section 2.3.1. Following the same approach, the phase distance relay *PhDsQ* was also adjusted, also depicted in Figure 5.2. In Table 5.2 are summarized the adjustments of the characteristic impedance reach characteristic of *PhDsQ*, as well as the time delays settings.

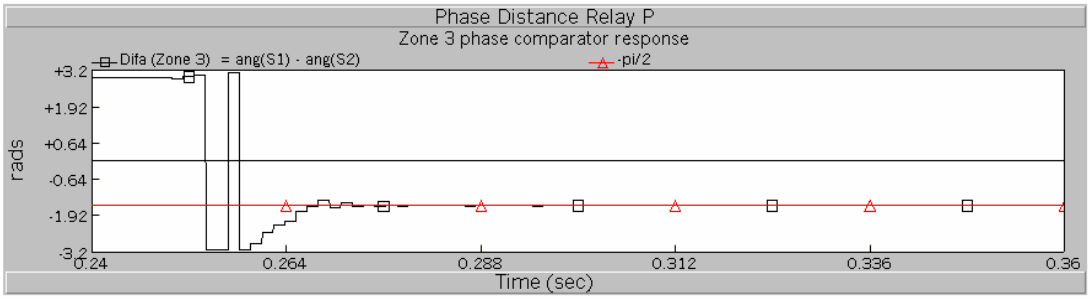


**(a)** View of the relevant information of the simulation

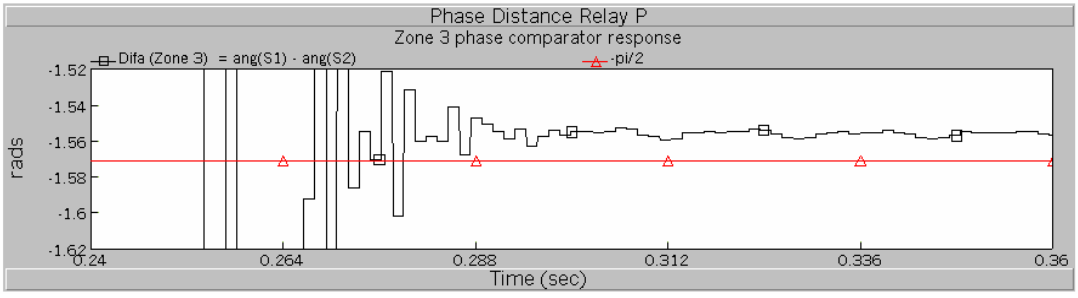


**(b)** Zooming of the previous figure

**Figure 5.11:** Phase comparator response, *PhDsP* zone-3, phase B-phase C-to-ground fault, 100% of remote line *T6*

| Zone | Characteristic | Reach impedance setting (ohms) | Time delay (seconds) |
|---|---|---|---|
| 1 | Mho | 24.07 | 0.02 |
| 2 | Mho | 40.997 | 0.2 |
| 3 | Mho | 51.93 | 0.4 |

**Table 5.1:** Zone adjustments and time delay settings of the phase distance relay *PhDsP*

| Zone | Characteristic | Reach impedance setting (ohms) | Time delay (seconds) |
|---|---|---|---|
| 1 | Mho | 24.03 | 0.02 |
| 2 | Mho | 60.5 | 0.2 |
| 3 | Mho | 95 | 0.4 |

**Table 5.2:** Zone adjustments and time delay settings of the phase distance relay *PhDsQ*

### 5.6.1.2 Setting and adjustment of a ground phase distance relay

To illustrate this study, the ground distance relay model *GrDsP* was adjusted to protect phase A of transmission line *T5*. Mho characteristics were chosen for the three zones of *GrDsP*, all of them employing phase comparators. The purpose of this study was to set the reach adjustments of zone-1, -2 and -3 of *GrDsP*. A trial-and-error procedure similar to the used for adjusting the phase distance relay model *PhDsP* was employed to adjust the ground distance relay model *GrDsP* using the simulation of a phase A-to-ground fault at a time $t = 0.2481$ seconds, with location depending of the zone to adjust.

#### 5.6.1.2.1 Zone-1 characteristic reach adjustment of ground distance relay

To adjust the zone-1 mho characteristic of ground distance relay *GrDsP*, a phase A-to-ground fault was performed at 80% of *T5*, with the arrangement showed in Figure 5.3. The reach of the mho characteristic of zone-1 of the ground distance relay model *GrDsP* obtained was 23.3 ohms. In Figure 5.12(a) is shown the relevant information of the angular difference *Difa* of the zone-1 phase comparator when the reach of the mho characteristic was adjusted at 23.3 ohms. In Figure 5.12(b) is shown a zooming of Figure 5.12(a), to observe the proximity of *Difa* to the value of $-\pi/2$.

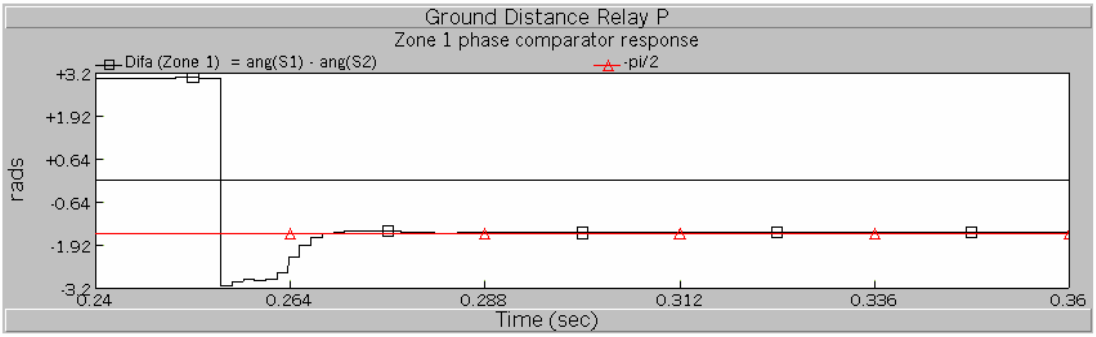


**(a)** View of the relevant information of the simulation

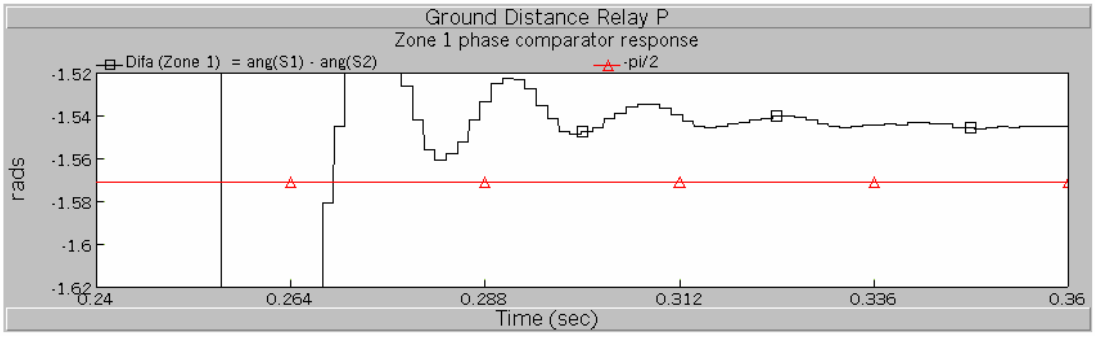


**(b)** Zooming of the previous figure

**Figure 5.12:** Phase comparator response, *GrDsP* zone-1, phase A-to-ground fault, 80% of *T5*

#### 5.6.1.2.2 Zone 2 characteristic reach adjustment of a ground distance relay

To adjust zone-2 mho characteristic of ground distance relay *GrDsP*, a phase A-to-ground fault was performed at 50% of *T6*. The reach of the mho characteristic of zone-2 of the ground distance relay model *GrDsP* obtained was 40.15 ohms. In Figure 5.13(a) is shown the angular difference *Difa* of the zone-2 phase comparator when the reach of the mho characteristic was adjusted at 40.15 ohms. In Figure 5.13(b) is shown a zooming of Figure 5.13(a).

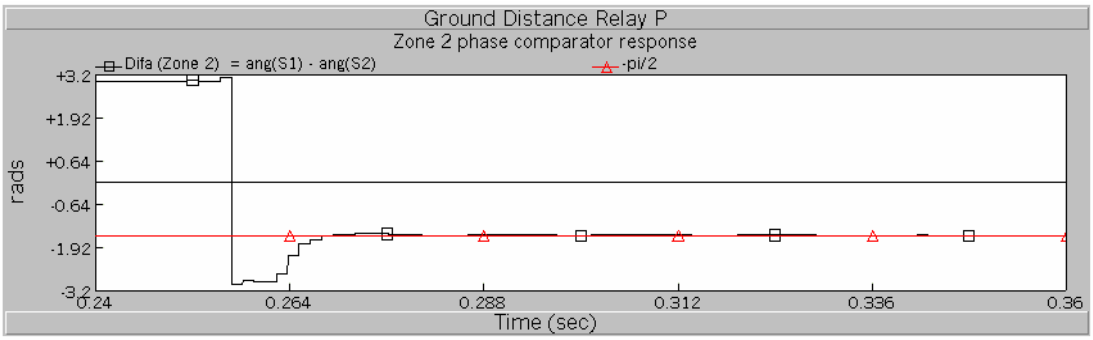


**(a)** View of the relevant information of the simulation

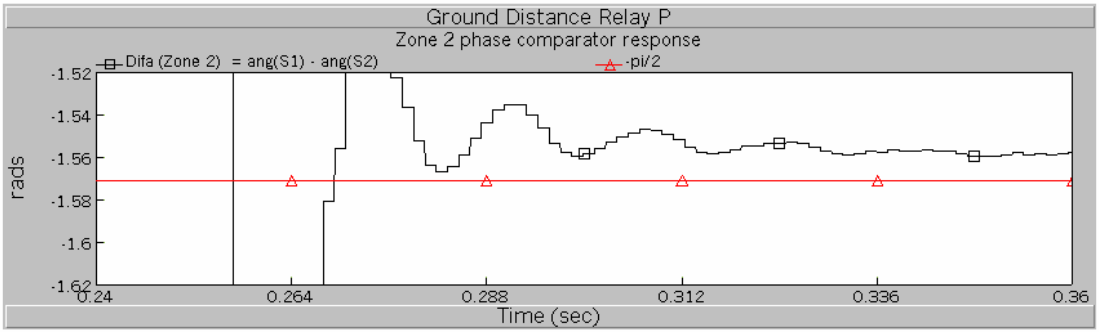


**(b)** Zooming of the previous Figure

**Figure 5.13:** Phase comparator response, *GrDsP* zone-2, phase A-to-ground fault, 50% of remote line *T6*

#### 5.6.1.2.3 Zone 3 characteristic reach adjustment of a ground distance relay

To adjust zone-3 mho characteristic of ground distance relay *GrDsP*, a phase A-to-ground fault was performed at 100% of remote line *T6*. The reach of the mho characteristic of zone-3 of the ground distance relay model *GrDsP* obtained was 51.9 ohms. In Figure 5.14(a) is shown the angular difference *Difa* of the zone-3 phase comparator when the reach of the mho characteristic was adjusted at 51.9 ohms. In Figure 5.14(b) is shown a zooming of Figure 5.14(a).

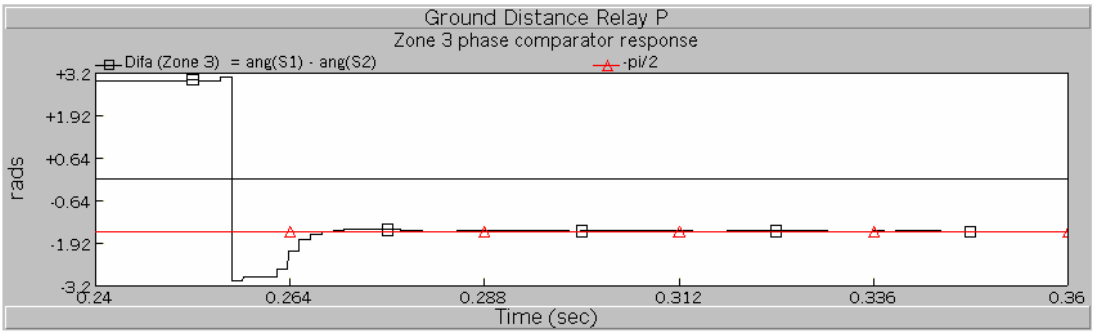


**(a)** View of the relevant information of the simulation

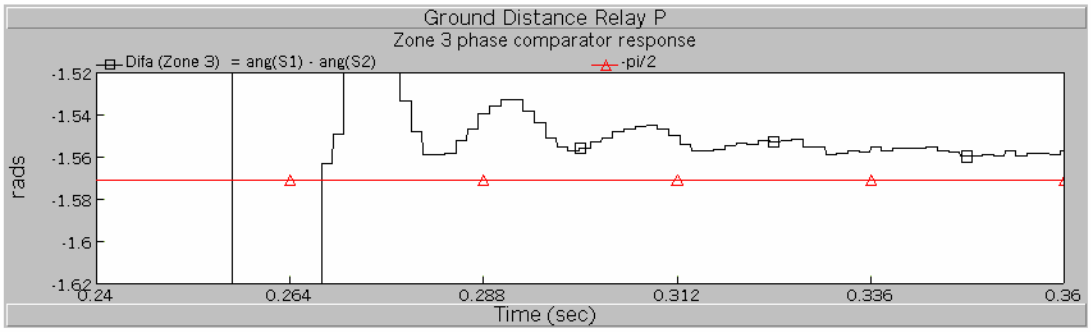


**(b)** Zooming of the previous Figure

**Figure 5.14:** Phase comparator response, *GrDsP* zone-3, phase A-to-ground fault, 100% of remote line *T6*

#### 5.6.1.2.4 Summary of adjustments of a ground distance relay

In Table 5.3 are presented the adjustment obtained of the zones-1, -2 and -3 of the ground distance relay *GrDP*. Time delays were given to the zones of *GrDsP*, in accordance with the suggestions stated in section 2.3.1.

| Zone | Characteristic | Reach impedance setting (ohms) | Time delay (seconds) |
|---|---|---|---|
| 1 | Mho | 23.3 | 0.02 |
| 2 | Mho | 40.15 | 0.2 |
| 3 | Mho | 51.9 | 0.4 |

**Table 5.3:** Ground distance relay *GrDsP* zones adjustments and settings

### 5.6.2 Local distance protection of a faulted transmission line

The purpose of this study was to observe the performance of the distance protection when different faults occur in the transmission line where the distance relay is providing primary local protection. In the study, the phase distances relays *PhDsP* and *PhDsQ*, designed and adjusted in previous sections, were employed to protect the transmission line *T5*. Phase B-phase C-to ground faults were simulated at 10%, 50% and 90% of the length of line *T5*, respect to the location of *PhDsP*, on *Bus 3*, or 90%, 50% and 10% of the length of line *T5*, respect to *PhDsQ*, on *Bus 4* at a time $t$=0.2481 seconds.

In Figure 5.15(a), 5.17(a), and 5.19(a) are shown the curves of the angular difference of the distance comparator signal $S_1$ and $S_2$ (*Difa*) of zone-1, -2, and -3 of *PhDsP*, correspondent to the phases B-phase C-to-ground faults at 10%, 50%, and 90% of the length of *T5* from the relay location, respectively. In Figure 5.15(b), 5.17(b), and 5.19(b) are shown the related trip signal that the phase comparators of zone-1, -2, and -3 issued to these faults, respectively. In Figure 5.16(a), 5.18(a), and 5.20(a) are shown the curves of *Difa* of zone-1, -2, and -3 of the phase distance relay *PhDsQ*, correspondent to

the phases B-phase C-to-ground faults at 90%, 50%, and 10% of the length of *T5* from the relay location, respectively. In Figure 5.16(b), 5.18(b), and 5.20(b) are shown the related trip signal that the phase comparators of zone-1, -2, and -3 issued to these faults, respectively.

In Figure 5.15(a) and 5.15(b) was shown that, for the fault at 10% of *T5* from the location of *PhDsP*, the phase comparator of zone-3 of *PhDsP* was the first in fulfilling its operating condition , followed by zone-2 and zone-1, respectively. However, zone-1 was the first in issuing a trip signal, followed by zones-2 and zone-3, respectively, due to the delay time given to the zones, as specified in Table 5.1. In Figure 5.16(a) and 5.16(b) was observed that, for the same fault, the operating condition of zone-1 of *PhDsQ* was not fulfilled and that zones-2 and zone-3 of *PhDsQ* fulfilled their operating conditions and issued their respective trip signals, accordingly with their time delays.

In Figure 5.17(a) and 5.17(b) was observed that, for the fault at 50% of *T5*, zone-1, zones-2 and zone-3 of *PhDsP* fulfilled their operating conditions and issued their respective trip signals. In Figure 5.18(a) and 5.18(b) was observed that the zones and related trip signal of *PhDsQ* showed a correct operation as well.

In Figure 5.19(a) and 5.19(b) was observed that, for the fault at 90% of *T5* from the location of *PhDsP*, the operation condition of zone-1 of *PhDSP* was not met and that the operating conditions of zones-2 and zone-3 of *PhDsP* met their operating condition and issued their respective trip signals. In Figure 5.20(a) and 5.20(b) was observed that the phase comparator of zone-3 of *PhDsQ* was the first in meeting its operating condition, followed by zone-2 and zone-1, respectively. However, it was zone-1 of *PhDsQ* the first in issuing a trip signal, followed by zones-2 and zone-3, respectively.

The analysis of the figures has demonstrated that the studies of the local protection of a faulted transmission line showed correct outcomes.

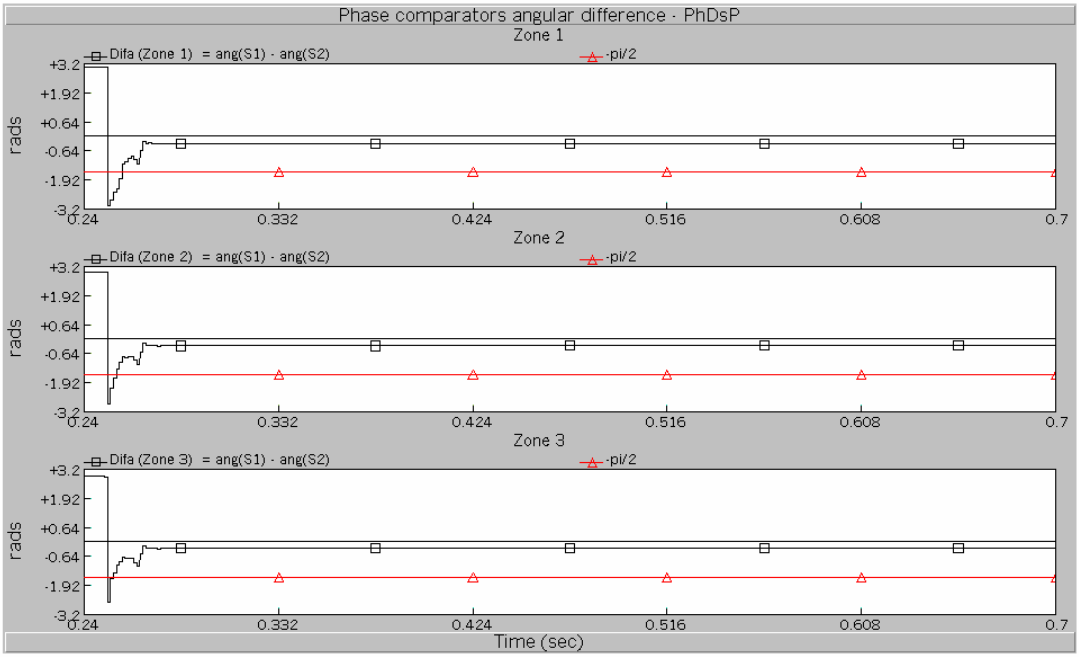


**(a)** Phase comparators response, *PhDsP*, zone-1, zone-2, and zone-3 respectively

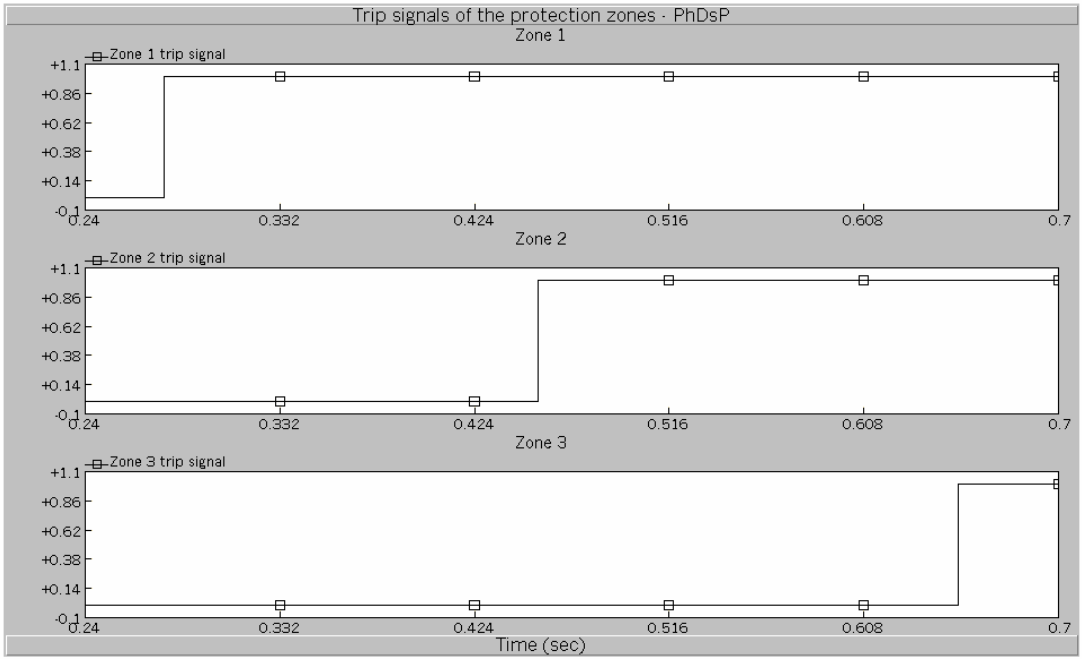


**(b)** Trip signals issued by the phase comparators of *PhDsP*, zone-1, zone-2, and zone-3 respectively

**Figure 5.15:** *PhDsP* responses for a phase B-phase C-to-ground fault at 10% of *T5* from the relay location

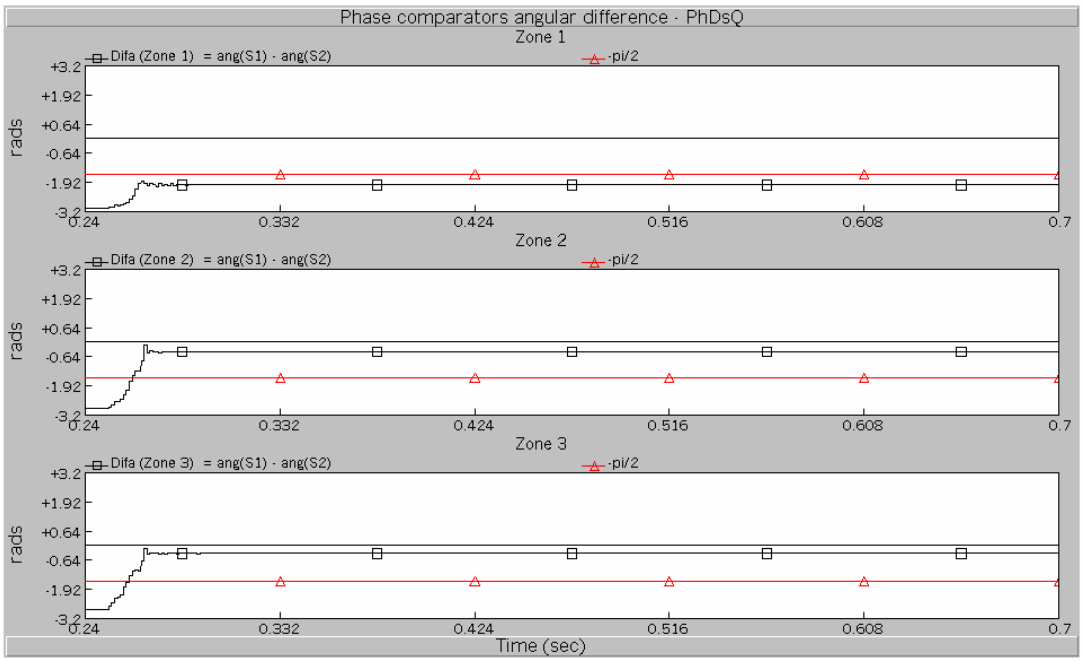


**(a)** Phase comparators response, *PhDsQ*, zone-1, zone-2, and zone-3 respectively

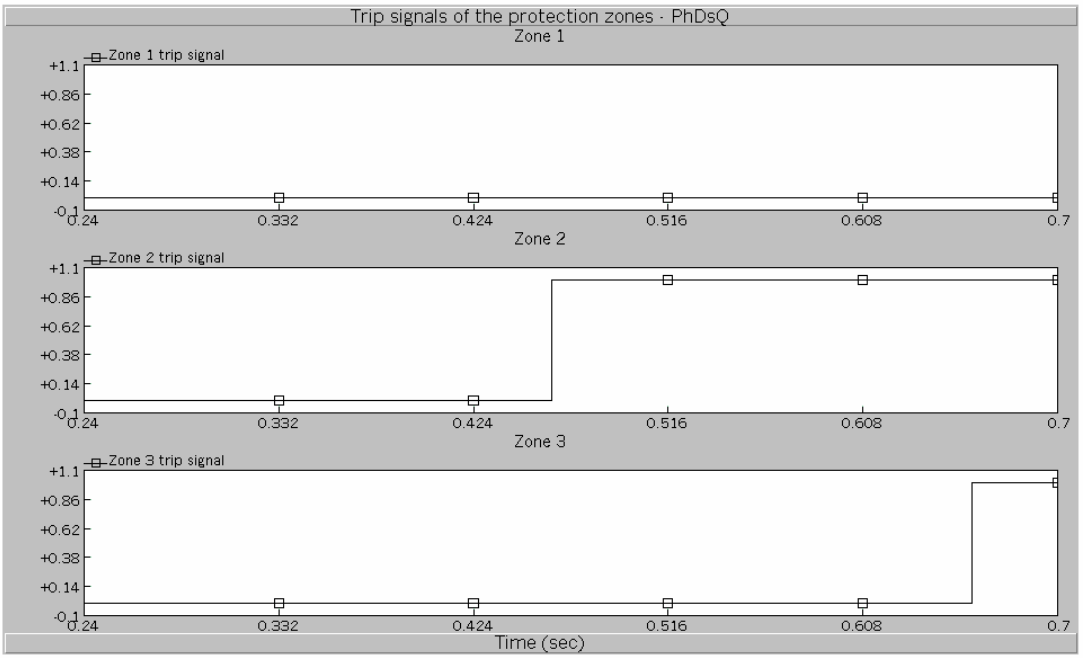


**(b)** Trip signals issued by the phase comparators of *PhDsQ*, zone-1, zone-2, and zone-3 respectively

**Figure 5.16:** *PhDsQ* responses for a phase B-phase C-to-ground fault at 90% of *T5* from the relay location

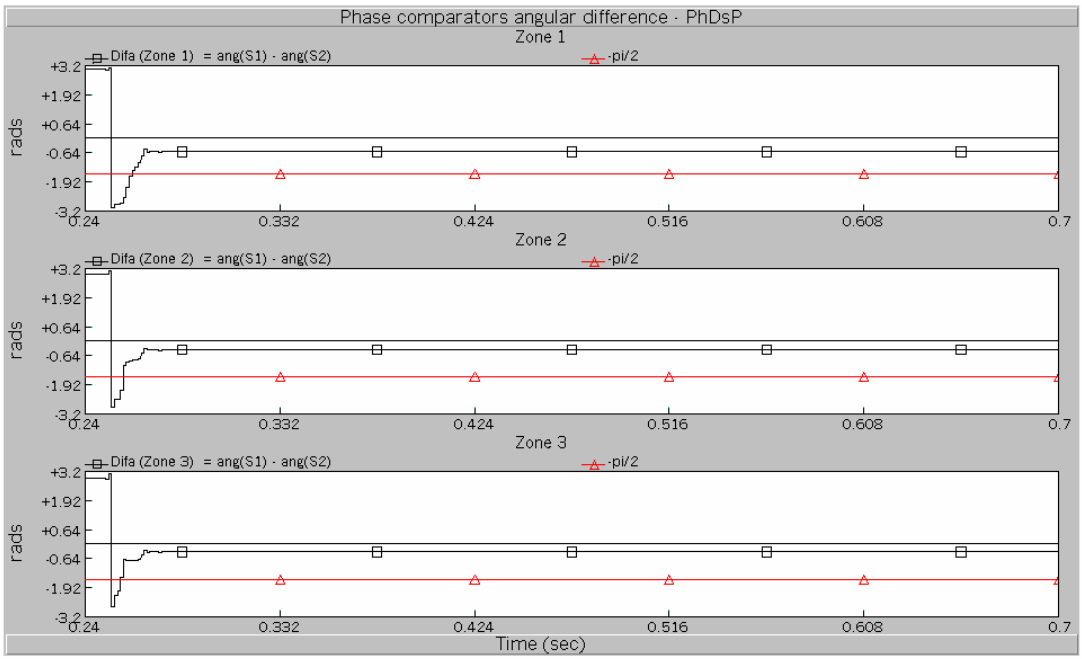


**(a)** Phase comparators response, *PhDsP*, zone-1, zone-2, and zone-3 respectively

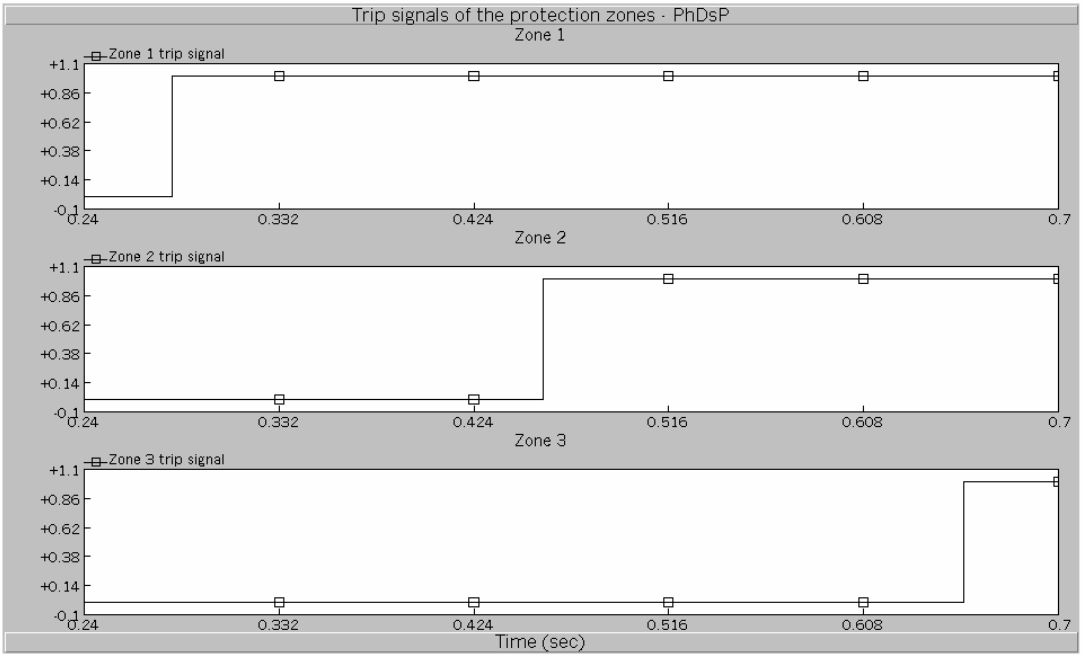


**(b)** Trip signals issued by the phase comparators of *PhDsP*, zone-1, zone-2, and zone-3 respectively

**Figure 5.17:** *PhDsP* responses for a phase B-phase C-to-ground fault at 50% of *T5*

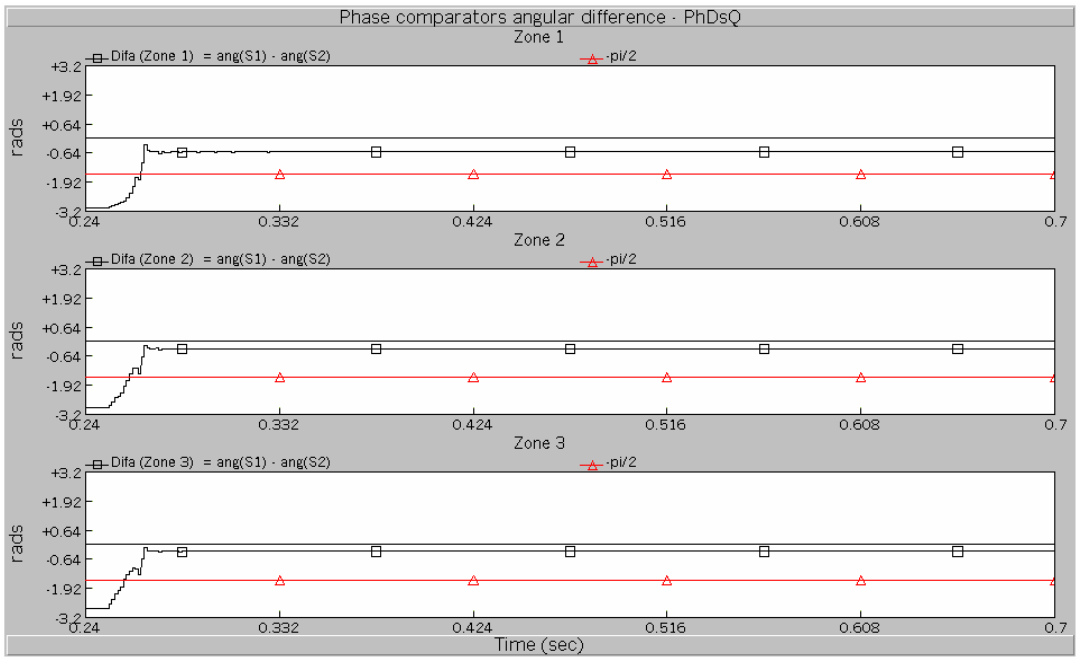


**(a)** Phase comparators response, *PhDsQ*, zone-1, zone-2, and zone-3 respectively

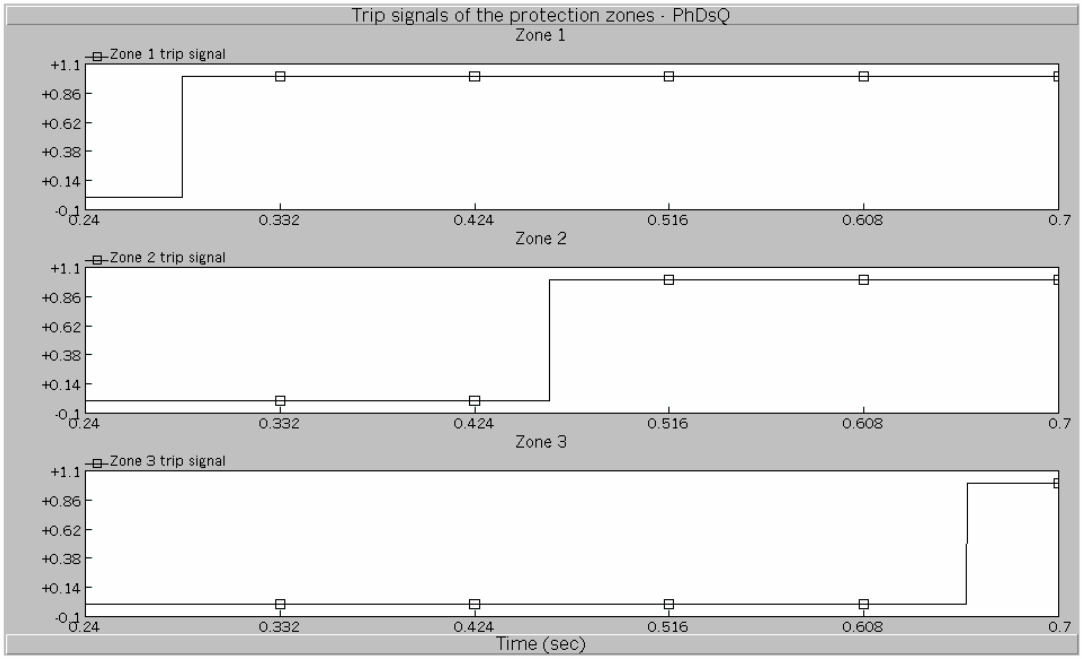


**(b)** Trip signals issued by the phase comparators of *PhDsQ*, zone-1, zone-2, and zone-3 respectively

**Figure 5.18:** *PhDsQ* responses for a phase B-phase C-to-ground fault at 50% of *T5*

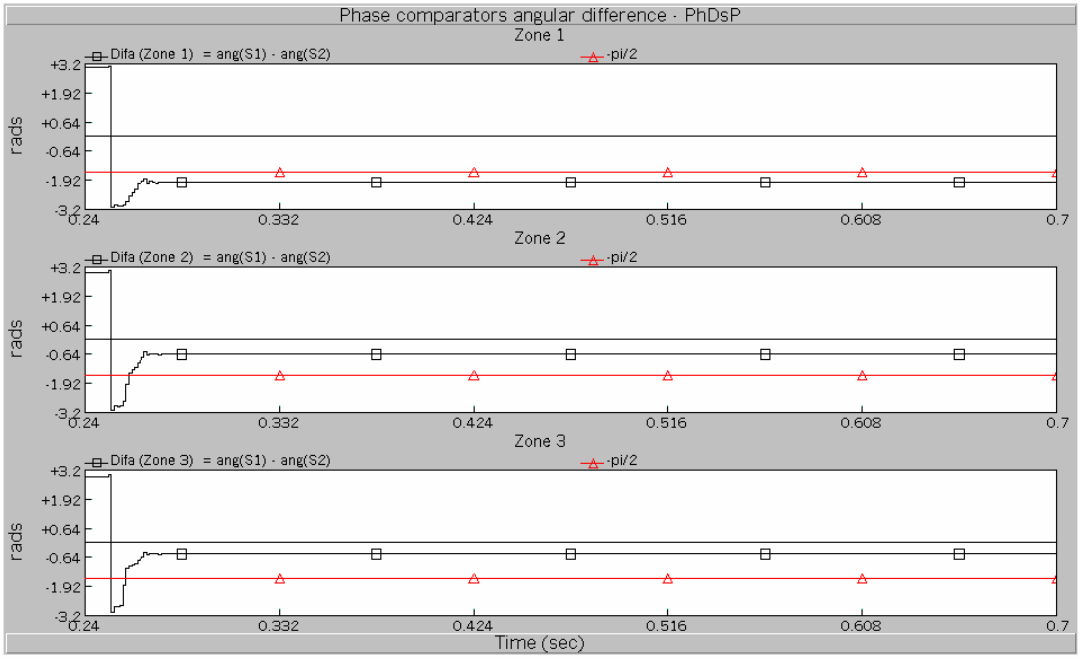


**(a)** Phase comparators response, *PhDsP*, zone-1, zone-2, and zone-3 respectively

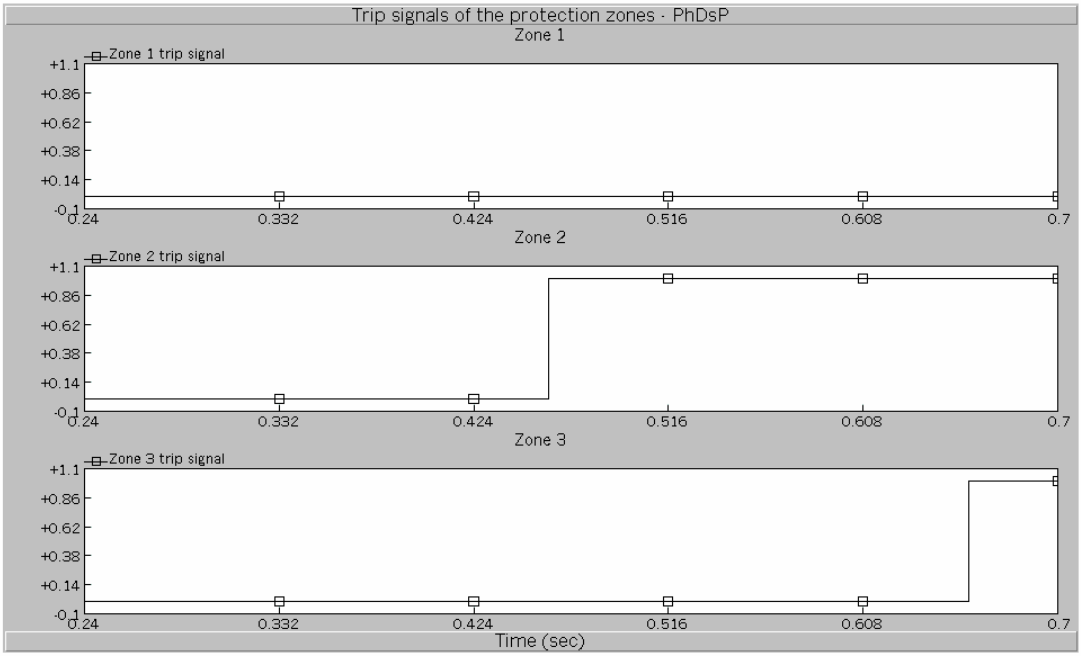


**(b)** Trip signals issued by the phase comparators of *PhDsP*, zone-1, zone-2, and zone-3 respectively

**Figure 5.19:** *PhDsP* responses for a phase B-phase C-to-ground fault at 90% of *T5* from relay location

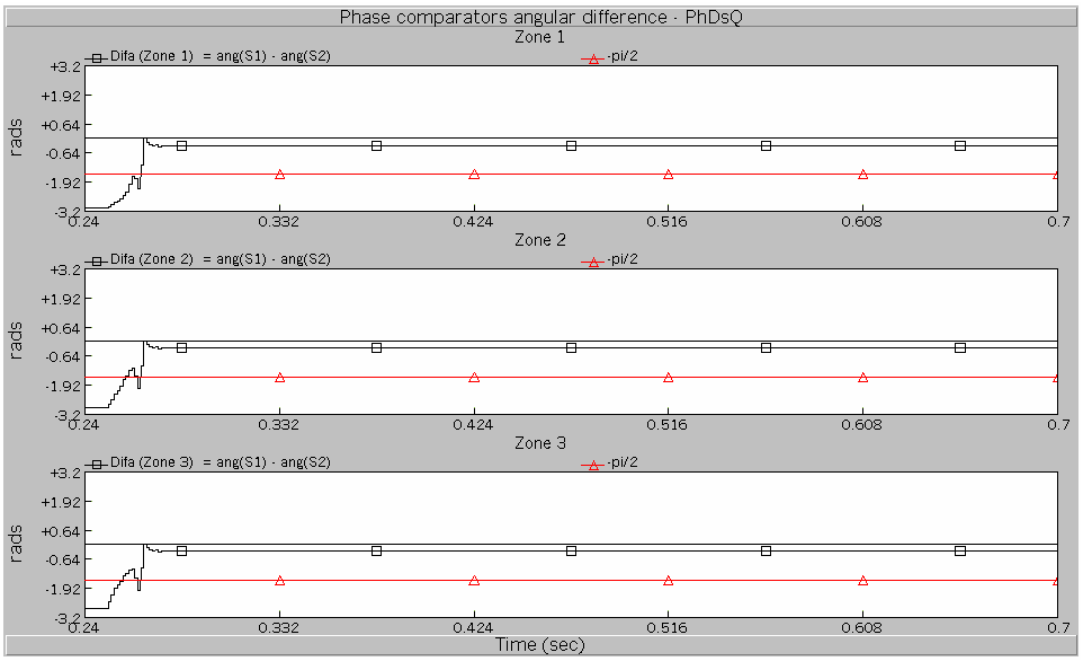


**(a)** Phase comparators response, *PhDsQ*, zone-1, zone-2, and zone-3 respectively

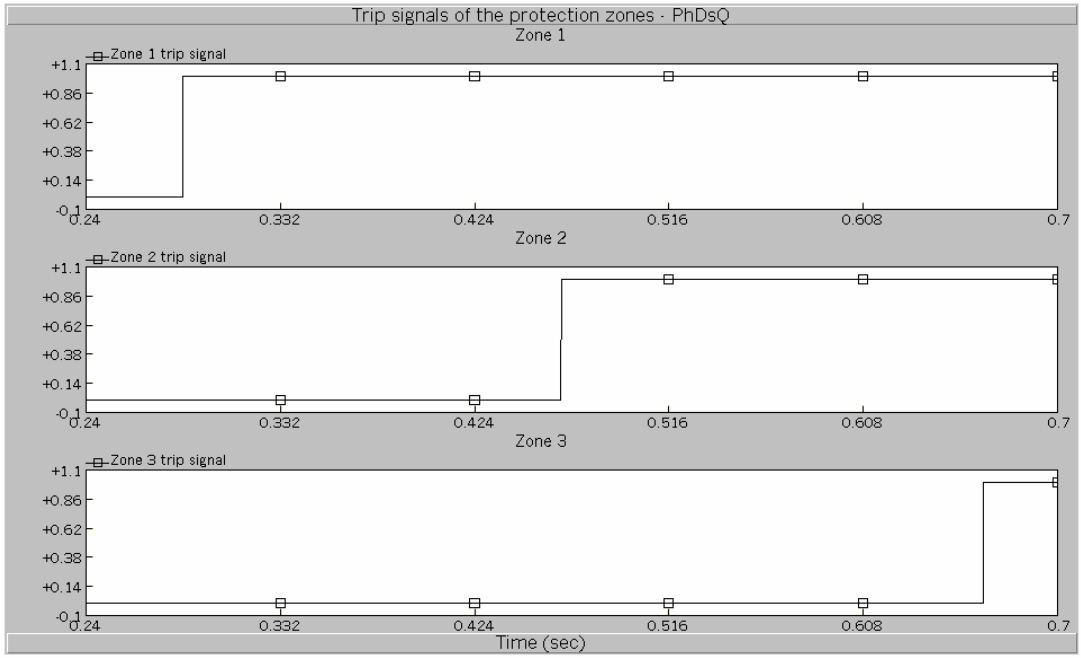


**(b)** Trip signals issued by the phase comparators of *PhDsQ*, zone-1, zone-2, and zone-3 respectively

**Figure 5.20:** *PhDsQ* responses for a phase B-phase C-to-ground fault at 10% of *T5* from the relay location

### 5.6.3 Remote backup protection

The purpose of this study was to investigate the performance of the numerical distance relay models when providing remote backup protection. The relay *PhDsP* was employed in this study to provide remote backup protection to emanating lines *T6* and *T11* of the remote *Bus 4*, as showed in Figure 5.21.

The study consisted in simulating that the primary distance protection of line *T6* or line *T11*, located on *Bus 4*, did not operate for an internal fault. Since Zone-2 and -3 of *PhDsP* were adjusted to protect up to 50% and 100% of the shortest line *T6* respectively, then *PhDsP* would eventually operate to open its sideward in-feed circuit of the remote lines *T6* and *T11*, depending of the location of those faults.

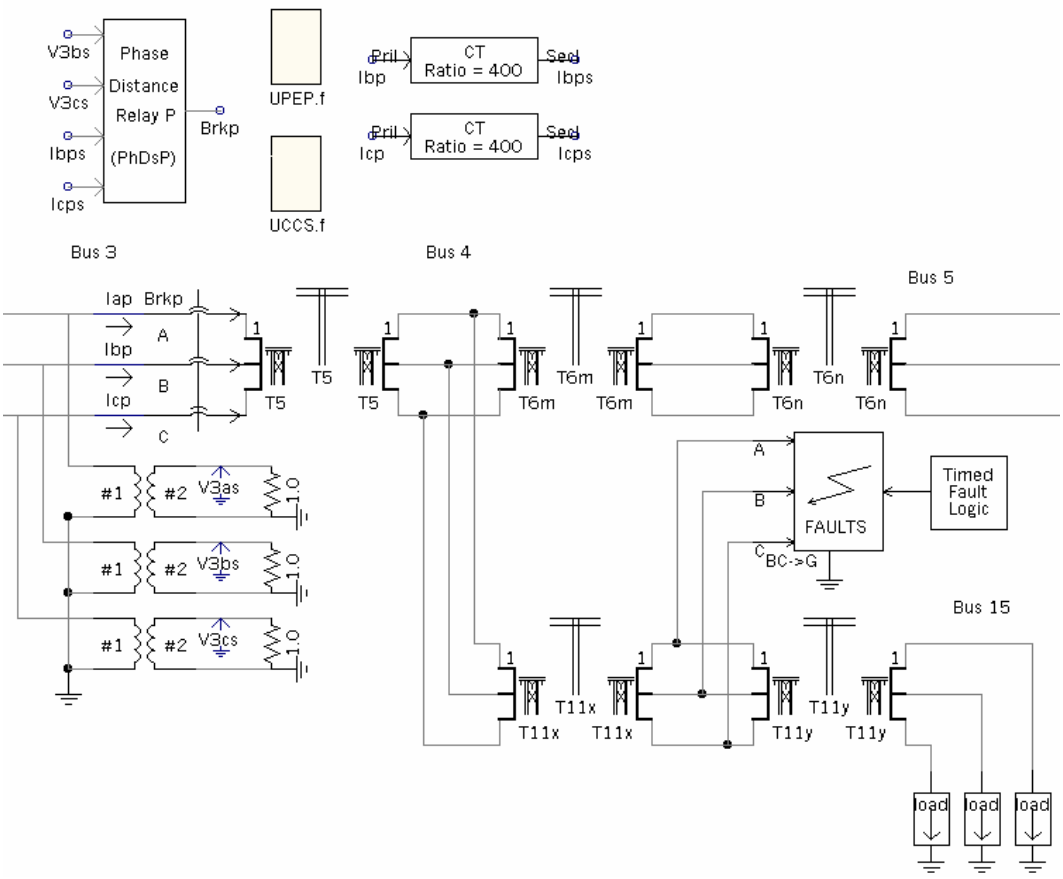


**Figure 5.21:** Relay *PhDsP* providing remote backup protection to lines *T6* and *T11*

The remote backup protection study was divided in faults over remote line *T6*, and faults over remote line *T11*. Phase B-phase C-to-ground faults were simulated at 25%, 50%, 75%, and 100% of remote lines *T6* and *T11*, at a time of $t$=0.2481 seconds.

### 5.6.3.1 Remote backup protection for faults over remote line *T6*

The response of the angular difference of signal $S_1$ and $S_2$ (*Difa*) of the phase comparators of zone-1, -2, and -3 of *PhDsP*, for phase B-phase C-to-ground faults at 25%, 50%, 75%, and 100% of the length of remote line *T6* are shown in Figure 5.22, Figure 5.24, Figure 5.26, and Figure 5.28, respectively.

The trip signals issued by zone-1, -2, and -3 of *PhDsP* for phase B-phase C-to-ground faults at 25%, 50%, 75%, and 100% of the length of remote line *T6* are shown in Figure 5.23, Figure 5.25, Figure 5.27, and Figure 5.29, respectively.

For the phase B-phase C-to-ground fault at 50% of *T6*, the response of *Difa* of zone-2 in Figure 5.24 was zoomed to show that the operating condition in zone-2 was marginally fulfilled. For the phase B-phase C-to-ground fault at 100% of *T6*, the response of *Difa* of zone-3 in Figure 5.28 was zoomed to show that the operating condition in zone-3 was also marginally met.

The trip signals of Figure 5.23, 5.25, 5.27 and 5.29 were issued correctly according with their related operation condition showed on Figure 5.22, 5.24, 5.26, and 5.28, and with the respective time delays, established in Table 5.1.

### 5.6.3.2 Remote backup protection for faults over remote line *T11*

The response of the angular difference of signal $S_1$ and $S_2$ (*Difa*) of the phase comparators of zone-1, -2, and -3 of *PhDsP*, for phase B-phase C-to-ground faults at

25%, 50%, and 75% of the length of remote line *T11* are shown in Figure 5.30, Figure 5.32, and Figure 5.34, respectively.

The trip signals issued by zone-1, -2, and -3 of *PhDsP* for phase B-phase C-to-ground faults at 25%, and 50% of the length of remote line *T11* are shown in Figure 5.31, and Figure 5.33, respectively. There were no trip signals issued when the fault was at 75% of *T11*.

For the phase B-phase C-to-ground fault at 25% of *T11*, the response of *Difa* of zone-2 in Figure 5.30 was zoomed to show that the operating condition in zone-2 was marginally fulfilled.

The trip signals of Figure 5.31 and 5.33 were issued correctly according with their related operation condition showed on Figure 5.30, and 5.32, and with the respective time delays established in Table 5.1.

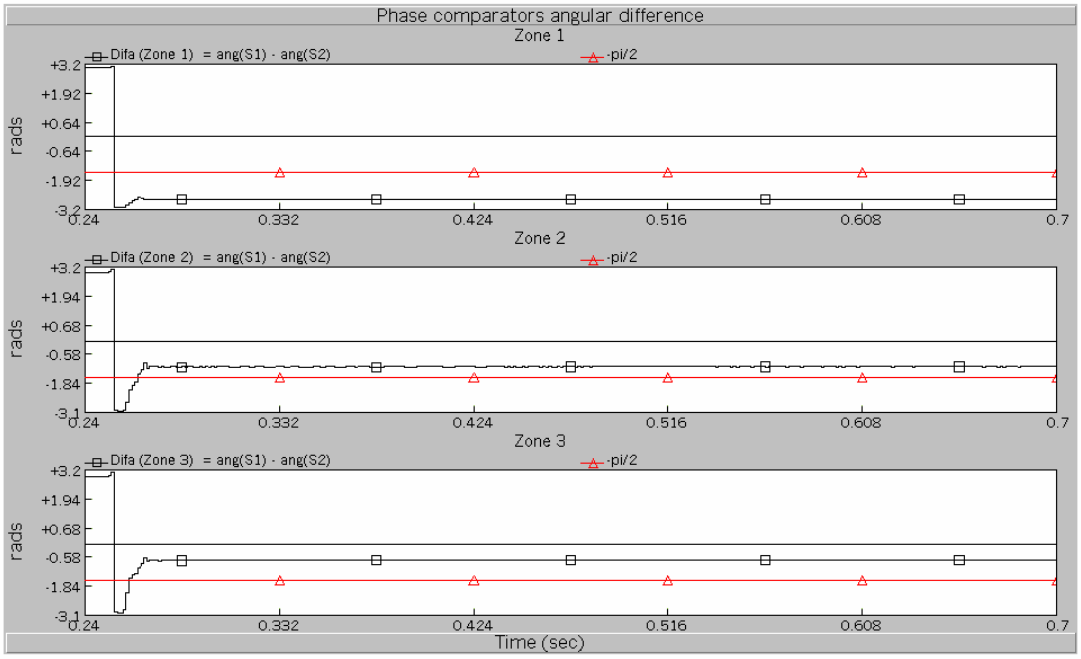


**Figure 5.22:** Response of the phase comparators of *PhDsP*, zone-1, -2, and -3, phase B-phase C-to-ground fault, 25% of remote line *T6*

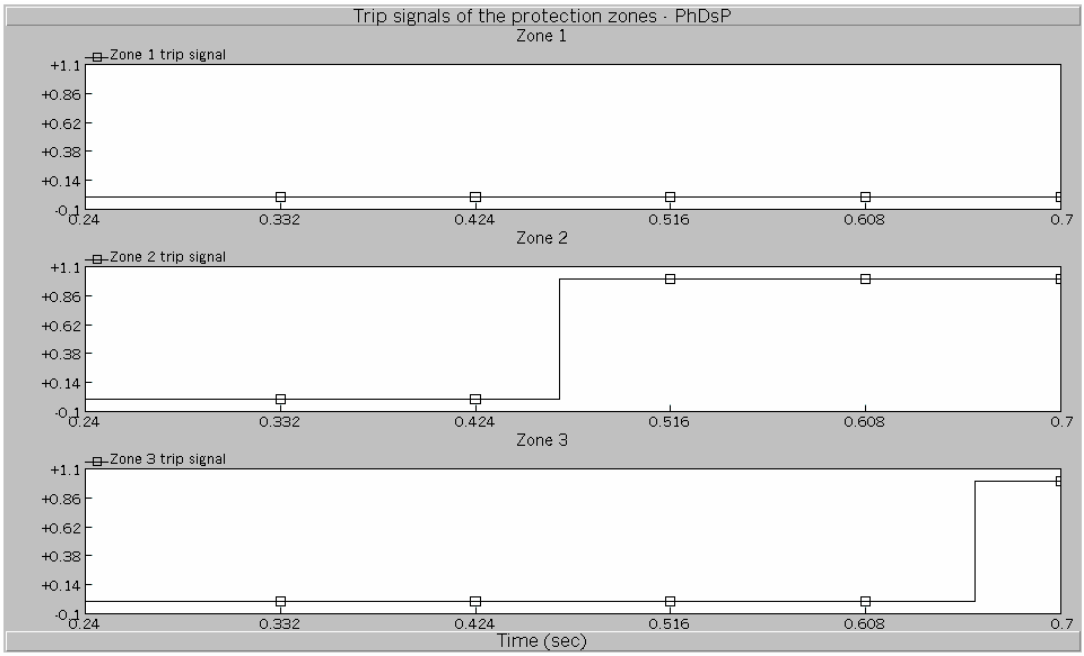


**Figure 5.23:** Trip signals issued by the phase comparators of *PhDsP*, zone-1, -2, and -3, phase B-phase C-to-ground fault, 25% of remote line *T6*

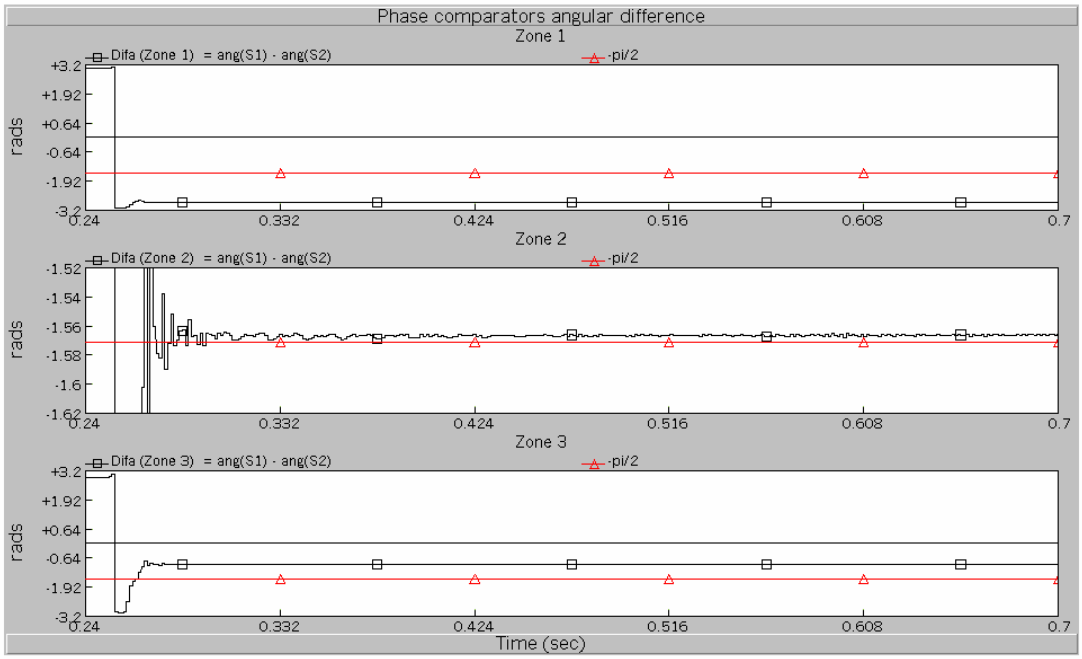


**Figure 5.24:** Response of the phase comparators of *PhDsP*, zone-1, -2, and -3, phase B-phase C-to-ground fault, 50% of remote line *T6*

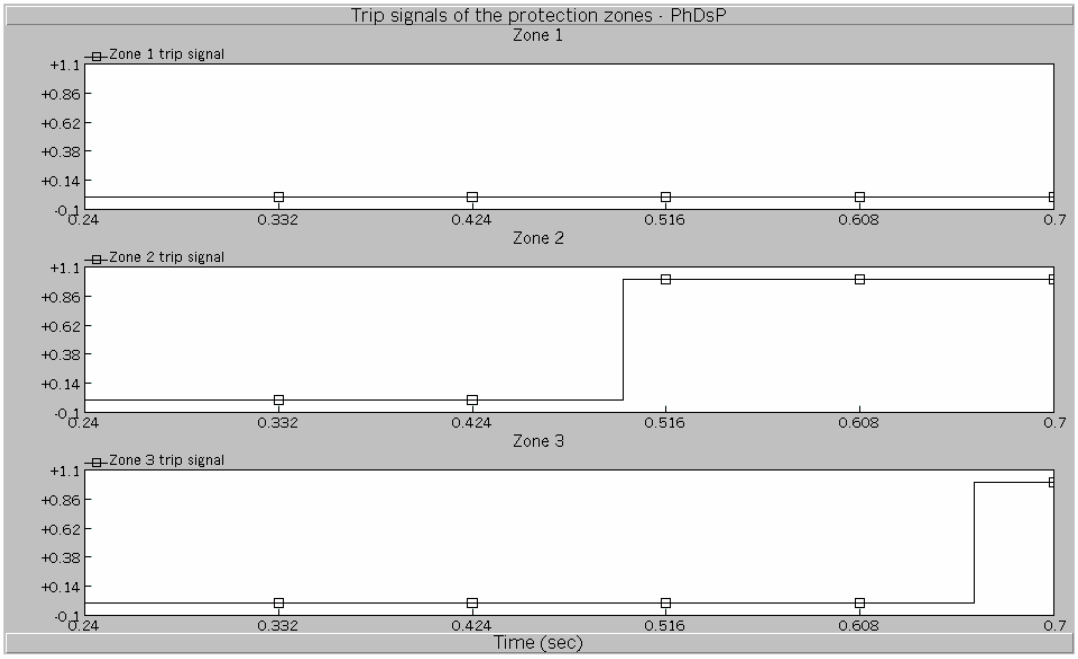


**Figure 5.25:** Trip signals issued by the phase comparators of *PhDsP*, zone-1, -2, and -3, phase B-phase C-to-ground fault, 50% of remote line *T6*

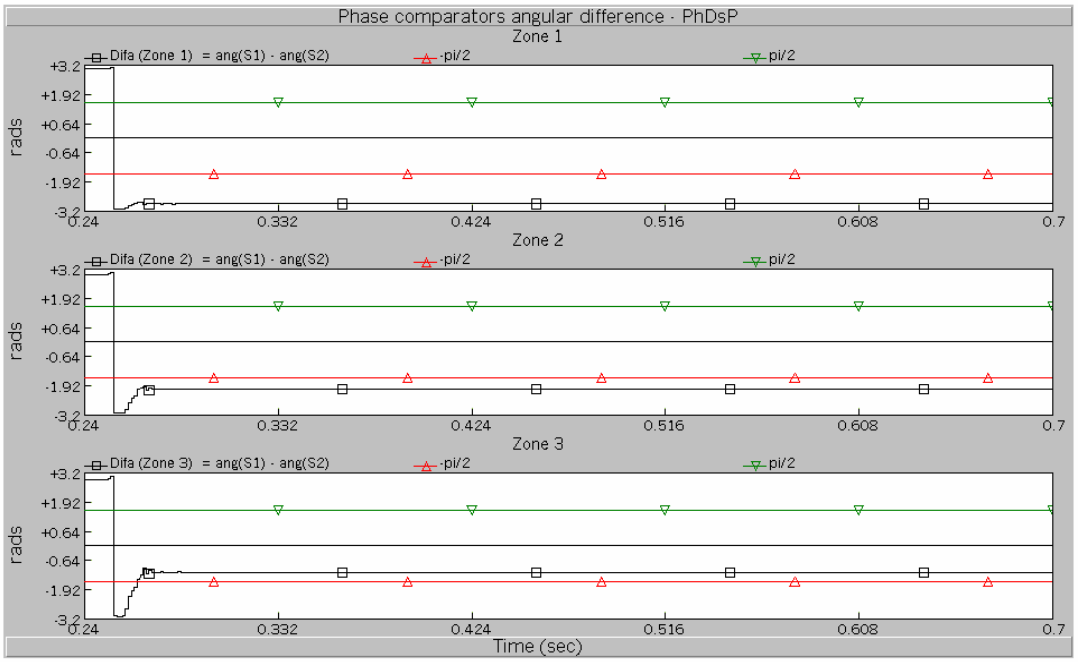


**Figure 5.26:** Response of the phase comparators of *PhDsP*, zone-1, -2, and -3, phase B-phase C-to-ground fault, 75% of remote line *T6*

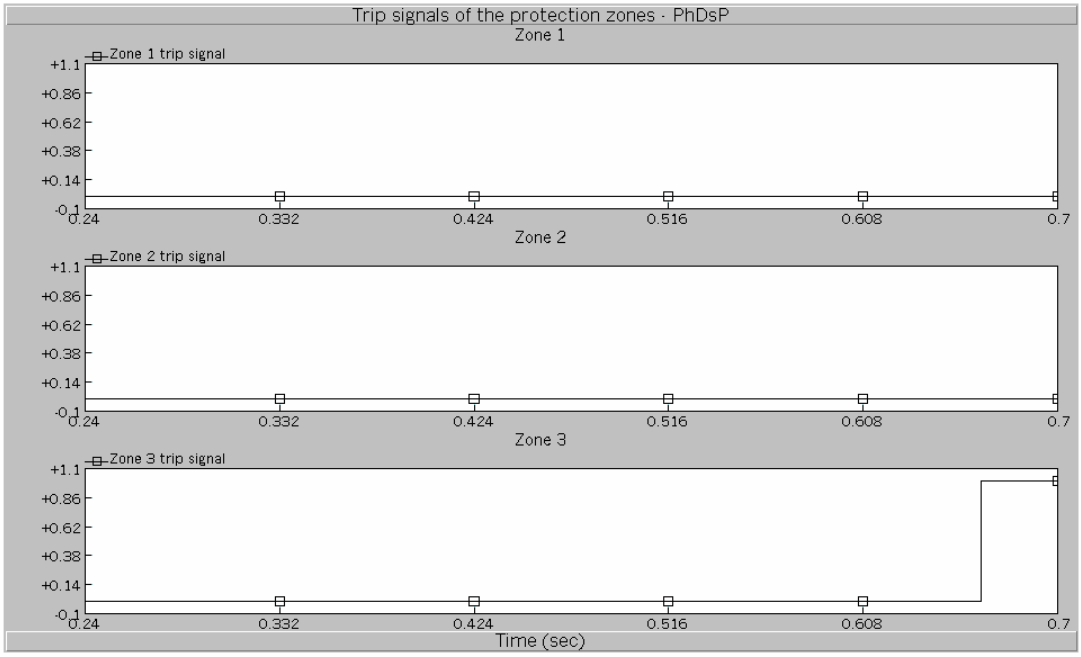


**Figure 5.27:** Trip signals issued by the phase comparators of *PhDsP*, zone-1, -2, and -3, phase B-phase C-to-ground fault, 75% of remote line *T6*

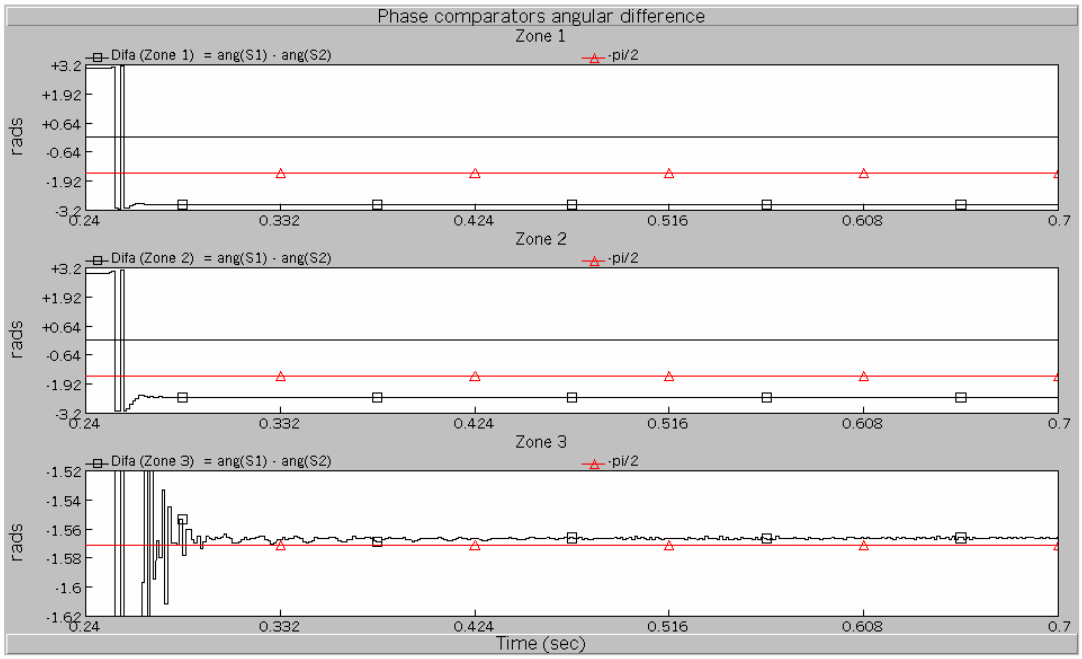


**Figure 5.28:** Response of the phase comparators of *PhDsP*, zone-1, -2, and -3, phase B-phase C-to-ground fault, 100% of remote line *T6*

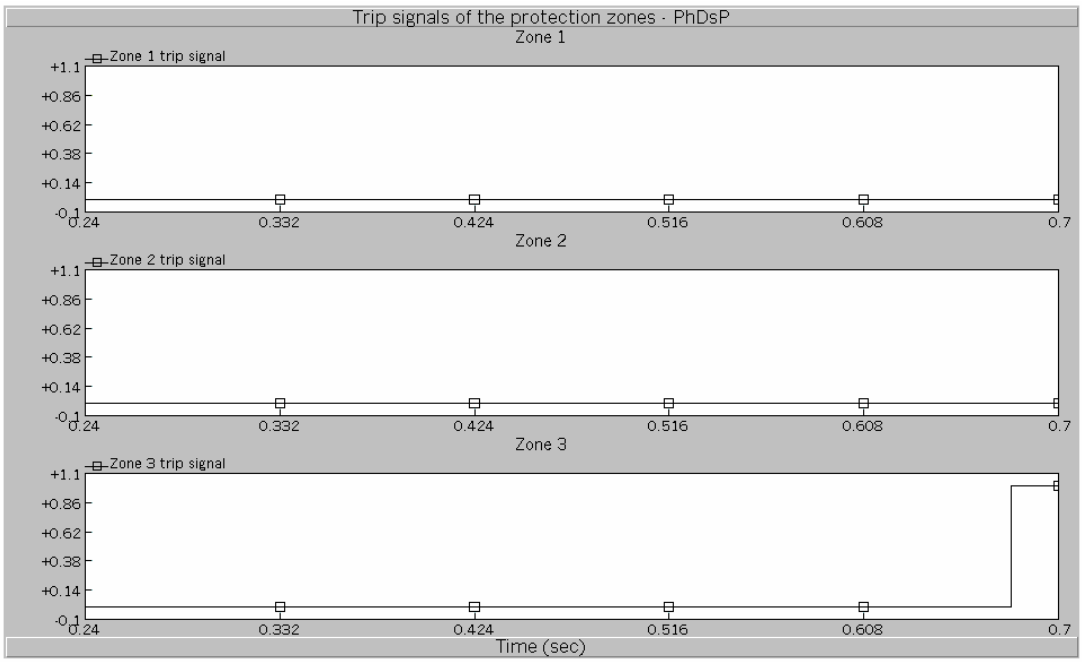


**Figure 5.29:** Trip signals issued by the phase comparators of *PhDsP*, zone-1, -2, and -3, phase B-phase C-to-ground fault, 100% of remote line *T6*

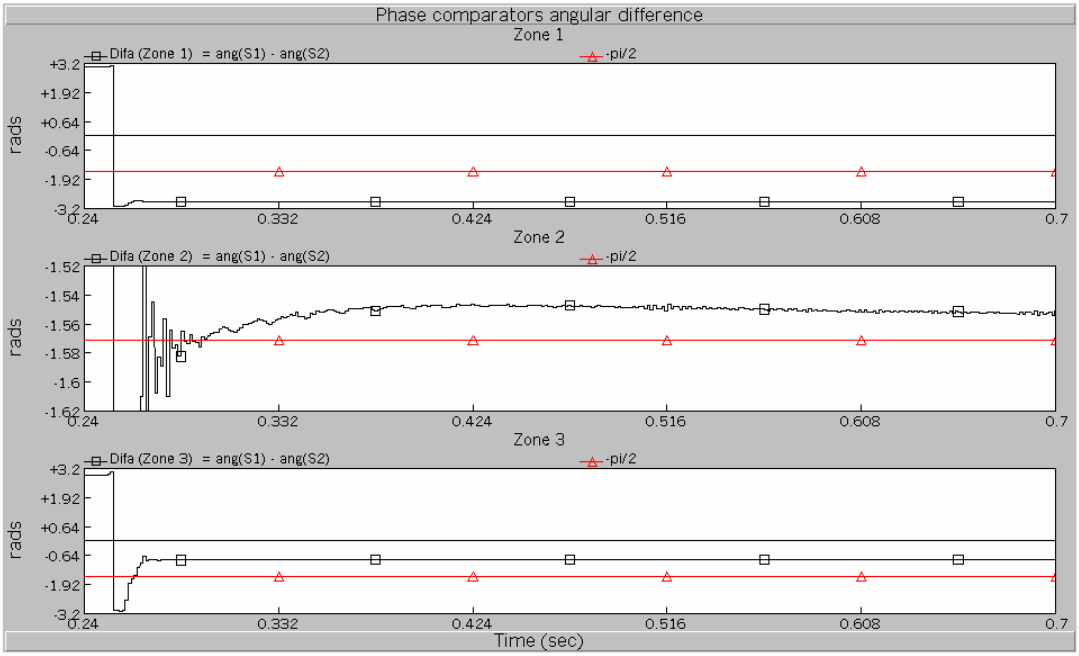


**Figure 5.30:** Response of the phase comparators of *PhDsP*, zone-1, -2, and -3, phase B-phase C-to-ground fault, 25% of remote line *T11*

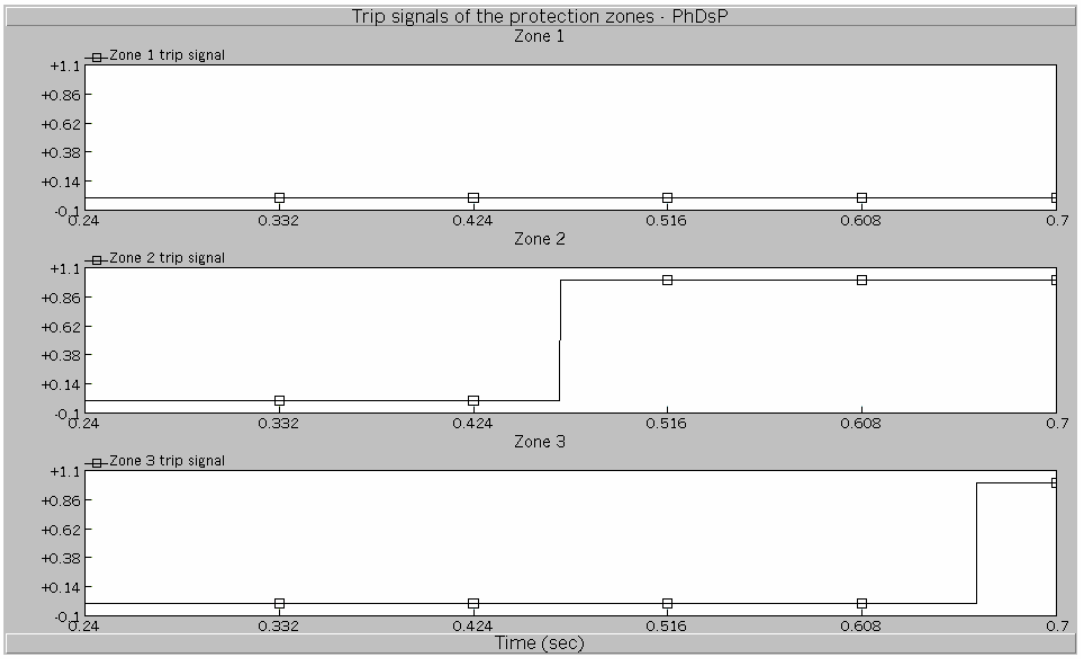


**Figure 5.31:** Trip signals issued by the phase comparators of *PhDsP*, zone-1, -2, and -3, phase B-phase C-to-ground fault, 25% of remote line *T11*

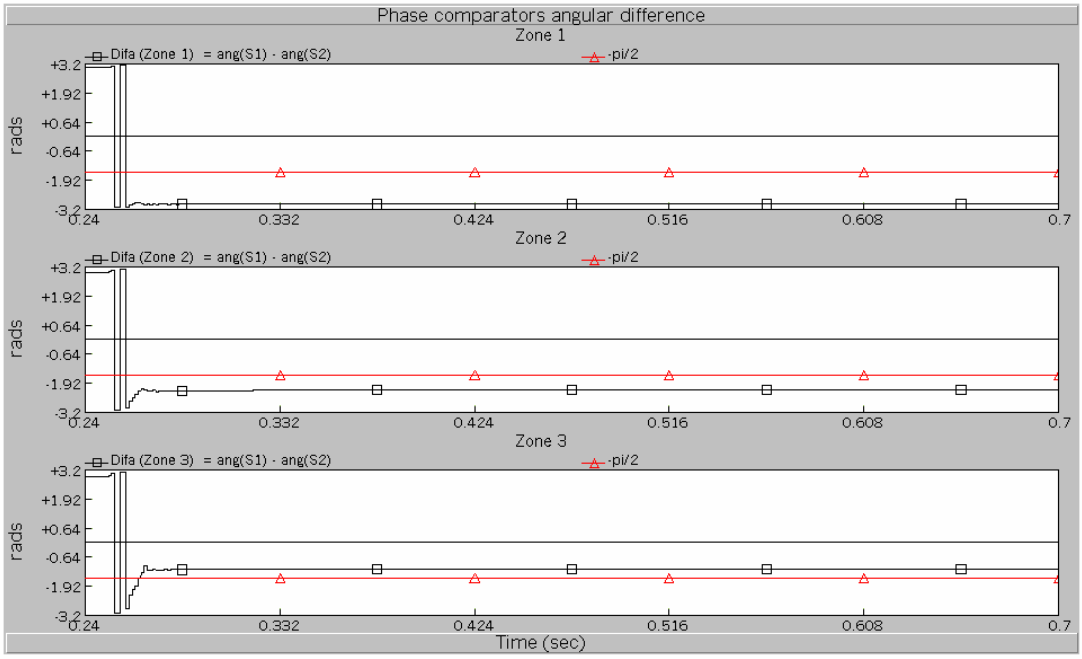


**Figure 5.32:** Response of the phase comparators of *PhDsP*, zone-1, -2, and -3, phase B-phase C-to-ground fault, 50% of remote line *T11*

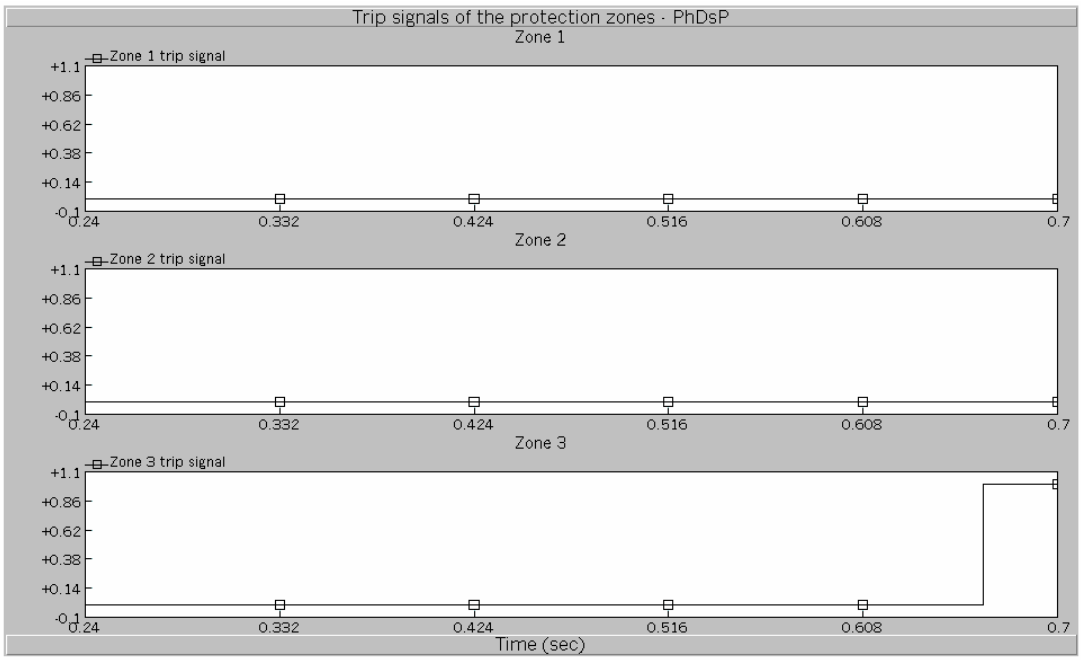


**Figure 5.33:** Trip signals issued by the phase comparators of *PhDsP*, zone-1, -2, and -3, phase B-phase C-to-ground fault, 50% of remote line *T11*

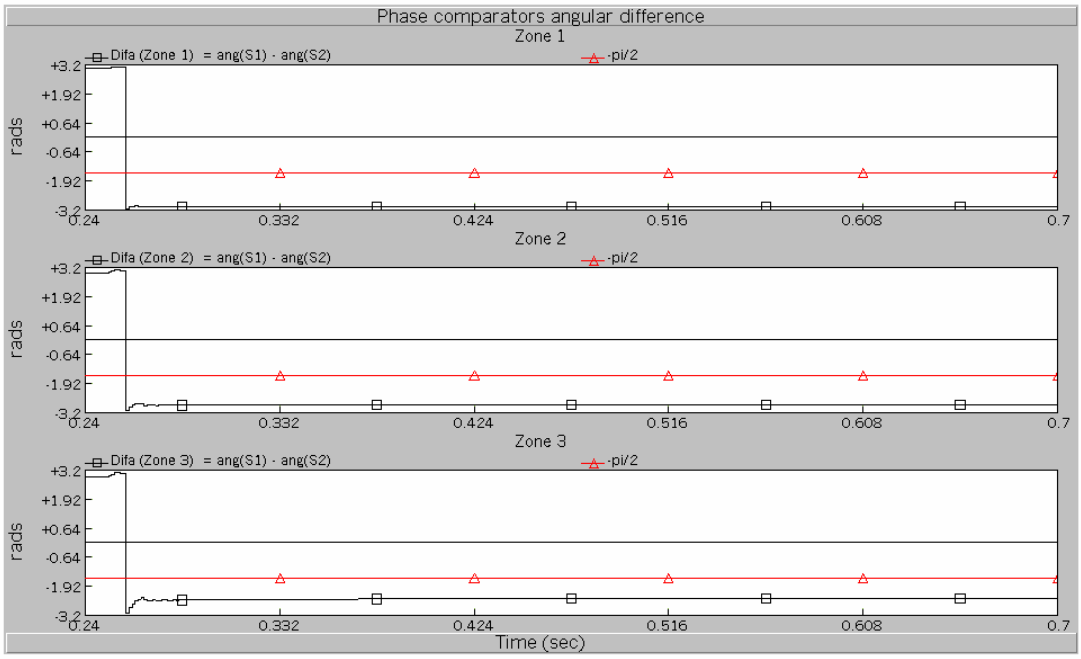


**Figure 5.34:** Response of the phase comparators of *PhDsP*, zone-1, -2, and -3, phase B-phase C-to-ground fault, 75% of remote line *T11*

#### 5.6.3.3 Conclusions to the remote backup protection studies

The remote backup protection studies of faulted remote transmission line *T6* showed correct results. Zone-1, -2, and -3 of *PhDsP* operated correctly for the phase B-phase C-to-ground faults at 25%, 50%, 75%, and 100% of remote line *T6*.

For the double line-to-ground fault at 50% of *T6*, zone-2 of *PhDsP* operated marginally, as shown in Figure 5.24, given that the adjustment of zone-2 was set based in the impedance of the double line-to-ground fault at 50% of *T6*. For the double line-to-ground fault at 100% of *T6*, zone-3 of *PhDsP* operated marginally, as shown in Figure 5.28, given that the adjustment of zone-3 was set based in the impedance of the double line-to-ground fault at 100% of *T6*.

The remote backup protection studies of faulted transmission line *T11* showed correct operation. The operation of the zones of the distance relay *PhDsP* for the different faults could not be anticipated, since the adjustment of zone-2 and -3 of *PhDsP* were based in the impedance of the remote line *T6*. However, it was expected that the reach of the zone-2 and -3 of *PhDsP* would not protect entirely the remote line *T11*.

For the phase B-phase C-to-ground fault at 25% of *T11*, zone-2 and -3 of the distance relay *PhDsP* operated. Zone-2 operated marginally, as shown in Figure 5.30. For the phase B-phase C-to-ground fault at 50% of *T11*, only zone-3 of *PhDsP* operated. For the double line-to-ground fault at 75% of *T11*, none of the zones of *PhDsP* operated. These results corroborated that the reach of the zones of *PhDsP* did not protect the entire remote line *T11*.

### 5.6.4 Distance protection performance under different fault types

This study had the purpose of investigating the response of the distance relay models to different type faults simulated at different lengths of the protected transmission line.

Comparison of the responses of the phase comparator and the apparent impedance estimated by distance relays were also made. The phase distance relay models *PhDsP* and *PhDsQ* protecting phases B and C of transmission line *T5* were employed in this study.

The three different single line-to-ground faults, the three double line-to-ground faults and the three-phase-to-ground fault were simulated at the 10% and 50% of the length of transmission line *T5*, from to the location of *PhDsP* (*Bus 3*). The time of the fault inception was $t$=0.2481 seconds. The graphs showing the results of this study were plotted from $t$=0.24 seconds to $t$=0.36 seconds, period of time that covered the most relevant information of the numerical relay models.

### 5.6.4.1 Distance protection performance for fault at 10% of line *T5*

The angle difference of the phase comparator signals $S_1$ and $S_2$ (*Difa*) of the phase distance relay model *PhDsP*, zone-1 and zone-2, for phase A-to-ground, phase B-to-ground, phase C-to-ground, phase A-phase B-to-ground, phase B-phase C-to-ground, phase C-phase A-to-ground, and three-phase-to-ground faults, located at 10% of transmission line *T5* referred to *Bus 3*, at a time $t$=0.2481, are shown in Figure 5.35, Figure 5.37, Figure 5.39, Figure 5.41, Figure 5.43, Figure 5.45, and Figure 5.47, respectively.

The *Difa* of the phase distance relay model *PhDsQ*, zone-1 and zone-2, for phase A-to-ground, phase B-to-ground, phase C-to-ground, phase A-phase B-to-ground, phase B-phase C-to-ground, phase C-phase A-to-ground, and three-phase-to-ground faults, located at 10% of transmission line *T5* referred to *Bus 3*, at a time $t$=0.2481, are shown in Figure 5.36, Figure 5.38, Figure 5.40, Figure 5.42, Figure 5.44, Figure 5.46, and Figure 5.48, respectively. It is important to notice that the fault located at 10% of *T5* from the location of *PhDsP* is the same fault located at 90% of *T5* from the location of *PhDsQ*.

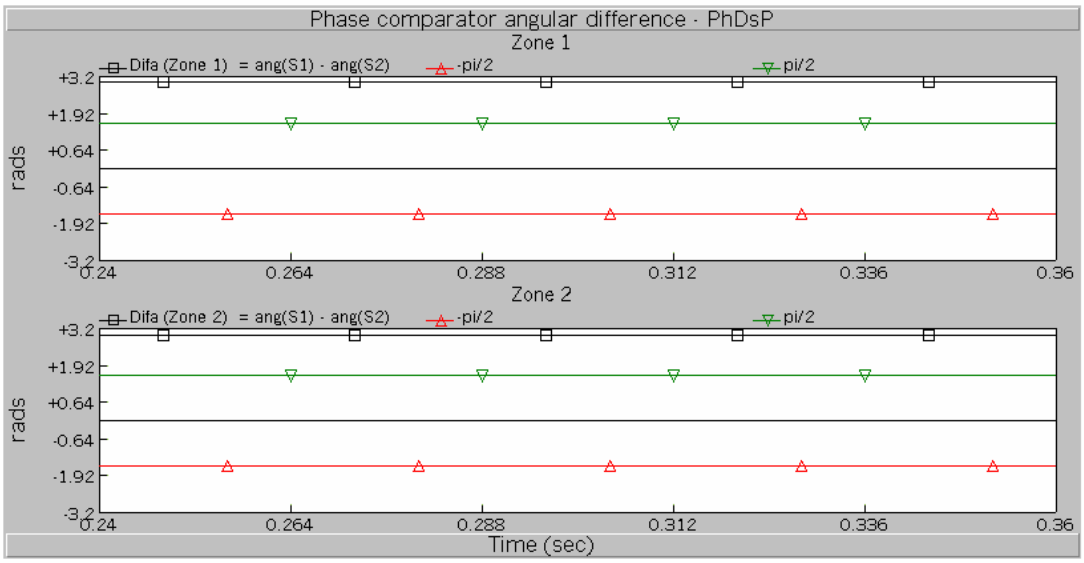


**Figure 5.35:** Response of the phase comparators of *PhDsP*, zone-1 and zone-2, phase A-to-ground fault, 10% of *T5* from relay location

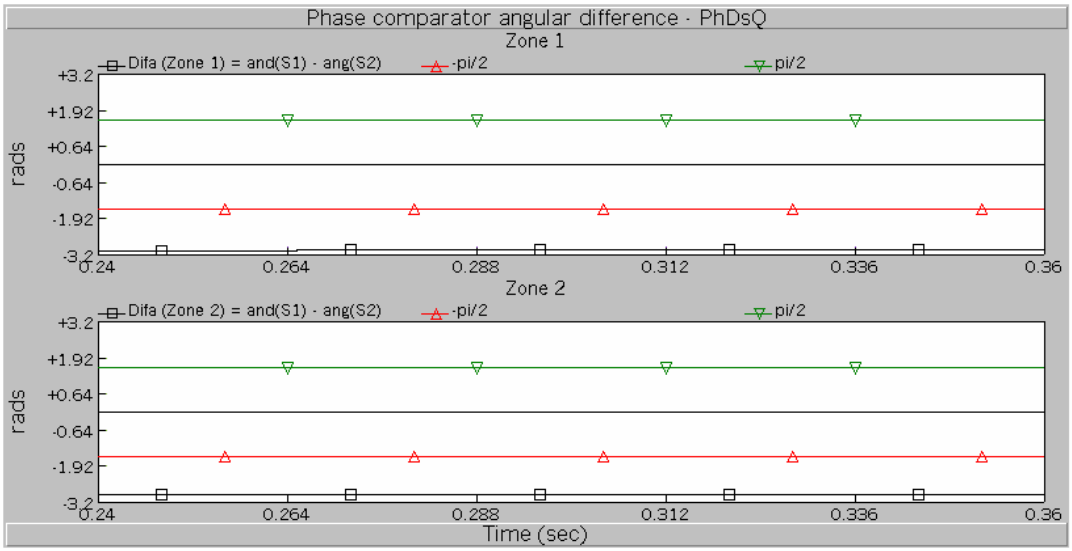


**Figure 5.36:** Response of the phase comparators of *PhDsQ*, zone-1 and zone-2, phase A-to-ground fault, 90% of *T5* from relay location

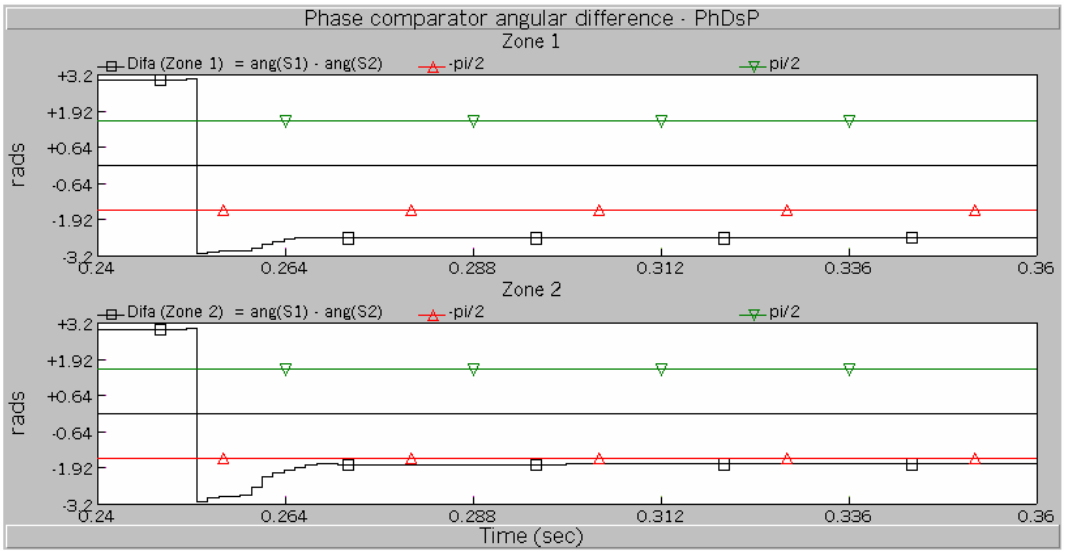


**Figure 5.37:** Response of the phase comparators of *PhDsP*, zone-1 and zone-2, phase B-to-ground fault, 10% of *T5* from relay location

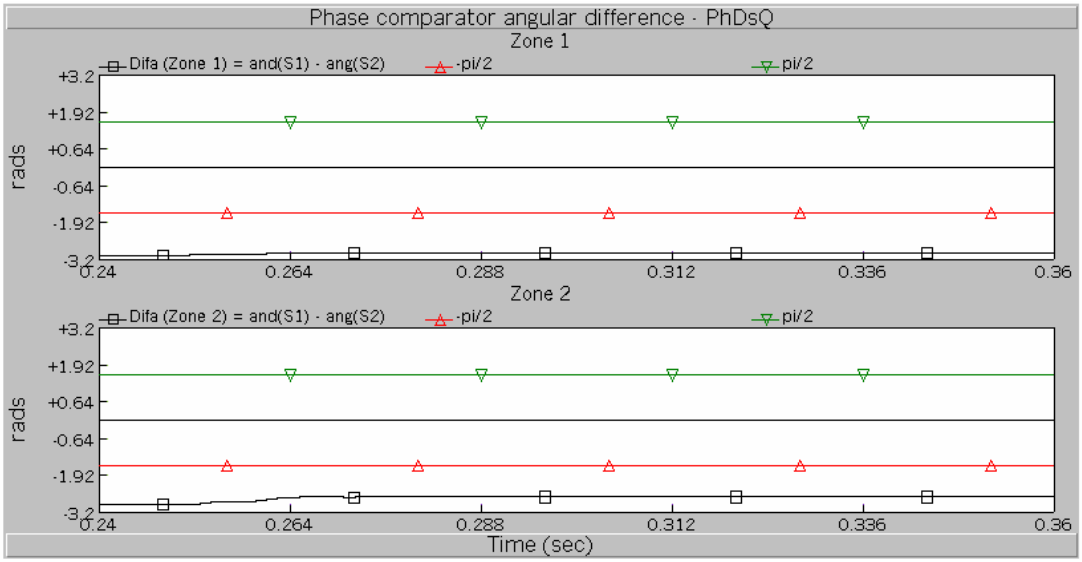


**Figure 5.38:** Response of the phase comparators of *PhDsQ*, zone-1 and zone-2, phase B-to-ground fault, 90% of *T5* from relay location

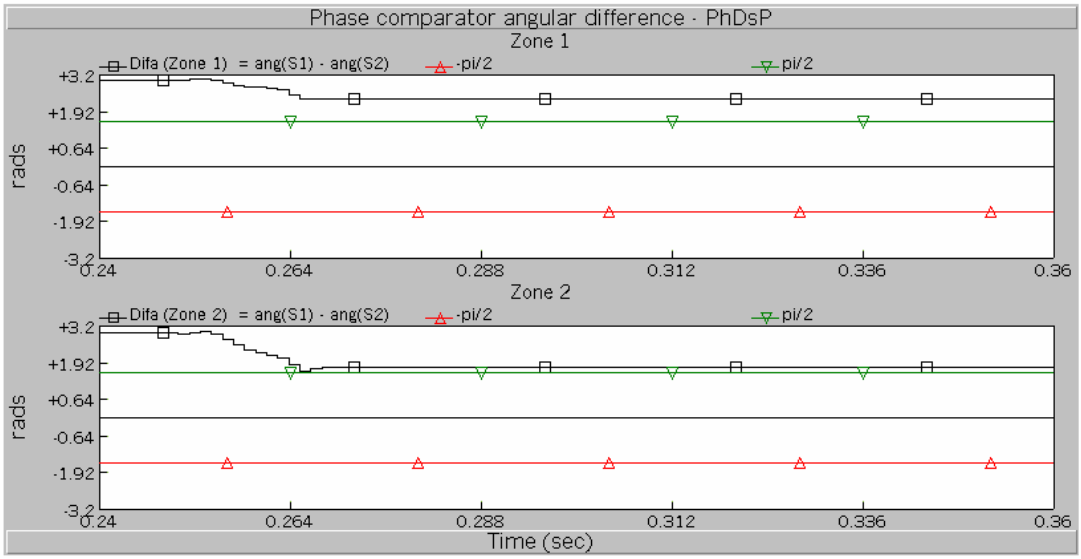


**Figure 5.39:** Response of the phase comparators of *PhDsP*, zone-1 and zone-2, phase C-to-ground fault, 10% of *T5* from relay location

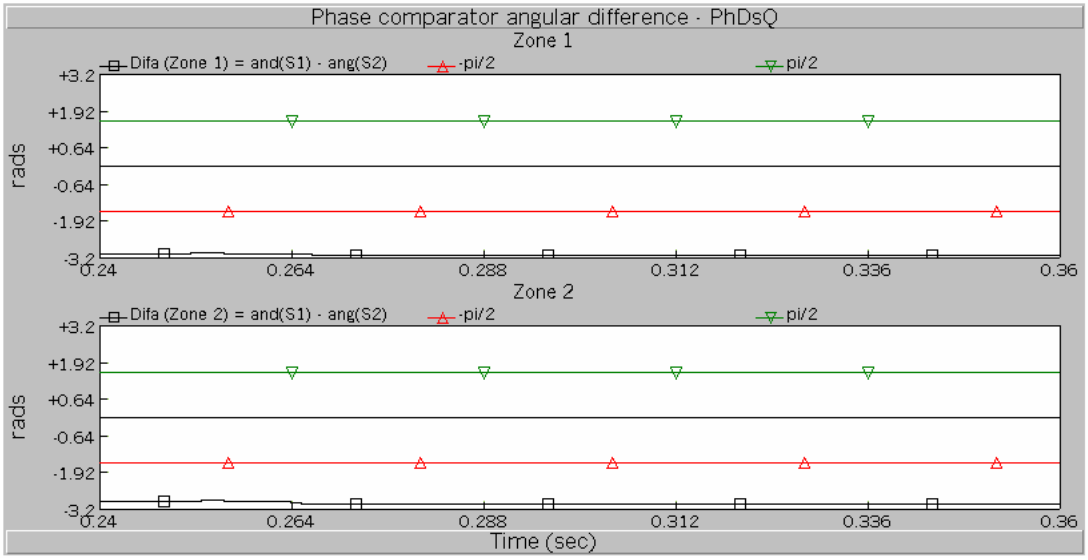


**Figure 5.40:** Response of the phase comparators of *PhDsQ*, zone-1 and zone-2, phase C-to-ground fault, 90% of *T5* from relay location

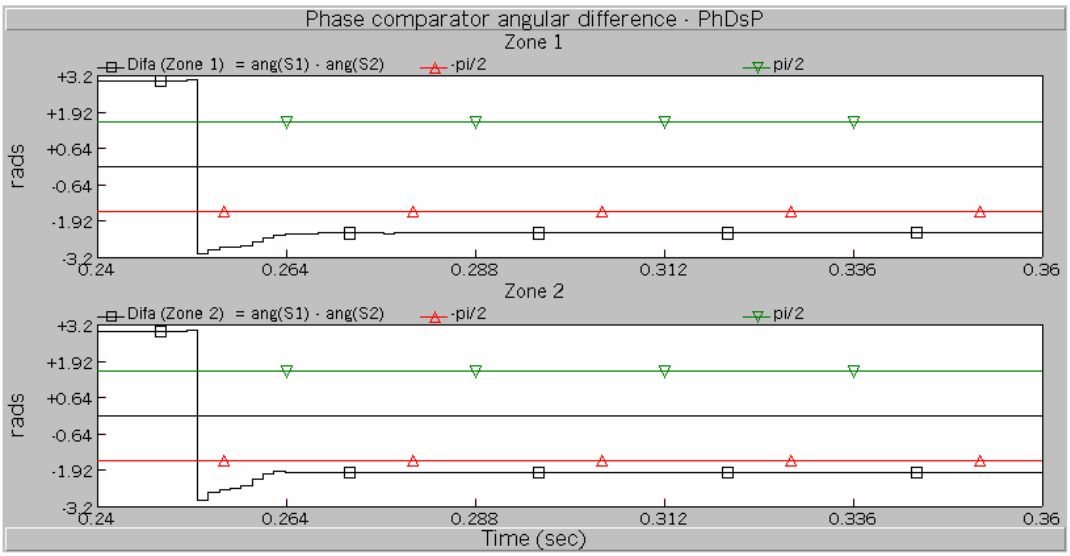


**Figure 5.41:** Response of the phase comparators of *PhDsP*, zone-1 and zone-2, phase A-phase B-to-ground fault, 10% of *T5* from relay location

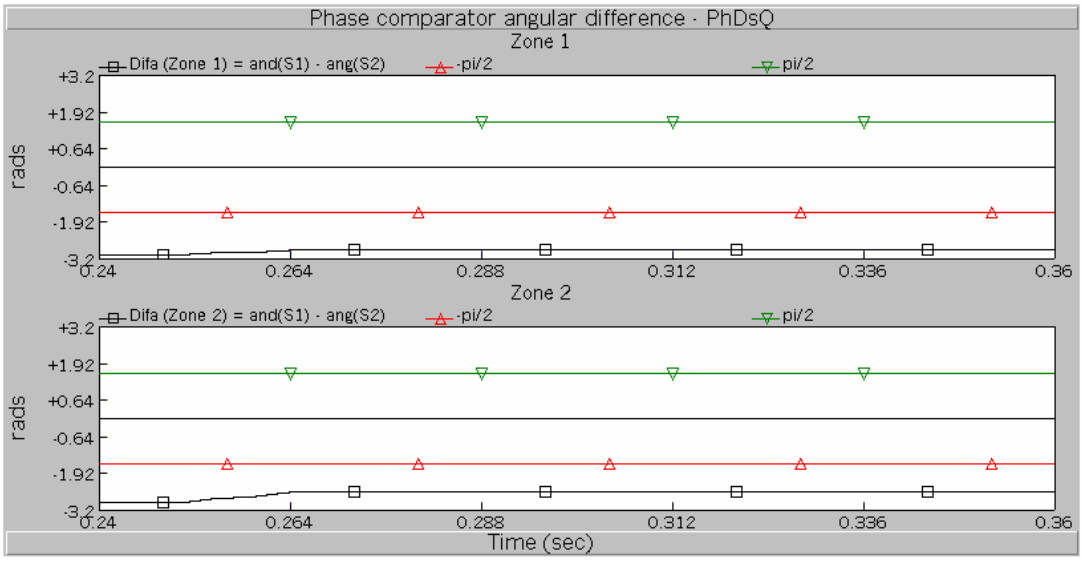


**Figure 5.42:** Response of the phase comparators of *PhDsQ*, zone-1 and zone-2, phase A-phase B-to-ground fault, 90% of *T5* from relay location

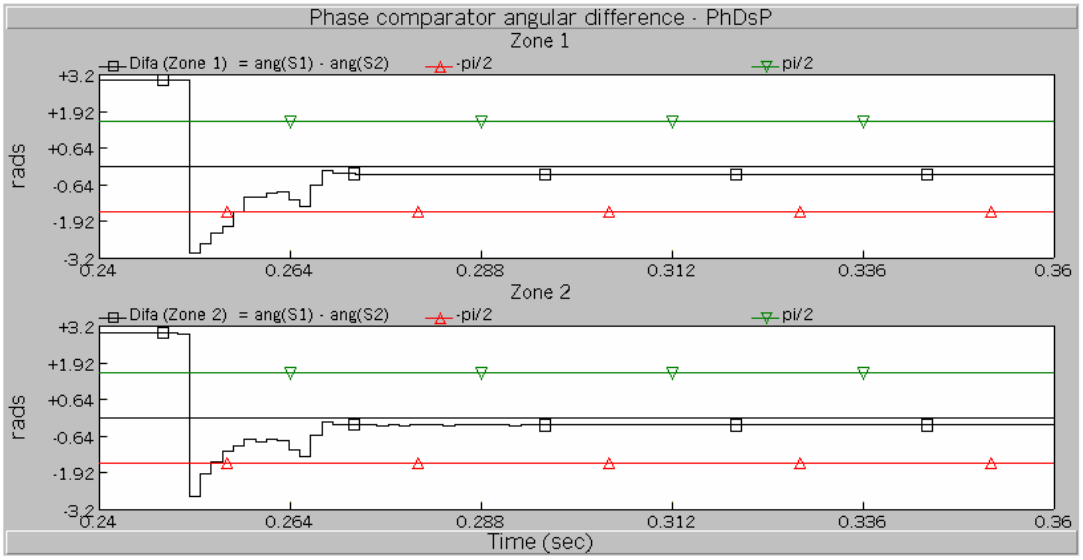


**Figure 5.43:** Response of the phase comparators of *PhDsP*, zone-1 and zone-2, phase B-phase C-to-ground fault, 10% of *T5* from relay location

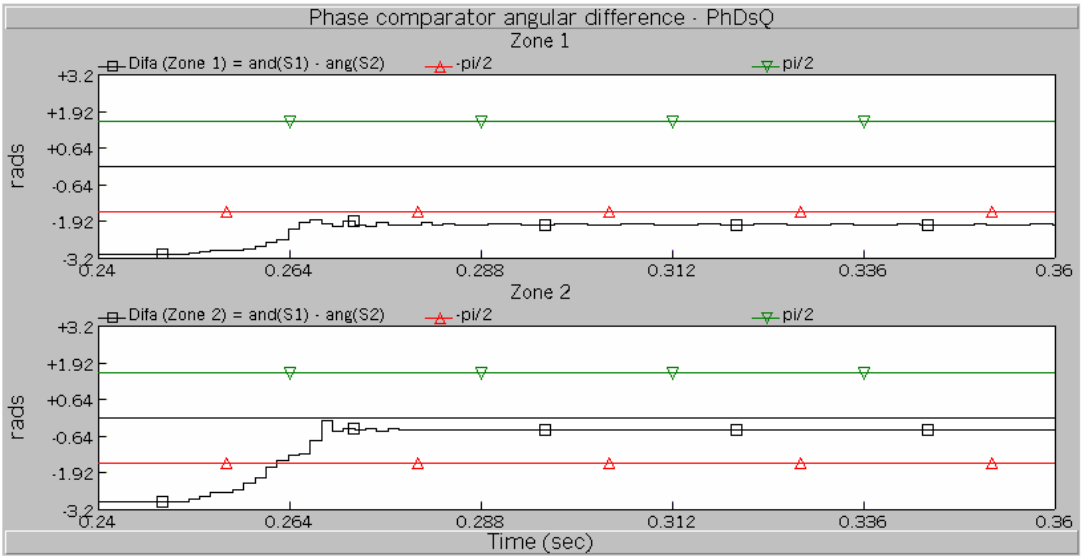


**Figure 5.44:** Response of the phase comparators of *PhDsQ*, zone-1 and zone-2, phase B-phase C-to-ground fault, 90% of *T5* from relay location

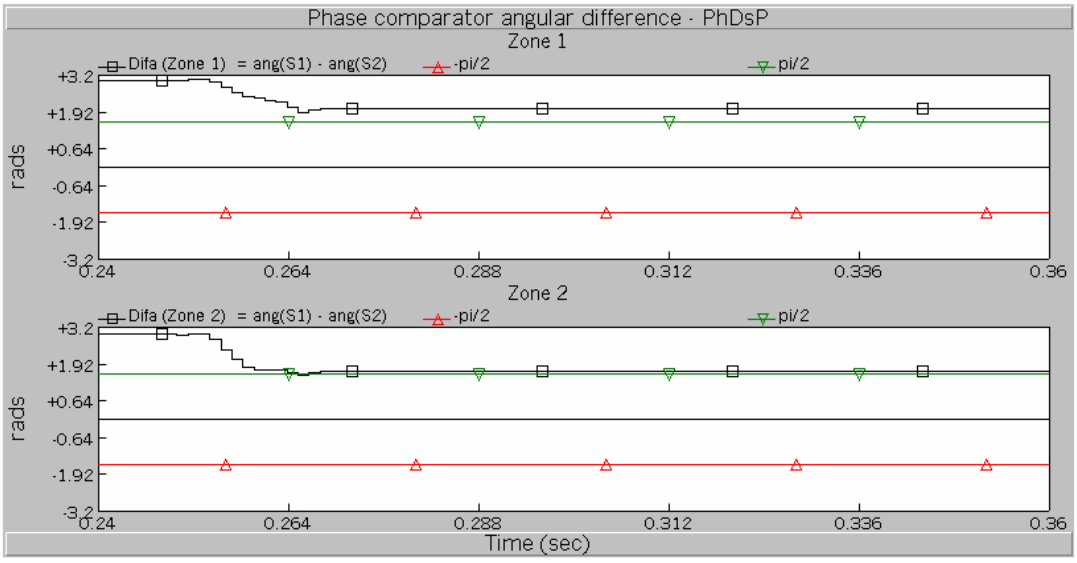


**Figure 5.45:** Response of the phase comparators of *PhDsP*, zone-1 and zone-2, phase C-phase A-to-ground fault, 10% of *T5* from relay location

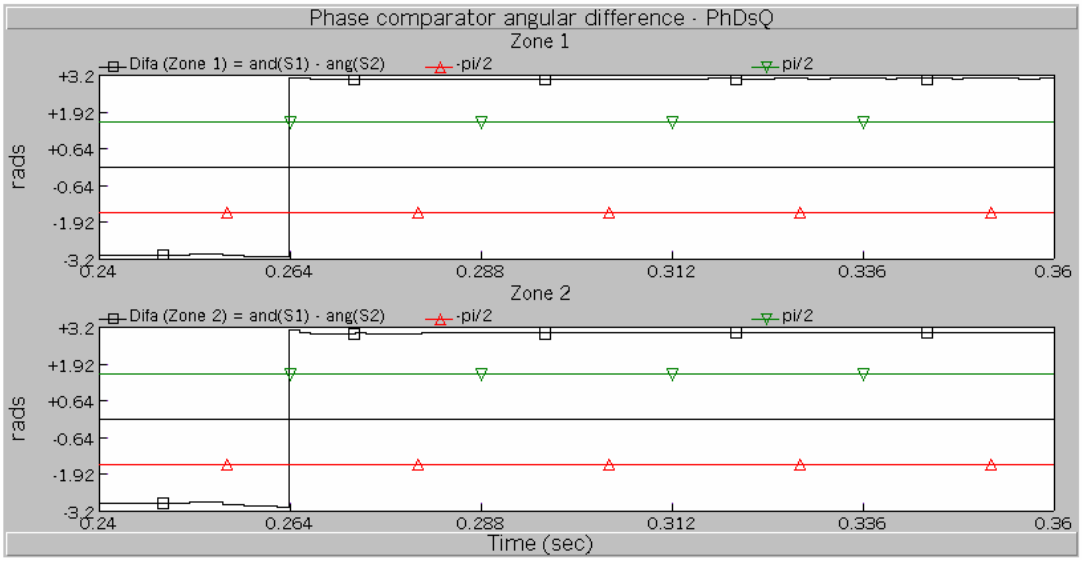


**Figure 5.46:** Response of the phase comparators of *PhDsQ*, zone-1 and zone-2, phase C-phase A-to-ground fault, 90% of *T5* from relay location

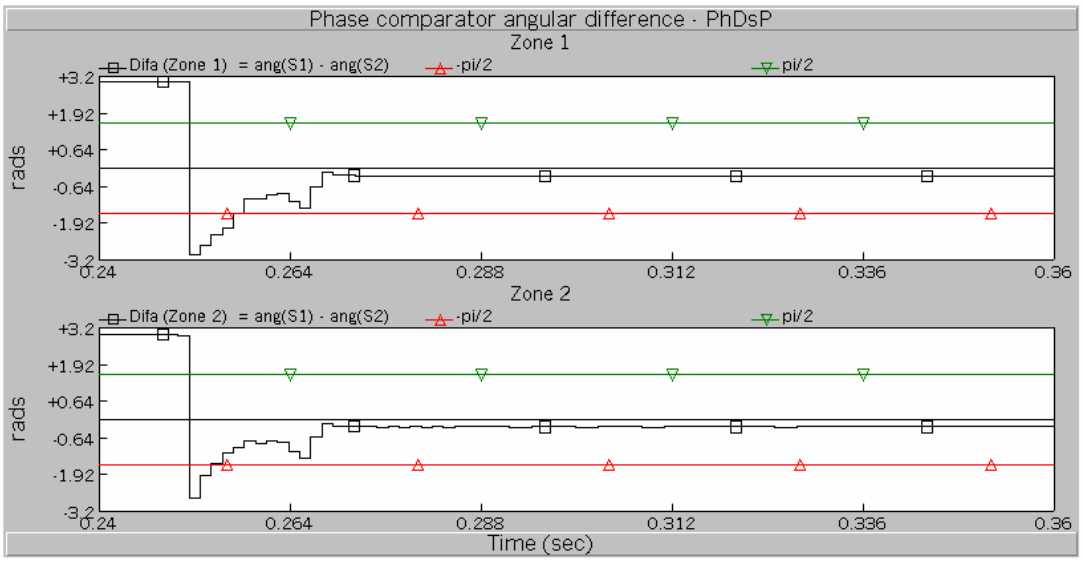


**Figure 5.47:** Response of the phase comparators of *PhDsP*, zone-1 and zone-2, three-phase-to-ground fault, 10% of *T5* from relay location

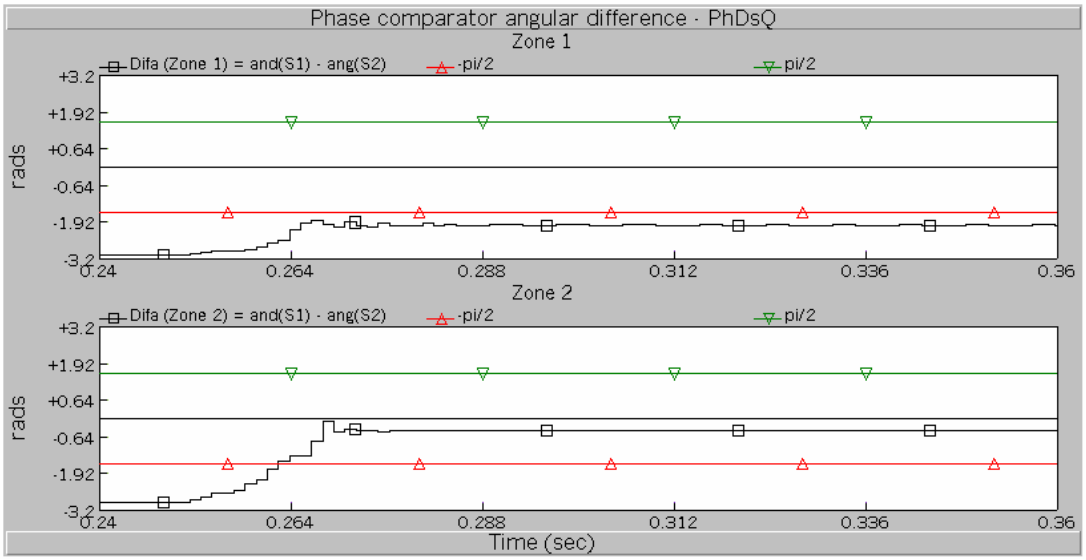


**Figure 5.48:** Response of the phase comparators of *PhDsQ*, zone-1 and zone-2, three-phase-to-ground fault, 90% of *T5* from relay location

### 5.6.4.2 Apparent impedances of the faults at 10% of line T5

In this section are presented the plottings in the impedance plane of the impedance faults calculated by the distance relay models *PhDsP* and *PhDsQ*, for the faults at 10% of transmission line *T5* from *Bus 3*, simulated in the previous section. The plottings were generated using Matlab and PSCAD/EMTDC output files containing the values of the apparent impedances seen by *PhDsP* and *PhDsQ* on the faults at 10% of line *T5*.

In Figures 5.49, 5.50 and 5.51 are shown the plottings of impedance faults calculated by the phase distance relay model *PhDsP* for the single line-to-ground, double line-to-ground and three-phase-to-ground faults at 10% of *T5*, from relay location, respectively.

In Figures 5.52, 5.53 and 5.54 are shown the plottings of impedance faults calculated by the phase distance relay model *PhDsQ* for the single line-to-ground, double line-to-ground and three-phase-to-ground faults at 90% of transmission line *T5*, from relay location, respectively.

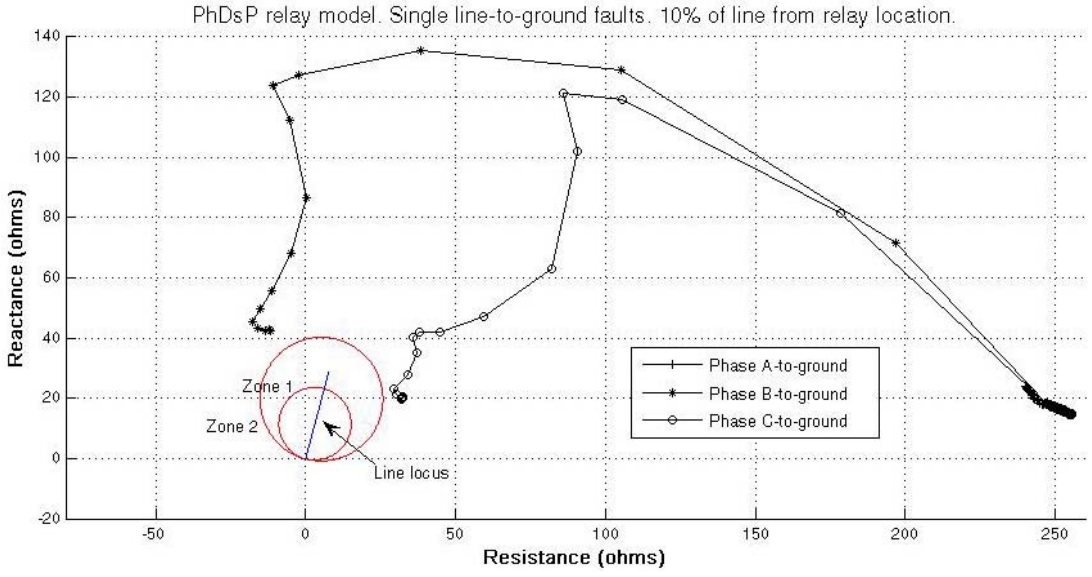


**Figure 5.49**: Apparent impedances seen by *PhDsP* on the single line-to-ground faults at 10% of *T5* from Bus 3

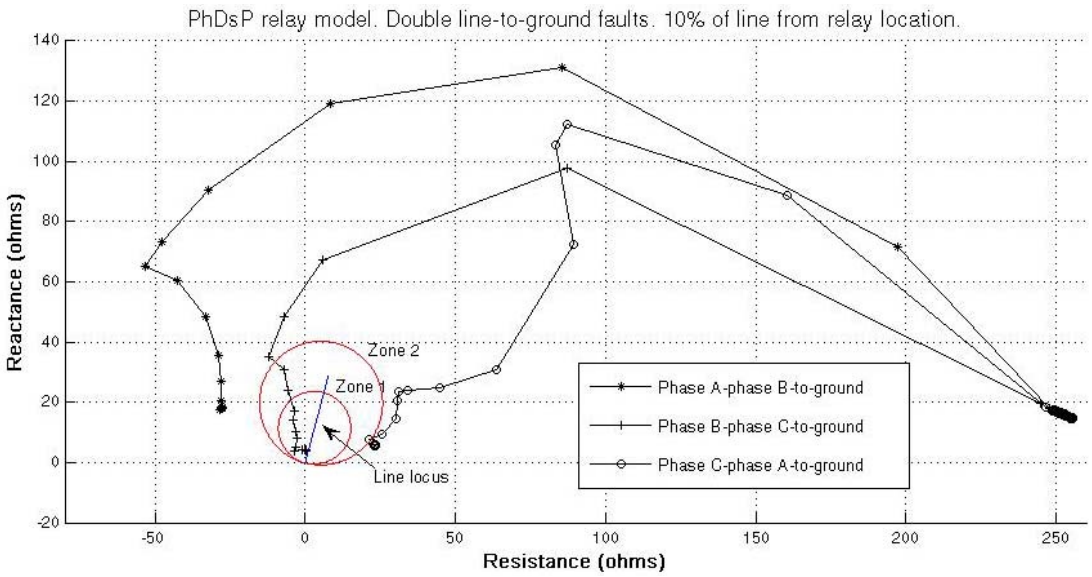


**Figure 5.50:** Apparent impedances seen by *PhDsP* on the double line-to-ground faults at 10% of *T5* from Bus 3

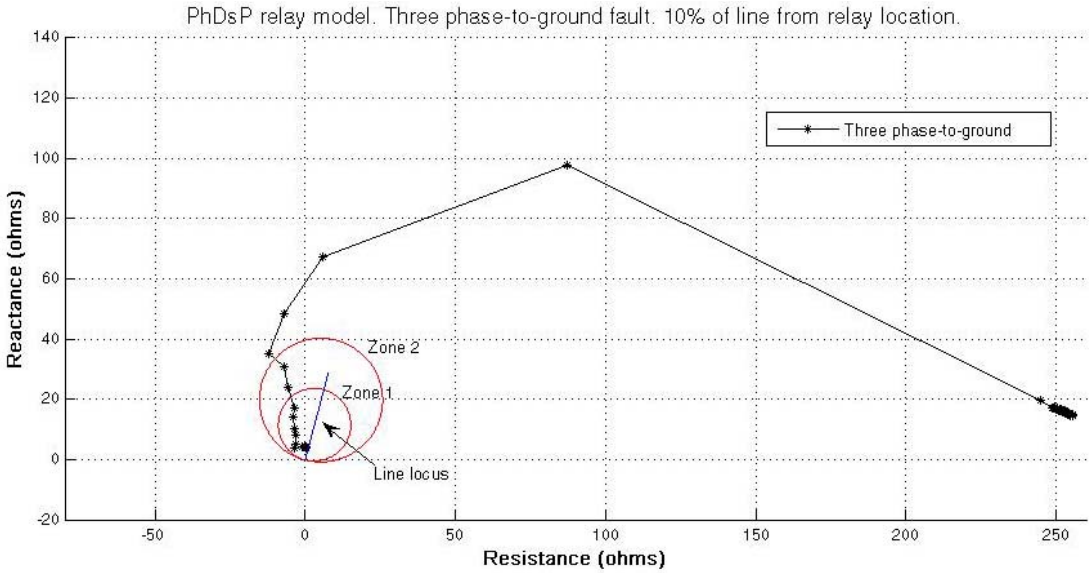


**Figure 5.51:** Apparent impedances seen by *PhDsP* on the three-phase-to-ground fault at 10% of *T5* from Bus 3

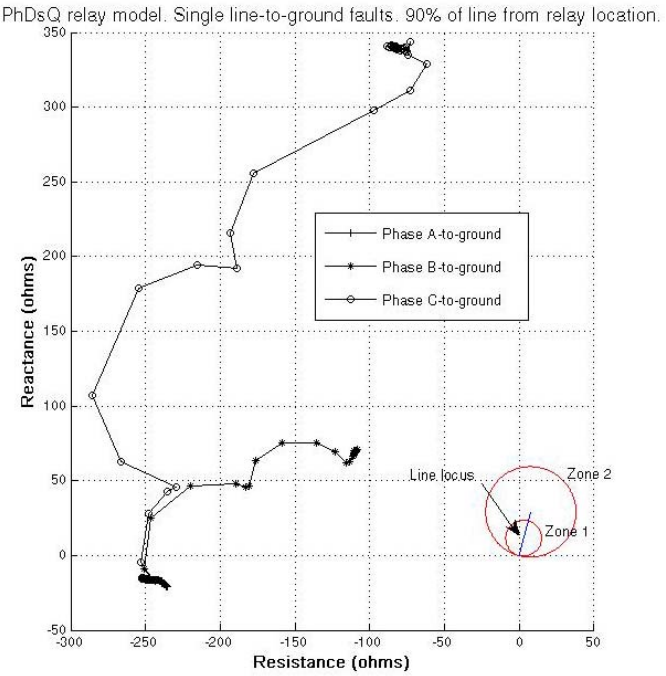


**Figure 5.52:** Apparent impedances seen by *PhDsQ* on the single line-to-ground faults at 10% of *T5* from Bus 3 (90% of *T5*from Bus 4)

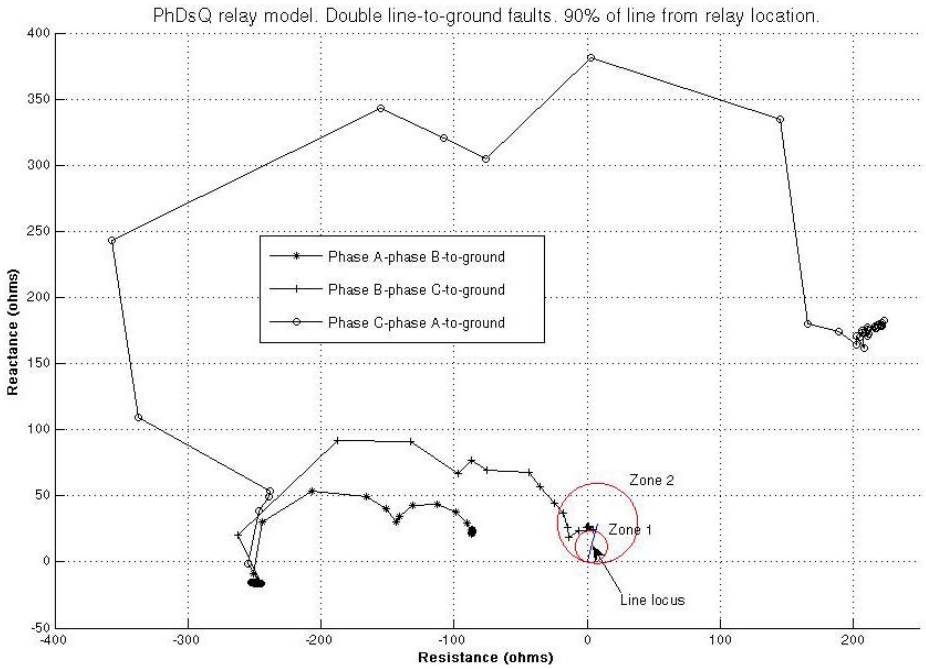


**Figure 5.53:** Apparent impedances seen by *PhDsQ* on the double line-to-ground faults at 10% of *T5* from Bus 3 (90% of *T5* from Bus 4)

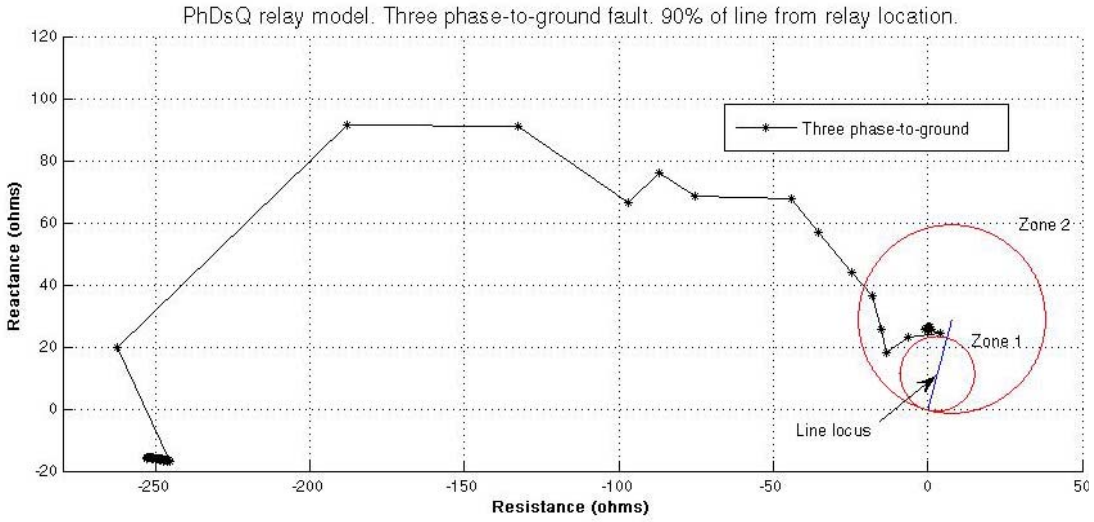


**Figure 5.54:** Apparent impedances seen by *PhDsQ* on the three-phase-to-ground fault at 10% of *T5* from Bus 3 (90% of *T5* from Bus 4)

### 5.6.4.3 Distance protection performance for fault at 50% of line *T5*

The angle difference of the phase comparator signals $S_1$ and $S_2$ (*Difa*) of the phase distance relay model *PhDsP*, zone-1 and zone-2, for phase A-to-ground, phase B-to-ground, phase C-to-ground, phase A-phase B-to-ground, phase B-phase C-to-ground, phase C-phase A-to-ground, and three-phase-to-ground faults, located at 50% of transmission line *T5*, at a time $t$=0.2481, are shown in Figure 5.55, Figure 5.57, Figure 5.59, Figure 5.61, Figure 5.63, Figure 5.65, and Figure 5.67, respectively.

The *Difa* of the phase distance relay model *PhDsQ*, zone-1 and zone-2, for phase A-to-ground, phase B-to-ground, phase C-to-ground, phase A-phase B-to-ground, phase B-phase C-to-ground, phase C-phase A-to-ground, and three-phase-to-ground faults, located at 50% of transmission line *T5*, at a time $t$=0.2481, are shown in Figure 5.56, Figure 5.58, Figure 5.60, Figure 5.62, Figure 5.64, Figure 5.66, and Figure 5.68, respectively.

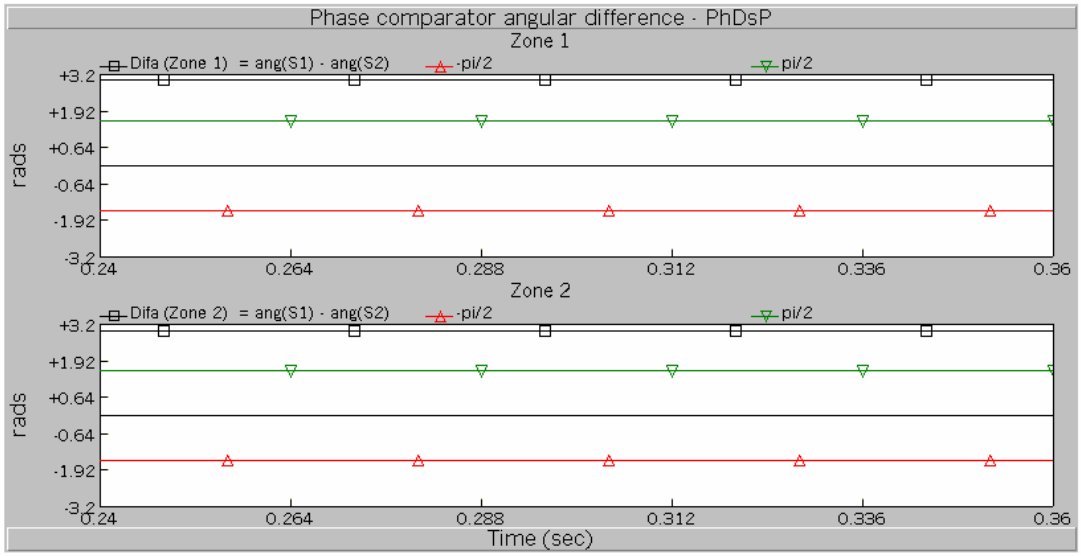


**Figure 5.55:** Response of the phase comparators of *PhDsP*, zone-1 and zone-2, phase A-to-ground fault, 50% of *T5*

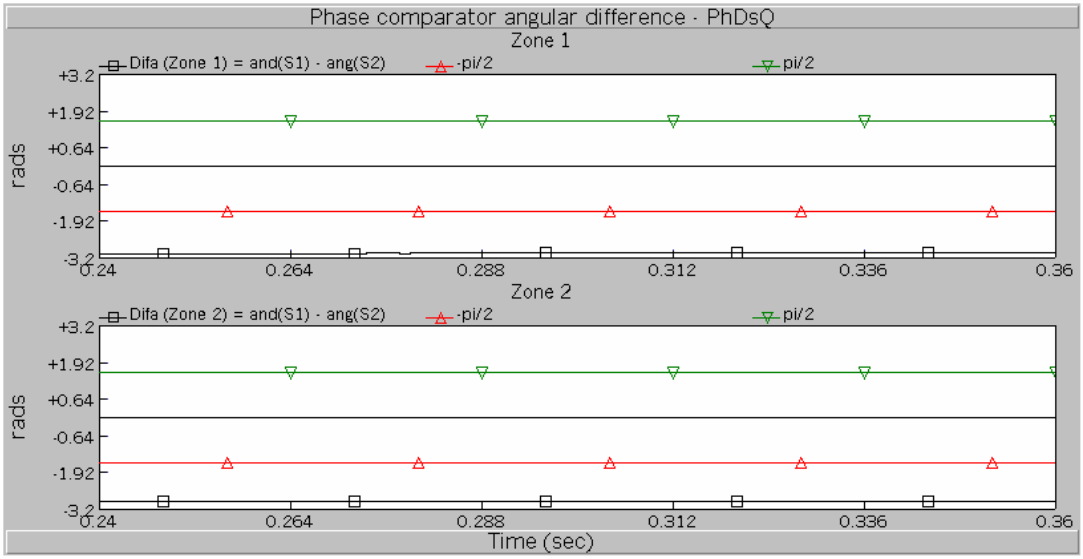


**Figure 5.56:** Response of the phase comparators of *PhDsQ*, zone-1 and zone-2, phase A-to-ground fault, 50% of *T5*

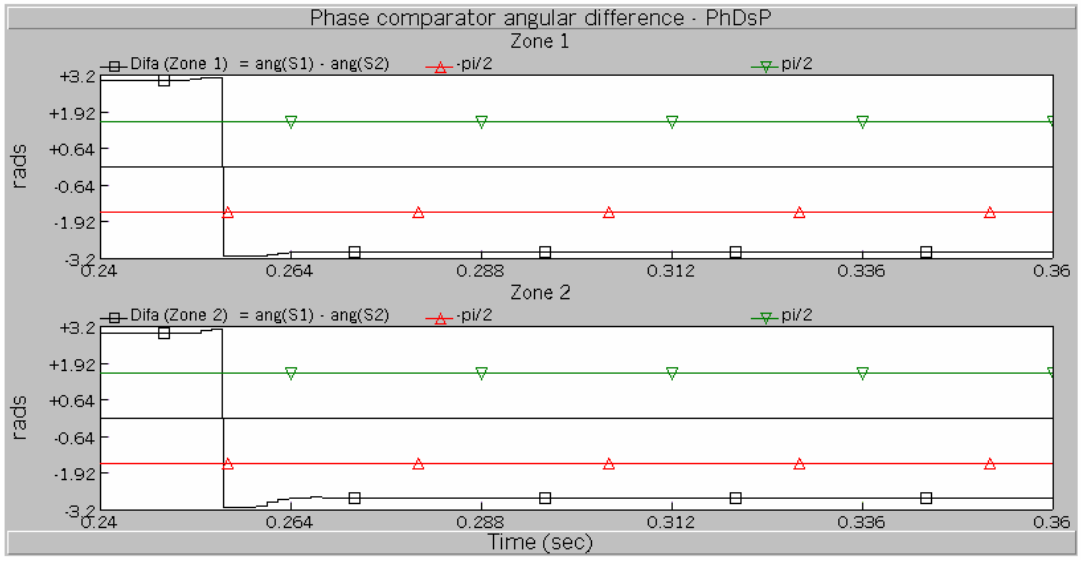


**Figure 5.57:** Response of the phase comparators of *PhDsP*, zone-1 and zone-2, phase B-to-ground fault, 50% of *T5*

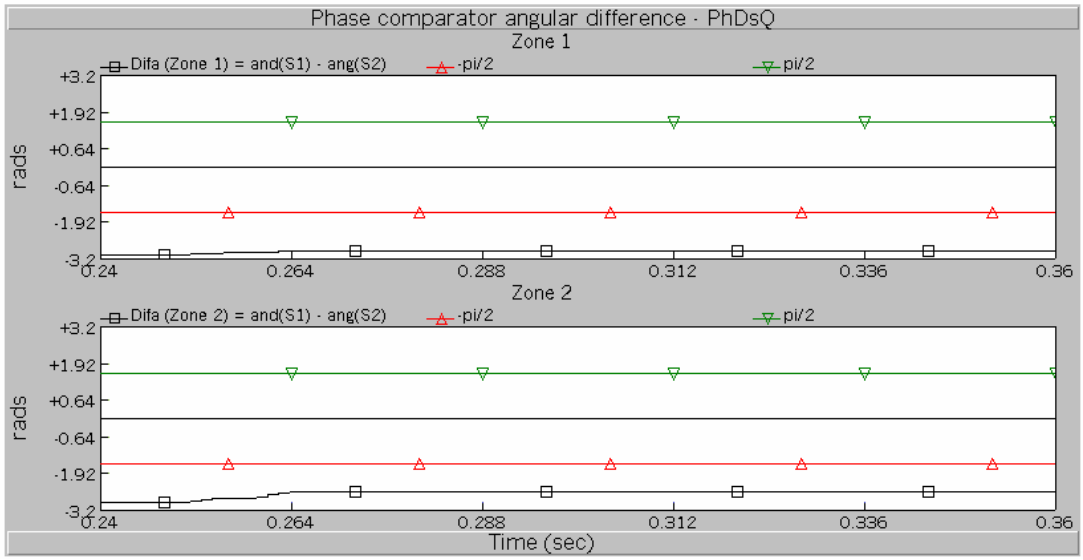


**Figure 5.58:** Response of the phase comparators of *PhDsQ*, zone-1 and zone-2, phase B-to-ground fault, 50% of *T5*

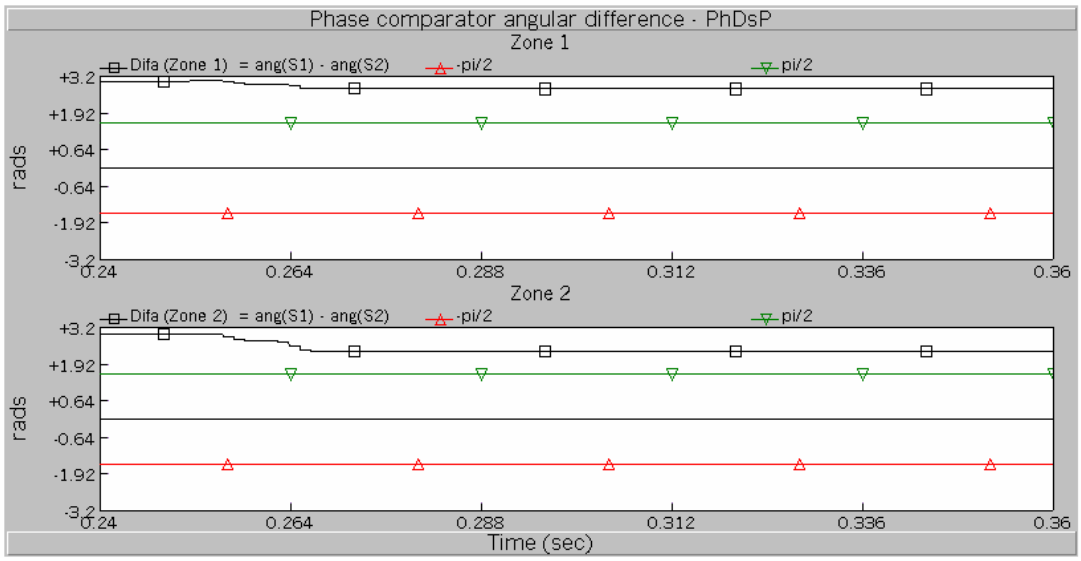


**Figure 5.59:** Response of the phase comparators of *PhDsP*, zone-1 and zone-2, phase C-to-ground fault, 50% of *T5*

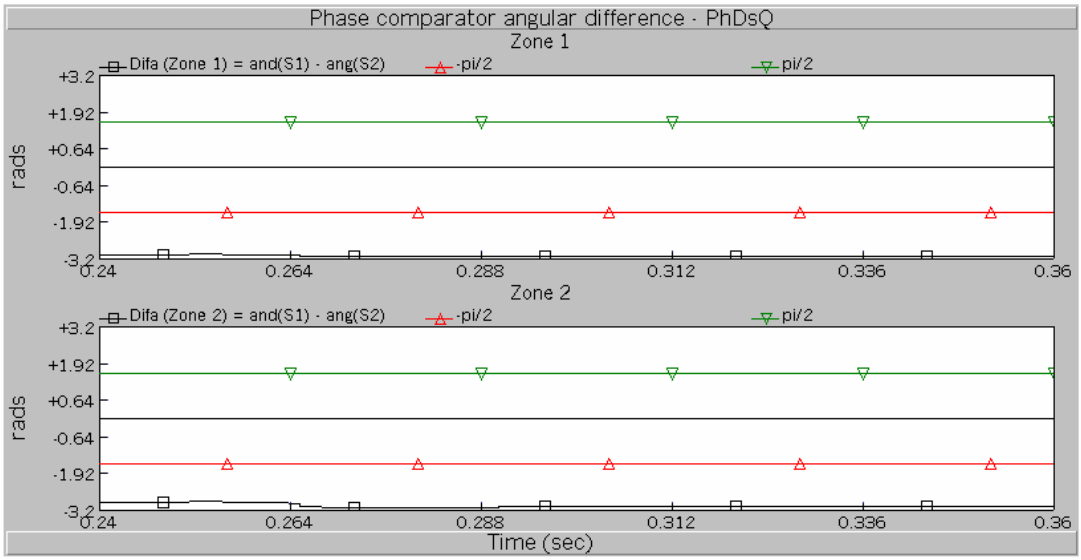


**Figure 5.60:** Response of the phase comparators of *PhDsQ*, zone-1 and zone-2, phase C-to-ground fault, 50% of *T5*

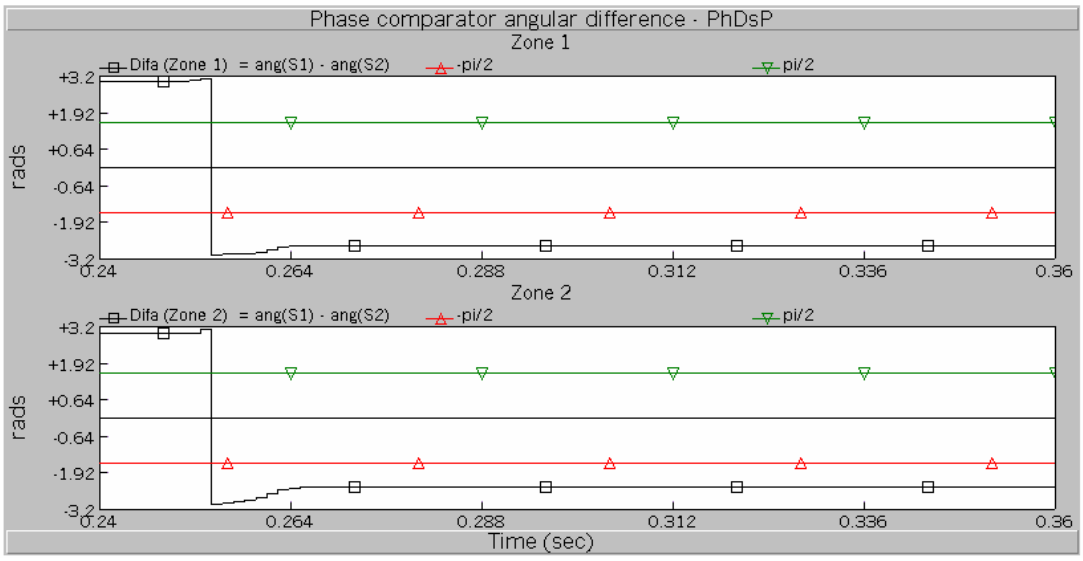


**Figure 5.61:** Response of the phase comparators of *PhDsP*, zone-1 and zone-2, phase A-phase B-to-ground fault, 50% of *T5*

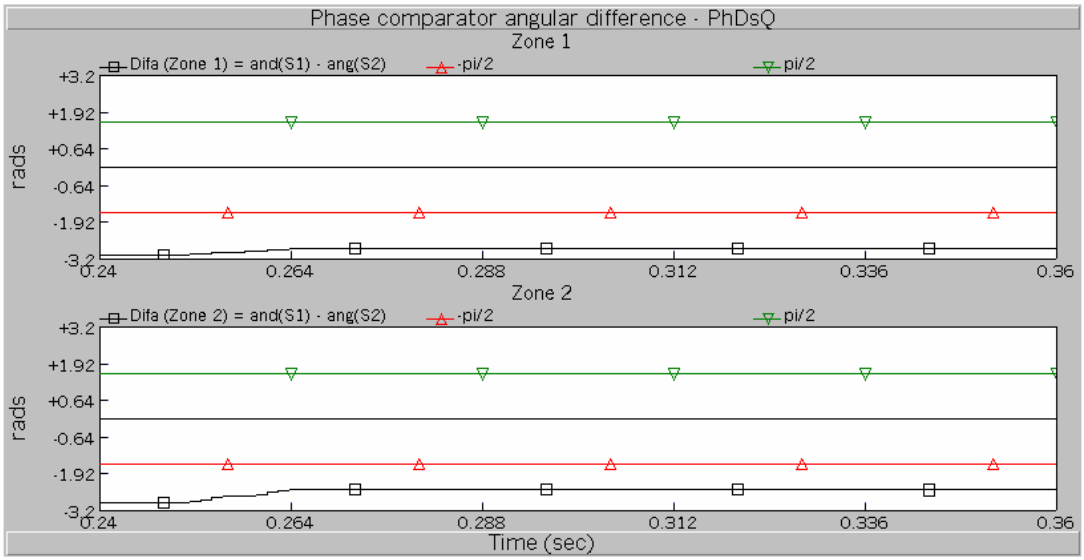


**Figure 5.62:** Response of the phase comparators of *PhDsQ*, zone-1 and zone-2, phase A-phase B-to-ground fault, 50% of *T5*

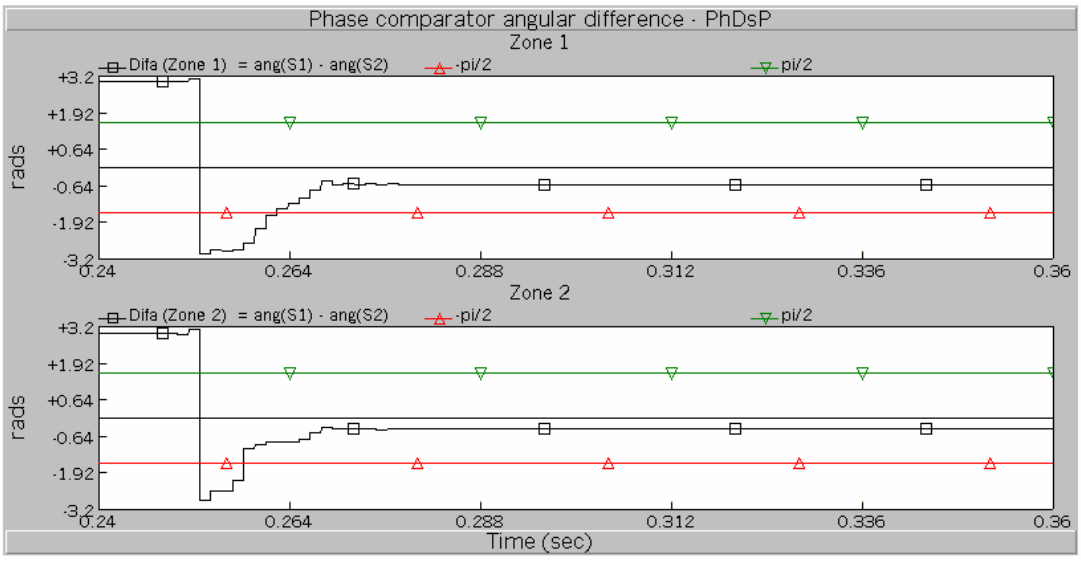


**Figure 5.63:** Response of the phase comparators of *PhDsP*, zone-1 and zone-2, phase B-phase C-to-ground fault, 50% of *T5*

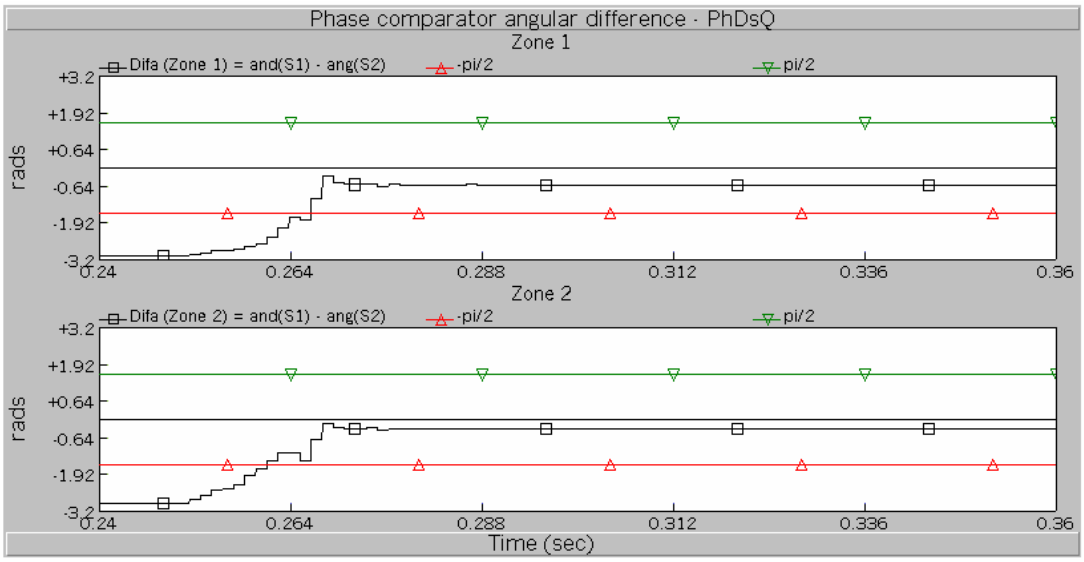


**Figure 5.64:** Response of the phase comparators of *PhDsQ*, zone-1 and zone-2, phase B-phase C-to-ground fault, 50% of *T5*

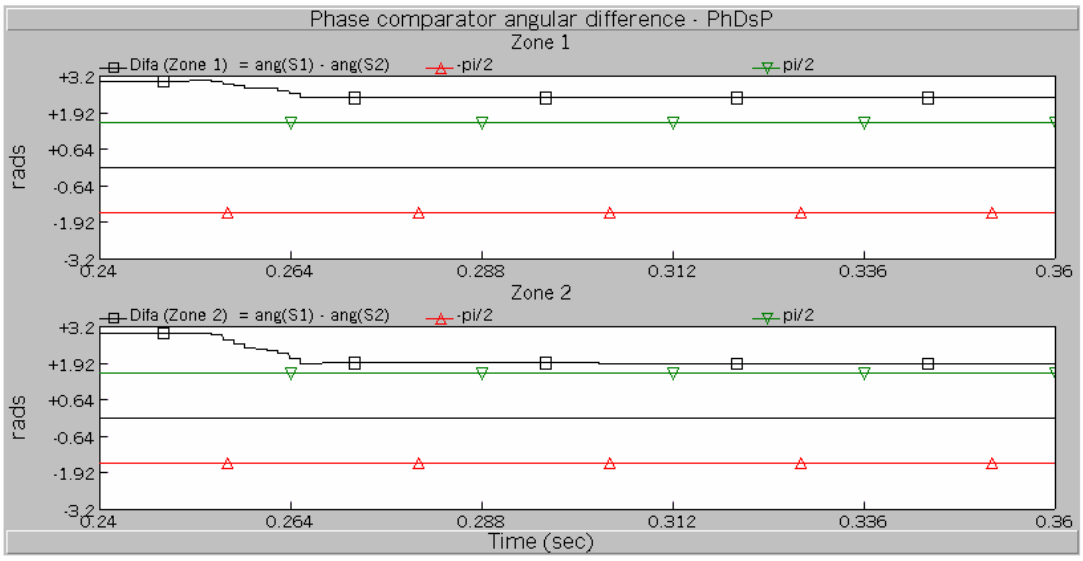


**Figure 5.65:** Response of the phase comparators of *PhDsP*, zone-1 and zone-2, phase C-phase A-to-ground fault, 50% of *T5*

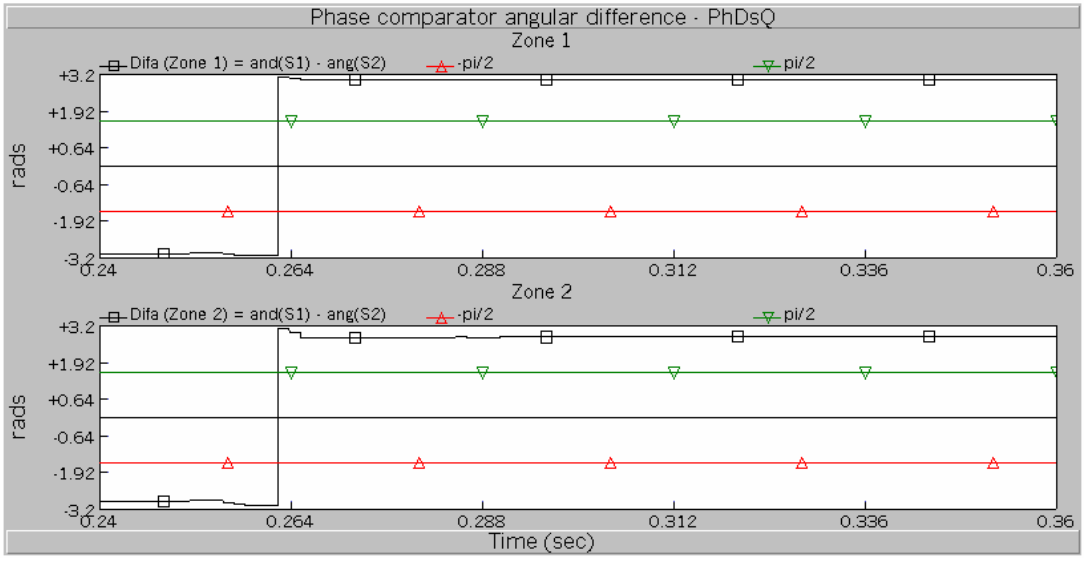


**Figure 5.66:** Response of the phase comparators of *PhDsQ*, zone-1 and zone-2, phase C-phase A-to-ground fault, 50% of *T5*

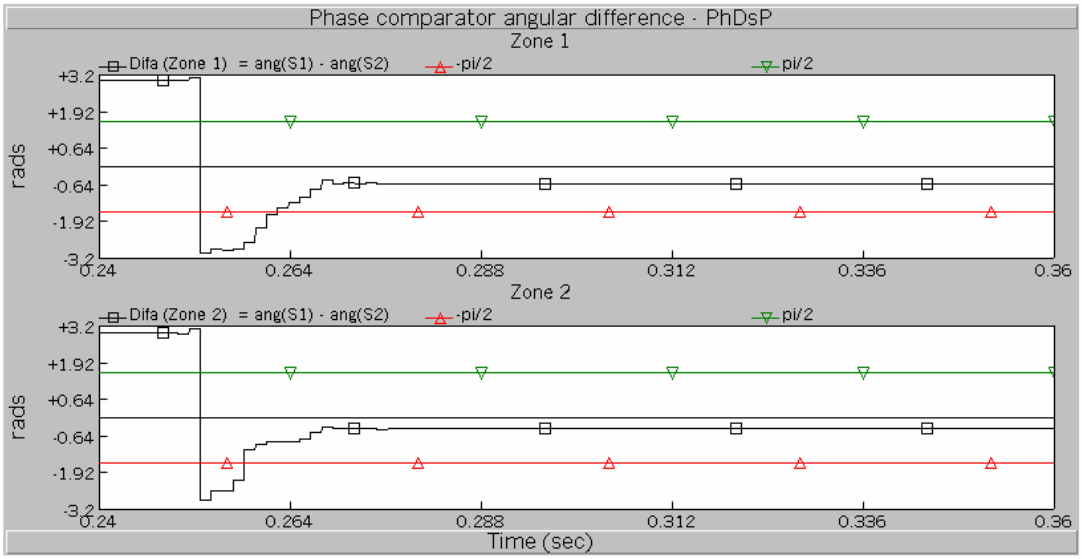


**Figure 5.67:** Response of the phase comparators of *PhDsP*, zone-1 and zone-2, three phase-to-ground fault, 50% of *T5*

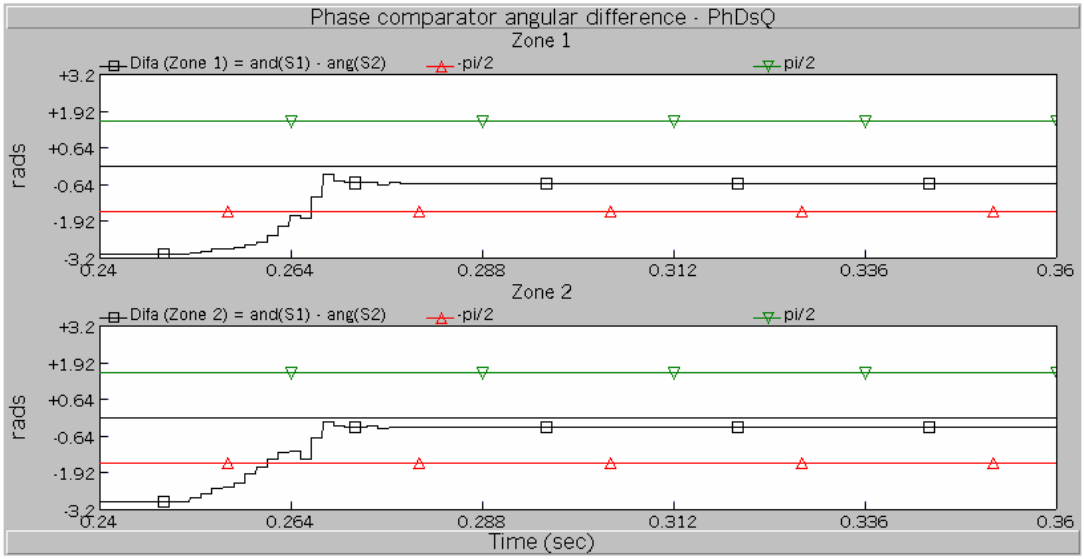


**Figure 5.68:** Response of the phase comparators of *PhDsQ*, zone-1 and zone-2, three phase-to-ground fault, 50% of *T5*

### 5.6.4.4 Apparent impedances of the faults at 50% of line *T5*

In this section are presented the plottings in the impedance plane of the impedance faults calculated by the distance relay models *PhDsP* and *PhDsQ*, for the faults at 50% of transmission line *T5*, simulated in the previous section. The plottings were generated using Matlab and PSCAD/EMTDC output files containing the values of the apparent impedances seen by *PhDsP* and *PhDsQ* on the faults at 50% of line *T5*.

In Figures 5.69, 5.70 and 5.71 are shown the plottings of impedance faults calculated by the phase distance relay model *PhDsP* for the single line-to-ground, double line-to-ground and three-phase-to-ground faults at 50% of *T5*, respectively. In Figures 5.72, 5.73 and 5.74 are shown the plottings of impedance faults calculated by the phase distance relay model *PhDsQ* for the single line-to-ground, double line-to-ground and three-phase-to-ground faults at 50% of transmission line *T5*, respectively.

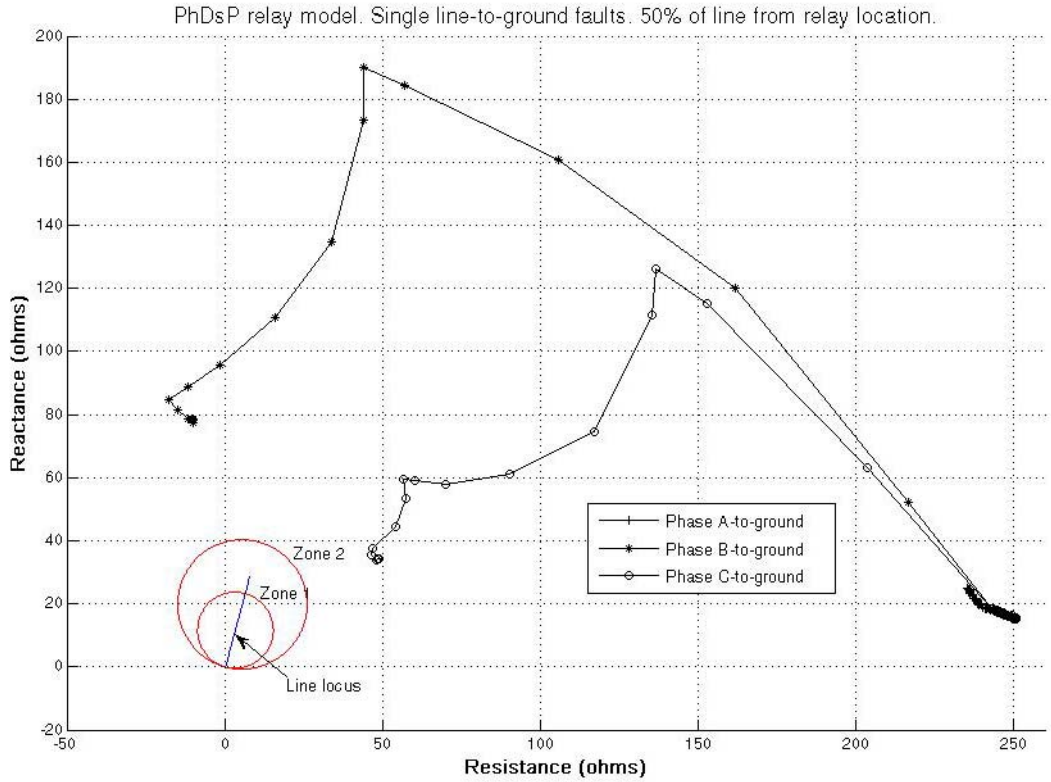


**Figure 5.69:** Apparent impedances seen by *PhDsP* on the single line-to-ground faults at 50% of *T5*

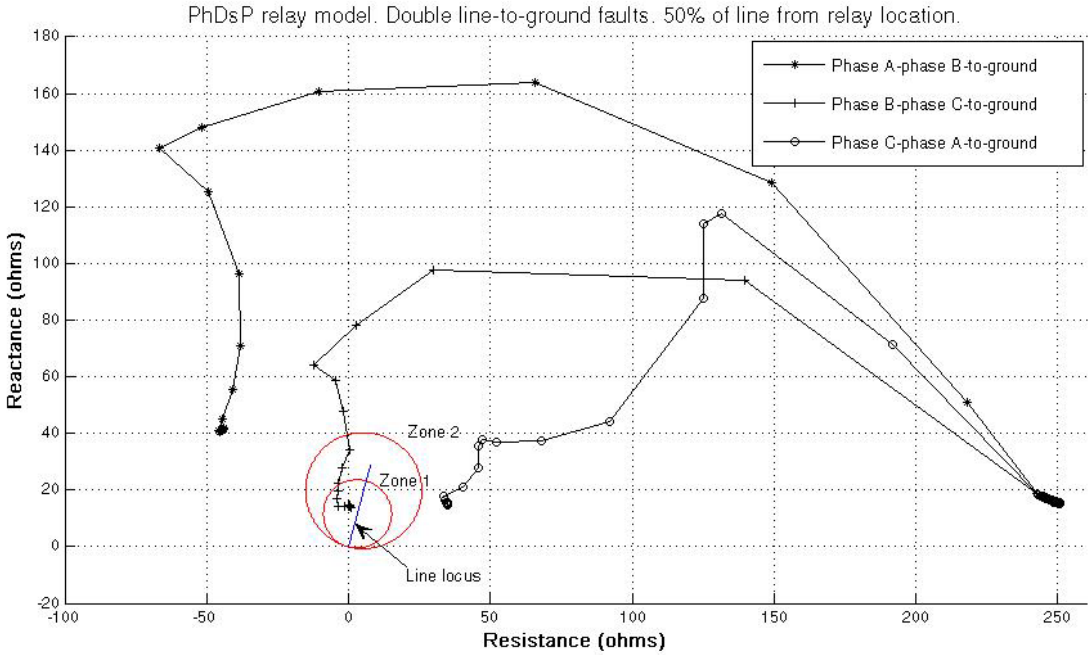


**Figure 5.70:** Apparent impedances seen by *PhDsP* on the double line-to-ground faults at 50% of *T5*

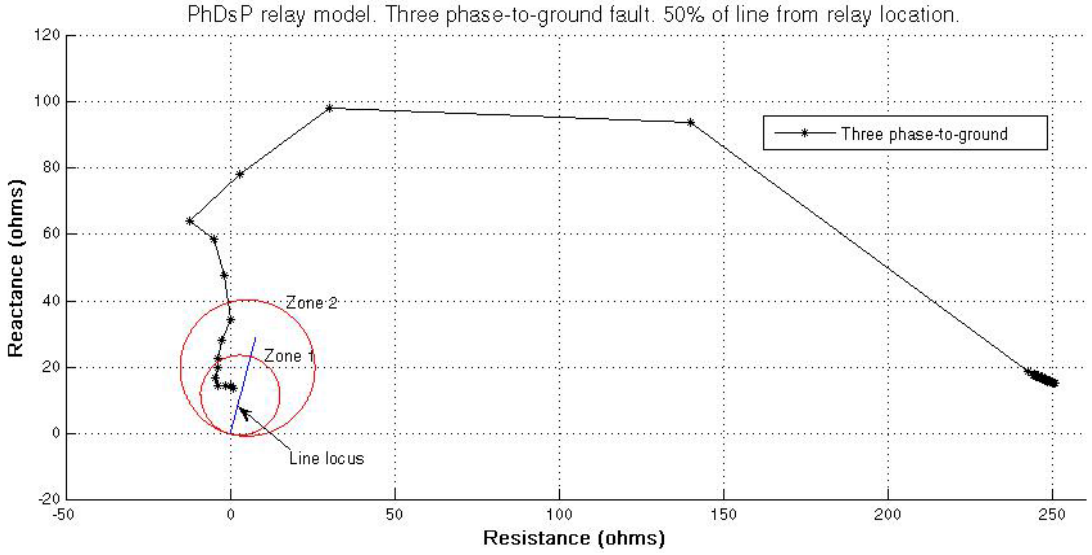


**Figure 5.71:** Apparent impedances seen by *PhDsP* on the three phase-to-ground fault at 50% of *T5*

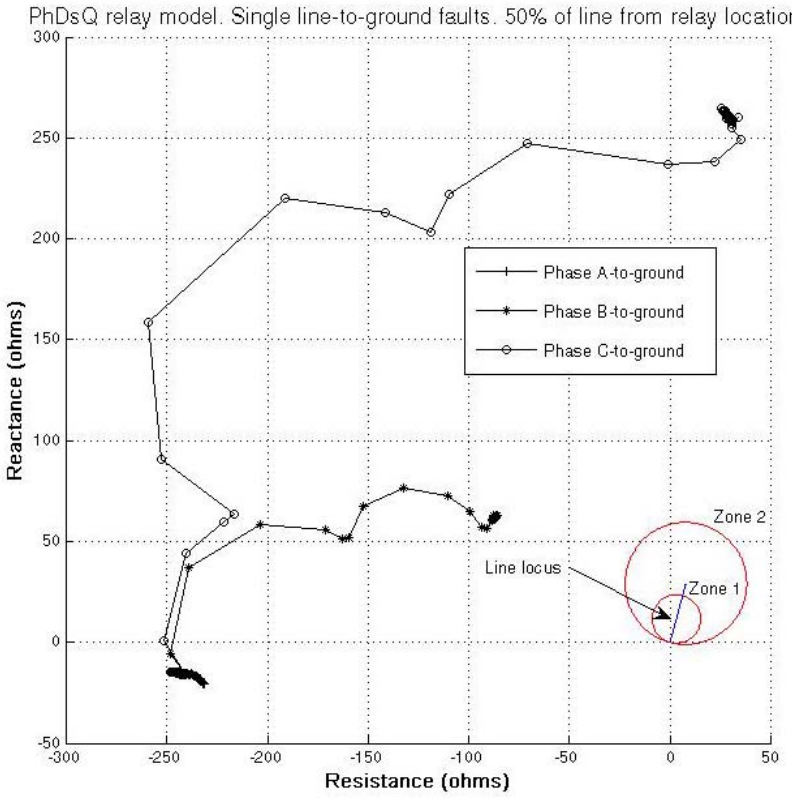


**Figure 5.72:** Apparent impedances seen by *PhDsQ* on the single line-to-ground faults at 50% of *T5*

### 5.6.4.5 Conclusion of the studies of distance protection performance for different fault types

In section 5.6.4 different fault types were simulated in two different locations of transmission line *T5*. Two distance relay models were adjusted and placed in both ends of such transmission line. The distance relay models identified correctly the nature of the event they were monitoring, and they showed the required discrimination in their operation. The distance relay models also calculated the apparent impedance of the transmission line, and the plotting of these apparent impedances in the impedance plane corroborated the correct operation of the relay models designed with the proposed protection system model designing methodology.

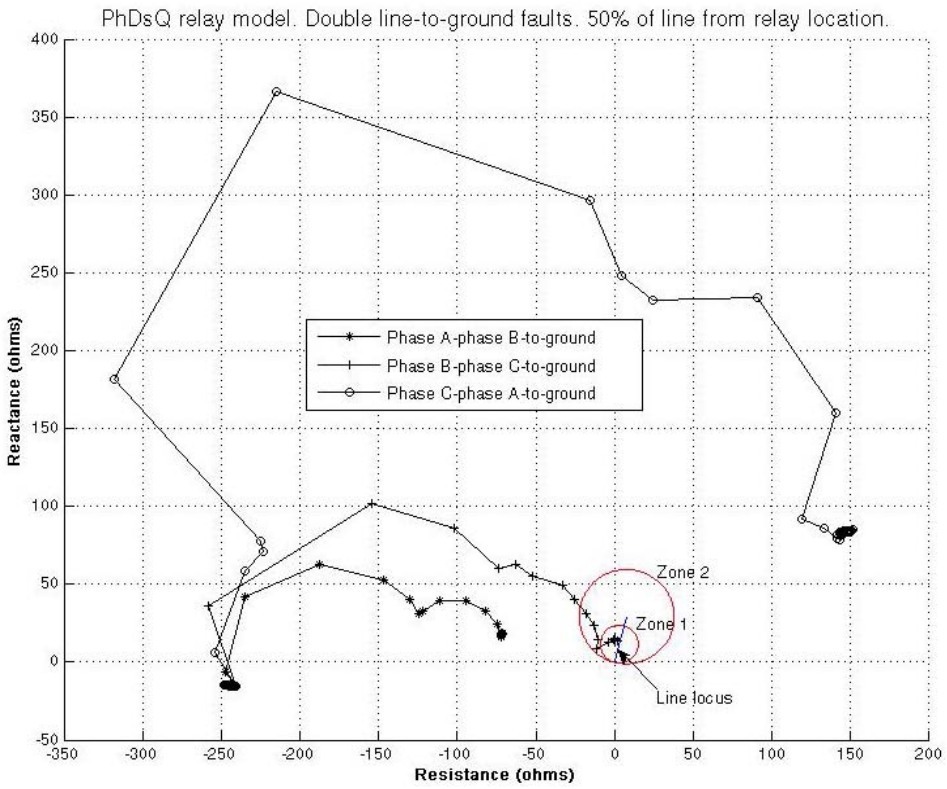


**Figure 5.73:** Apparent impedances seen by *PhDsQ* on the double line-to-ground faults at 50% of *T5*

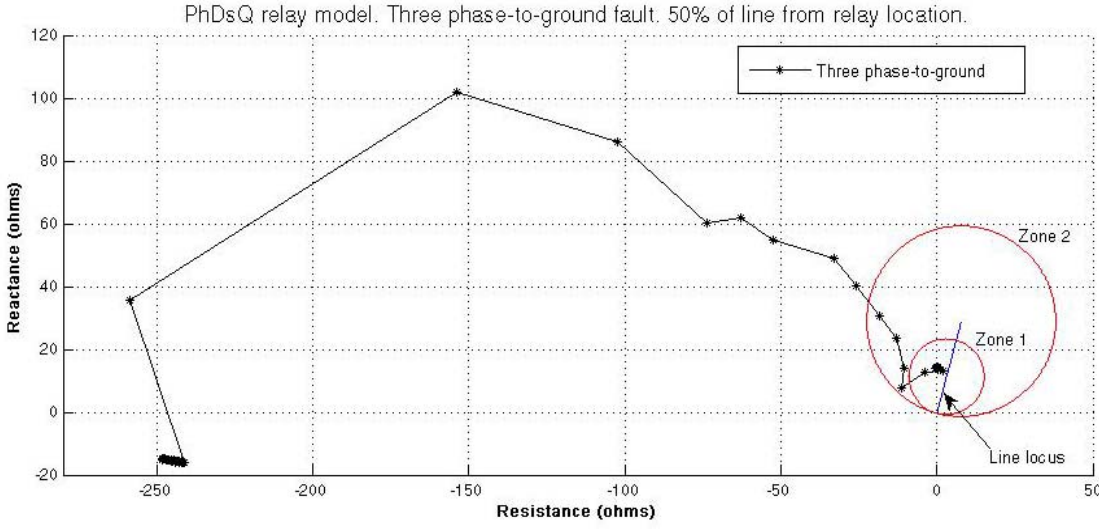


**Figure 5.74:** Apparent impedances seen by *PhDsQ* on the three phase-to-ground fault at 50% of *T5*

### 5.6.5 Distance protection performance for a fault behind its location

The purpose of this study was to investigate the performance of the distance protection in the occurrence of a fault behind its location. Location is the electrical point where the current and voltage transformers feeding the numerical relay are connected to the power system. In these terms, a fault behind the numerical distance relay is placed behind the current transformers.

For this study, the numerical distance relay *PhDsP* was employed. In Figure 5.75 is depicted the fault arrangement of this study in PSCAD/EMTDC. A phase B-phase C-to-ground fault was simulated directly over *Bus 3*, just behind the current transformers of *PhDsP*.

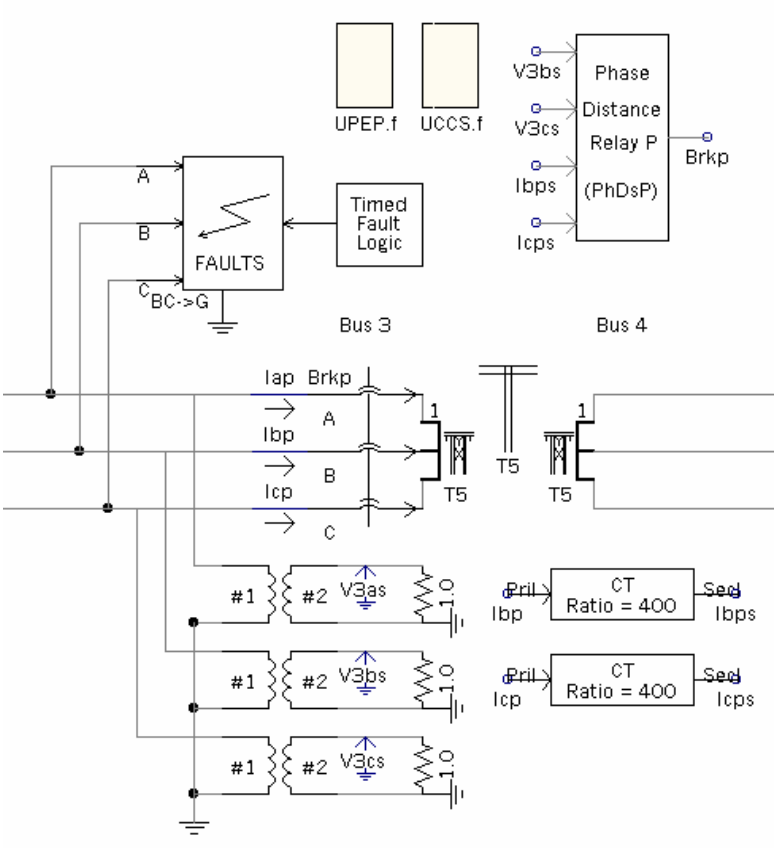


**Figure 5.75:** Phase B-phase C-to-ground fault simulated behind the location of *PhDsP*

In Figure 5.76 is shown the response of the angular difference of the signals $S_1$ and $S_2$ of the phase comparator (*Difa*) of *PhDsP*, zone-1, zone-2 and zone-3. It is observed that, just before the fault inception, the *Difa* of *PhDsP* was positive and outside of the range of the operating condition of Equation 5.1. In Figure 2.6(b) is depicted a condition like this in a mho characteristic. In Figure 2.6(b), the fault impedance $Z_r\angle\varphi_r$ in the first quadrant implies that the fault current is lagging the fault voltage by an angle $\varphi_r$ and, because the system is reactive, the conventional flow current had the same direction than which *PhDsP* was "seeing" the line *T5*.

In figure 5.76, after the fault inception, the value of *Difa* crossed the characteristics of zone-1, zone-2, and zone-3 of *PhDsP*, to keep a negative value outside the operating zones. From this, it is inferred that the conventional current was flowing in the opposite direction of the direction in which *PhDsP* was "seeing" the line *T5*, and that the event did not represent a fault for the distance relay, which was expected.

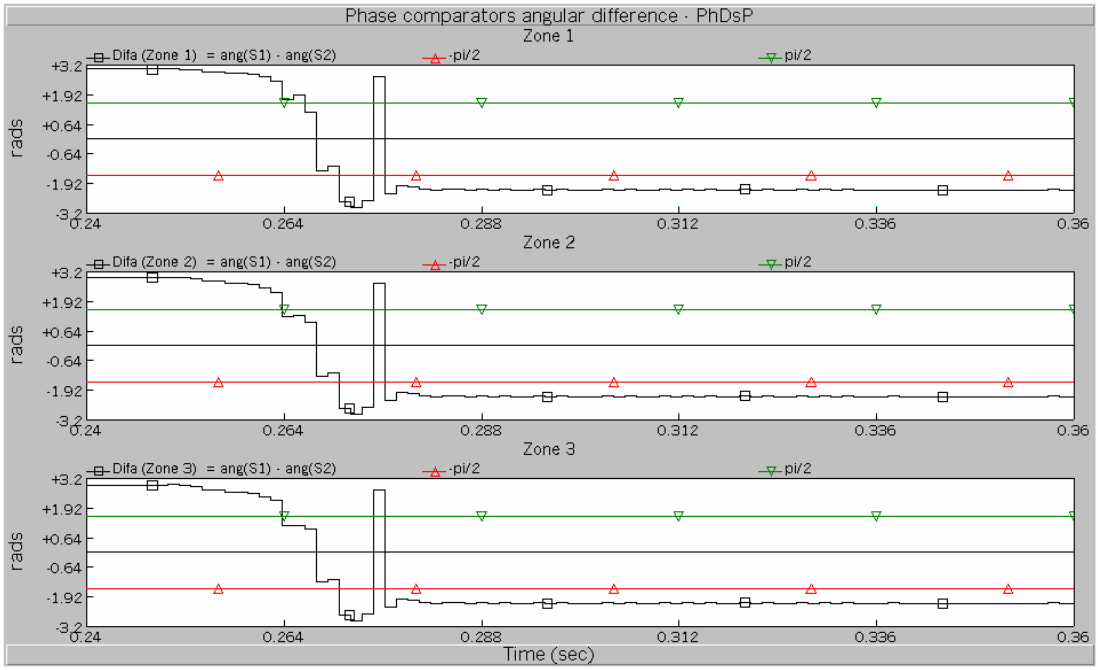


**Figure 5.76:** Response of the phase comparators of *PhDsP*, phase B-phase C-to-ground fault, just behind the relay location

### 5.6.6 Distance protection performance under current transformer saturation

The purpose of this study was to observe the behavior of the numerical distance relay model under current transformer saturation. The current transformers of the numerical distance relay model *PhDsP* were used to simulate its saturation, and to observe the effect that this event had in the performance of *PhDsP*. An analysis of these current transformers was made to know theirs saturation characteristics.

The current transformers supplying *PhDsP* have a rate of 2000 amperes to 5 amperes. The knee point of the excitation curve of the CT's is over 400 volts in the secondary side [52]. The knee point of the excitation curve divides the linear operation region and the saturated operation of the CT. Therefore, driving the operation of the CT over 400 V in the secondary circuit saturates the CT.

The voltage in the secondary side of the CT is proportional to the current flowing on the secondary windings of the CT and to the burden connected to the secondary terminals of the CT, as expressed in the following equation [50].

$$E_s = I_s Z_B, \tag{5.2}$$

where,

$E_s$ is the secondary current of the CT

$I_s$ is the secondary excitation current of CT

$Z_B$ is the impedance burden connected to the secondary of the CT

The maximum fault current experienced by *PhDsP* is 17 kA in the primary circuit. Therefore, value of the maximum fault current in the secondary of the CT is:

$$I_s = \frac{I_p}{CTR} = \frac{17000\ \text{A}}{400} = 42.5\ \text{A}\,, \tag{5.3}$$

where,

$I_p$ is the current in the primary circuit of the CT

$CTR$ is the CT ratio

According to Equation 5.2, the maximum impedance which should be connected to the secondary terminals of the CT, without saturating it, is

$$Z_B = \frac{E_s}{I_s} = \frac{400\ \text{V}}{42.5\ \text{A}} = 9.412\ \Omega\,. \tag{5.4}$$

To saturate the CT it is necessary that the burden connected to its secondary terminals is larger than 9.412 Ω. For the study, the burden impedance chosen was 10 Ω.

The secondary current of the CT supplying current signal to *PhDsP* for a phase B-phase C-to-ground fault, at 80% of the length of line *T5* is shown in Figure 5.77(a). The CT burden impedance was 0.7 Ω. The secondary current of the same CT, under the same fault conditions, but with a burden impedance of 10 Ω, is shown in Figure 5.77(b). Comparing Figure 5.77(a) and 5.77(b) it is observed the degradation suffered by the secondary current in the saturated CT.

The *Difa* of zone-1 of *PhDsP* is shown in Figure 5.78. For a better appreciation of the corruption suffered by *Difa*, in Figure 5.79(a) and Figure 5.79(b) are presented the zoomings of *Difa* for a phase B-phase C-to-ground fault, at 80% of the length of line *T5*, saturated and non-saturated CT cases, respectively.

In Figure 5.79(b) it is observed that the saturation of the CT's made the *Difa* of *PhDsP* to be incorrectly out of the operating condition for a short period of time. The

comparison made of the non-saturated and saturated CT's cases in Figure 5.79 shows that the response of the distance relay was greatly affected by the saturation of the CT's.

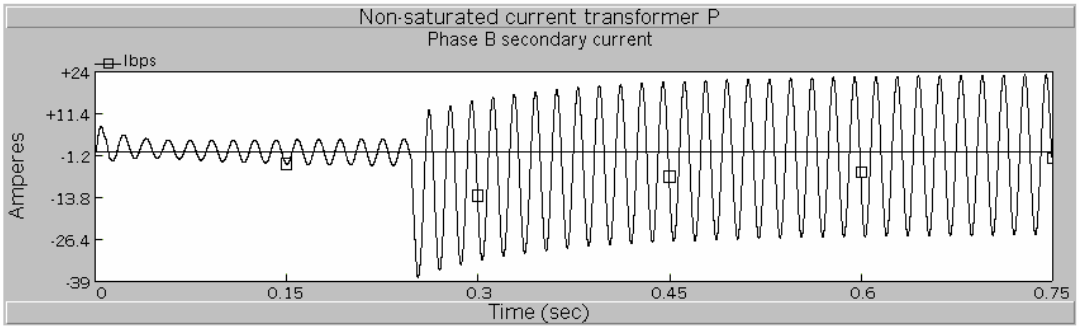


**(a)** Non saturated CT, 0.7 Ω burden

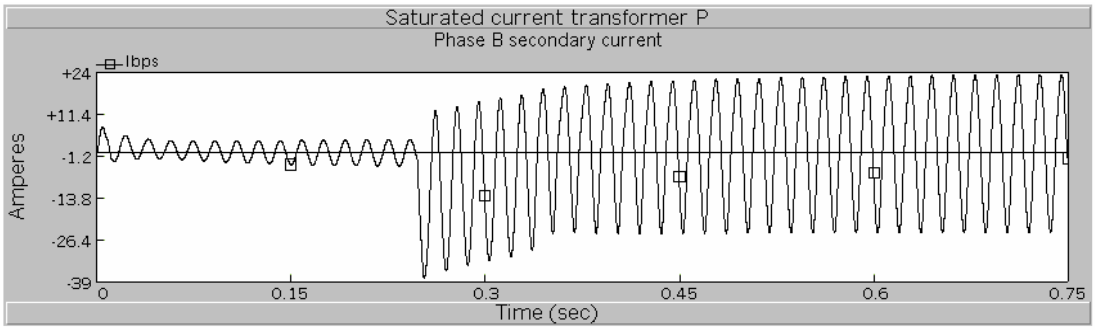


**(b)** Saturated CT, 10 Ω burden

**Figure 5.77:** Secondary current of the CT of phase B of *PhDsP*, phase B-phase C-to-ground fault, 80% of *T5*.

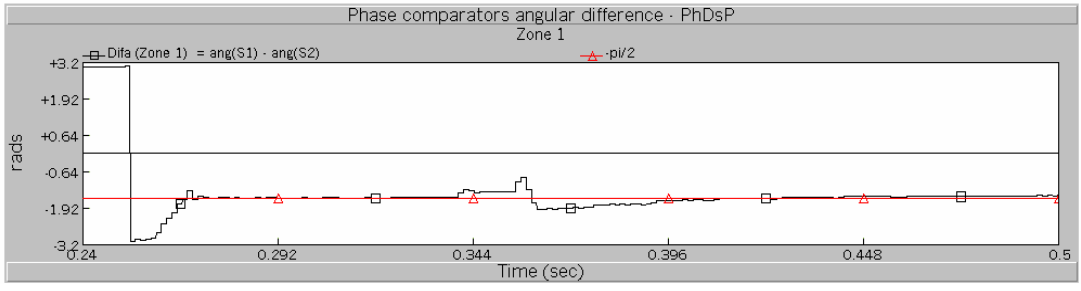


**Figure 5.78:** Response of the phase comparators of *PhDsP*, CT saturated case, phase B-phase C-to-ground fault, 80% of *T5*

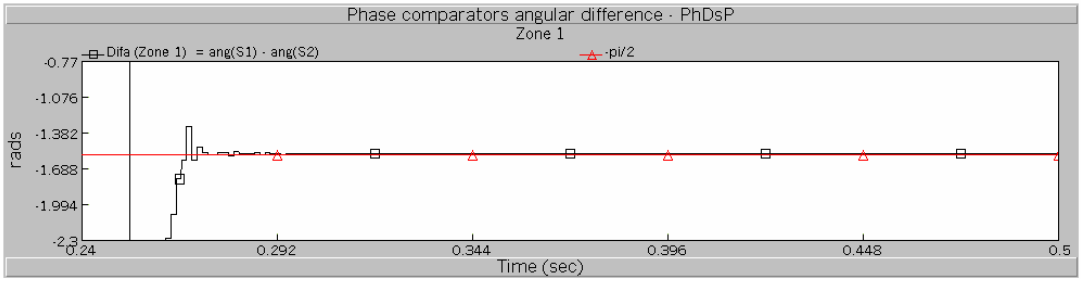


**(a)** Non-saturated CT case

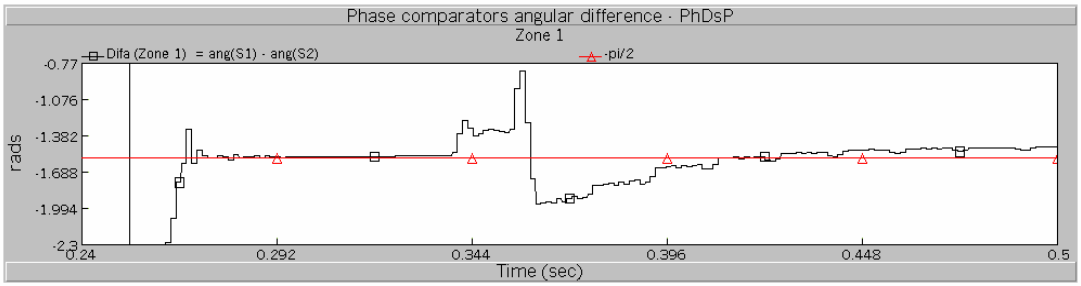


**(b)** Saturated CT case

**Figure 5.79:** Zooming of the response of the phase comparators of *PhDsP*, phase B-phase C-to-ground fault, 80% of *T5*

### 5.6.7 Distance protection performance when anti-aliasing filter removed

The purpose of this study was to investigate the effect that the presence of the anti-aliasing filter has over the response of the numerical distance relay model. The study consisted in comparing the response of a numerical distance relay model that had the anti-aliasing filter module with the response of the same numerical distance relay model that had the anti-aliasing filter module removed.

The numerical distance relay model *PhDsP* was used in the study. A phase B-phase C-to-ground fault was simulated at 80% of the length of line *T5*, from *Bus 3*. The voltage waveform of phase B after the analog signal scaling and sample-and-hold modules of the relay model *PhDsP* were monitored to show the effect of the presence and the absence of the anti-aliasing filter in the performance of the numerical distance relay model.

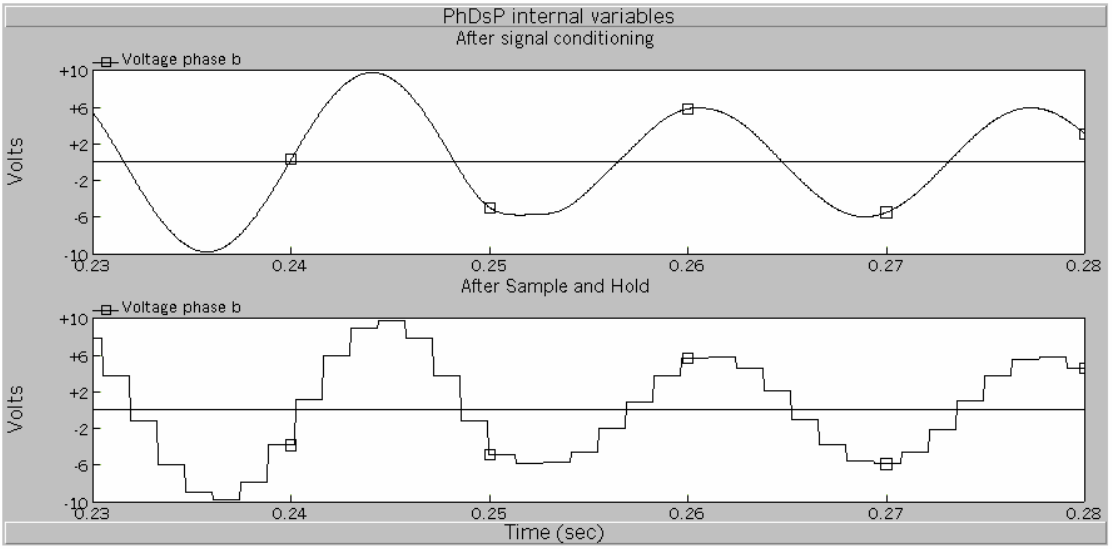


**(a)** After analog signal scaling and sample and hold modules, with anti-aliasing filtering

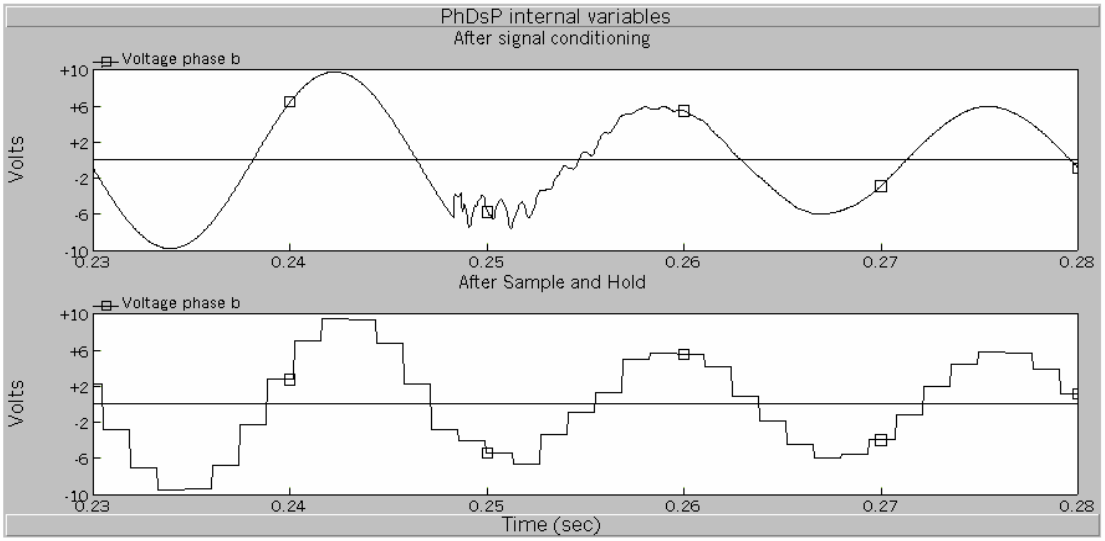


**(b)** After analog signal scaling and sample and hold modules, without anti-aliasing filtering

**Figure 5.80:** Comparison of voltage waveform of phase B of *PhDsP* with and without anti-aliasing filtering

The voltage waveform of phase B after the analog signal scaling and sample-and-hold modules at the interior of the relay model *PhDsP*, when *PhDsP* employed anti-aliasing filtering is shown in Figure 5.80(a). The same voltage waveform is shown in Figure 5.80(b) for the case when *PhDsP* did not employ anti-aliasing filtering.

The phasor estimation of the filtered and unfiltered voltage waveforms of Figure 5.80 is shown in Figure 5.81. The filtered voltage of phase B magnitude and phase calculated by the phasor estimator algorithm in *PhDsP* is shown in Figure 5.81(a). The magnitude and phase of the unfiltered voltage of phase B calculated by the phasor estimator algorithm in *PhDsP* is shown in Figure 5.81(b).

The filtered and unfiltered voltage and current waveform were then employed to calculate the angular difference of the signals $S_1$ and $S_2$ of the phase comparator (*Difa*) of the phase comparator of *PhDsP*. The calculated *Difa* for the filtered and unfiltered cases, zone-1, -2, and -3 of *PhDsP* are shown in Figure 5.82. The calculated *Difa* for the filtered case are shown in Figure 5.82(a) shows, and *Difa* for the unfiltered case are shown in Figure 5.82(b).

In Figure 5.82(b) it is observed that the absence of the anti-aliasing filter produced a delay in the identification of the fault to the zone-1 of distance relay *PhDsP*, compared to the case when the relay had the anti-aliasing filter, showed in Figure 5.82(a). Zone-2 and -3 had relatively no difficult to identify the fault.

Based in these observations, it is concluded that the absence of the anti-aliasing filter in the distance relay model did not represent a major problem in the performance of the *PhDsP*, in general terms. However, the performance of the distance relay model was slightly affected when the fault impedance was close to the reach of the zone characteristic.

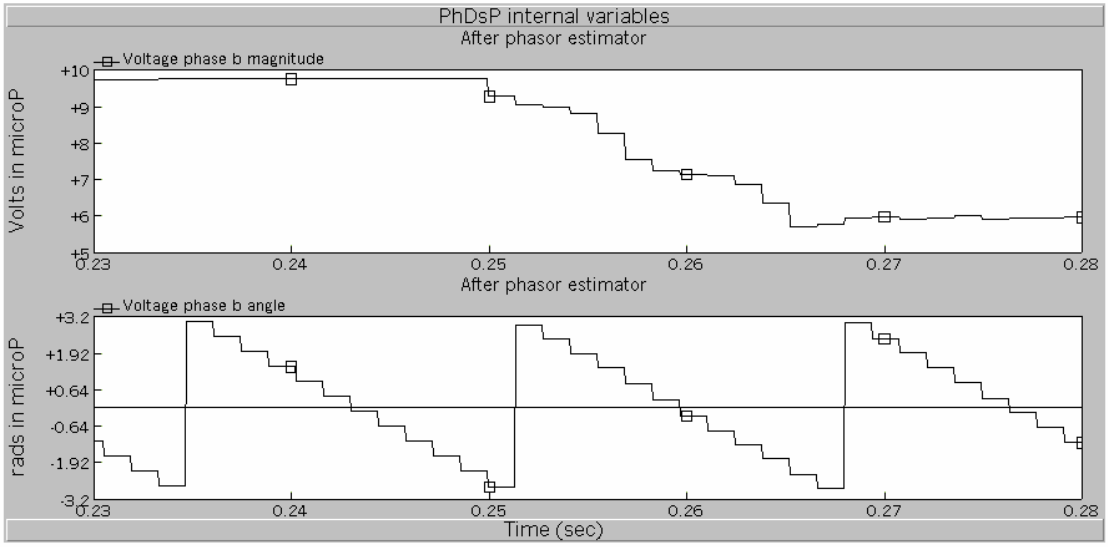


**(a)** Magnitude and phase of the filtered voltage

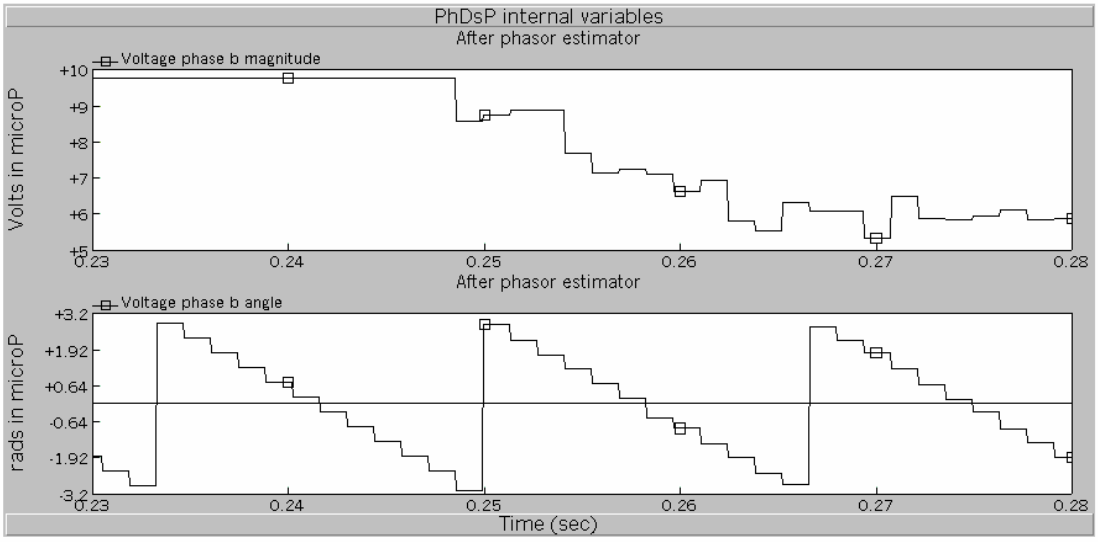


**(b)** Magnitude and phase of the unfiltered voltage

**Figure 5.81:** Phasor estimation of the filtered and unfiltered voltage of phase B of Figure 5.80

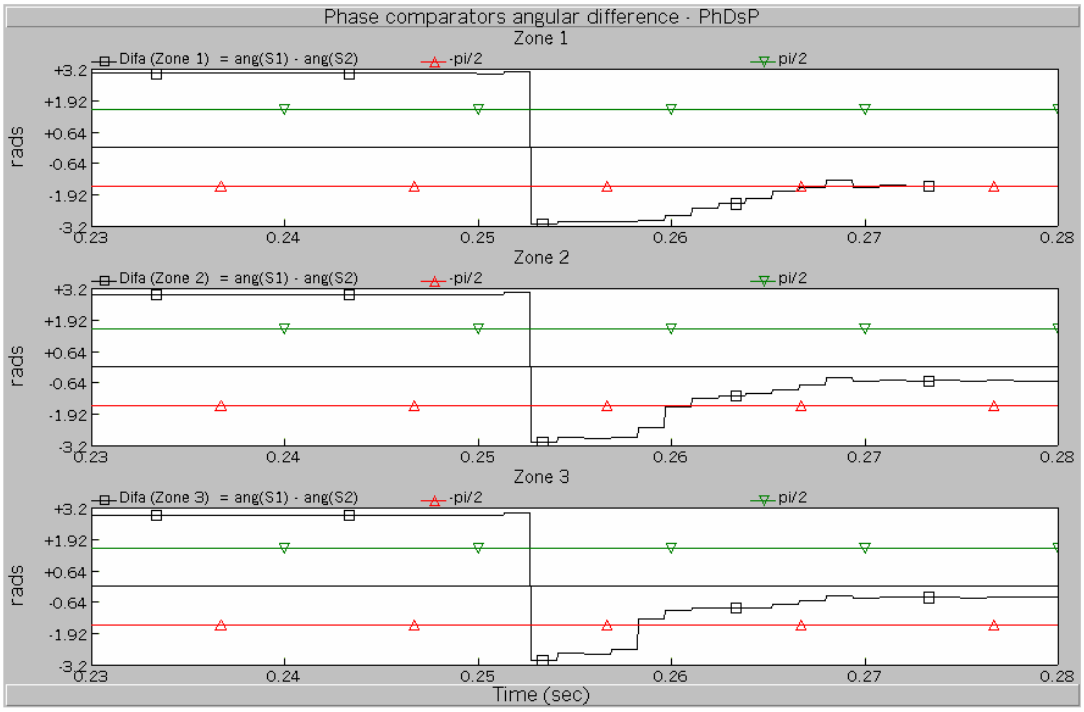


**(a)** *Difa* of the filtered case

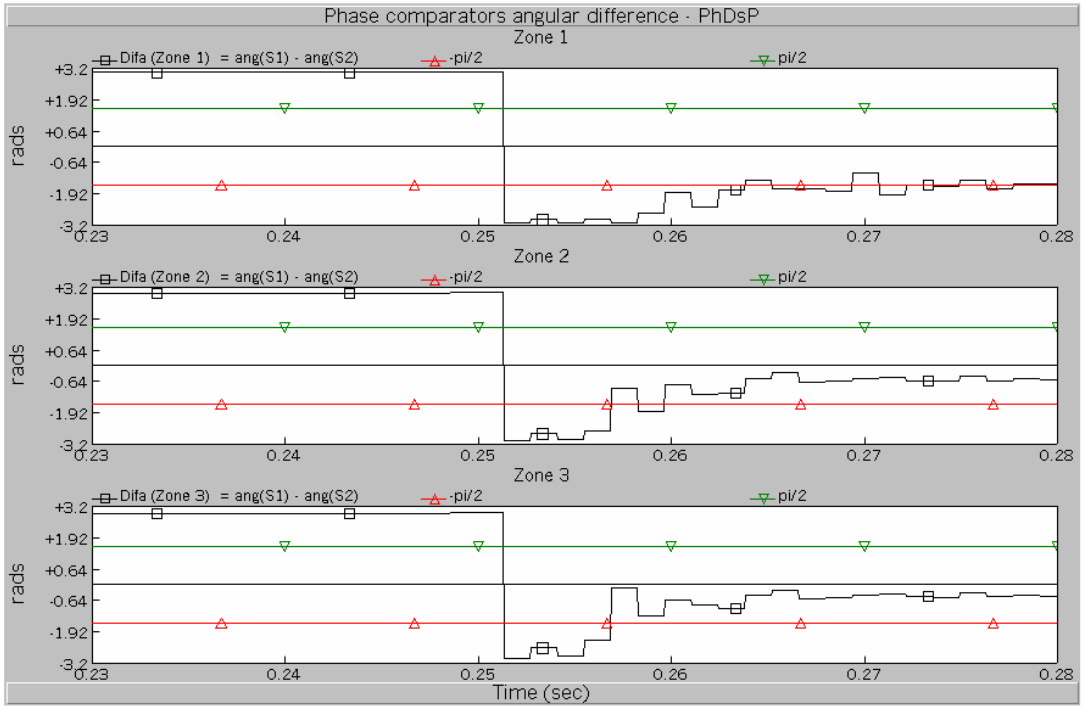


**(b)** *Difa* of the unfiltered case

**Figure 5.82:** Response of the phase comparators of *PhDsP*, filtered and unfiltered cases, zone-1, -2, and -3, phase B-phase C-to-ground fault, 80% of *T5*

## 5.7 Differential relay studies

Under this section are presented the studies of the differential protection designed with the proposed protection system model designing methodology. In section 5.3 are presented the test power system and the differential numerical relay model designed with the proposed methodology in PSCAD/EMTDC used to develop the differential relay studies. The power transformer $Tr_7$ and the single-phase differential relay (*SPhDiffR1*) designed to protect $Tr_7$ are shown in Figure 5.4.

### 5.7.1 Setting and adjustment of differential relay protecting a power transformer

The purpose of this study was to adjust the parameters of a numerical percentage restraint differential relay model, designed with the proposed protection system model designing methodology, protecting a power transformer.

In section 2.4.2, the operation of the percentage restraint differential relay is established in Equation 2.60. The adjustment of the numerical percentage restraint differential relay model consisted in evaluate the value of the slope of the differential characteristic (*SLP*) to achieve a correct operation of the differential relay during normal operation and in the event of a fault. The evaluation of *SLP* is based in the behavior of the operating and unfiltered restraint current during normal operation and in the event of a fault.

In Figure 5.83 are presented the unfiltered restraining current and the operating current of *SPhDiffR1* for the three-phase fault showed in Figure 5.4, occurring at the time of $t=0.4$ seconds. Equations 2.56 and 2.57 were employed to calculate the operating and unfiltered restraint currents, respectively. The unfiltered restrain current used a value of $k$=0.5. In Figure 5.83(a) are observed two different stages in the behavior of the differential relay curves.

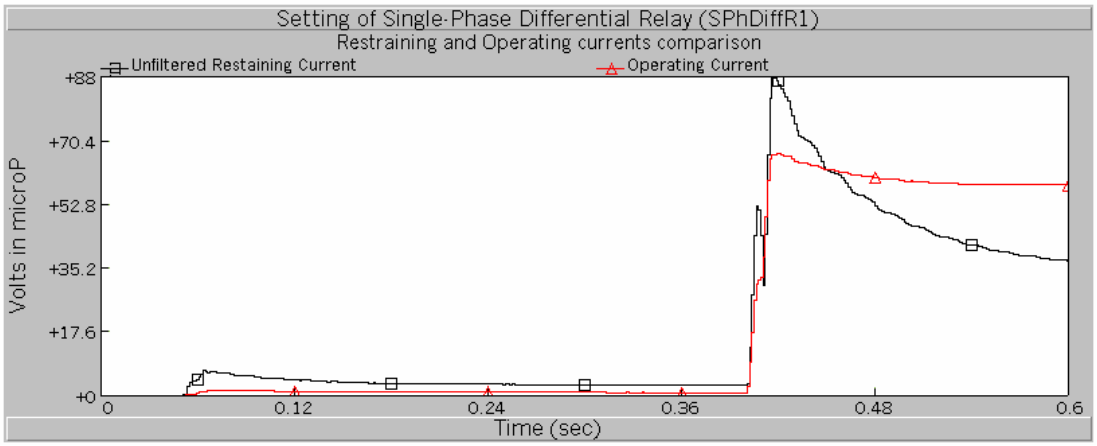


**(a)** Complete simulation graph showing the normal operation and fault event

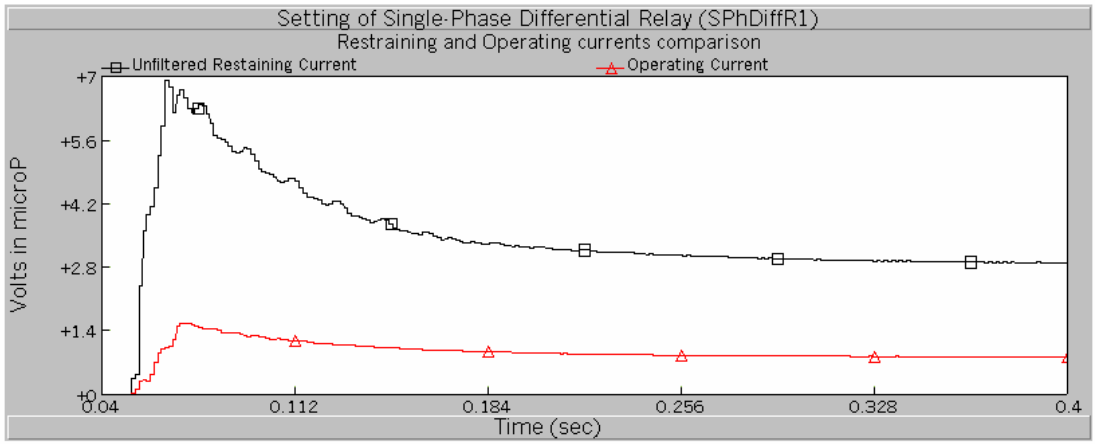


**(b)** Zooming of the differential currents during normal operation

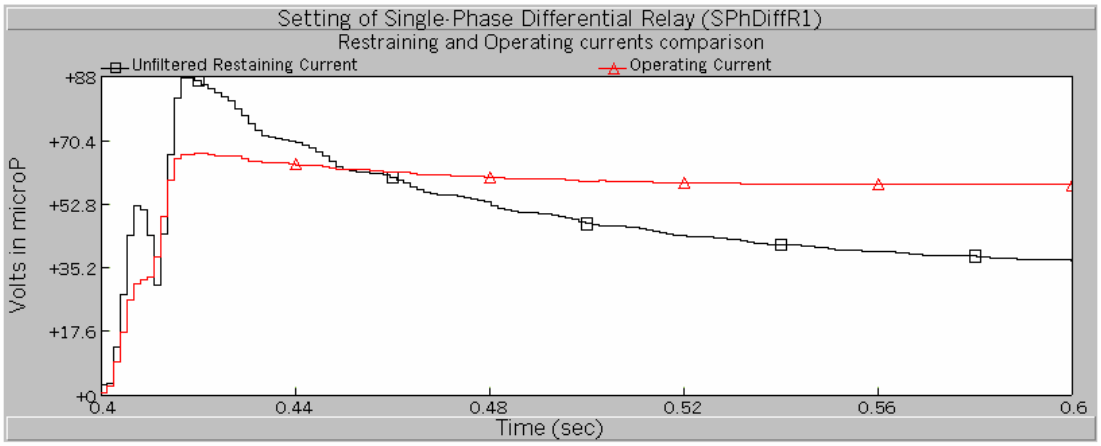


**(c)** Zooming of the differential currents after fault inception

**Figure 5.83:** *SPhDiffR1* differential currents for the three-phase fault of Figure 5.4

The first part is the behavior of the differential relay currents during the normal operation of the power transformer. The second part is the behavior of the differential relay currents after the occurrence of the fault. In Figure 5.83(b) and Figure 5.83(c) are shown zooming of the differential currents during normal operation and after the occurrence of the fault, respectively. In Table 5.4 are summarized the relevant values for adjusting purposes of the unfiltered restraining current and the operating current.

According to Equation 2.60, during normal operation, the operating current must be smaller than the restraining current, and in a fault, the operating current must be larger than the restraining current. In the normal operation shown in Figure 5.83(b), it was observed that these differential currents fulfilled the requirements of a correct operation. After the fault inception, as shown in Figure 5.83(c), it was only in the transitory part that the differential currents did not fulfill the requirements of a correct operation. Therefore, the selected value of *SLP* must make the unfiltered restraining current value smaller than the operating current during the transitory part of the fault, while keeping the restraining current larger than the operating current during normal operation.

From Table 5.4, the ratio of the operating current to the unfiltered restraining current during the transitory part of the normal operation was *1.55/6.78=0.229*. The same ratio during the stable part of the normal operation was *0.8/2.87=0.279*. This means that *SLP* must be larger than 0.279 to keep the unfiltered restraining current larger than the operating current during normal operation. Also from Table 5.4, the ratio of the operating current to the unfiltered restraining current during the transitory part of the fault was *30.4/52.8=0.576*. The same ratio during the stable part of the fault was *58/32=1.81*. This means that *SLP* must be smaller that 0.576 to make the unfiltered restraining current smaller than the operating current after the fault.

Based on the above-mentioned evaluations, the value of *SLP=0.35* was chosen. This value of *SLP=0.35* corresponds to a differential characteristic of 19.29 degrees. The differential currents of *SPhDiffR1* for the three-phase fault showed in Figure 5.4, occurring at a time *t=0.4* seconds, with the unfiltered restraining current multiplied by a

factor equal to *SLP = 0.35* is shown in Figure 5.84. In order to make a distinction, the unfiltered restraining current multiplied by *SLP* is hereafter called as restraining current. The complete simulation plotting of the differential currents is depicted in Figure 5.84(a). The differential currents during the normal operation are shown in Figure 5.84(b). The differential currents after the fault inception are shown in Figure 5.84(c).

| **Differential current** | **Normal operation (Volts in the μP)** | | **After the fault (Volts in the μP)** | |
|---|---|---|---|---|
| | **Transitory** | **Stable** | **Transitory** | **Stable** |
| Operating | 1.55 | 0.80 | 30.4 | 58 |
| Unfiltered Restraining | 6.78 | 2.87 | 52.8 | 32 |

**Table 5.4:** Relevant values of the differential currents shown in Figure 5.83.

In Figure 5.84(c) it is observed that assigning *SLP=0.35* corrected the operation of the differential relay *SPhDiffR1* during the fault. In Figure 5.84(b) is also observed that the chosen value of *SLP* preserved a safety margin between the differential currents during normal operation.

## 5.7.2 Setting and adjustment of differential protection against inrush current presented on a power transformer

As explained in section 2.4.3.2.1, inrush current is the most important issue related with differential protection of power transformers. The purpose of this study was to set and adjust a harmonic-restrained differential relay to overcome the effects of the presence of inrush current on a power transformer. To exemplify this study, the single-phase differential relay *SPhDiffR1* adjusted in the previous section was employed.

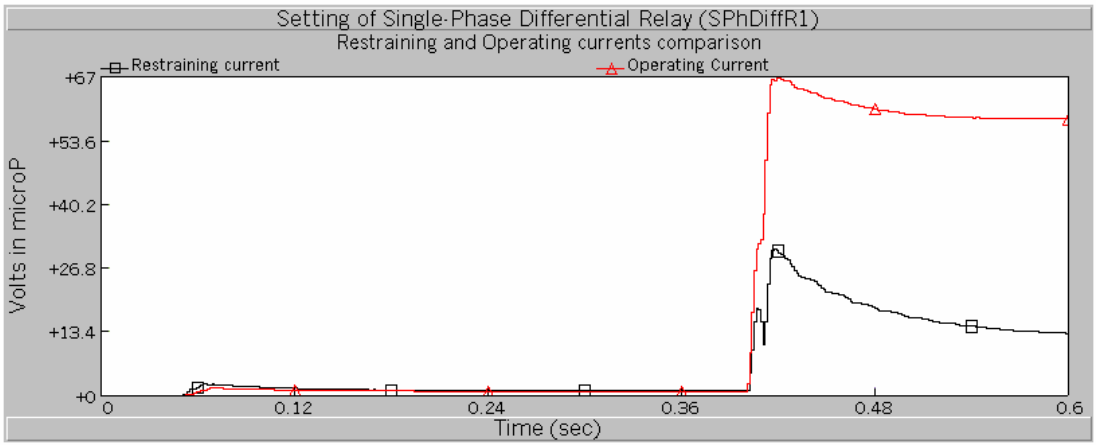


**(a)** Complete simulation graph showing the normal operation and fault event

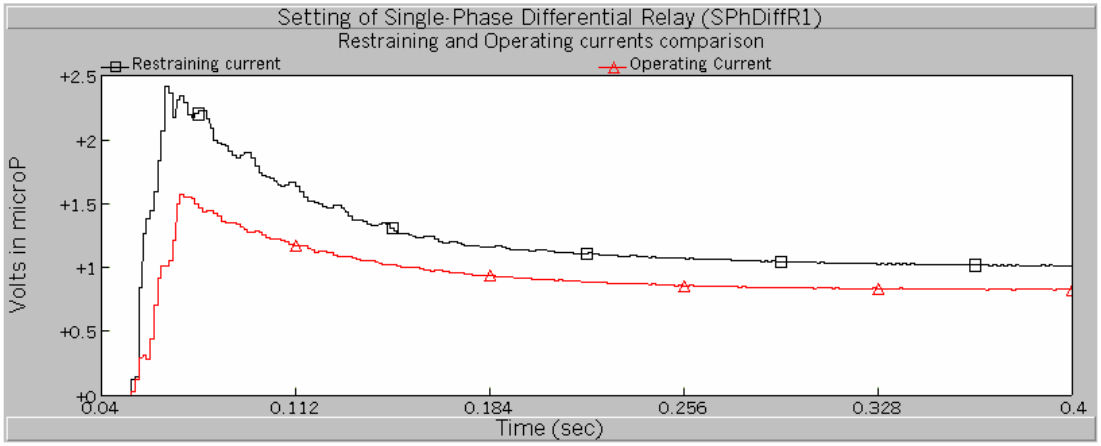


**(b)** Zooming of the differential currents during normal operation

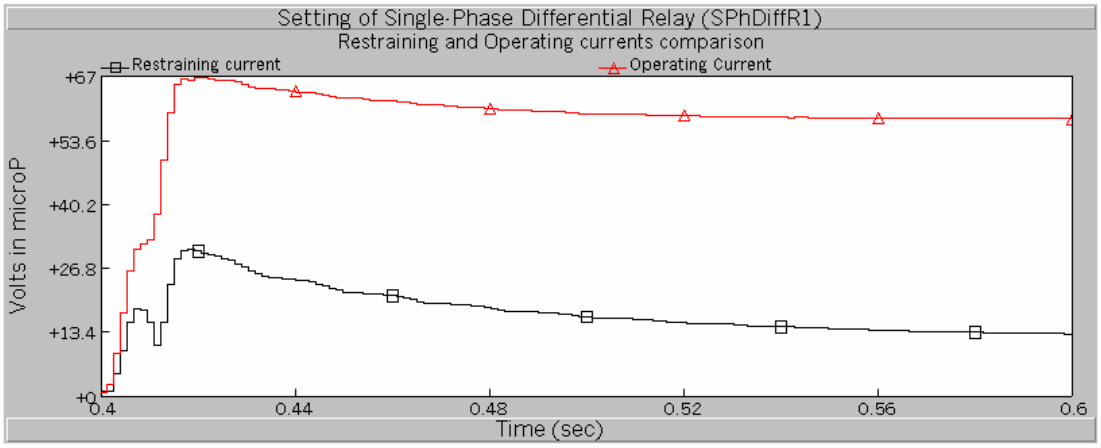


**(c)** Zooming of the differential currents after fault inception

**Figure 5.84:** *SPhDiffR1* differential currents with adjusted restraining current

To recreate an inrush current in the power transformer $Tr_7$, the breakers *Brk6* and *Brk9*, shown in Figure 5.4, were opened during the first 0.1 seconds of the simulation. After this time, the breakers *Brk6* and *Brk9* were closed, causing the energization of the power transformer $Tr_7$. Due to the sudden energization, an inrush current appeared in the windings of the power transformer $Tr_7$. After certain time, the inrush current disappeared, and the currents through the power transformer became stable. A three-phase fault, as showed in Figure 5.4, was simulated at a time of $t=0.55$ seconds.

The behavior of the differential currents of the differential relay *SPhDiffR1* in the presence of the inrush current is shown in Figure 5.85. In Figure 5.85(a) are depicted the differential currents during the entire simulation. In Figure 5.85(b) it is observed the effect of the presence of the inrush current in the operating and restraining currents before the fault. From the time of breakers closing, up to 0.25 seconds, the operating current was larger that the restraining current, which means that the differential relay *SPhDiffR1* would operate incorrectly, since the presence of inrush current due to energization of the transformer is not a fault. In Figure 5.85(a) is observed that the differential currents after the fault were unaffected by the presence of inrush current.

As stated in section 2.4.3.3.1, the harmonic-restrained differential relay employs the second harmonic of the operating relay to overcome the problems in the protection of power transformers due to the presence of inrush current. Equation 2.62, rewritten in Equation 5.5, suggests that the second harmonic of the operating current must be multiplied by a factor $k_2$, and the product must be added to the restraint current.

$$I_{op} > m_i \cdot I_{rt} + k_2 I_{2h} \tag{5.5}$$

In Figure 5.86 is depicted the second harmonic phasor magnitude of the operating current generated in the simulation case. The factor $k_2$ was estimated considering the difference in magnitude between the restraining and operating currents and the magnitude value of the second harmonic of the operating current during the presence of the inrush current.

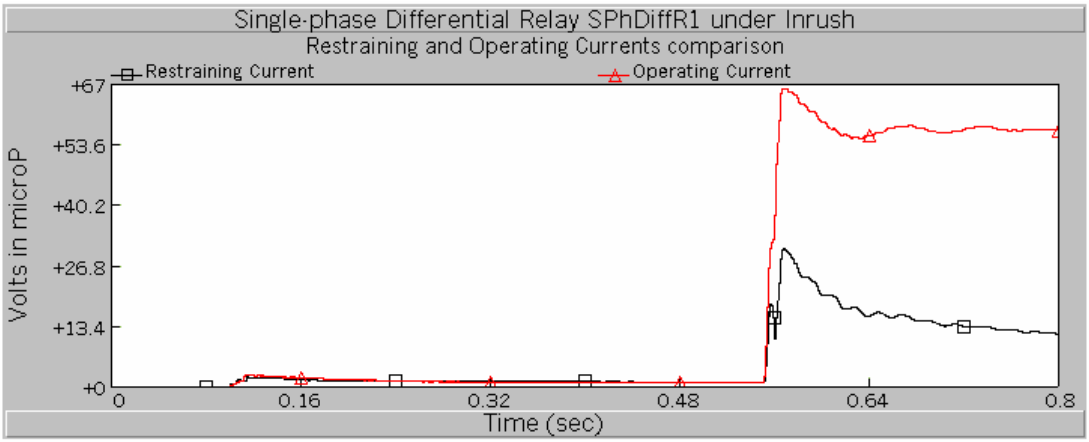


**(a)** Complete simulation graph showing the normal operation and fault event

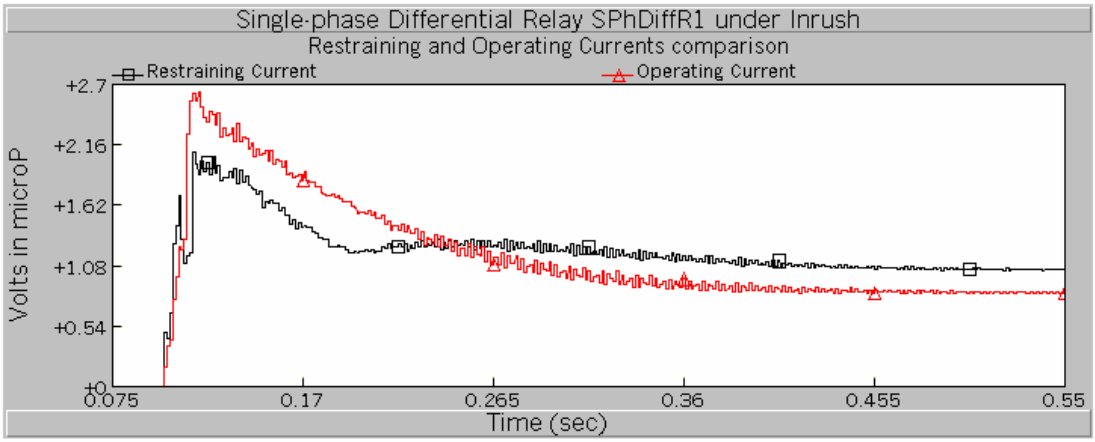


**(b)** Zooming of the differential currents during normal operation

**Figure 5.85:** *SPhDiffR1* differential currents behavior in the presence of inrush current

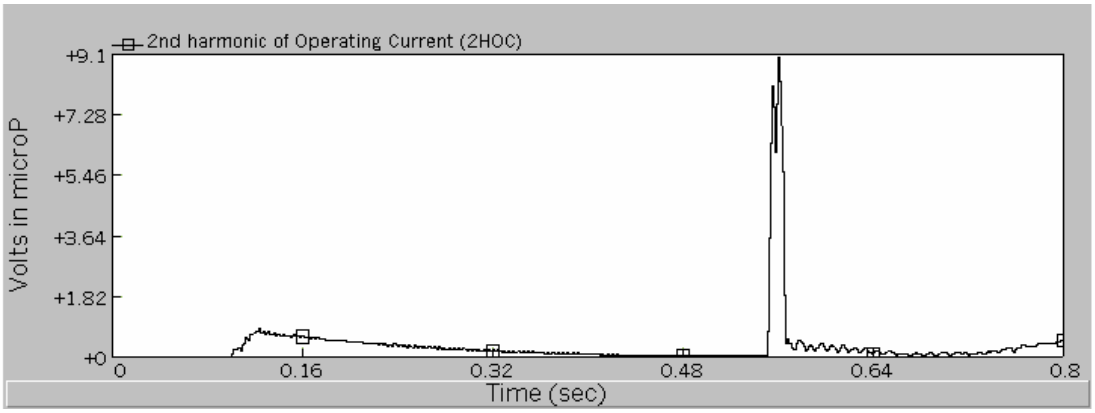


**Figure 5.86:** Second harmonic phasor magnitude of the operating current

In Figure 5.87 is shown a zooming of Figure 5.85(a) for the time when the inrush current effect was present, and below it, the zooming of the second harmonic of the operating current of Figure 5.86 for the same period of time. In Figure 5.87 is observed that the biggest difference between the restraining and the operating current occurred at *t=0.115* seconds, and it was approximately 1.4 volts in the microprocessor, and that the value of the second harmonic at that time was approximately 0.52 volts in the microprocessor. Therefore,

$$k_2 = \frac{1.4}{0.52} = 2.7 \tag{5.6}$$

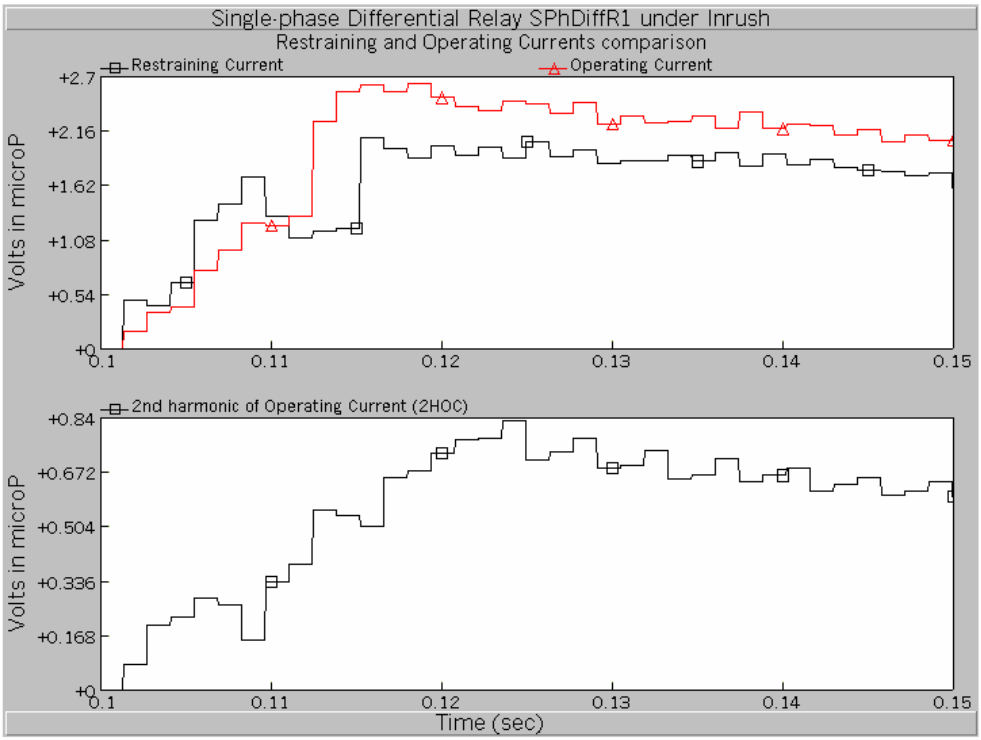


**Figure 5.87:** *SPhDiffR1* differential currents and second harmonic of operating current during the affect of the inrush current

The addition of the multiplication of the second-harmonic of the operating current by $k_2=2.7$ to the restraining current assured that this current was larger than the operating current during the time of the inrush current effect.

However, the previous action had a temporary negative effect in the operation of *SPhDiffR1* after fault inception. In Figure 5.88 is shown the zooming of the differential currents in the Figure 5.85(a) just after the fault inception, and below it, the zooming of the second harmonic magnitude of the operating current of Figure 5.86 for the same period of time. In Figure 5.88 is observed that the second harmonic of the operating current had pick values from the time of the fault inception *t=0.55* seconds up to *t=0.562* seconds. These pick values of the second harmonic were furthermore increased by the multiplication by the factor $k_2$=*2.7*. The difference between operating current and restraining current during the pick values of the second harmonic was not large enough to avoid making the restraining current temporarily larger than the operation current just after the fault inception, which caused a delaying in the identification of the fault condition by the *SPhDiffR1* differential relay.

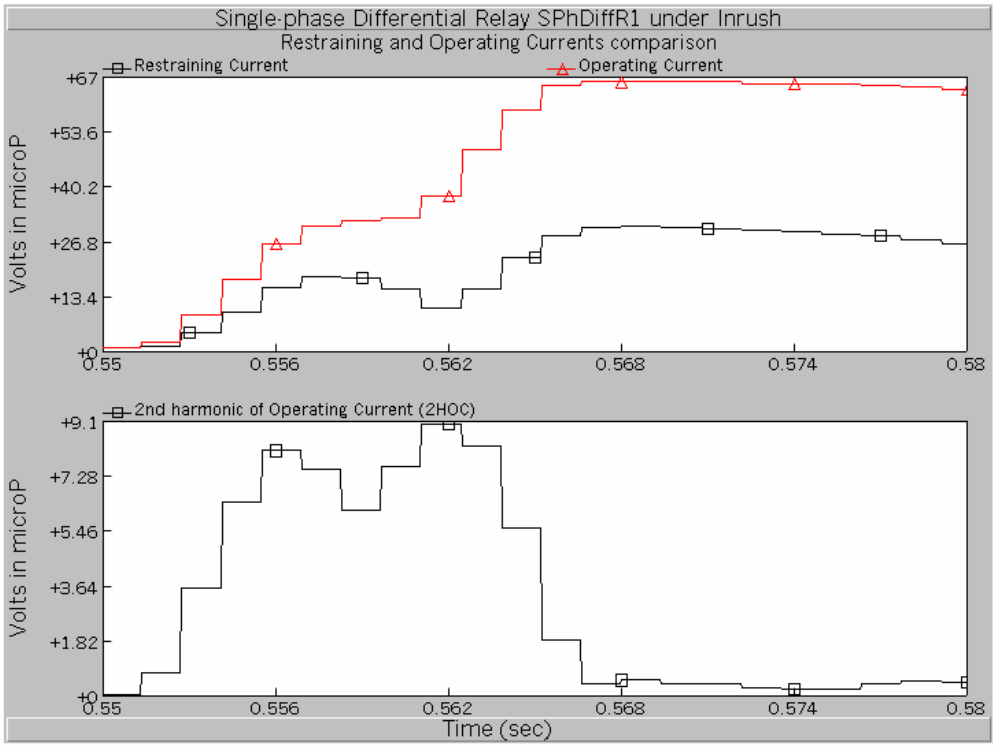


**Figure 5.88:** *SPhDiffR1* differential currents and second harmonic of operating current just after fault inception

In Figure 5.89 is shown the operating current and the restraining current modified by the addition of the multiplication of the second harmonic of the operating current by the factor $k_2=2.7$, for the same simulation case study. In Figure 5.89(a) is presented the entire simulation of the case. In Figure 5.89(b) is shown the zooming of the differential currents during the affect of the inrush current. In Figure 5.89(c) is depicted the zooming of the differential currents just after fault inception.

In Figure 5.89(b) it is observed that the restraining current was larger than the operating current during the effect of the inrush current and for the rest of the normal operation. However, in Figure 5.89(c) it is observed that the restraining current was larger than the operating current during the first 7 samples after fault inception, time that represents the delay of the differential relay to identify the fault condition. This means that the differential relay *SPhDiffR1* made a compromise by delaying the identification of a fault (loss of dependability) in order to avoid false tripping during the presence of inrush current (increment of reliability).

### 5.7.3 Performance of the differential protection of a power transformer under internal faults

The purpose of this study was to investigate the response of differential relays to internal faults in the protected transformer. The differential relay *SPhDiffR1* adjusted in previous sections was used to carry out this study. The study was divided in the simulation of internal fault in the side of *Bus 6*, and in the simulation of internal faults in the side of *Bus 9*, as shown in Figure 5.4.

The response of the differential currents of *SPhDiffR1* for a three-phase internal fault in front of the CT's of the side of *Bus 6* –considering that the CT's "see" toward the transformer location- is shown in Figure 5.90. The response of the differential currents of *SPhDiffR1* for a phase A-to-ground internal fault in front of the CT's of the side of *Bus 6* is shown in Figure 5.91.

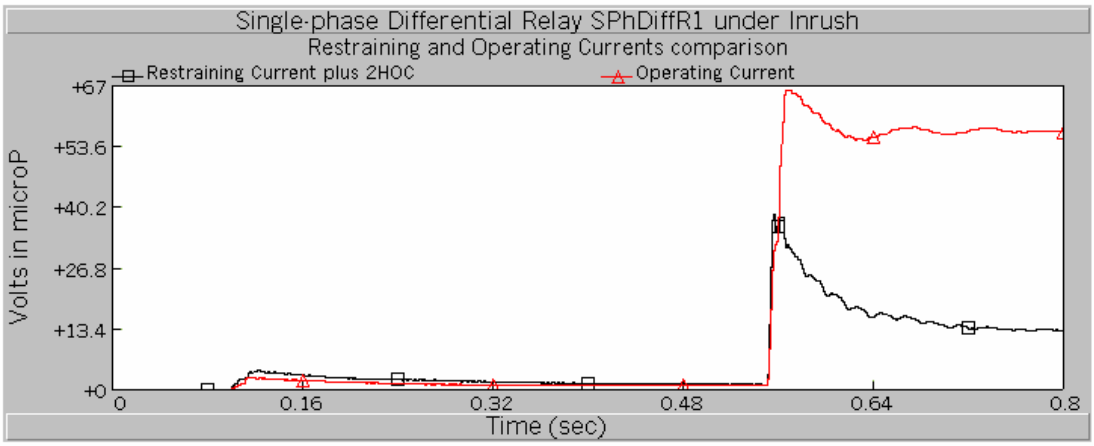


**(a)** Complete simulation graph showing the normal operation and fault event

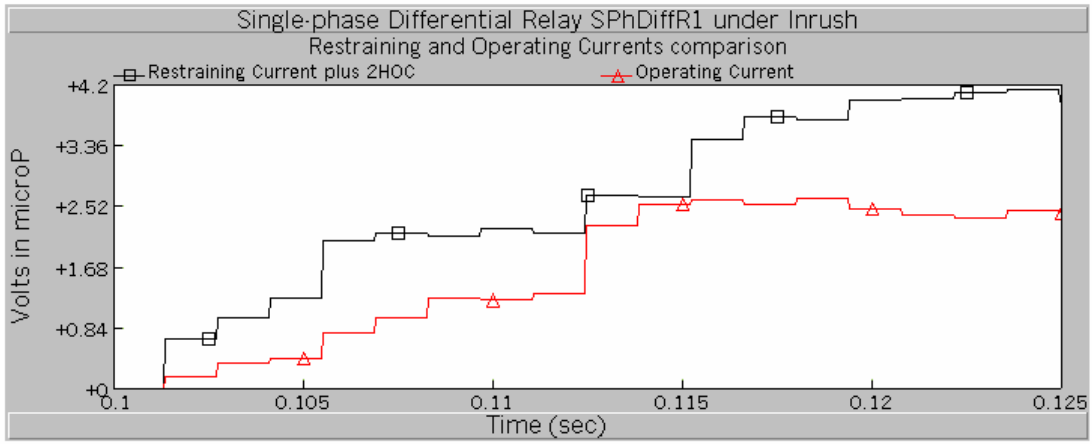


**(b)** Zooming of the differential currents during the effect of the inrush current

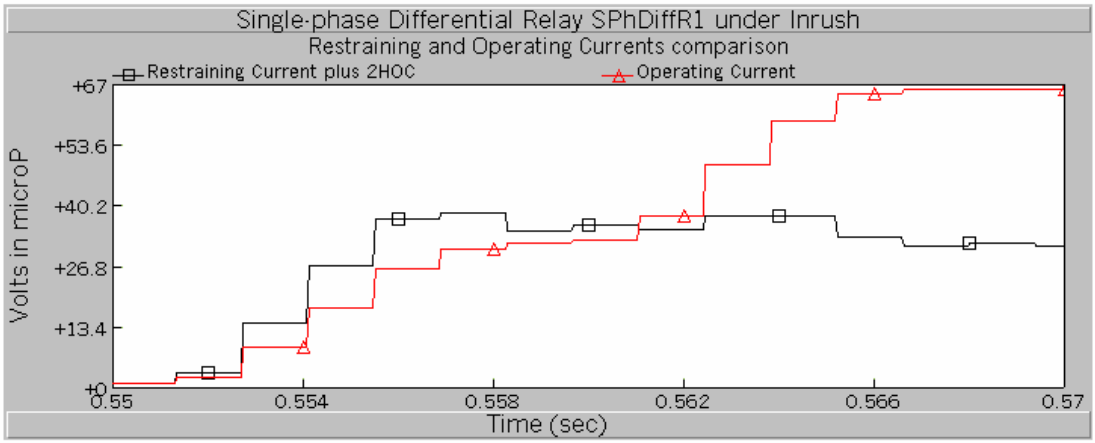


**(c)** Zooming of the differential currents after fault inception

**Figure 5.89:** *SPhDiffR1* differential currents adjusted to overcome inrush current issues

The differential relay *SPhDiffR1* showed correct operation for the simulated faults. Both responses also showed the delay in the identification of the fault condition, as discussed in the previous section.

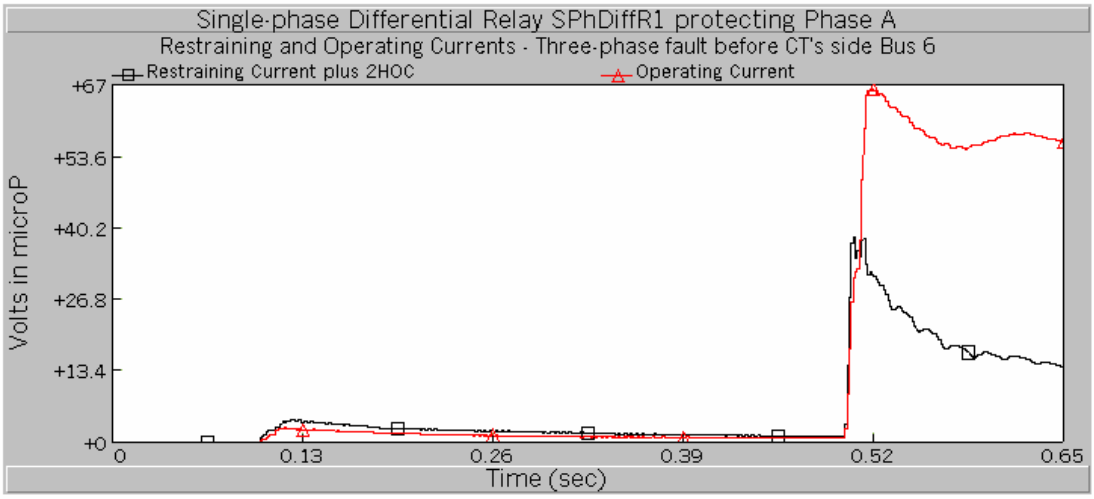


**Figure 5.90:** *SPhDiffR1* differential currents, three-phase internal fault, *Bus 6* side

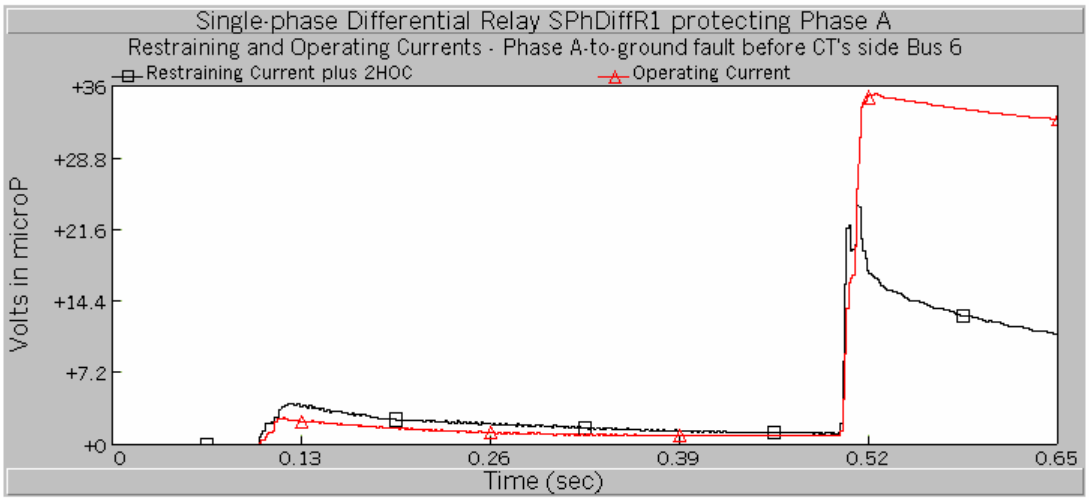


**Figure 5.91:** *SPhDiffR1* differential currents, phase A-to-ground internal fault, *Bus 6* side

The response of the differential currents of *SPhDiffR1* for a three-phase internal fault in front of the CT's of the side of *Bus 9* is shown in Figure 5.92. The response of the differential currents of *SPhDiffR1* for a phase A-to-ground internal fault in front the

CT's of the side of *Bus 9* is shown in Figure 5.93. The differential relay *SPhDiffR1* showed correct operation for the simulated faults. The responses of *SPhDiffR1* to the internal faults of side of *Bus 9* showed a shorter delay in the identification of the fault conditions, which improved the differential relay performance.

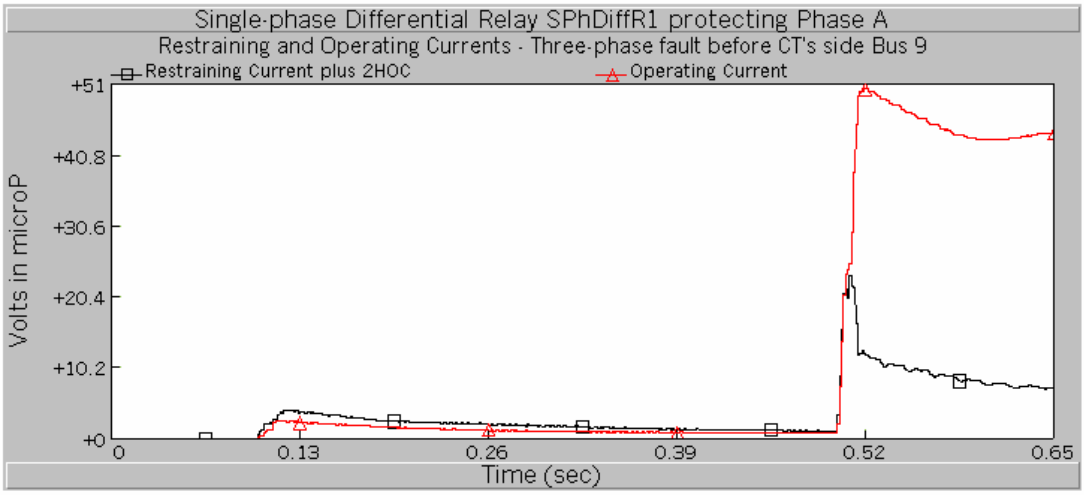


**Figure 5.92:** *SPhDiffR1* differential currents, three-phase internal fault, *Bus 9* side

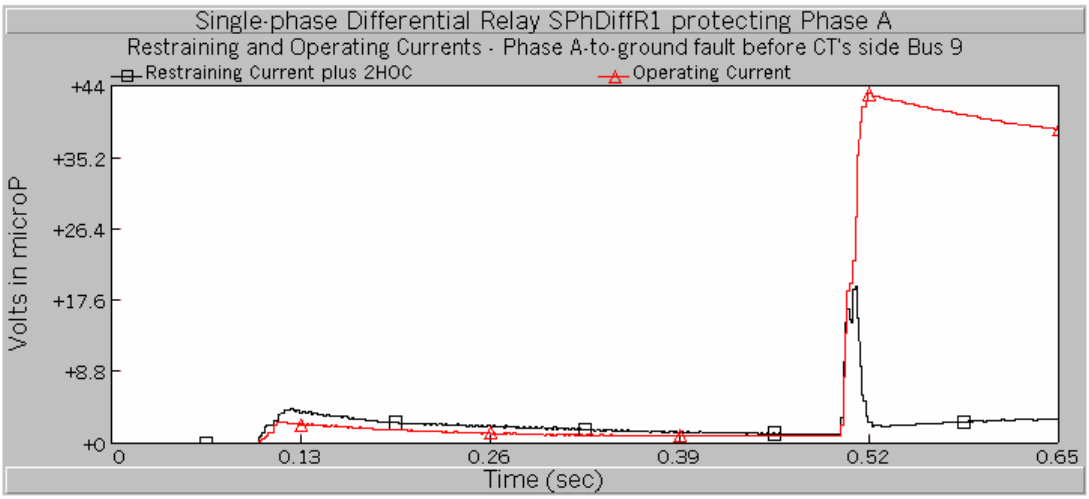


**Figure 5.93:** *SPhDiffR1* differential currents, phase A-to-ground internal fault, *Bus 9* side

### 5.7.4 Performance of the differential protection of a power transformer under external faults

The purpose of this study was to investigate the response of differential relays to external faults to the protected transformer. The differential relay *SPhDiffR1* adjusted in previous sections was used in this study. The study was divided in simulation of external faults (at the back of the CT's) in the side of *Bus 6*, and simulation of external faults in the side of *Bus 9*.

The response of the differential currents of *SPhDiffR1* for a three-phase external fault, located directly over *Bus 6* is shown in Figure 5.94. The response of the differential currents of *SPhDiffR1* for a phase A-to-ground external fault located directly over *Bus 6* is shown in Figure 5.95. The differential relay *SPhDiffR1* showed correct operation for the simulated faults.

The restraining current in both faults remained above the value of the operating current during all the simulation time, which meant that the differential relay identified correctly the event as an external fault. The response of the differential currents of *SPhDiffR1* for a three-phase external fault located directly over *Bus 9* is shown in Figure 5.96. The response of the differential currents of *SPhDiffR1* for a phase A-to-ground external located at *Bus 9* is shown in Figure 5.97. The differential relay *SPhDiffR1* showed correct operation for the simulated faults, identifying both events as external faults.

### 5.7.5 Performance of the differential protection of a power transformer during CT saturation

The purpose of this study was to observe the behavior of the numerical differential relay model under CT saturation. The CT of the numerical differential relay model *SPhDiffR1* were used to simulate its saturation, and to observe the effect that this event had in the performance of *SPhDiffR1*.

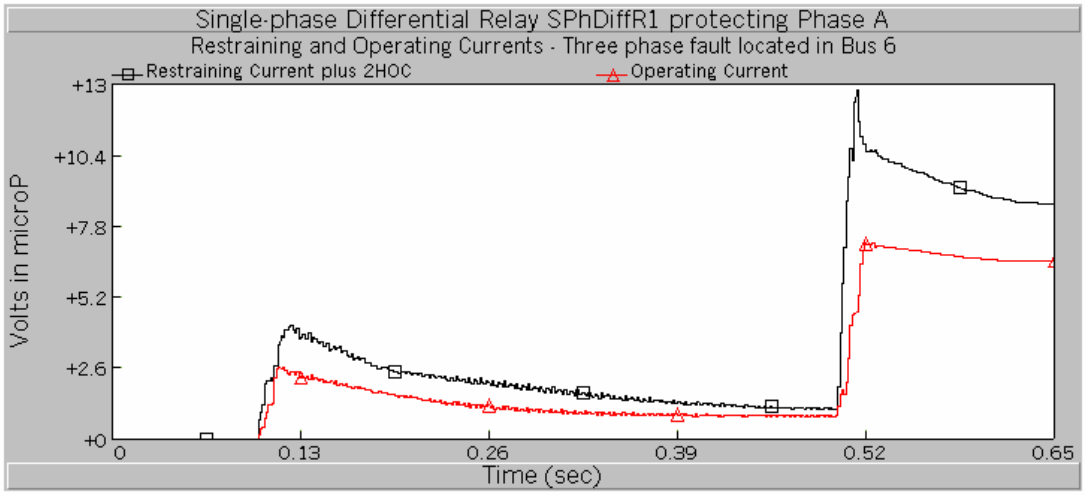


**Figure 5.94:** *SPhDiffR1* differential currents, three-phase external fault, on *Bus 6*

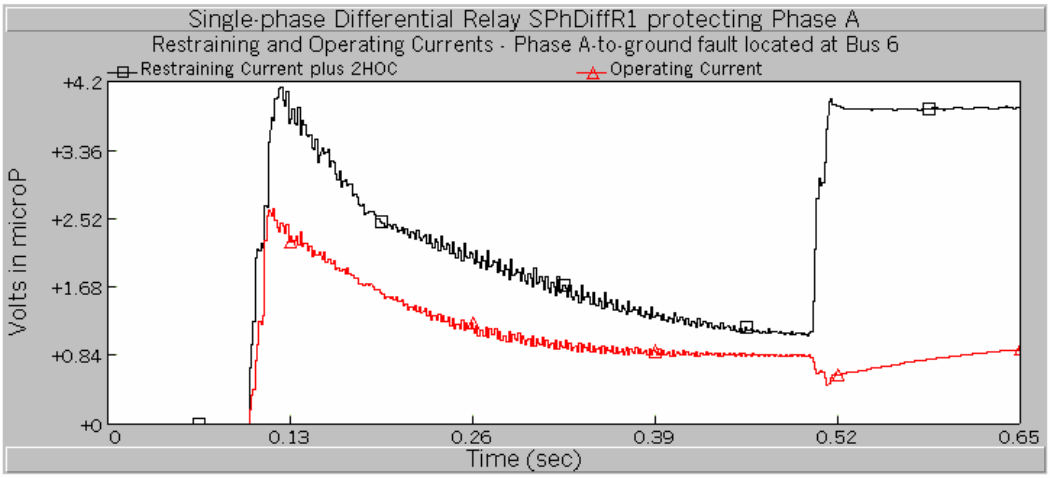


**Figure 5.95:** *SPhDiffR1* differential currents, phase A-to-ground external fault *Bus 6*

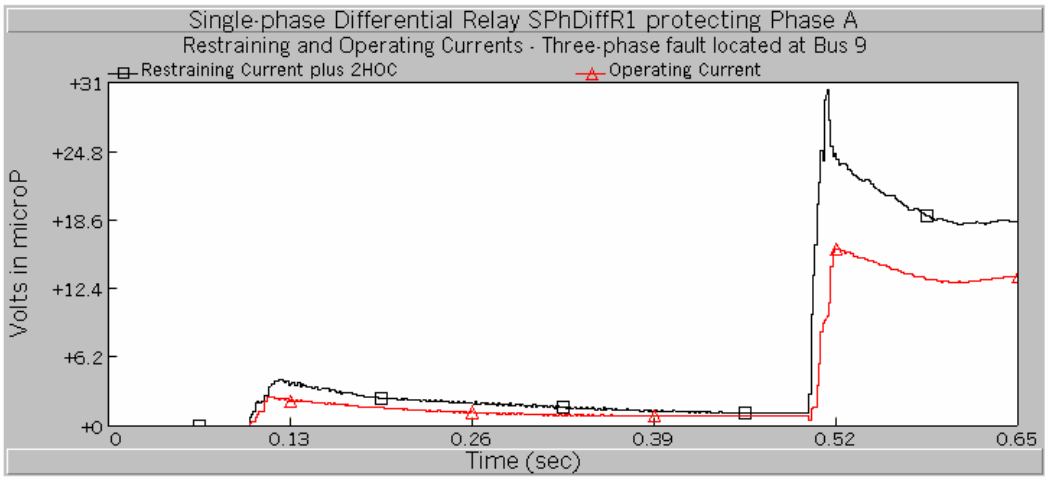


**Figure 5.96:** *SPhDiffR1* differential currents, three-phase external fault, on *Bus 9*

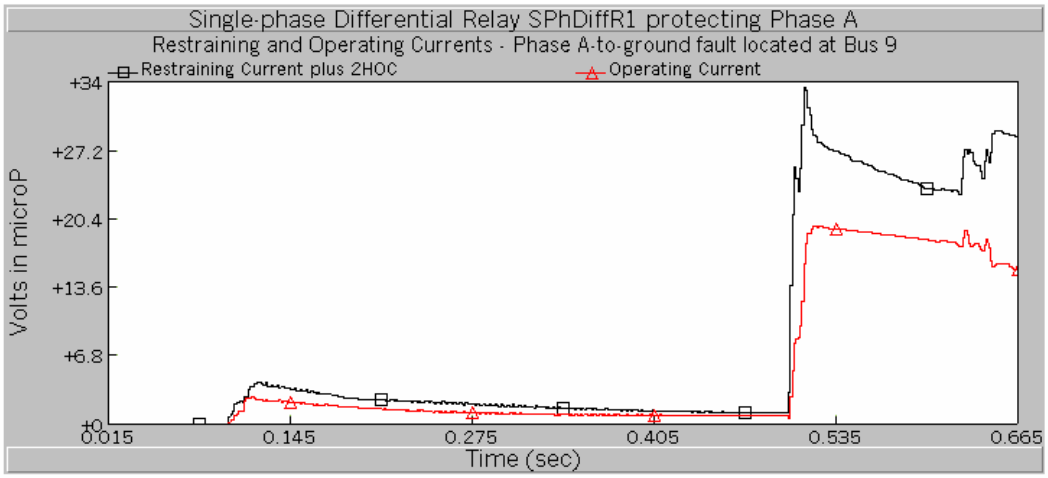


**Figure 5.97:** *SPhDiffR1* differential currents, phase A-to-ground external fault *Bus 9*

An analysis of the CT's was done to determine their saturation characteristics. In Figure 5.4 are shown the CT's *I6* and *I9* of *SPhDiffR1* with transforming ratios 1750 A/5 A and 1200 A/5 A, respectively. The knee points of the excitation curves of these CT's are 350 and 240 volts in the secondary side, respectively [52]. The CT's will saturate when the secondary circuits voltages of the CT's are larger than 350 and 240 V, respectively.

A method to increase the secondary circuit voltages is incrementing the burden. The maximum fault currents in the primary circuit of the CT's *I6* and *I9* were 100 kA and 26 kA, respectively. The maximum fault currents in the secondary terminals of the CT's *I6* and *I9* are determined by the following expressions, respectively [50].

$$I_s = \frac{I_p}{CTR} = \frac{100000\ A}{350} = 285.7\ A, \tag{5.7}$$

$$I_s = \frac{I_p}{CTR} = \frac{26000\ A}{240} = 108.3\ A, \tag{5.8}$$

According to Equation 5.2, the maximum allowed impedance burden that can be connected to the secondary terminals of the CT's *I6* and *I9* without saturating their cores were established by the following expressions, respectively.

$$Z_B = \frac{E_s}{I_s} = \frac{350\ V}{285.7\ A} = 1.22\ \Omega, \tag{5.9}$$

$$Z_B = \frac{E_s}{I_s} = \frac{240\ V}{108.3\ A} = 2.21\ \Omega, \tag{5.10}$$

To saturate the CT's *I6* and *I9* it is necessary to provide their secondary terminals with burden impedances larger than 1.22 and 2.21 Ω, respectively. The burden impedance chosen to saturate the CT's *I6* and *I9* was 10 Ω.

In Figure 5.98 is shown secondary current of phase A of the CT's *I6* and *I9*, respectively, for a three-phase fault as in Figure 5.4, for the cases of non-saturated CT's burden impedances of 0.7 Ω and saturated CT's burden impedances of 10 Ω.

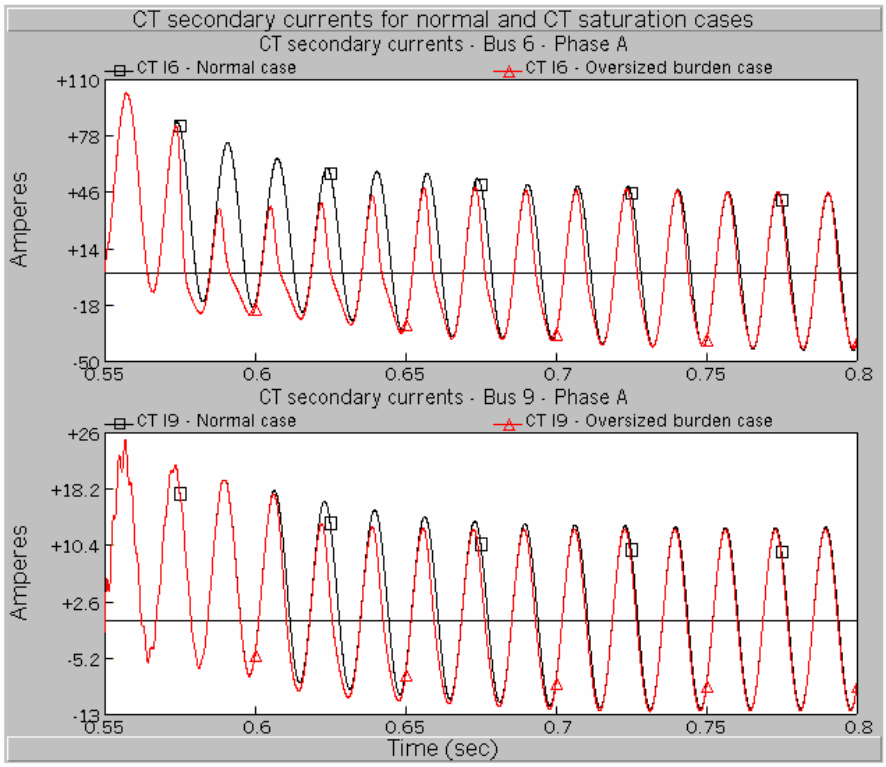


**Figure 5.98:** Secondary current of phase A of the *I6* and *I9* CT's of phase B of *SPhDiffR1*, three phase-to-ground fault

The response of the differential currents of *SPhDiffR1* for the non-saturated CT's case is shown in Figure 5.99(a). The response of the differential currents of *SPhDiffR1* for the saturated CT's case is shown in Figure 5.99(b). Comparing Figure 5.99(a) and 5.99(b) it was observed the degree of corruption that the differential currents suffered due to the saturation of the CT's. This corruption in the differential currents made difficult to the differential relay *SPhDiffR1* to identify clearly the fault event. The fact that the differential relay *SPhDiffR1* employed second harmonic blocking worsened the identification of the event as a fault.

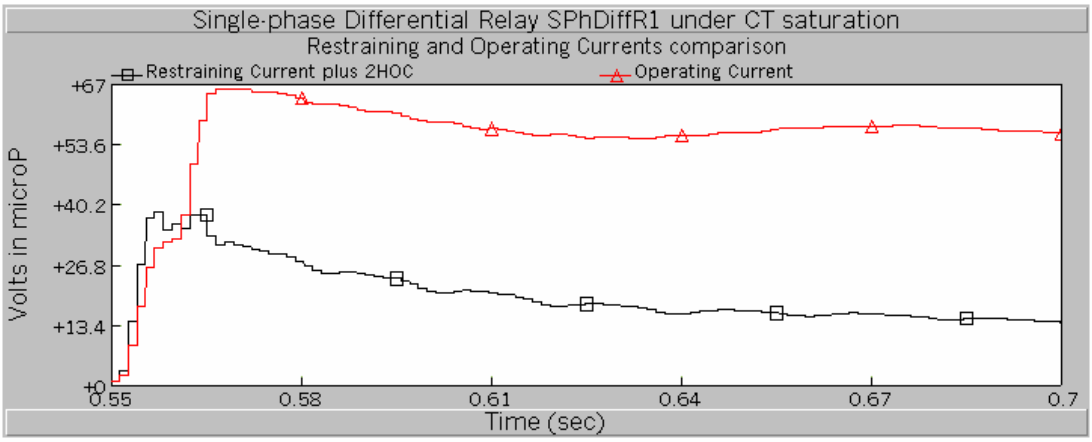


**(a)** Zooming of the differential currents after fault inception, non-saturated CT's case

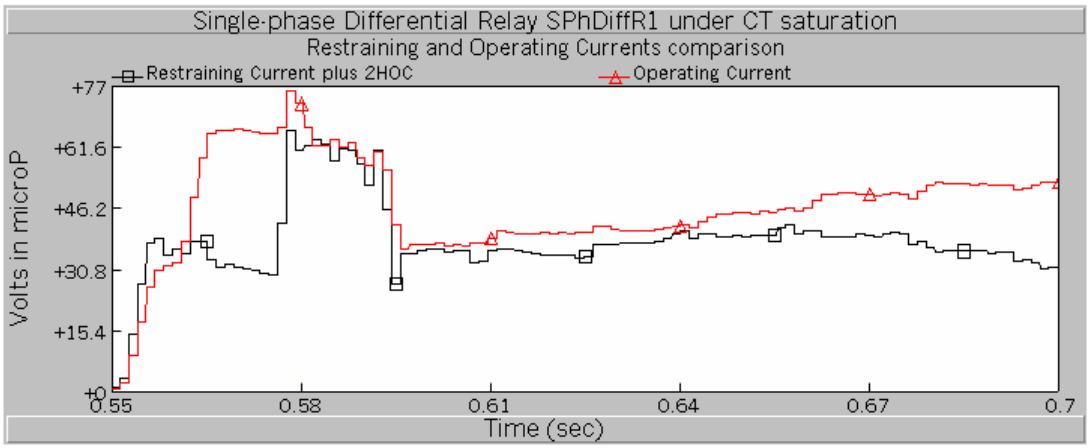


**(b)** Zooming of the differential currents after fault inception, saturated CT's case

**Figure 5.99:** *SPhDiffR1* differential currents response, three-phase fault, located as shown in Figure 5.4, non-saturated and saturated CT's cases

### 5.7.6 Performance of the differential protection of a power transformer when anti-aliasing filter removed

The purpose of this study was to investigate the effect that the absence of the anti-aliasing filter has over the response of the numerical differential relay model. To illustrate this study, the numerical differential relay model *SPhDiffR1* was employed.

The differential current response of *SPhDiffR1* on normal operation when the anti-aliasing filter was removed is illustrated in Figure 5.100. In Figure 5.100(b) is shown a zooming of Figure 5.100(a), to better appreciate the response of the differential currents during the effect of the inrush current.

The response of the differential currents of *SPhDiffR1* after the fault when the anti-aliasing filter was removed is depicted in Figure 5.101. In Figure 5.101(b) is shown a a better perspective of the transitory part of the fault.

The differential currents responses in Figures 5.100 and 5.101 showed that the differential relay *SPhDiffR1* had a better performance when the anti-aliasing filter was removed. The difference between the operating and restraining current during the effect of inrush current was larger than the case when the anti-aliasing filter was present, as shown in Figure 5.89(b). It was also observed that the operating current reached values above the restraining current faster during the transitory part of the fault when the anti-aliasing filter was removed, compared with the case when the anti-aliasing filter was employed, shown in Figure 5.89(c). It seems that the presence of harmonic in the operating current improved the differential relay performance.

## 5.8 Summary

The present chapter has developed a series of protection system studies designed with the proposed protection system model designing methodology. Studies related to the

protection of transmission lines with distance relay have been developed. These studies include the setting and adjustment of distance relays, local and remote protection of transmission lines, distance protection performance for fault behind the relay location, distance protection performance under CT saturation and distance protection performance when the anti-aliasing filter has been removed. The response of the distance relay models to these studies has been satisfactory.

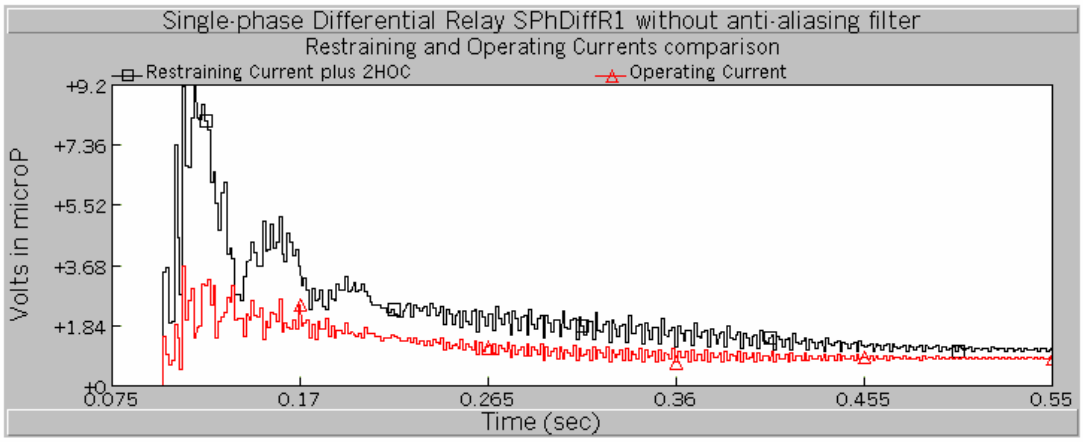


**(a)** Differential currents during normal operation

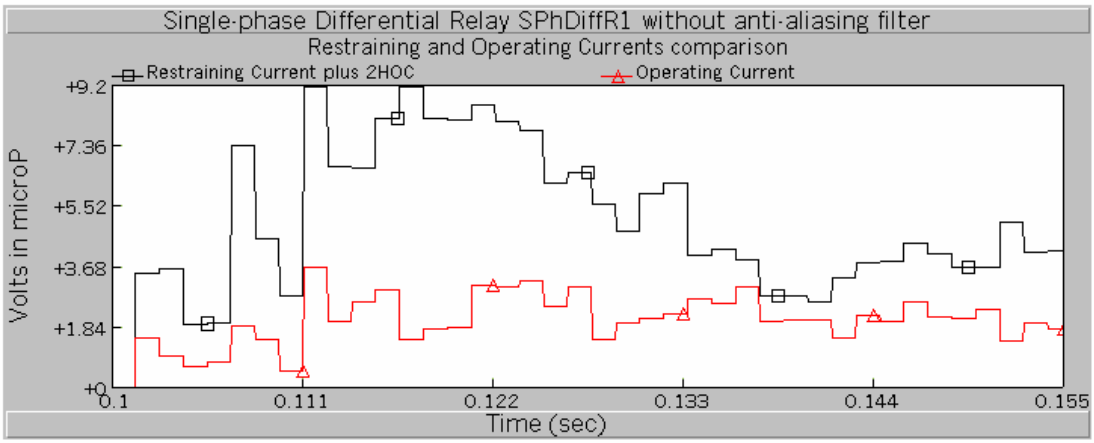


**(b)** Zooming of the differential currents during the effect of the inrush current

**Figure 5.100:** *SPhDiffR1* differential currents response, normal operation, no anti-aliasing filter

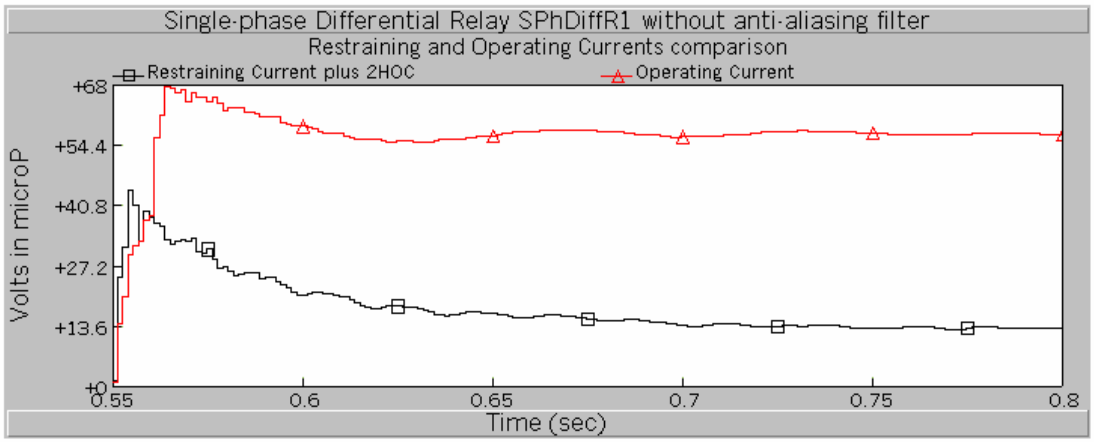


**(a)** Differential currents after the fault inception

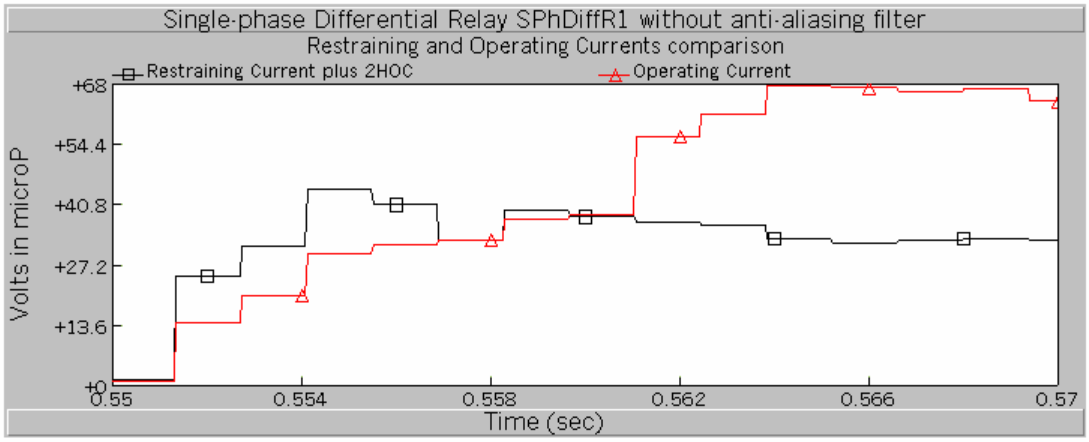


**(b)** Zooming of differential currents in the transitory part of the fault

**Figure 5.101:** *SPhDiffR1* differential currents response, fault inception, three-phase fault, located as shown in Figure 5.4, no anti-aliasing filter

Studies related to the protection of power transformers with differential relays have also been developed. These studies include setting and adjustment of numerical differential relays protecting a power transformer, differential protection adjustment against the effects of inrush current, performance of the differential protection for power transformer internal and external faults, performance of the differential protection under current transformer saturation and differential protection performance when anti-aliasing filter has been removed. The response of the differential protection system has been satisfactory in the developed studies.

# 6. CONSISTENCY OF NUMERICAL RELAY MODELS

## 6.1 Introduction

In chapter 5 the protection studies designed with the proposed protection system model designing methodology have been developed. In the present chapter a number of consistency tests are developed. These consistency tests investigate other aspects of the response of the numerical relay models designed with the proposed protection system model designing methodology that are not directly related with their response to a fault event. The results of these consistency tests are known in advance. The responses of the numerical relay models are compared to the results known. The similarity of the known result and the response of the numerical relay models is a measure of the validity and consistency of the numerical relay models with their real counterpart.

The developed consistency tests are described in this chapter. The consistency test of the distance relay characteristics is developed. The results are shown and conclusions are drawn. Decimation applied to the consistency of numerical relay models is described. The outcomes of this test are presented and conclusions are established.

## 6.2 List of developed consistency tests

The consistency tests developed in the present chapter are the following.

- Consistency test of the distance relay characteristics
    - Impedance characteristic, phase and ground distance relays
    - Offset-impedance characteristic, phase and ground distance relays
    - Mho characteristic, phase and ground distance relays
    - Reactance characteristic, phase and ground distance relays
- Decimation applied to the consistency of numerical relay models
    - Distance relay models
    - Differential relay models

## 6.3 Consistency test of the distance relay characteristics

The purpose of this test was to observe the accuracy of the relay model to identify different system operation points as apparent impedances along its characteristic curve.

To develop this consistency test, a special circuit was designed in PSCAD/EMTDC. The circuit designed for the consistency test of distance relay characteristics is shown in Figure 6.1. This circuit consists on a generator feeding a balanced three-phase load, and a numerical distance relay acquiring the voltage and current signals in front of the load.

The distance relay model characteristics were set to protect an impedance of 10 ohms at 75 degrees. For every characteristic under test a set of points of the characteristic was picked. For circular characteristics, these points were equal-spaced over the circumference. Every point of the characteristic curve represented a resistance and reactance in the impedance plane. The three-phase load impedance of the consistency circuit was set at these resistance and reactance values. Simulations were run and the relay model response was obtained and analyzed. In the test, some points of the characteristic curves had negative resistances, therefore the values of resistance of the three-phase load were set negative, which is unrealistic, but it was necessary for the purposes of the consistency test.

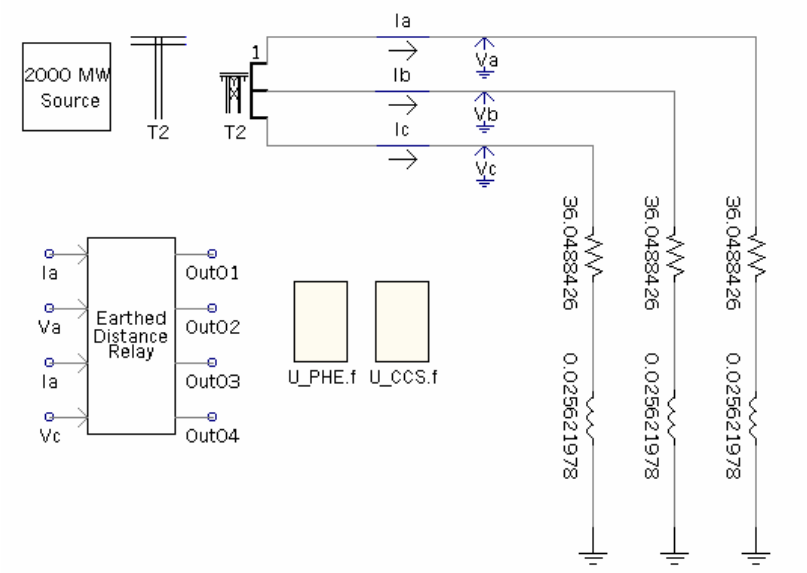


**Figure 6.1:** Consistency test circuit of the characteristics of distance relay models

### 6.3.1 Impedance characteristic consistency test

In Figure 6.2 is shown the impedance characteristic of a distance relay with an impedance reach of 10 ohms and 75 degrees. Twelve equally separated points were chosen of the characteristic curve. The data used for the consistency test of the impedance characteristic curve of a phase distance relay model and the outcomes of the test are shown in Table 6.1. The data used for the consistency test of the impedance characteristic curve of a ground distance relay model and the results of the test are shown in Table 6.2.

### 6.3.2 Offset-impedance characteristic consistency test

In Figure 6.3 is shown the offset-impedance characteristic of a distance relay with an impedance reach of 10 ohms and 75 degrees. Twelve equally separated points were chosen of the characteristic curve.

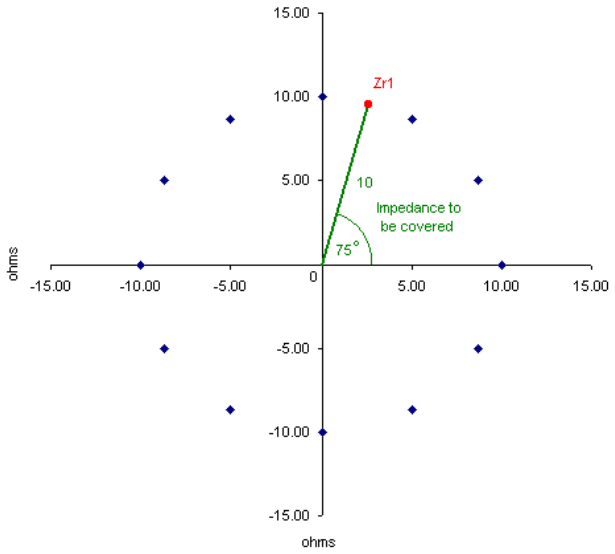


**Figure 6.2:** Points for consistency test of an impedance characteristic curve

| Resistance | Reactance | Expected magnitude | Estimated magnitude | Error in magnitude (%) | Expected phase | Estimated phase | Error in phase (%) |
|---|---|---|---|---|---|---|---|
| 10.0000 | 0.0000 | 10.0000 | 10.0031 | -0.0310 | 0.0000 | 0.0013 | N/A |
| 8.6603 | 5.0000 | 10.0000 | 10.0034 | -0.0340 | 30.0000 | 29.9969 | 0.0103 |
| 5.0000 | 8.6603 | 10.0000 | 10.0029 | -0.0290 | 60.0000 | 60.0042 | -0.0070 |
| 0.0000 | 10.0000 | 10.0000 | 10.0037 | -0.0370 | 90.0000 | 90.0040 | -0.0044 |
| -5.0000 | 8.6603 | 10.0000 | 10.0032 | -0.0320 | 120.0000 | 119.9980 | 0.0017 |
| -8.6603 | 5.0000 | 10.0000 | 10.0033 | -0.0330 | 150.0000 | 149.9990 | 0.0007 |
| -10.0000 | 0.0000 | 10.0000 | 10.0033 | -0.0330 | 180.0000 | 179.9970 | 0.0017 |
| -8.6603 | -5.0000 | 10.0000 | 10.0030 | -0.0300 | -150.0000 | -150.0010 | -0.0007 |
| -5.0000 | -8.6603 | 10.0000 | 10.0028 | -0.0280 | -120.0000 | -120.0010 | -0.0008 |
| 0.0000 | -10.0000 | 10.0000 | 10.0030 | -0.0300 | -90.0000 | -89.9989 | 0.0012 |
| 5.0000 | -8.6603 | 10.0000 | 10.0027 | -0.0270 | -60.0000 | -59.9971 | 0.0048 |
| 8.6603 | -5.0000 | 10.0000 | 10.0035 | -0.0350 | -30.0000 | -30.0002 | -0.0007 |

**Table 6.1:** Consistency test results, phase distance relay, impedance characteristic

| Resistance | Reactance | Expected magnitude | Estimated magnitude | Error in magnitude (%) | Expected angle | Estimated angle | Error in phase (%) |
|---|---|---|---|---|---|---|---|
| 10.0000 | 0.0000 | 10.0000 | 10.0031 | -0.0310 | 0.0000 | -0.0020 | N/A |
| 8.6603 | 5.0000 | 10.0000 | 10.0035 | -0.0350 | 30.0000 | 30.0026 | -0.0087 |
| 5.0000 | 8.6603 | 10.0000 | 10.0037 | -0.0370 | 60.0000 | 59.9981 | 0.0032 |
| 0.0000 | 10.0000 | 10.0000 | 10.0026 | -0.0260 | 90.0000 | 90.0037 | -0.0041 |
| -5.0000 | 8.6603 | 10.0000 | 10.0033 | -0.0330 | 120.0000 | 119.9902 | 0.0082 |
| -8.6603 | 5.0000 | 10.0000 | 10.0034 | -0.0340 | 150.0000 | 150.0039 | -0.0026 |
| -10.0000 | 0.0000 | 10.0000 | 10.0032 | -0.0320 | 180.0000 | 179.9997 | 0.0002 |
| -8.6603 | -5.0000 | 10.0000 | 10.0045 | -0.0450 | -150.0000 | -150.0021 | -0.0014 |
| -5.0000 | -8.6603 | 10.0000 | 10.0034 | -0.0340 | -120.0000 | -119.9990 | 0.0008 |
| 0.0000 | -10.0000 | 10.0000 | 10.0029 | -0.0290 | -90.0000 | -89.9994 | 0.0007 |
| 5.0000 | -8.6603 | 10.0000 | 10.0027 | -0.0270 | -60.0000 | -59.9977 | 0.0038 |
| 8.6603 | -5.0000 | 10.0000 | 10.0032 | -0.0320 | -30.0000 | -30.0022 | -0.0073 |

**Table 6.2:** Consistency test results, ground distance relay, impedance characteristic

The data used for the consistency test of the offset-impedance characteristic curve of a phase distance relay model and results of the test are shown in Table 6.3. The data used for the consistency test of the offset-impedance characteristic curve of a ground distance relay model and the results of the test are shown in Table 6.4.

### 6.3.3 Mho characteristic consistency test

In Figure 6.4 is shown the mho characteristic of a distance relay with a reach impedance of 10 ohms and 75 degrees. Twelve equally separated points were chosen of the characteristic curve.

The data used for the consistency test of the mho characteristic curve of a phase distance relay model and results of the test are shown in Table 6.5. The data used for the consistency test of the mho characteristic curve of a phase distance relay model and results of the test are shown in Table 6.6.

### 6.3.4 Reactance characteristic consistency test

In Figure 6.5 is shown the reactance characteristic of a distance relay with a reach impedance of 10 ohms and 75 degrees. The impedance points from the reactance characteristic curve were chosen in pairs equally distant from the reactance axis. Not all the chosen points of the reactance characteristic curve are included in Figure 6.5.

The data used for the consistency test of the reactance characteristic curve of a phase distance relay model and results of the test are shown in Table 6.7. The word *failed* in Table 6.7 means that the estimation of the quantity by the phase and magnitude comparators was erroneous. The data used for the consistency test of the reactance characteristic curve of a ground distance relay model and results of the test are shown in Table 6.8. The meaning of the word *failed* is the same as in Table 6.7.

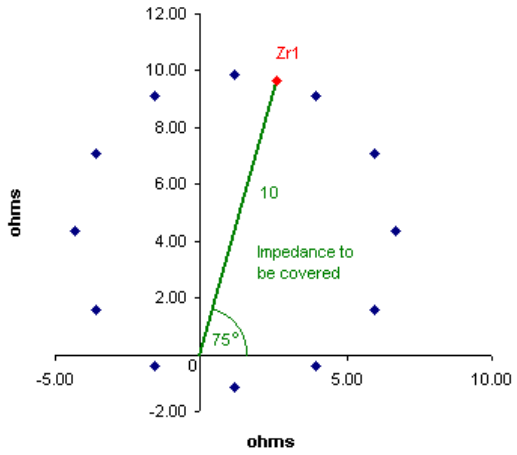


**Figure 6.3:** Points for consistency test of an offset-impedance characteristic curve

| Resistance | Reactance | Expected magnitude | Estimated magnitude | Error in magnitude (%) | Expected phase | Estimated phase | Error in phase (%) |
|---|---|---|---|---|---|---|---|
| 6.6647 | 4.3467 | 7.9569 | 7.9596 | -0.0347 | 33.1121 | 33.1092 | 0.0089 |
| 5.9278 | 7.0967 | 9.2467 | 9.2500 | -0.0358 | 50.1281 | 50.1267 | 0.0028 |
| 3.9147 | 9.1098 | 9.9153 | 9.9191 | -0.0379 | 66.7457 | 66.7458 | -0.0001 |
| 1.1647 | 9.8467 | 9.9153 | 9.9186 | -0.0331 | 83.2543 | 83.2544 | -0.0002 |
| -1.5853 | 9.1098 | 9.2467 | 9.2498 | -0.0329 | 99.8719 | 99.8711 | 0.0008 |
| -3.5985 | 7.0967 | 7.9569 | 7.9593 | -0.0304 | 116.8879 | 116.8861 | 0.0015 |
| -4.3353 | 4.3467 | 6.1391 | 6.1411 | -0.0329 | 134.9251 | 134.9260 | -0.0007 |
| -3.5985 | 1.5967 | 3.9368 | 3.9380 | -0.0306 | 156.0727 | 156.0700 | 0.0017 |
| -1.5853 | -0.4165 | 1.6391 | 1.6393 | -0.0136 | -165.2806 | -165.2850 | -0.0027 |
| 1.1647 | -1.1533 | 1.6391 | 1.6394 | -0.0185 | -44.7194 | -44.7201 | -0.0015 |
| 3.9147 | -0.4165 | 3.9368 | 3.9377 | -0.0239 | -6.0727 | -6.0723 | 0.0073 |
| 5.9278 | 1.5967 | 6.1391 | 6.1410 | -0.0309 | 15.0749 | 15.0742 | 0.0047 |

**Table 6.3:** Consistency test results, phase distance relay, offset impedance characteristic

| Resistance | Reactance | Expected magnitude | Estimated magnitude | Error in magnitude (%) | Expected angle | Estimated angle | Error in phase (%) |
|---|---|---|---|---|---|---|---|
| 6.6647 | 4.3467 | 7.9569 | 7.9594 | -0.0317 | 33.1121 | 33.1159 | -0.0114 |
| 5.9278 | 7.0967 | 9.2467 | 9.2504 | -0.0399 | 50.1281 | 50.1319 | -0.0076 |
| 3.9147 | 9.1098 | 9.9153 | 9.9185 | -0.0324 | 66.7457 | 66.7363 | 0.0141 |
| 1.1647 | 9.8467 | 9.9153 | 9.9188 | -0.0347 | 83.2543 | 83.2505 | 0.0045 |
| -1.5853 | 9.1098 | 9.2467 | 9.2501 | -0.0366 | 99.8719 | 99.8796 | -0.0077 |
| -3.5985 | 7.0967 | 7.9569 | 7.9595 | -0.0331 | 116.8879 | 116.8940 | -0.0053 |
| -4.3353 | 4.3467 | 6.1391 | 6.1413 | -0.0364 | 134.9251 | 134.9250 | 0.0001 |
| -3.5985 | 1.5967 | 3.9368 | 3.9380 | -0.0306 | 156.0727 | 156.0740 | -0.0008 |
| -1.5853 | -0.4165 | 1.6391 | 1.6395 | -0.0252 | -165.2806 | -165.2810 | -0.0002 |
| 1.1647 | -1.1533 | 1.6391 | 1.6396 | -0.0289 | -44.7194 | -44.7141 | 0.0119 |
| 3.9147 | -0.4165 | 3.9368 | 3.9379 | -0.0280 | -6.0727 | -6.0738 | -0.0174 |
| 5.9278 | 1.5967 | 6.1391 | 6.1410 | -0.0311 | 15.0749 | 15.0770 | -0.0138 |

**Table 6.4:** Consistency test results, ground distance relay, offset mho characteristic

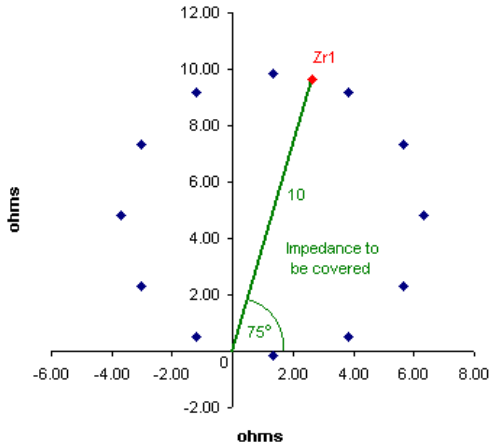


**Figure 6.4:** Points for consistency test of a mho characteristic curve

| Resistance | Reactance | Expected magnitude | Estimated magnitude | Error in magnitude (%) | Expected phase | Estimated phase | Error in phase (%) |
|---|---|---|---|---|---|---|---|
| 6.2941 | 4.8296 | 7.9335 | 7.9357 | -0.0268 | 37.5000 | 37.4975 | 0.0067 |
| 5.6242 | 7.3296 | 9.2388 | 9.2421 | -0.0362 | 52.5000 | 52.4979 | 0.0040 |
| 3.7941 | 9.1598 | 9.9144 | 9.9181 | -0.0368 | 67.5000 | 67.4977 | 0.0034 |
| 1.2941 | 9.8296 | 9.9144 | 9.9177 | -0.0328 | 82.5000 | 82.5064 | -0.0078 |
| -1.2059 | 9.1598 | 9.2388 | 9.2422 | -0.0363 | 97.5000 | 97.4991 | 0.0009 |
| -3.0360 | 7.3296 | 7.9335 | 7.9358 | -0.0291 | 112.5000 | 112.5030 | -0.0027 |
| -3.7059 | 4.8296 | 6.0876 | 6.0894 | -0.0300 | 127.5000 | 127.5020 | -0.0016 |
| -3.0360 | 2.3296 | 3.8268 | 3.8279 | -0.0289 | 142.5000 | 142.4990 | 0.0007 |
| -1.2059 | 0.4995 | 1.3053 | 1.3054 | -0.0090 | 157.5000 | 157.5010 | -0.0006 |
| 1.2941 | -0.1704 | 1.3053 | 1.3053 | -0.0060 | -7.5000 | -7.5020 | -0.0272 |
| 3.7941 | 0.4995 | 3.8268 | 3.8279 | -0.0278 | 7.5000 | 7.4991 | 0.0120 |
| 5.6242 | 2.3296 | 6.0876 | 6.0891 | -0.0237 | 22.5000 | 22.5005 | -0.0022 |

**Table 6.5:** Consistency test results, phase distance relay, mho characteristic

| Resistance | Reactance | Expected magnitude | Estimated magnitude | Error in magnitude (%) | Expected angle | Estimated angle | Error in phase (%) |
|---|---|---|---|---|---|---|---|
| 6.2941 | 4.8296 | 7.9335 | 7.9359 | -0.0300 | 37.5000 | 37.5029 | -0.0077 |
| 5.6242 | 7.3296 | 9.2388 | 9.2424 | -0.0388 | 52.5000 | 52.5013 | -0.0025 |
| 3.7941 | 9.1598 | 9.9144 | 9.9173 | -0.0291 | 67.5000 | 67.5016 | -0.0024 |
| 1.2941 | 9.8296 | 9.9144 | 9.9182 | -0.0373 | 82.5000 | 82.4989 | 0.0013 |
| -1.2059 | 9.1598 | 9.2388 | 9.2420 | -0.0351 | 97.5000 | 97.4971 | 0.0030 |
| -3.0360 | 7.3296 | 7.9335 | 7.9367 | -0.0404 | 112.5000 | 112.4990 | 0.0009 |
| -3.7059 | 4.8296 | 6.0876 | 6.0895 | -0.0305 | 127.5000 | 127.4970 | 0.0024 |
| -3.0360 | 2.3296 | 3.8268 | 3.8279 | -0.0284 | 142.5000 | 142.4970 | 0.0021 |
| -1.2059 | 0.4995 | 1.3053 | 1.3053 | -0.0060 | 157.5000 | 157.4980 | 0.0013 |
| 1.2941 | -0.1704 | 1.3053 | 1.3054 | -0.0113 | -7.5000 | -7.5033 | -0.0435 |
| 3.7941 | 0.4995 | 3.8268 | 3.8278 | -0.0242 | 7.5000 | 7.5002 | -0.0021 |
| 5.6242 | 2.3296 | 6.0876 | 6.0897 | -0.0338 | 22.5000 | 22.5006 | -0.0027 |

**Table 6.6:** Consistency test results, ground distance relay, mho characteristic

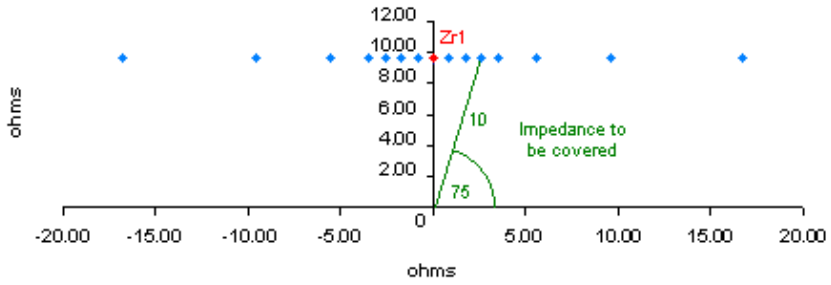


**Figure 6.5:** Points for consistency test of a reactance characteristic curve

| Resistance | Reactance | Expected magnitude | Estimated magnitude | Error in magnitude (%) | Expected phase | Estimated phase | Error in phase (%) |
|---|---|---|---|---|---|---|---|
| -36.0488 | 9.6593 | 37.3205 | failed | N/A | 165.0000 | failed | N/A |
| -16.7303 | 9.6593 | 19.3185 | failed | N/A | 150.0000 | failed | N/A |
| -9.6593 | 9.6593 | 13.6603 | 13.6646 | -0.0318 | 135.0000 | 135.0000 | 0.0000 |
| -5.5768 | 9.6593 | 11.1536 | 11.1575 | -0.0354 | 120.0000 | 119.9990 | 0.0008 |
| -3.5157 | 9.6593 | 10.2792 | 10.2827 | -0.0344 | 110.0000 | 110.0010 | -0.0009 |
| -2.5882 | 9.6593 | 10.0000 | 10.0038 | -0.0380 | 105.0000 | 104.9990 | 0.0010 |
| -1.7032 | 9.6593 | 9.8083 | 9.8121 | -0.0387 | 100.0000 | 100.0040 | -0.0040 |
| -0.8451 | 9.6593 | 9.6962 | 9.6999 | -0.0381 | 95.0000 | 95.0005 | -0.0005 |
| 0.0000 | 9.6593 | 9.6593 | 9.6631 | -0.0398 | 90.0000 | 89.9991 | 0.0010 |
| 0.8451 | 9.6593 | 9.6962 | 9.6996 | -0.0353 | 85.0000 | 84.9998 | 0.0002 |
| 1.7032 | 9.6593 | 9.8083 | 9.8118 | -0.0360 | 80.0000 | 79.9987 | 0.0016 |
| 2.5882 | 9.6593 | 10.0000 | 10.0036 | -0.0360 | 75.0000 | 75.0024 | -0.0032 |
| 3.5157 | 9.6593 | 10.2792 | 10.2831 | -0.0383 | 70.0000 | 70.0081 | -0.0116 |
| 5.5768 | 9.6593 | 11.1536 | 11.1574 | -0.0345 | 60.0000 | 59.9971 | 0.0048 |
| 9.6593 | 9.6593 | 13.6603 | 13.6651 | -0.0355 | 45.0000 | 45.0002 | -0.0004 |
| 16.7303 | 9.6593 | 19.3185 | 19.3257 | -0.0372 | 30.0000 | 30.0003 | -0.0010 |
| 36.0488 | 9.6593 | 37.3205 | 37.3349 | -0.0386 | 15.0000 | 14.9993 | 0.0047 |

**Table 6.7:** Consistency test results, phase distance relay, reactance characteristic

### 6.3.5 Conclusion of the consistency test of the distance relay characteristics

In Tables 6.1 to 6.8 the estimated magnitude and angle of the impedance seen by the phase and ground distance relay models presented a maximum error value of 0.0435% between the expected value and the estimation of the relay model. Based on this, it is possible to affirm that the numerical phase and ground distance relay models showed consistency in the proper estimation of system impedances.

| Resistance | Reactance | Expected magnitude | Estimated magnitude | Error in magnitude (%) | Expected angle | Estimated angle | Error in phase (%) |
|---|---|---|---|---|---|---|---|
| -36.0488 | 9.6593 | 37.3205 | failed | N/A | 165.0000 | failed | N/A |
| -16.7303 | 9.6593 | 19.3185 | failed | N/A | 150.0000 | failed | N/A |
| -9.6593 | 9.6593 | 13.6603 | 13.6653 | -0.0369 | 135.0000 | 134.9970 | 0.0022 |
| -5.5768 | 9.6593 | 11.1536 | 11.1576 | -0.0363 | 120.0000 | 119.9980 | 0.0017 |
| -3.5157 | 9.6593 | 10.2792 | 10.2833 | -0.0402 | 110.0000 | 110.0000 | 0.0000 |
| -2.5882 | 9.6593 | 10.0000 | 10.0033 | -0.0330 | 105.0000 | 105.0010 | -0.0010 |
| -1.7032 | 9.6593 | 9.8083 | 9.8121 | -0.0389 | 100.0000 | 99.9981 | 0.0019 |
| -0.8451 | 9.6593 | 9.6962 | 9.6993 | -0.0325 | 95.0000 | 94.9973 | 0.0028 |
| 0.0000 | 9.6593 | 9.6593 | 9.6621 | -0.0291 | 90.0000 | 90.0024 | -0.0027 |
| 0.8451 | 9.6593 | 9.6962 | 9.6992 | -0.0313 | 85.0000 | 85.0036 | -0.0042 |
| 1.7032 | 9.6593 | 9.8083 | 9.8117 | -0.0351 | 80.0000 | 80.0000 | 0.0000 |
| 2.5882 | 9.6593 | 10.0000 | 10.0034 | -0.0340 | 75.0000 | 74.9967 | 0.0044 |
| 3.5157 | 9.6593 | 10.2792 | 10.2823 | -0.0305 | 70.0000 | 70.0012 | -0.0017 |
| 5.5768 | 9.6593 | 11.1536 | 11.1570 | -0.0309 | 60.0000 | 59.9983 | 0.0028 |
| 9.6593 | 9.6593 | 13.6603 | 13.6641 | -0.0282 | 45.0000 | 44.9996 | 0.0009 |
| 16.7303 | 9.6593 | 19.3185 | 19.3249 | -0.0330 | 30.0000 | 29.9984 | 0.0053 |
| 36.0488 | 9.6593 | 37.3205 | 37.3328 | -0.0329 | 15.0000 | 14.9996 | 0.0027 |

**Table 6.8:** Consistency test results, ground distance relay, reactance characteristic

## 6.4 Decimation applied to the consistency of relay models in a power system

Decimation was the second consistency test of the numerical relay models developed in the thesis. Decimation means to down-sample by an entire multiple the original sampling frequency on a numerical relay model. Current and voltage waveforms have a determined frequency response. Sampling the signals provokes that the frequency response of these waveforms is repeated periodically on periods of time determined by the sampling frequency. Down-sampling the original sampling frequency causes a decreasing of the period of the periodic response and aliasing at high frequencies may appear. The decimation consistency test to numerical relay models had the following process.

1. A numerical relay was designed with the proposed protection system modeling methodology. The designed relay model samples the voltage and current inputs at an original sampling frequency $f_0$.

2. The same numerical relay model was modified to sample signals to a down-sampled frequency $f_d$. The original sampling frequency $f_0$ was a multiple of the down-sampled frequency $f_d$, i.e., $f_0 = n\, f_d$, where $n$ is a positive integer.
3. To avoid aliasing provoked by the down-sampling, an additional low pass filter was designed to filter the relay input signals before entering the relay model.
4. The operational behavior of the relay model, as well as the shape of the signal inside the numerical relay model when sampling at $f_0$ and $f_d$, must be similar, but unmatched in time due to the additional filter delaying.

### 6.4.1 Developed decimation tests

Four decimation consistency tests of numerical relay models were developed. Two were decimation tests applied to numerical distance relay models, and two were decimation tests applied to numerical differential relay models.

#### 6.4.1.1 Decimation test 1 - Distance relay model

A phase-distance relay model was designed to protect the phases B and C of the transmission line *T5* from the test power system employed in chapter 5. The distance relay model sampled the input current and voltage signals at a rate of 1440 Hz. A phase-to-phase fault on phases B and C was simulated at 50% of the length of transmission line *T5*, at a time of 0.248 seconds. Another simulation was run employing the same relay, but in this case the relay sampled the input signals at a rate of 720 Hz. An additional $5^{th}$ order, 360 Hz cut-off frequency, Butterworth low-pass filter was designed to filter the current and voltage signals before entering the relay model of the latter simulation. In Figure 6.6 are shown the estimated angle of the signal $S_1$ of the distance relay model, 1440 and 720 Hz sampling frequency cases, respectively. In Figure 6.7 are shown the estimated angle of the signal $S_2$, 1440 and 720 Hz sampling frequency cases, respectively.

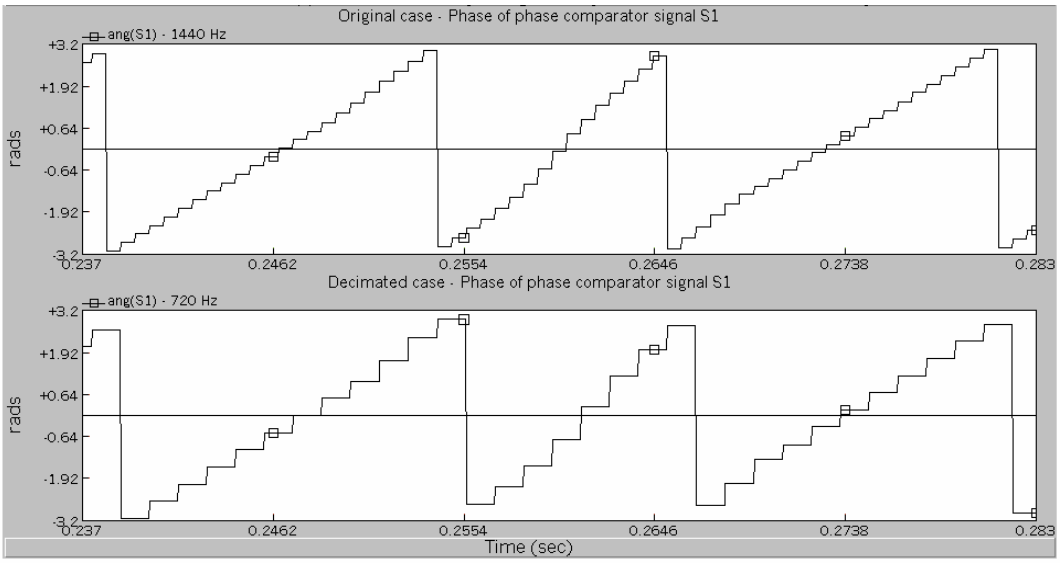


**Figure 6.6:** Estimated angle of signal $S_1$, 1440 Hz (original sampling frequency) and 720 Hz (down-sampled sampling frequency) cases, test 1

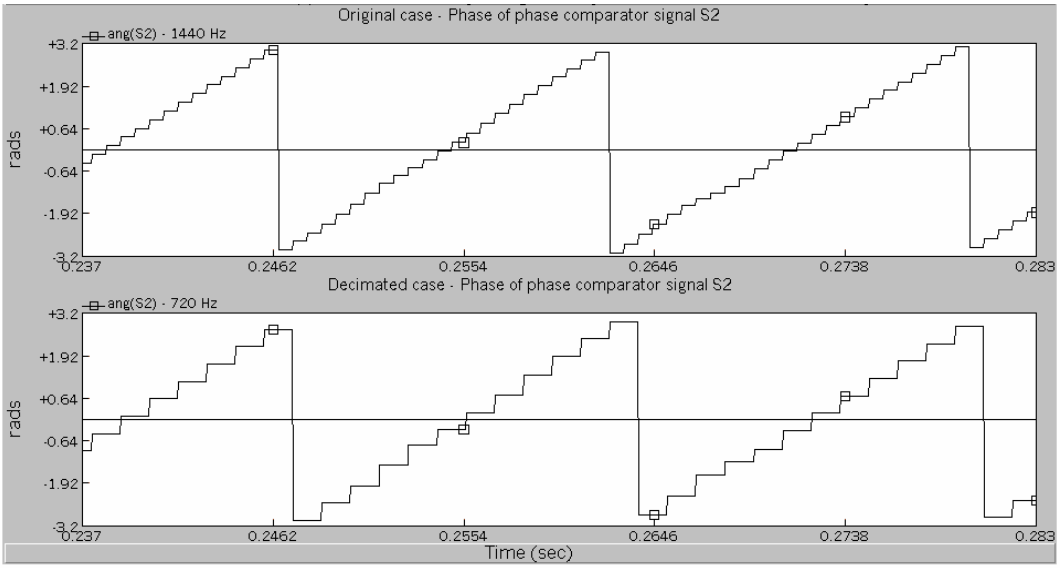


**Figure 6.7:** Estimated angle of signal $S_2$, 1440 Hz (original sampling frequency) and 720 Hz (down-sampled sampling frequency) cases, test 1

Distance relays identify fault conditions when the difference between the angles of $S_1$ and $S_2$ lies in the range of $-\pi/2$ and $\pi/2$. In Figure 6.8 are shown the angle differences of signals $S_1$ and $S_2$ of the original and down-sampled sampling frequency cases. In Figure 6.9 is shown the trigger signals of the numerical phase distance relay model of the

original and down-sampled sampling frequency cases. The original case issued a logic trip signal at 0.26245 seconds and the down-sampled case tripped at 0.26384 seconds. The delay observed was of 0.0014 seconds.

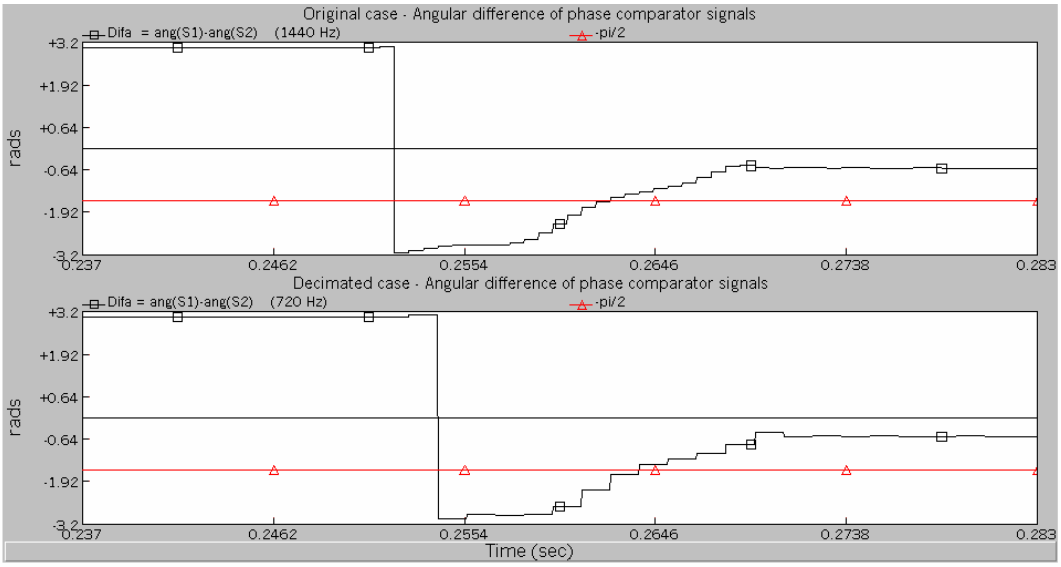


**Figure 6.8:** Angle difference of signals $S_1$ and $S_2$, 1440 Hz (original) and 720 Hz (down-sampled) cases, test 1

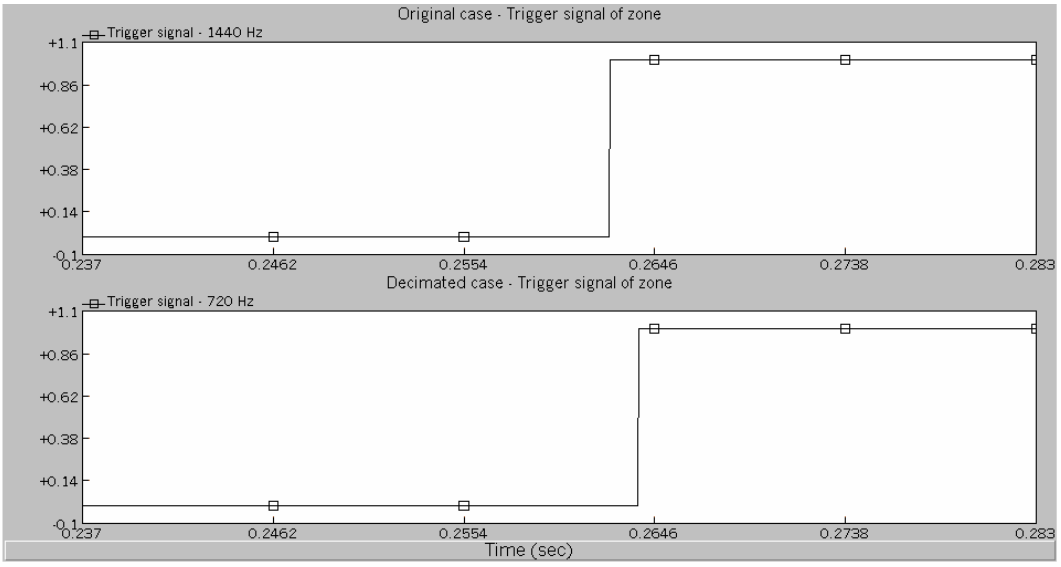


**Figure 6.9:** Trip signals of 1440 Hz (original sampling frequency) and 720 Hz (down-sampled sampling frequency) cases, test 1

### 6.4.1.2 Decimation test 2 - Distance relay model

The conditions of test 2 were the same than the employed for test 1, but the fault was located behind the distance relay, at 65% of the adjacent transmission line *T1*, divided in *T1i* and *T1h* for fault simulation, as shown in Figure 6.10.

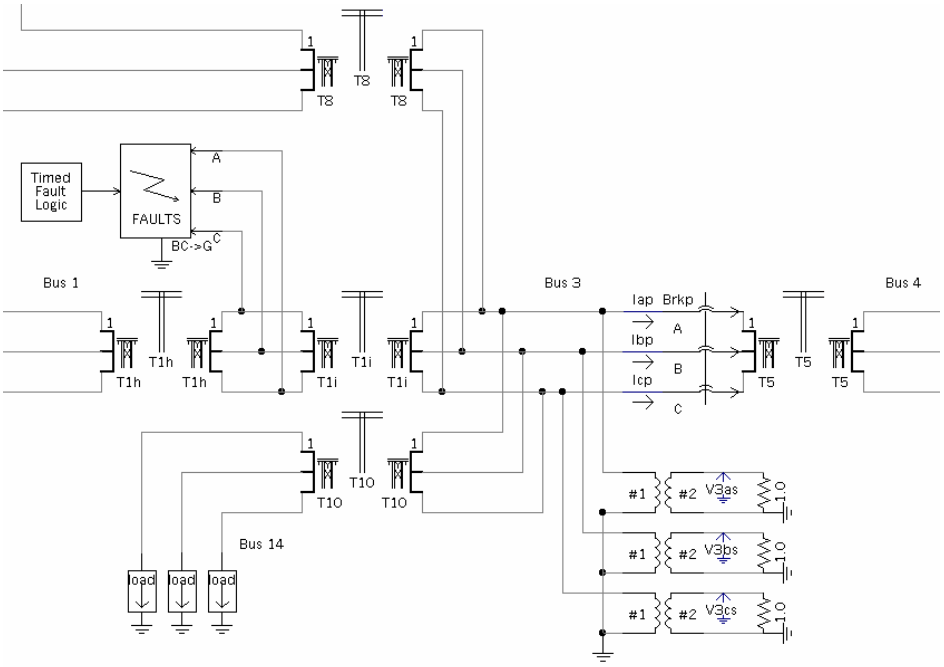


**Figure 6.10:** Location of the fault for decimation test 2

In Figure 6.11 are shown the estimated angle of the signal $S_1$ of the distance relay model, 1440 and 720 Hz sampling frequency cases for test 2, respectively. In Figure 6.12 are shown the estimated angle of the signal $S_2$, 1440 and 720 Hz sampling frequency cases for test 2, respectively.

In Figure 6.13 is shown the difference between $S_1$ and $S_2$, for the original and down-sampled sampling frequency cases of decimation consistency test 2. The angle difference between $S_1$ and $S_2$ did not fall in the range of $-\pi/2$ and $\pi/2$, in both the original and down-sampled sampling frequency cases, as shown in Figure 6.13. Therefore, the distance relay model did not produce a trip signal.

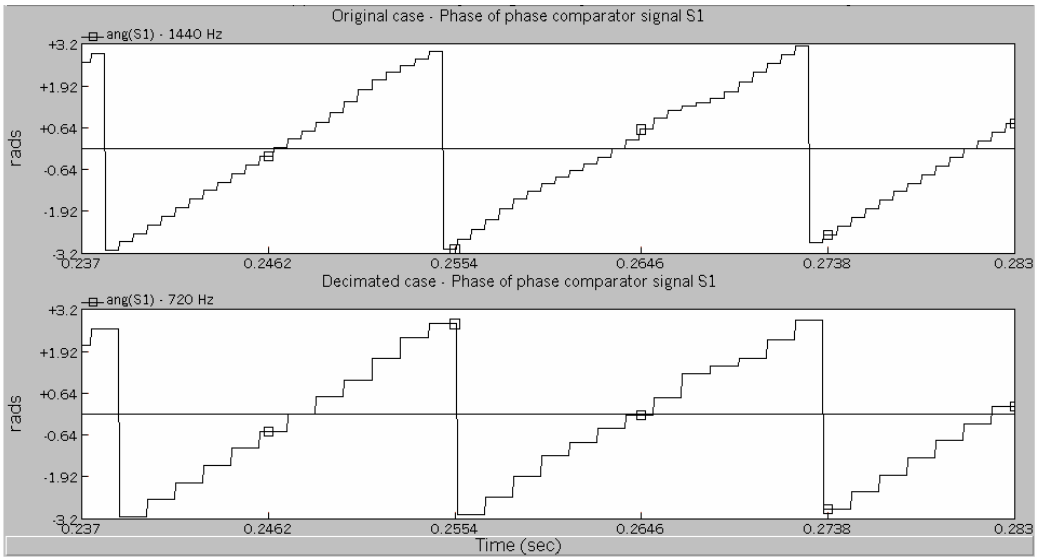


**Figure 6.11:** Estimated angle of signal $S_1$, 1440 Hz (original sampling frequency) and 720 Hz (down-sampled sampling frequency) cases, test 2

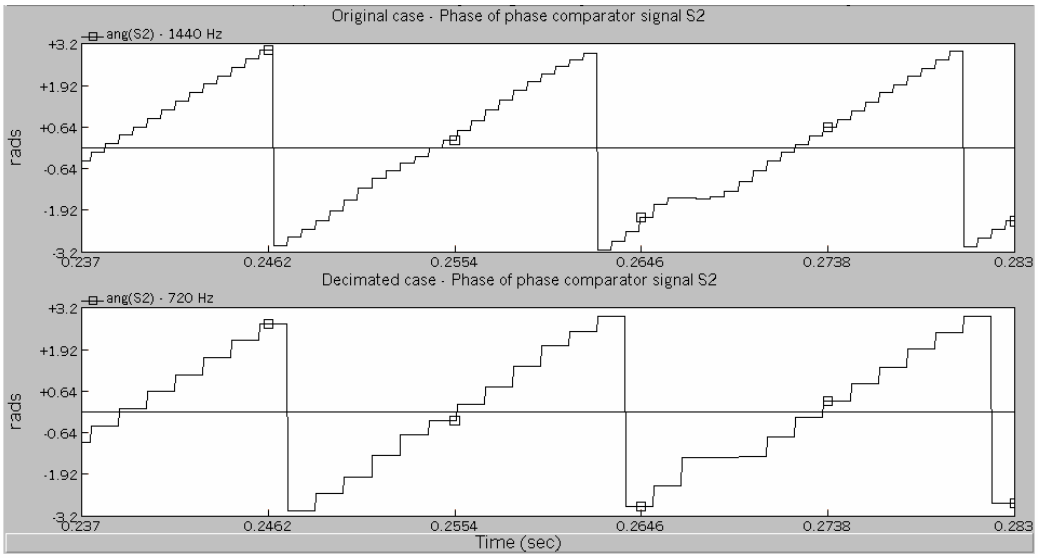


**Figure 6.12:** Estimated angle of signal $S_2$, 1440 Hz (original sampling frequency) and 720 Hz (down-sampled sampling frequency) cases, test 2

### 6.4.1.3 Decimation test 3 - Differential relay model

A single-phase differential relay model was designed to protect the phase A of power transformer *Tr7* of the test power system employed in chapter 5. The relay model

sampled originally the input current signals at a rate of 1440 Hz. A phase A-to-ground fault was simulated in the internal zone of the differential relay, marked by the current transformers *I6a* and *I9a* at a time of 0.35 seconds, as shown in Figure 6.14.

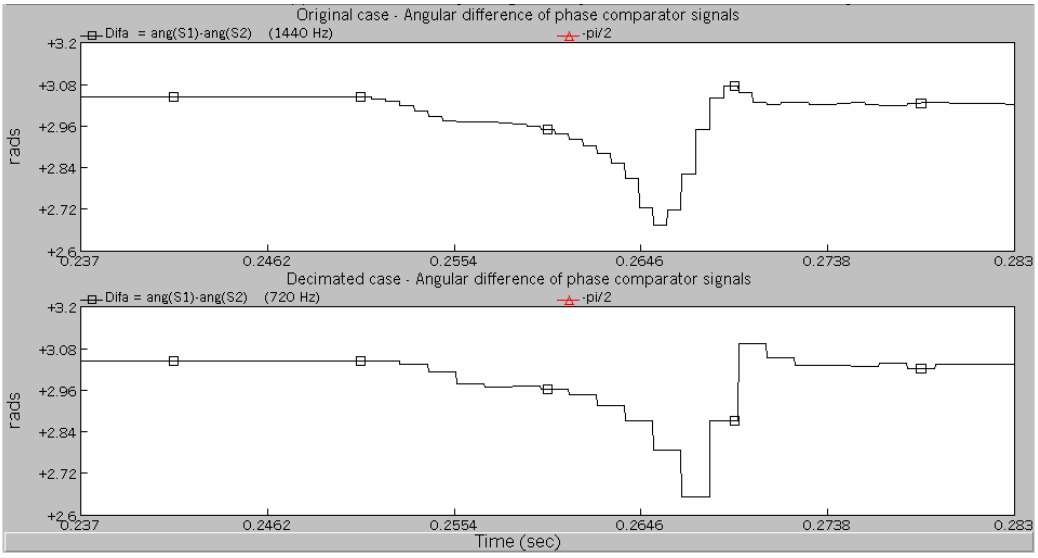


**Figure 6.13:** Angle difference of signals $S_1$ and $S_2$, 1440 Hz (original) and 720 Hz (down-sampled) cases, test 2

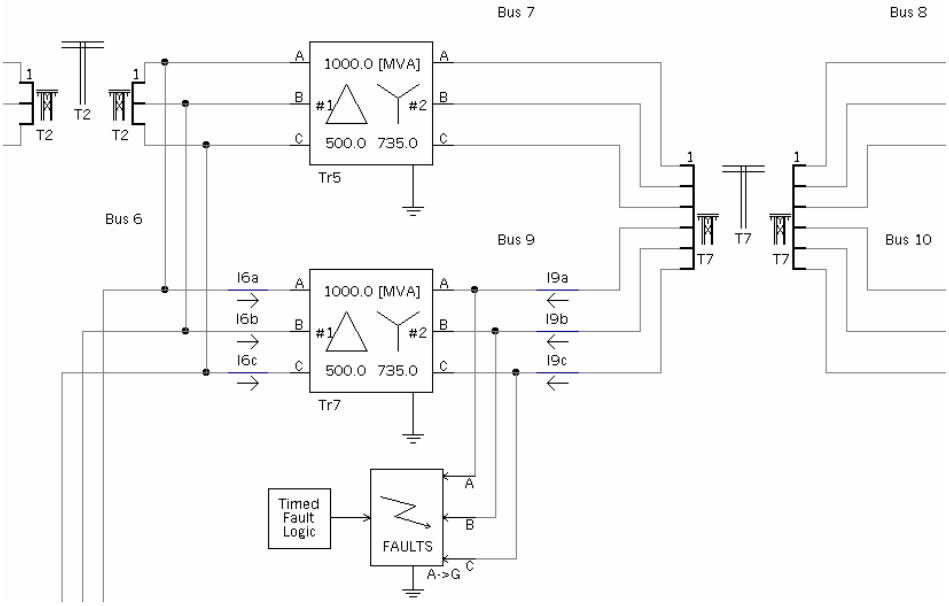


**Figure 6.14:** Phase A-to-ground fault inside the differential protecting zone of a power transformer *Tr7*, test 3

Another simulation was run under the same conditions, but in this case the relay model sampled the input signals at a rate of 720 Hz. An additional 5th order, 360 Hz cut-off frequency, Butterworth low-pass filter was used to filter the input current signals before entering the relay model.

The comparison between the estimated restraining signals employing the original sampling frequency of 1440 Hz and the down-sampled sampling frequency of 720 Hz is shown in Figure 6.15. The comparison of the respecting estimated operating currents is shown in Figure 6.16.

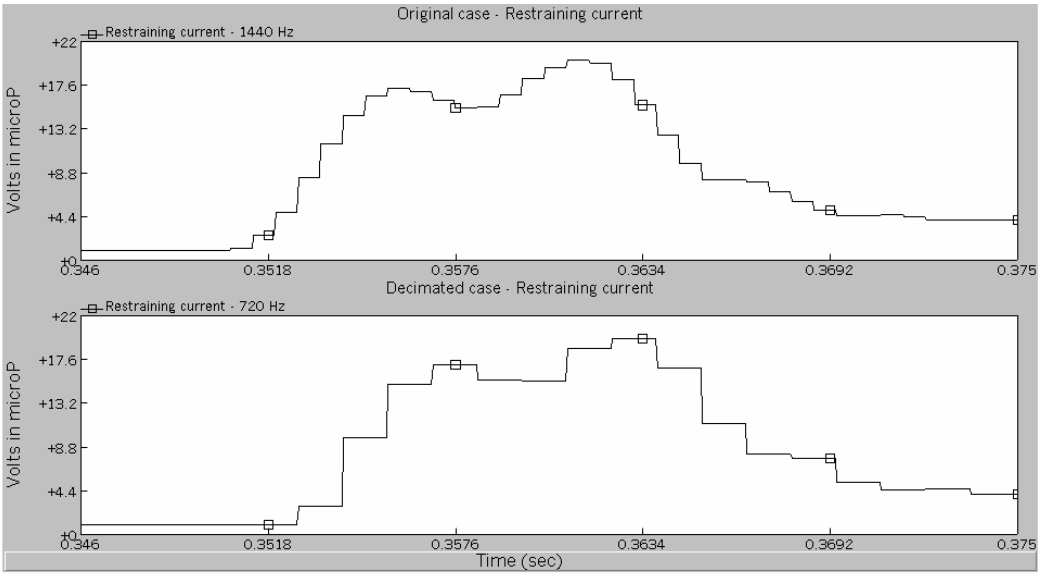


**Figure 6.15:** Estimated restraining currents, 1440 Hz (original sampling frequency) and 720 Hz (down-sampled sampling frequency) cases, test 3

In Figure 6.17 are shown the logic trip signals of test 3 of the original and down-sampled sampling frequencies. The trip signal for the original frequency case was issued at a time of 0.3521 seconds, while in the down-sampled case the trip was issued at a time of 0.3542 seconds. The delay observed was of 0.0021 seconds.

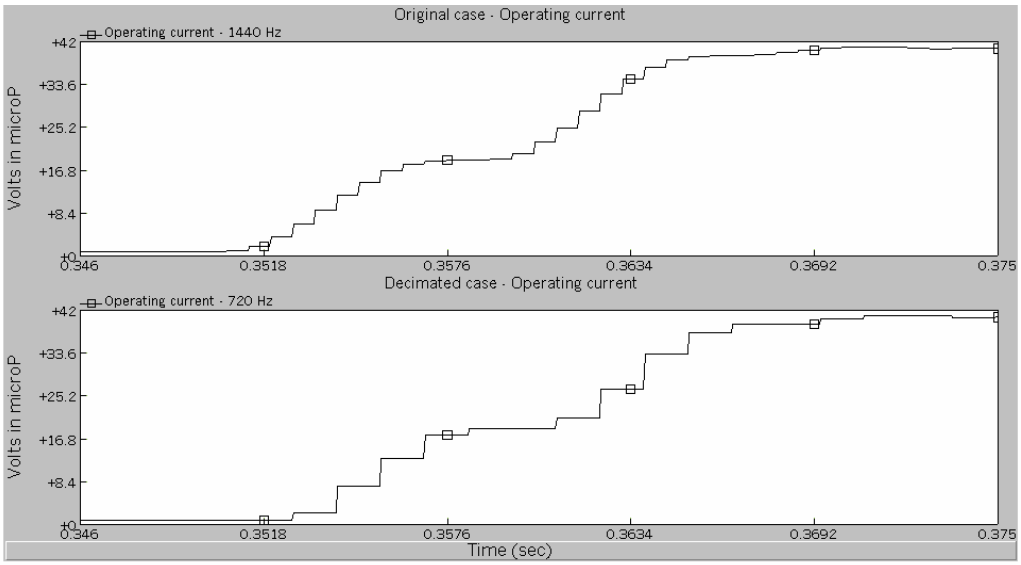


**Figure 6.16:** Estimated operating currents, 1440 Hz (original sampling frequency) and 720 Hz (down-sampled sampling frequency) cases, test 3

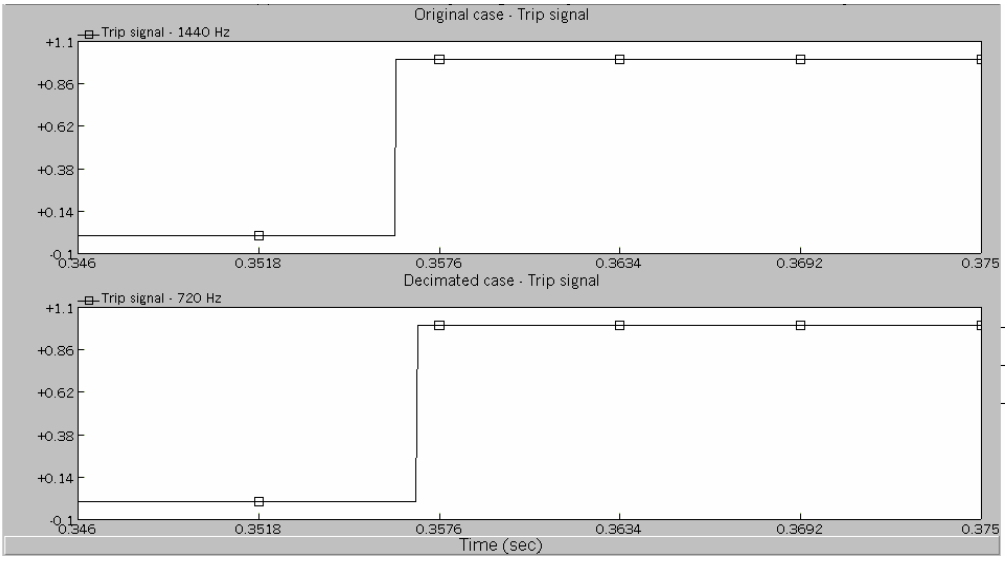


**Figure 6.17:** Trip signals of 1440 Hz (original sampling frequency) and 720 Hz (down-sampled sampling frequency) cases, test 3

### 6.4.1.4 Decimation test 4 - Differential relay model

The conditions for the test 4 were the same than the employed for test 3, but in test 4 the fault was located outside the differential relay protection zone, as shown in Figure 6.18.

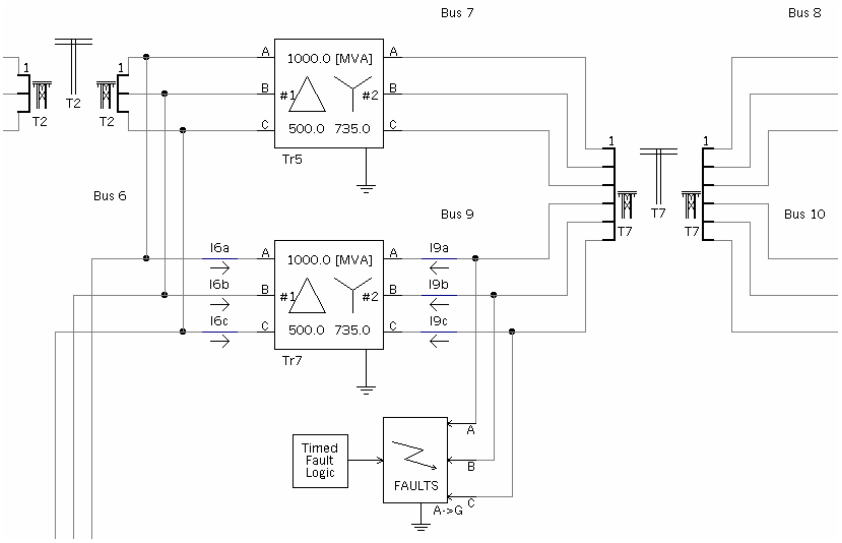


**Figure 6.18:** Phase A-to-ground fault outside the differential protecting zone of a power transformer, test 4

The comparison between the estimated restraining signals using the original frequency sampling of 1440 Hz and the down-sampled sampling frequency of 720 Hz are shown in Figure 6.19. The comparison of respecting estimated operating currents are shown in Figure 6.20.

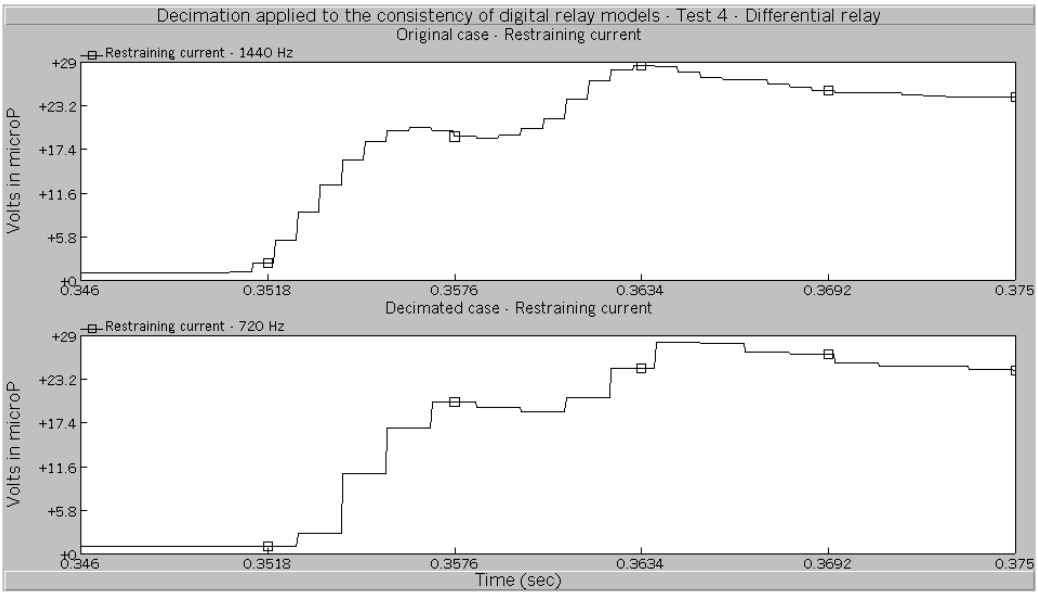


**Figure 6.19:** Estimated restraining currents, 1440 Hz (original sampling frequency) and 720 Hz (down-sampled sampling frequency) cases, test 4

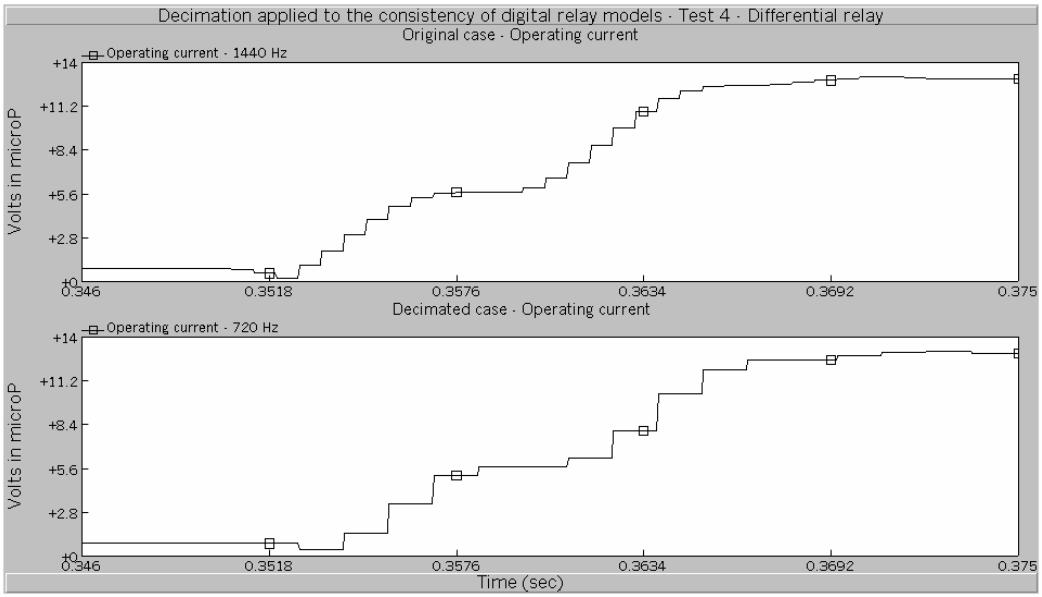


**Figure 6.20:** Estimated operating currents, 1440 Hz (original sampling frequency) and 720 Hz (down-sampled sampling frequency) cases, test 4

### 6.4.2 Conclusion of the decimation consistency tests of the distance relay models

In the graphs of the decimation consistency tests it was observed that the curves of the signals of the original sampling frequency and of the down-sampled sampling frequency cases were similar in shape and magnitude. Slight delays were also noticed in the curves of the down-sampled cases respect to the original cases. These delays were due to the anti-aliasing filtering of the input signal employed in the down-sampling cases. Based on this, it is possible to affirm that the numerical distance and differential models showed consistency in their response, regardless of the sampling frequency employed.

## 6.5 Summary

The present chapter has presented the consistency tests applied to the numerical relay models designed using the proposed protection system model designing methodology.

The consistency tests applied to the characteristic curve of distance relay models has been developed. The impedance, offset-mho, mho, and reactance characteristic of phase and ground distance relay have been tested with a special circuit designed to test their consistency. The results obtained have been satisfactory.

Basic concepts of decimation have been explained. Decimation applied to test the consistency of relay models has been distance and differential numerical relay models designed with the proposed protection system model designing methodology, and the results have been satisfactory as well.

# 7. Summary and Conclusions

Electrical power systems are one of the more complex and important systems ever built by human civilization. The role of electrical power systems in the development, sustenance and expansion of the economical activity of modern societies is of the first order of importance. However, power systems sometimes fail due to adverse environment and aging of equipment. When the failures happen, protection of power systems acquires a vital significance to minimize the damages and to keep the operation of the systems safe.

Numerical relays are a result of the application of microprocessor technology in the protection industry. These relays are in an extensive use in modern protection schemes, and are also a very active area of research. Modeling of numerical relays provides a valuable source of information for manufacturers, utility engineers, educators and trainers.

A literature review has shown that most of the modeling techniques applied to numerical relays lack automation and generalization. This means that the modeling techniques are not computer-aided for designing successive relay models. A new modeling process has to be planned and implemented every time a new relay model has to be produced. Those techniques that do offer generality in the modeling process [53] employ software that is not an industry standard. The techniques that model power systems and numerical relays in the same emtp need to set up a link between the electromagnetic transient engine and the relay model. To do this, it is necessary to have an in-depth knowledge of the structure of the emtp. The amount of work that this task takes can be as big as the modeling process itself.

This research project has developed a new methodology of modeling protection systems that overcomes these problems. The proposed methodology automates and generalizes the design process. The methodology embeds the designed numerical relay models within a power system model in the PSCAD/EMTDC environment in closed-loop structure. This structure recreates the interaction of the protection system model and the power system model. The structure allows the user to analyze the performance of the designed relay models at the level of the internal response of different modules that constitute the numerical relays, and at the level of the interaction between different numerical relays that constitute the protection system.

In Chapter 1 are described the subject and organization of the thesis. The importance of power systems and their protection systems is emphasized. Previously proposed techniques for modeling numerical relays are reviewed and discussed as well. The outline and objectives of the thesis are also established in chapter 1. Some background in protection of power systems and in the structure and functionality of numerical relays is also provided.

In Chapter 2, an overview of power system protection and protection philosophy are presented. In this chapter the protection of transmission lines with distance relays, and the protection of power transformers with differential relays are discussed. Emphasis is given to the description and operating principles of distance and differential relays. The setting and adjustment of protection zones, comparators and operating characteristics of distance relays are discussed. The calculation of apparent impedance and zero-sequence compensation for ground distance relays are also included. The principle of operation of differential relays is examined. Percentage restrain differential relays are introduced. Finally, the protection of power transformers with differential relays is addressed.

In Chapter 3, the structure of a generalized numerical relay is introduced. The major internal modules of the generalized relay model are described. These modules are the analog signal scaling module, analog anti-aliasing filtering module, analog-to-digital

conversion module, phasor estimation algorithm module and relay logic module. The most common techniques and methods employed in each module of the generalized numerical relay are enumerated and reviewed.

A new methodology for designing models of protection systems developed during this research is described in Chapter 4. The proposed methodology consists of two major steps. The first step consists of designing numerical relay models by using the computer software, called PLSA, which was designed for this project. The PLSA software and the relay modeling procedure are described in Chapter 4. The second step consists of incorporating the numerical relay models designed with PLSA in a power system case modeled in the PSCAD/EMTDC environment. *Components* in PSCAD/EMTDC are also introduced in chapter 4. These components consist of user-custom structures of PSACD/EMTDC that are needed for embedding the numerical relay models in the PSCAD/EMTDC case. The details related to putting the numerical relay models in service in the PSCAD/EMTDC case are also addressed.

The structure created with the proposed methodology is flexible and stable, and allows the entire capability of PSCAD/EMTDC to be used without decreasing the computational speed or computational memory. The methodology allows investigating the protection system in two different levels. In the first level, the behavior of the internal variables of a numerical relay model can be observed. In the second level, the interactions between the relay models and other elements of the power system are analyzed. In Chapter 5, protection system studies performed with the proposed methodology are presented. The studies are divided in studies of distance relays protecting a transmission line and studies of differential relays protecting a power transformer. The studies performed with distance and differential relay models are enumerated. The adjustment and parameter setting of the distance and differential relays are reported. The performance of the distance and differential relay models in the event of faults of different nature are included. The responses of the distance and differential relay models to CT saturation as well as the response of the relay models when anti-

aliasing filter are not used are reviewed. The response and the issues of differential relay models in the presence of inrush current are also reported.

In Chapter 6, a set of tests dedicated to corroborate the consistency of the numerical relay models are described. For this purpose, response of the models is checked for cases for which results were known in advance. It was expected that the relay models would respond as close as possible to the anticipated result. The distance relay characteristic curve consistency tests are introduced. Results obtained with the distance relay characteristic curve consistency tests are reported and the conclusions are drawn. Decimation applied to the consistency of numerical relay models is described. The outcomes obtained with decimation applied to the consistency of numerical relay models are shown and conclusions are developed.

The objective of this research project was to develop a methodology that would allow a relay model to be built in a single computational structure that would analyze the performance of a protection system and the power system in which the relay is installed. The analyses allow the user to examine the internal variables of the relay as well as the interaction between different relay models and with other elements of the power system. The work reported in this thesis shows that the objectives have been fulfilled successfully. Specifically, the project has made the following contributions.

- A new methodology for designing models of protection systems and including digital and numerical relay models in a PSCAD/EMTDC case have been developed. This methodology establishes a closed loop structure between the protection systems and power systems. In depth analysis of the internal variables of the numerical relay models and observations of the interactions of the numerical relay models between themselves or with other elements of the power system are feasible with this structure. The structure flexibility permits the simulation of practically any power and protection system study. Additionally, the proposed methodology can be employed in designing new numerical relay prototypes, new protection algorithms and methods.

- A user-friendly Visual C++-based program (PLSA), which helps in designing numerical relay models, for use with PSCAD/EMTDC has been developed. PLSA acquires from the user data and parameters of a numerical relay to generate computational equivalents of the relay. Additionally, PLSA may be enhanced to design other relay elements.
- A technique for embedding numerical relay models designed with PLSA in cases of the electromagnetic transient program PSCAD/EMTDC has been introduced. The technique employs a user-custom structure to insert numerical relay models inside a PSCAD/EMTDC case.

The proposed protection system model designing methodology does not require an external program to perform the analog and digital signal processing of the numerical relay, given that this process is coded and placed inside the relay model. Additionally, since the relay models use a structure that is common to the models that conform the PSCAD/EMTDC library, the relay model are natural elements of PSCAD/EMTDC, and the engine EMTDC directly and naturally attains every computational process they generate or suffer. This methodology represents an advantage over other modeling techniques because the simulation of the power system and its related protection system are running only in PSCAD/EMTDC, and there is no need of creating a loop, closed or open, between PSCAD/EMTDC and an external program where the relay models would be running, as in previous approaches. Besides, there is no need to perform complex modification to the main code of PSCAD/EMTDC, maximizing the efficiency of computational resources and simplifying the interaction between protection and power system models.

# REFERENCES


[1] A. Guzman, S. Zocholl, G. Benmouyal, and H. J. Altuve, "Performance Analysis of Traditional and Improved Transformer Differential Protective Relays", *SEL Technical Papers*.

[2] J. Lewis Blackburn, "Protective Relaying," Marcel Dekker Inc., 1987.

[3] ALSTOM T&D Energy Automation & Information, "Network Protection and Automation," First Edition, July 2002.

[4] IEE, "Power System Protection: Volume 1 – Principles and Components", 2nd Edition by the Electricity Training Association, London 1995.

[5] B. Kasztenny, A. Kulidjian, B. Campbell, M. Pozzuoli, "Operate and Restraint Signals of a Transformer Differential Relay", *54th Annual Georgia Tech Protective Relaying Conference*, May 2000.

[6] W. A. Elmore, "Protective Relaying. Theory and Applications," Second Edition, Marcel Dekker Inc., 2004.

[7] L F. Kennedy and C. D. Hayward, "Harmonic-Current-Restrained Relays for Differential Protection," *AIEE Transactions*, Vol. 57, May 1938, pp. 262-266.

[8] C. D. Hayward, "Harmonic-Current-Restrained Relays for Transformer Differential Protection," *AIEE Transactions*, Vol. 60, 1941, pp. 377-382.

[9] C. A. Mathews, "An Improved Transformer Differential Relay," *AIEE Transactions*, Vol. 73, Part III, June 1954, pp. 645-650.

[10] R. L. Sharp and W. E. Glassburn, "A Transformer Differential Relay with Second-Harmonic Restrain," *AIEE Transactions*, Vol. 77, Part III, Dec. 1958, pp. 913-918.

[11] C. H. Einval and J. R. Linders, "A Three-Phase Differential Relay for Transformer Protection," *IEEE Transactions PAS*, Vol. PAS-94, No. 6, Nov/Dec 1975, pp. 1971-1980.

[12] G. Bartula, "Enhanced Transformer Protection through Inrush-Proof Ratio Differential Relays," Brown Boveri Review, Vol. 32, 1945, pp. 129-133.

[13] G. D. Rockefeller, "Fault Protection with a Digital Computer," *IEEE Transactions PAS*, Vol. PAS-98, April 1969, pp. 438-464.

[14] A. M. Dmitrenko, “Semiconductor Pulse-Duration Differential Restrain Relay,” Izvestiya Vysshikh Uchebnykh Zavedenii, Elektromekhanika, No. 3, March 1970, pp. 335-339 (in Russian).

[15] A. Giuliante and G. Clough, “Advances in the Design of Differential Protection for Power Transformers,” *1991 Georgia Tech. Protective Relaying Conference*, Atlanta, GA, May 1-3, 1991, pp. 1-12.

[16] M. Hegazy, “New Principle for Using Full-Wave Rectifiers in Differential Protection of Transformers,” *IEE Proceedings*, Vol. 116, March 1969, pp. 425-428.

[17] A. M. Dimitrenko, “The Use of Currentless Pause for Detuning Differential Protection from Transient Imbalances Currents,” *Elektrichestvo*, No. 1, January 1979, pp. 55-58 (in Russian)

[18] E. L. Michelson, “Rectifier Relay for Transformer Protection,” *AIEE Transactions*, Vol. 64, May 1945, pp. 252-254.

[19] E. V. Podgornyi and E. M. Ulianitskii, “A Comparison of Principles for Detuning Differential Relays from Transformer Inrush Currents,” *Elektrichestvo*, No. 10, October 1969, pp. 26-32 (in Russian).

[20] S. B. Wilkinson, Transformer Differential Relay, U. S. Patent No. 5627712, May 6th, 1997.

[21] Mason C. Russell, “The Art and Science of Protective Relaying,” New York Wiley, 1956.

[22] M.S. Sachdev, M. Nagpal, and T. Adu, "Interactive Software for Evaluating and Teaching Digital Relaying Algorithms", *IEEE Transactions on Power Systems*, Vol. 5, No. 1, February 1990, pp. 346-352

[23] T. S. Sidhu, M. Hfuda and M. S. Sachdev, “Generating Relay Models for Protection Studies”, *IEEE Computer Applications in Po*wer, Vol. 11, No. 4, 1998, pp. 33-38

[24] M. S. Sachdev (Coordinator) et al, "Advancements in Microprocessor Based Protection and Communication", 1997, *A tutorial publication of the IEEE*, Piscataway, NJ: IEEE Cat. No. 97TP120-0, pp. 127

[25] P. G. McLaren, K. Mustaphi, G. Benmouyal, S. Chano, A. Girgis, C. Henville, M. Kezunovic, L. Kojovic, R. Marttila, M. Meisinger, G. Michel, M. S. Sachdev, V. Skendzic, T. S. Sidhu, and D. Tziouvaras, " Software Models for Relays", *IEEE Transactions on Power Delivery*, Vol. 16, No. 12, April 2001, pp. 238-45,

[26] Canadian/American EMTP users Group, Alternative Transient Program (ATP)-Rule book, Portland, Oregon, 1992

[27] A.K.S. Chaudhary, Kwa-sur Tam, and A. G.Phadke, "Protection System Representation in the Electromagnetic Transient Program," *IEEE Transactions on Power Delivery*, Vol. 9, No. 2, April 1994, pp. 700-711

[28] J. Mahseredjian, G. Benmouyal, X. Lombard, M. Zouiti, B. Bressac, and L. Gérin-Lajoie, " A link between EMTP and MATLAB for user-defined modeling," *IEEE Transactions on Power Delivery*, Vol. 13, Issue 2, April 1998, pp. 667-674

[29] Kesunovic M., and Chen Q., "A novel approach for interactive protective system simulation," *IEEE Trans. on Power Systems*, vol. 12, no. 2, pp. 668-694, Apr. 1997

[30] M. Gole. and A. Daneshpooy, "Towards Open Systems: A PSCAD/EMTDC to MATLAB Interface," *International Conference on Power Systems Transients (IPST97)*, Seattle, June22-26, 1997., pp. 145-149

[31] P. G. McLaren, G. W. Swift, A. Neufeld, Z. Zhang, E. Dirks, M. Haywood, "Open System Relaying," *IEEE Trans. on Power Delivery*, Vol. 9, no. 3, July 1994.

[32] IEEE Standard Dictionary of Electrical and Electronics Terms, *IEEE*, Wiley Interscience, 1972

[33] M. S. Sachdev -Course Coordinator-, Microprocessor Relay and Protection System, *IEEE Tutorial Course*, Piscataway, NJ: IEEE Cat. No 88EH0269-1-PWR.

[34] B. Porat, A Course in Digital Signal Processing, John Wiley and Sons Inc., 1997.

[35] B. P. Lathi., Signal Processing and Linear Systems, Berkeley-Cambridge Press, Carmichael California, 1998.

[36] T. W. Parks, C. S. Burrus, Digital Filter Design, John Wiley & Sons, Inc., 1987.

[37] R. C. Jaeger, "Tutorial: Analog Data Acquisition Technology," *IEEE Micro*, February 1982.

[38] G. Benmouyal, “Removal of DC-offset in current waveform using digital mimic filtering," *IEEE Transactions on Power Delivery*, Vol. 10, No. 2, pp. 621-628, April 1995.

[39] V. Cook, Analysis of Distance Protection, Research Studies Press, John Wiley and Sons, 1985.

[40] G. Ziegler, Numerical Distance Protection, Siemens AG, Berlin and Munich, 1999.

[41] J. G. Andrichak, G. E. Alexander, “Distance Relay Fundamentals,” General Electric Co Technical Papers.

[42] H. W. Dommel, “Digital Computer Solution of Electromagnetic Transient in Single- and Multiphase Networks,” *IEEE Transactions on Power Apparatus and Systems*, Vol. PAS-88, No. 4, April 1969.

[43] H. Dommel, “EMTP Reference Manual,” Bonneville Power Administration 1986.

[44] Introduction to PSCAD/EMTDC V3, Manitoba HVDC Research Centre Inc., Canada, 2000.

[45] J. Singh, M. S. Sachdev, R. J. Fleming, E. Krause, “Digital IDTM Overcurrent Relays,” *Proceedings of IEE 1980 DPSP Conference*, IEE Publication No. 185, pp. 84-87.

[46] E. O. Schweitzer and A. Aliaga, “Digital Programmable Time-Parameter Relay Offers Versatility and Accuracy,” *IEEE Transactions on Power Apparatus and Systems*, Vol. PAS-89, No. 1, pp. 152-157, Jan./Feb. 1980.

[47] Z. Peng, M. S. Li, C. Y. Wu, T. C. Cheng, and T. S. Ning, “A dynamic State Space Model of a Mho Distance Relay,” *IEEE Transactions on Power Apparatus and Systems*, Vol. PAS-104, No. 12, December 1985.

[48] R. E. Wilson, J. M. Nordstrom, “EMTP Transient Modeling of a Distance Relay and a Comparison with EMTP Laboratory Testing,” *IEEE Transactions on Power Delivery*, Vol. 8, No. 3, July 1993.

[49] Chul-Hwan Kim, Myung-Hee Lee, R. K. Aggarwal, A. T. Johns, “Educational Use of EMTP MODELS for the Study of a Distance Relay Algorithm for Protecting Transmission Lines,” *IEEE Transactions on Power Systems*, Vol. 15, No. 1, February 2000.

[50] Westinghouse Electric Corporation, “Relaying Current Transformer Application Guide,” *Industrial and Commercial Power System Applications Series*, July 1986.

[51] MATLAB, High-Performance Numeric Computation and Visualization Software. External Interface Guide, January 1993. The MathWorks, Inc.

[52] The Institute of Electrical and Electronics Engineers, Inc., “IEEE Standard Requirements for Instrument Transformer, ANSI/IEEE C57.13-1978,” June 1986.

[53] M. Kezunovic, B. Kasztenny, “New SIMULINK Libraries for Modeling Digital Protective Relays and Evaluating Their Performance Under Fault Transients”, *Proceedings of the International Conference on Power System Transients IPST '99*. Budapest, Hungary. June 1999.

[54] MATLAB 6.1, Reference Manual, MathWorks, Inc. 2001.

[55] SIMULINK 4.1, Reference Manual, MathWorks, Inc. 2001.

[56] Power System Block Set, Reference Manual, MathWorks, Inc. 2001.

[57] A. M. Gole, A. Daneshpooy, “Towards Open Systems: A PSCAD/EMTDC to MATLAB Interface,” *Proceedings of the International Conference on Power System Transients IPST '97*. Seattle, USA. June 1997.

[58] R. W. Wall, B. K. Johnson, “Using TACS Functions within EMTP to Teach Protective Relaying Fundamentals,” IEEE Transactions on Power Systems, Vol. 12, No. 1, February 1997.

[59] P. G. McLaren, G. W. Swift, Z. Zhang, E. Dirks, R. P. Jayasinghe, and I. Fernando, “A New Directional Element for Numerical Distance Relays,” IEEE Transactions on Power Delivery, Vol. 10, No. 2, April 1995.

[60] G. E. Alexander, J. G. Andrichak, “Ground Distance Relaying: Problems and Principles,” *Nineteenth Annual Western Protective Relay Conference*, Washington, October 1991.

# APPENDIX A
# VISUAL C++ BRIEF

## A.1 Forewords

The program for generating digital relay models (PLSA), developed in this doctoral project, has been programmed employing the Microsoft Foundation Class (MFC) Library included in Microsoft Visual C++.

In order to prepare the terrain to the description of the structure and functionality of PLSA, this appendix presents a series of concepts and definitions related with the MFC Library and Visual C++. Concepts of the philosophy of object-oriented programming are also included in order to understand the theory behind MFC.

## A.2. Object-oriented programming philosophy and principles

Object-oriented programming is different from procedural programming languages (C, Pascal, etc.) in several ways, but the most important difference is that everything in object-oriented programming is grouped as *objects* in categories named *classes*. Object-oriented programming, defined in the purest sense, is implemented by establishing a communication system between objects; this is, by sending messages to objects.

### A.2.1 Objects and classes

An *object* is a computational element that can perform a set of activities. The set of activities that the object performs defines the behavior of the object. For example, a **Student** object can tell you its name or its address. The two broad categories of objects are *Classes* and *Instances*. Users of object-oriented technology usually think of classes as containing the information necessary to create instances, i.e., the structure and capabilities of an instance is determined by its corresponding class. A class is a logic method that consists of both a pattern and a mechanism for creating items based on that pattern. This is the class as an instance factory view. Instances are the individual items that are created using the class creation mechanism.

#### A.2.1.1 Messages

The interface between objects consists of a flux of messages, each message performing a specific action. An object asks another object to perform an action by sending it a message. For example, a **School** object asks the **Student** object for its name by sending it a message asking for its name. The receiving **Student** object returns the name back to the sending object.

A message can also contain information the sending objects needs to pass to the receiving object, called the argument in the message. A receiving object always returns a value back to the sending object. This returned value may or may not be useful to the sending object. For example, the **School** object now wants to change the name of the **Student** object. It does this by sending the **Student** object a message to set its name to a new name. The new address is passed as an argument in the message. In this case, the **School** object does not care about the return value from the message.

### A.2.1.2 Sequential operation

It is very common that a message will cause other messages to be sent, either to itself or to other objects, in order to complete its task. This is called sequential operation. Control will not return to the original sending object until all other messages have been completed.

### A.2.1.3 Methods

Each message received by an object has code that is associated with it. When an object receives a message, the code associated with the message is executed. In other words, these messages determine the behavior of the object and the code determines how the object carries out each message. The code associated with each message is called a method. The message name is also called the method name due to its close association with the method. When an object receives a message, it determines what method is being requested and passes control to the method. An object has as many methods as it takes to perform its designed actions.

Methods that operate on specific objects are instance methods and messages that invoke instance methods are called instance message. Methods that operate on specific classes are class methods.

Methods are similar to subroutines, procedures, or functions found in procedural languages (C, Pascal). For example, a method name equates to a subroutine name, and the code for the method equates to the code found in a subroutine. Sending a message to an object is similar to calling a subroutine.

### A.2.1.4 Data of objects

Each object needs to keep the information on how to perform its defined behavior. Some objects also contain variables that support their behavior. These variables are called instance variables. The only methods that can refer to the values stored in the instance variables, or the only ones that can change them, are the instance methods. The instance methods for other objects cannot refer to this object data. The previous

characteristic is called encapsulation. Encapsulation assures that there is a secure process for accessing object data.

Unlike procedural programming, where common data areas are often used for sharing information, object-oriented programming discourages direct access to common data (other than the use of global variables) by other programs. Only the object that *owns* the data can change them. Other objects can view or change this data by sending message to the *owner*.

## A.2.2 Object-oriented programming paradigm

A computer language is object-oriented if they support the four specific object properties, called abstraction, polymorphism, inheritance, and encapsulation.

### A.2.2.1 Data abstraction

Abstraction is the process of focusing on the essential details while ignoring the inessential details. In functional abstraction, it may be known a good deal about the interface information, but very little about how an actual function is accomplished.

Data abstraction is implemented on top of functional abstraction. In data abstraction, not only the function performed is an abstraction, but the interface data is also treated as an abstraction. For example, consider a *list object*. If the same *list object* can be used for a *list of names*, a *list of addresses*, or a *list of stacks*, then we can treat the objects that might be placed in the list as an abstraction.

### A.2.2.2 Encapsulation

In object-oriented programming, objects interact with each other by messages. The only thing that an object knows about another object is the object interface. Each object data and logic is hidden from other objects. In other words, the interface encapsulates the object code and data.

What is explained in the previous paragraph allows the developer to separate the implementation of an object from its behavior. This separation creates a *black-box* affect, where the user is isolated from implementation changes. As long as the interface remains the same, any changes to the internal implementation are transparent to the user. For example, if the name message is sent to the **Student** object, it does not matter to the user how the developer implemented the code to handle this message. All the sending object needs is the correct protocol for interacting with the **Student** object. The developer can change the implementation at any time, but the name message would still work because the interface is the same.

### A.2.2.3 Polymorphism

Another benefit of separating implementation from behavior is polymorphism. Polymorphism allows two or more objects respond to the same message. An analogy of polymorphism to daily life is how students response to a school bell. Every student knows the significant of the bell. When the bell (message) rings, however, it has its own meaning to different students (objects). Some students go home, some go to the library, and some go to other classes. Every student responds to the bell, but how they response to it might be different.

Polymorphism allows the sending object to communicate with receiving objects without having to understand what type of object it is, as long as the receiving objects support the messages.

### A.2.2.4 Inheritance

Inheritance can be defined as the process whereby one object acquires characteristics from one or more other objects. One of the most important features of object-oriented programming is the ability to modify existing solution to solve new problems. If a particular kind of problem has been solved using a certain class approach, a similar but slightly different problem can usually be solved by modifying the old class approach to create a new class approach that inherits from the old one the basic or useable structure.

## A.3 Microsoft Visual C++ introduction

C++ is a standard language that is not owned by any of the major compiler developers. A C++ compiler takes programming code written in C++, called **source code**, translates it into the language of the particular machine on which the program is going to run, and combines that machine language with other important programming code (called linking), and saves a complete, executable program.

The Microsoft Visual C++ compiler is only one of the compilers available that compiles the language called C++. The Visual C++ compiler can be used to create Windows programs or programs that run in a console window. Programs that run in a console window are often called console applications.

The Microsoft Visual C++ development system is a state-of-the-art compiler that is used to create full-blown applications for Windows. It employs a graphical user interface and a debugger. It includes a Microsoft Foundation Classes MFC Library, which makes possible to write advanced Windows-based applications. The compiler also allows you to compile standard C++ code and execute the code within a console window.

## A.3.1 Microsoft Foundation Class

The Microsoft Foundation Class **MFC** Library is a collection of classes that can be used to build application programs. The classes in the MFC Library are written in the C++ programming language. The MFC Library saves a programmer time by providing code that has already been written. It also provides an overall framework for developing the application program.

There are MFC Library classes for all graphical user interface elements (windows, frames, menus, tool bars, status bars, and so forth), for building interfaces to databases, for handling events such as messages from other applications, for handling keyboard and mouse input, and for creating ActiveX controls.

## A.3.2 Document/View architecture

By default, the MFC Application Wizard creates an application skeleton with a document class and a view class. MFC separates data management into these two classes. The document stores the data, manages printing the data, and coordinates updating multiple views of the data. The view displays the data, and manages user interaction with it, including selection and editing.

In this model, an MFC document object reads and writes data to persistent storage. The document may also provide an interface to the data wherever it resides (such as in a database). A separate view object manages data display, from rendering the data in a window to user selection and editing of data. The view obtains display data from the document and communicates back to the document any data changes.

The document/view model leave to separate view objects represent each view of the data, while code common to all views (such as a calculation engine) can reside in the document. The document also takes the task of updating all views whenever the data changes. The MFC document/view architecture makes it easy to support multiple views, multiple document types, splitter windows, and other valuable user-interface features.

## A.3.3 Document/View classes

The parts of the MFC framework most visible both to the user and to the programmer, are the document and view. Most of the work in developing an application with the framework goes into writing the document and view classes. However, at the heart of document/view are four key classes:

The CDocument class supports objects used to store or control the data of the program and provides the basic functionality for programmer-defined document classes. A document represents the unit of data that the user typically opens with the **Open** command on the **File** menu and saves with the **Save** command on the **File** menu.

The CView (or one of its derived classes) provides the basic functionality for programmer-defined view classes. A view is attached to a document and acts as an intermediary between the document and the user. The view renders an image of the document on the screen and interprets user input as operations upon the document. The view also renders the image for both printing and print preview.

CFrameWnd (or one of its variations) supports objects that provide the frame around one or more views of a document.

CDocTemplate supports an object that coordinates one or more existing documents of a given type and manages creating the correct document, view, and frame window objects for that type.

The document/view implementation in the class library separates the data itself from its display and from user operations on the data. All changes to the data are managed through the document class. The view calls this interface to access and update the data.

Documents, their associated views, and the frame windows that frame the views are created by a document template. The document template is responsible for creating and managing all documents of one document type.

# APPENDIX B
# PSCAD/EMTDC FORTRAN CODE

## B.1 Expression evaluation

PSCAD/EMTDC has a limited set of mathematical functions. Users may compose their own code and computations using the grammar of expressions shown in the following tables. Table B.1 shows trigonometric, hyperbolic and common mathematical functions. Table B.2 presents arithmetic operators. Table B.3 introduces logical operators, and table B.4 extra operators that are useful. In the tables, *a* is in radians, *x* is a real number and *c* is a complex number. FORTRAN 77 code must be indented by 6 spaces.

| Function | Expression |
|---|---|
| Sine | sin (a) |
| Cosine | cos (a) |
| Tangent | tan (a) |
| Angle sine | Asin (x) |
| Angle cosine | acos (x) |
| Angle tangent | atan (x) |
| Hyperbolic sinus | sinh (a) |
| Hyperbolic cosine | cosh (a) |
| Hyperbolic tangent | tanh (a) |
| Natural logarithm | log (x) |
| Exponential | exp (x) |
| Logarithm base 10 | log10 (x) |
| Absolute value | abs (x) |
| Real part of complex | real (c) |
| Imaginary part of complex | imag(c) |
| Integer portion | int (x) |
| Fractional portion | frac (x) |
| Random value between 0 and x | rand (x) |
| Rounding functions | round (x) |
| Rounding functions to lower entire | floor (x) |
| Rounding functions to higher entire | ceil (x) |

**Table B.1:** Mathematical functions for user-custom code in PSCAD/EMTDC

| Arithmetic operation | Operator |
|---|---|
| Addition | + |
| Subtraction | - |
| Multiplication | * |
| Division | / |
| Power | ** |
| Square root | sqrt (x) |

**Table B.2:** Arithmetic operators for user-custom code in PSCAD/EMTDC

| Logical operator | Operator |
|---|---|
| Equal | = |
| Not equal | != |
| Less than | < |
| Greater than | > |
| Less than or equal to | <= |
| Greater than or equal to | >= |
| Or | \|\| |
| And | && |

**Table B.3:** Logical operators for user-custom code in PSCAD/EMTDC

| Extra | Operator |
|---|---|
| Time-step increment specified in the Case Properties | DELT |
| Variables defined in parameter, graphics or computations sections are composed by the sign *$* followed by the variable name. | $*Variable* |

**Table B.4:** Extra functions for user-custom code in PSCAD/EMTDC

## B.2 Fortran, Dsdyn and Dsout sections

The Fortran, Dsdyn and Dsout sections are used when building a new user-custom model to include user code into the model. All computations that are used to control the network dynamics (for example, the calculation of a voltage source magnitude) must be written in Dsdyn. Dsout is employed to store code if this makes calculations using network solution quantities, such as currents and voltages variables. The network solution is done after the call of Dsdyn routine hence the latest network solution is

available when Dsout is called. When in doubt of where to locate the code of the user, it should be store in the Fortran section, since PSCAD decides the place to include the code of the user.

## B.3 Directives

Several directives are allowed in the Fortran, Dsdyn and Dsout sections to facilitate the creation of the code of the user. Each directive line begins with sign # in the first non-blank position. The principal directives employed are:

- Directives to store variable values of the network solution of a previous time step to be used in the current network solution
- Directives to indicate the use of a subroutine
- Directives to pass values from internal variables of the component to a case variable

### B.3.1 STORAGE directive

This directive tells PSCAD how many storage elements are used by this component. There are four types of storage arrays in EMTDC that can be used by user models. They are REAL, INTEGER, COMPLEX and LOGICAL. A model can use as many elements from as many arrays. The storage directive definition is given in the following manner:

#STORAGE *TYPE:Number*

Example: For a model that uses 10 real storage elements and 4 integer storage elements, the #STORAGE directive is shown in the example below. Note that the order of arrays is not important.

```
#STORAGE REAL:10 INTEGER:4
```

### B.3.2 SUBROUTINE directive

This directive declares the existence of a subroutine. The *Description* is included in comment lines at the top of the FORTRAN code.

#SUBROUTINE *Subroutine_name Description*

Example:

```
#SUBROUTINE G6P200 HVDC Valve group
```

### B.3.3 OUTPUT directive

If the content of a parameter of a component identified by Parameter_name is not empty, a local variable by the name specified by the contents of the parameter will be created and assigned the value of the FORTRAN expression within the curly braces "{...}". Type may be either REAL, INTEGER or LOGICAL.

#OUTPUT *Type Parameter_name {...}*

Example:

```
#OUTPUT INTEGER OUT1 {STORI(THIS+10)}
```

## B.4 User variables storage

EMTDC store arrays (*STORx*) are used to store user variables that have to be available for the next simulation time step. The *STORx* arrays provide storage for floating-point, integer, logical and complex variables. Each type of *STORx* arrays has a particular integer variable *NSTORx*, which is an index to control the access to its related *STORx* array. The *STORx* arrays and its related *NSTORx* indexes are shown in table B.5.

| Variable type | *STORx* array | Control index |
|---|---|---|
| Floating point | STORF(NSTORF) | NSTORF |
| Integer | STORI(NSTORI) | NSTORI |
| Logical | STORL(NSTORL) | NSTORL |
| Complex | STORC(NSTORC) | NSTORC |

**Table B.5:** *STORx* arrays type and associated access control variable

A keyword **STORAGE** should be put in the *Dsout* section of component definition to inform PSCAD of the total number of user variables of the main code and related subroutines to allocate in the *STORx* array. It is advised to make copies of the indexes of used *STORx* arrays and use the copies of indexes in the code. This approach allows calling other functions or subroutines which use *STORx* arrays while keeping unaffected the original values of the indexes.

Consider the following example, where variables UVR1 and UVR2 are floating point variables, UVR3 is an integer variable and UVR4 is a logical variable. The previous values of UVR1, UVR2, UVR3 and UVR4 are retrieved from the *STORx* arrays at beginning of the main code. The *STORx* arrays are updated with the new values of UVR1, UVR2, UVR3 and UVR4 at the end of the main code for using them in the next time step.

```
#STORAGE REAL:2
#STORAGE INTEGER:1
#STORAGE LOGICAL:1

!  Making copies of the original indexes
      MYNSTORF = NSTORF
      MYNSTORI = NSTORI
      MYNSTORL = NSTORL
!  Retrieving user variable values from STORx arrays
      UVR1 = STORF(MY_NSTORF)
      UVR2 = STORF(MY_NSTORF+1)
      UVR3 = STORI(MY_NSTORI)
      UVR4 = STORL(MY_NSTORL)
!  Body of the program where UVRx are used
      . . . . .
      . . . . .
      . . . . .
!  Saving the values of variables for use in the next time step
      STORF(MY_NSTORF) = UVR1
      STORF(MY_NSTORF+1) = UVR2
      STORI(MY_NSTORI) = UVR3
      STORL(MY_NSTORL) = UV4
```

# APPENDIX C
# VARIABLE NAMES EMPLOYED IN THE NUMERICAL RELAY MODELS

## C.1 Introduction

In order to gain access to specific internal variables, the following list enumerates the variable names used in the digital relay models. In order to differentiate variables from different relay models, it is important to notice that the variable names are composed by the denomination given in the following tables plus the particular three-letters given to a specific relay model by the user, during the designing of the model of the numerical relay with PLSA, as mentioned in section 4.5.1.1.

To facilitate the identification of a variable name, in Table C.1 are shown the letters and signs that are going to be employed in the present appendix to build the notation of the variable names. These signs and letters represent the numbers or letters that specify a particular variable. For example, the variable name of the signal that uses the *n*-th channel at the end of the signal conditioning and scaling module has the notation *CH*n*. This means that, if the relay model has four channels, and the extension used in the specific relay model is *GS*, then the name of signal variables using the four channels are *CHGS1*, *CHGS2*, *CHGS3* and *CHGS4*, respectively.

| Symbols | Representation |
|---|---|
| * | Represents the three letters particular of the specific relay model |
| *n* | Represents the *n*-th channel number |
| *z* | Represents the *z*-th zone of a distance relay |

**Table C.1:** Symbols employed in the appendix for notation purposes

## C.2 General-purpose variable names

In Table C.2 are presented the name of the variables that are of general purpose, such as storing pointer variables, variable name of the signals using the digital relay model channels and sampling variables.

## C.3 Phasor estimation variable names

In Table C.3 are presented the name of the variables corresponding to the real and imaginary components of the fundamental and harmonic phasors (second to fifth), as

well as the two first terms of the Taylor series of the DC component (see section 3.4.4.3 for definition) of the signals using the relay channels, at the end of the phasor estimation algorithm.

| Description | Notation |
|---|---|
| Storing pointer variable | *MNSTF** |
| Signal variable name of the n-th channel at the end of the signal conditioning and scaling module | *CH*n* |
| Signal variable name of the n-th channel at the end of the anti-aliasing filtering module | *CAF*n* |
| Signal variable name of the n-th channel at the end of the analog-to-digital conversion module | *CAD*n* |
| Sampling counter variable name | *SPCT** |

**Table C.2:** General purpose variable names

| Description | Notation |
|---|---|
| Real component of the fundamental phasor of the signal on the n-th channel | *FR*n* |
| Imaginary component of the fundamental phasor of the signal on the n-th channel | *FI*n* |
| Real component of the second harmonic phasor of the signal on the n-th channel | *DR*n* |
| Imaginary component of the second harmonic phasor of the signal on the n-th channel | *DI*n* |
| Real component of the third harmonic phasor of the signal on the n-th channel | *TR*n* |
| Imaginary component of the third harmonic phasor of the signal on the n-th channel | *TI*n* |
| Real component of the fourth harmonic phasor of the signal on the n-th channel | *QR*n* |
| Imaginary component of the fourth harmonic phasor of the signal on the n-th channel | *QI*n* |
| Real component of the fifth harmonic phasor of the signal on the n-th channel | *CR*n* |
| Imaginary component of the fifth harmonic phasor of the signal on the n-th channel | *CI*n* |
| First term of the DC component of the signal on the n-th channel | *D1*n* |
| Second term of the DC component of the signal on the n-th channel | *D2*n* |

**Table C.3:** Variable names of the phasors and DC component of the signals on the relay model channels

## C.4 Distance relay model variable names

In Table C.4 are presented the name of the variables corresponding to distance relay models comparator. The distance relay variables presented in Table C.4 correspond to the real and imaginary components of the fundamental phasor of the distance relay voltage and current, as well as their corresponding amplitude and phase. For the voltage and current of the distance relay it is understood the phase-to-ground voltage and the compensated current in a ground distance relay, and the phase-to-phase voltage and current in a phase distance relay. Other distance relay variables include the angle of the signals $S_1$ and $S_2$ and the difference between these signals in a phase comparator, as well as the amplitude of the signals $S_O$ and $S_R$ and their difference in an amplitude comparator.

| Description | Notation |
|---|---|
| Real component of the fundamental phasor of the distance relay voltage | *VR*R* |
| Imaginary component of the fundamental phasor of the distance relay voltage | *VR*I* |
| Amplitude of the fundamental phasor of the distance relay voltage | *VR*M* |
| Angle in radians of the fundamental phasor of the distance relay voltage | *VR*A* |
| Real component of the fundamental phasor of the distance relay current | *CR*R* |
| Imaginary component of the fundamental phasor of the distance relay current | *CR*I* |
| Amplitude of the fundamental phasor of the distance relay current | *CR*M* |
| Angle in radians of the fundamental phasor of the distance relay current | *CR*A* |
| Relative angle of the distance relay signal $S_1$ of the z-th phase comparator | *S1*zA* |
| Relative angle of the distance relay signal $S_2$ of the z-th phase comparator | *S2*zA* |
| Angle difference between the distance relay signals $S_1$ and $S_2$ on the z-th phase comparator | *D*zA* |
| Magnitude of the distance relay signal $S_O$ of the z-th amplitude comparator | *SO*zM* |
| Magnitude of the distance relay signal $S_R$ of the z-th amplitude comparator | *SR*zM* |
| Magnitude difference between the distance relay signals $S_O$ and $S_R$ on the z-th phase comparator | *D*zM* |
| Trip signal of the z-th comparator | *TR*z* |
| Apparent resistance seen by the distance relay (optional) | *RS** |
| Apparent reactance seen by the distance relay (optional) | *XS** |
| Trip signal of the distance relay | *TR21** |

**Table C.4:** Variable names of the distance relay comparator

## C.5 Differential relay model variable names

In Tables C.5, C.6, and C.7 are presented the name of the variables exclusive of differential relay model. The differential relay variables presented in Table C.5 correspond to the real and imaginary components of the fundamental and harmonic phasors (second to fifth), as well as the two first terms of the Taylor series of the DC component (section 3.4.4.3) of the restraint current in differential relay equation. In Table C.6 are presented the fundamental and harmonic phasors, and the DC component of the operating current. In Table C.7 are mentioned the variable names of the restraint and operating current phasors (which are the linear summation of the fundamental and harmonics presented in Tables C.5 and C.6), their difference and the trip signal variable name.

| Description | Notation |
|---|---|
| Real component of the fundamental phasor of the restraint current | *FR*nRC* |
| Imaginary component of the fundamental phasor of the restraint current | *FI*nRC* |
| Amplitude of the fundamental phasor of the restraint current | *F*nRC* |
| Real component of the second harmonic phasor of the restraint current | *DR*nRC* |
| Imaginary component of the second harmonic phasor of the restraint current | *DI*nRC* |
| Amplitude of the second harmonic phasor of the restraint current | *D*nRC* |
| Real component of the third harmonic phasor of the restraint current | *TR*nRC* |
| Imaginary component of the third harmonic phasor of the restraint current | *TI*nRC* |
| Amplitude of the third harmonic phasor of the restraint current | *T*nRC* |
| Real component of the fourth harmonic phasor of the restraint current | *QR*nRC* |
| Imaginary component of the fourth harmonic phasor of the restraint current | *QI*nRC* |
| Amplitude of the fourth harmonic phasor of the restraint current | *Q*nRC* |
| Real component of the fifth harmonic phasor of the restraint current | *CR*nRC* |
| Imaginary component of the fifth harmonic phasor of the restraint current | *CI*nRC* |
| Amplitude of the fifth harmonic phasor of the restraint current | *C*nRC* |
| First term of the DC component of the restraint current | *DC1*nRC* |
| Second term of the DC component of the restraint current | *DC2*nRC* |
| Magnitude of the DC component of the restraint current | *DC*nRC* |

**Table C.5:** Variable names of the harmonics of the restraint current of the differential relay model

| Description | Notation |
|---|---|
| Real component of the fundamental phasor of the operating current | *FR*nOC* |
| Imaginary component of the fundamental phasor of the operating current | *FI*nOC* |
| Amplitude of the fundamental phasor of the operating current | *OC*n* |
| Real component of the second harmonic phasor of the operating current | *DR*nOC* |
| Imaginary component of the second harmonic phasor of the operating current | *DI*nOC* |
| Amplitude of the second harmonic phasor of the operating current | *D*nOC* |

**Table C.6:** Variable names of the harmonics of the operating current of the differential relay model

| Description | Notation |
|---|---|
| Amplitude of the first slope restraint current phasor | *RC*n* |
| Amplitude of the second slope restraint current phasor | *RC2*n* |
| Amplitude of the operating current phasor | *OC*n* |
| Trip signal of the differential relay | *TR87** |

**Table C.7:** Variable names of the operating and restraint current of the differential relay model

# APPENDIX D
# TEST POWER SYSTEM PARAMETERS AND DATA

## D.1 Test power system description

In Figure D.1 is shown the 17-bus test system employed to develop the power system studies of Chapter 6. The test system has two sources representing power systems with excess generation, and two motors representing power systems that have load in excess of generation. Distance relays protect the transmission lines and differential relays protect the transformers. The relay models were designed using the developed PLSA software.

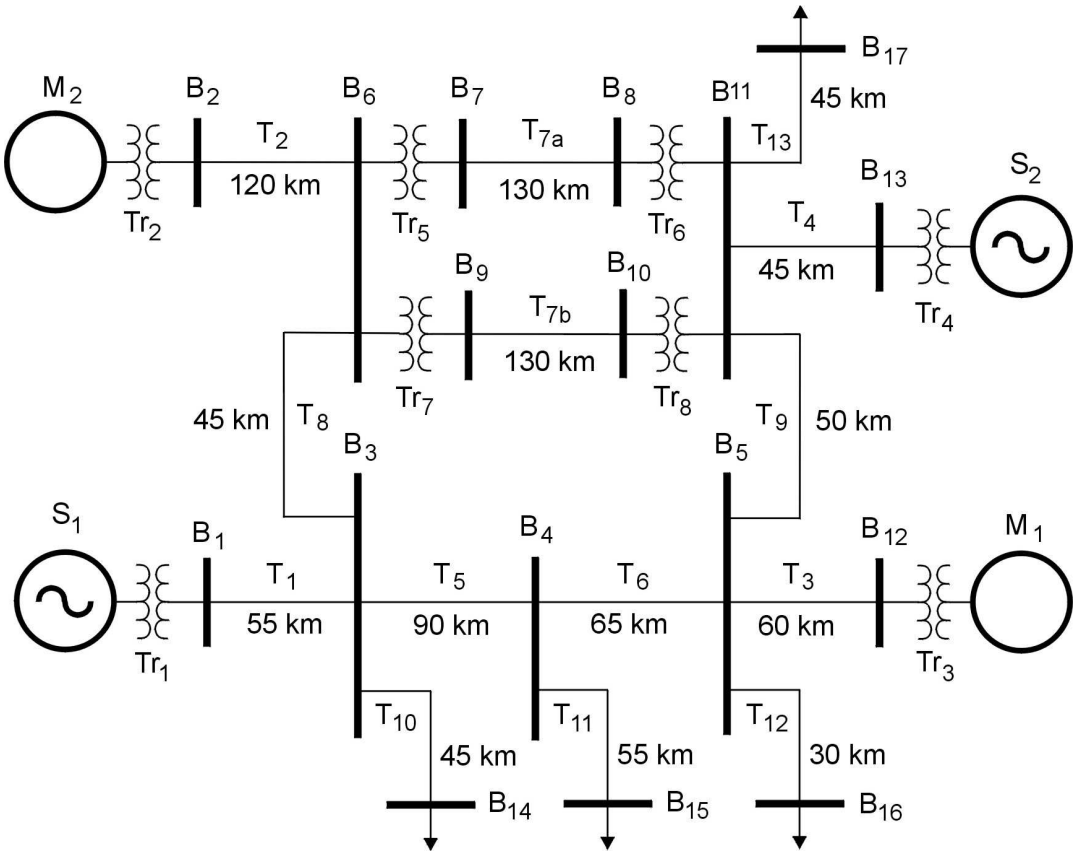


**Figure D.1:** Seventeen-bus test system

## D.1.1 Transmission Lines

The data and parameters of the transmission lines modeled in the test power system model shown in Figure D.1 are given in Table D.1.

| Name | Length (Km) | No Of Conductors | Sub-conductors in a bundle | Shunt Conductance (mhos/m) |
|---|---|---|---|---|
| L1 | 55 | 3 | 1 | 1.0 E-10 |
| L2 | 120 | 3 | 1 | 1.0 E-10 |
| L3 | 60 | 3 | 1 | 1.0 E-10 |
| L4 | 45 | 3 | 1 | 1.0 E-10 |
| L5 | 90 | 6 | 1 | 1.0 E-10 |
| L6 | 65 | 6 | 1 | 1.0 E-10 |
| L7a | 130 | 6 | 1 | 1.0 E-10 |
| L7b | 130 | 6 | 1 | 1.0 E-10 |
| L8 | 45 | 3 | 1 | 1.0 E-10 |
| L9 | 50 | 3 | 1 | 1.0 E-10 |
| L10 | 45 | 3 | 1 | 1.0 E-10 |
| L11 | 55 | 3 | 1 | 1.0 E-10 |
| L12 | 30 | 3 | 1 | 1.0 E-10 |
| L13 | 45 | 3 | 1 | 1.0 E-10 |

**Table D.1:** Transmission lines data and parameters

## D.1.2 Machines

Electric parameters of the machines modeled in the test power system model shown in Figure D.1 are given in Table D.2. Other important machines data and parameters are given in Table D.3.

| Name | Power | Power Factor | Voltage (L-L) | Xd" (p.u) |
|---|---|---|---|---|
| S1 – Source | 2000 MW | 0.866 lagging | 15 kV | 0.14 |
| S2 – Source | 1000 MW | 0.866 lagging | 15 kV | 0.14 |
| M1- Motor | 400 MW | 0.866 lagging | 15 kV | |
| M2 - Motor | 500 MW | 0.866 lagging | 15 kV | |

**Table D.2:** Electric parameters of machines

| | |
|---|---|
| **Stator to rotor turns ratio** | 1 |
| **Angular moment of inertia** | 0.3 |
| **Mechanical damping** | 0.05 p.u. |
| **Stator resistance** | 0.043 p.u. |
| **Wound rotor resistance** | 0 p.u. |
| **Mutual inductance** | 1 p.u. |
| **Stator leakage inductance** | 0.0613 p.u. |
| **Wound rotor leakage inductance** | 0.0613 p.u. |

**Table D.3:** General parameters of machines

### D.1.3 Transformers

Electric data of the power transformers modeled in the test power system model shown in Figure D.1 are given in Table D.4.

| Name | MVA Rating | Voltage Ratio | XT (p.u) |
|---|---|---|---|
| T1 | 2500 | 15 kV / 500 kV | 0.1 |
| T2 | 1800 | 15 kV / 500 kV | 0.1 |
| T3 | 500 | 500 kV /15 kV | 0.1 |
| T4 | 600 | 500 kV /15 kV | 0.1 |
| T5 | 600 | 500 kV /230 kV | 0.1 |
| T6 | 1000 | 500 kV /230 kV | 0.1 |
| T7 | 1000 | 500 kV /230 kV | 0.1 |
| T8 | 1000 | 230 kV / 500 kV | 0.1 |
| T9 | 1000 | 230 kV / 500 kV | 0.1 |

**Table D.4:** Power transformers electric data

### D.1.4 Loads

The electric data of the loads modeled in the test power system model shown in Figure D.1 are given in Table D.5.

| Name | Power (MW) | Voltage (kV) |
|---|---|---|
| L1 | 200 | 500 |
| L2 | 150 | 230 |
| L3 | 150 | 500 |
| L4 | 150 | 500 |

**Table D.5:** Loads electric data